

399  
/

THE UNIVERSITY OF NEW SOUTH WALES

SCHOOL OF METALLURGY

THESIS

FOR THE DEGREE OF DOCTOR OF PHILOSOPHY

THE MORPHOLOGY AND CRYSTALLOGRAPHY

OF WIDMANSTATTEN PRECIPITATES

John Donald Watson. B.Sc.

September, 1970.

T669.961

1

Form 2  
RETENTION

THE UNIVERSITY OF NEW SOUTH WALES

DECLARATION RELATING TO DISPOSITION OF THESIS

This is to certify that I John Donald Watson being a candidate for the degree of Doctor of Philosophy am fully aware of the policy of the University relating to the retention and use of higher degree theses, namely that the University retains the copies of any thesis submitted for examination, "and is free to allow the thesis to be consulted or borrowed. Subject to the provisions of the Copyright Act (<sup>1968</sup>~~1912-1950~~) the University may issue the thesis in whole or in part, in photostat or microfilm or other copying medium."

In the light of these provisions I declare that I wish to retain my full privileges of copyright in my thesis and request that neither the whole nor any portion of the thesis may be published by the University Librarian nor may he authorise the publication of the whole or any part of the thesis, and I further declare that this preservation of my copyright privileges in the thesis shall lapse from the 1st day of September 1972 unless it shall previously have been extended or revoked in writing over my hand.

Signature...

Witness.....

Date.....



BOUND BY  
**L. H. MOON & SON**  
PTY. LTD.  
MELBOURNE

### ACKNOWLEDGEMENTS

This work is part of a continuing programme of research into the properties of Widmanstätten precipitates initiated by Dr.P.G. McDougall, and it is to him that the author is indebted for the conscientious way in which he supervised this particular project throughout. His continued guidance, helpful discussion, criticism and intense personal interest are most gratefully acknowledged.

Thanks are also expressed to the various members of staff of the School of Metallurgy who assisted in bringing the work to completion. In this respect special mention must be made of Professor J.S. Bowles for his theoretical contributions, Mr. M. McGirr for his invaluable assistance with the mathematics and many helpful discussions, as well as Messrs. A.S. Malin and F. Scott for their assistance in a number of ways.

Finally the author wishes to thank his wife for her help in preparing the manuscript and for her continued support and encouragement.

This research was made possible by the provision of a Postgraduate Scholarship by the Commonwealth Government.

## TABLE OF CONTENTS

### SUMMARY

#### PART 1 - LITERATURE REVIEW

		Page No.	
CHAPTER	1	GENERAL INTRODUCTION.	1
CHAPTER	2	SOLID STATE PHASE TRANSFORMATIONS.	7
	2.1	<u>Introduction.</u>	7
	2.2	<u>Diffusional Precipitation Reactions.</u>	9
	2.2.1	General	9
	2.2.2	Nucleation	9
	2.2.3	Growth	13
	2.2.3.1	Time Dependence	13
	2.2.3.2	The Role of the Interface Structure	14
	2.2.4	Temperature Dependence of Morphology	19
	2.2.5	Orientation Relationships	23
	2.3	<u>Martensitic Transformations.</u>	27
	2.3.1	Geometric and Crystallographic Properties	27
	2.3.2	Strains Involved in Martensite Transformations	28
	2.3.2.1	The Correspondence and Total Lattice Strain	28
	2.3.2.2	The Shape Strain	30
	2.3.2.3	The Complementary Strain	32
	2.3.3	The Phenomenological Theories	33
	2.3.3.1	Wechsler, Lieberman and Read	33
	2.3.3.2	Bowles and Mackenzie	35
	2.3.3.3	Application of the Theories	39
	2.3.4	The Martensite Interface	41
	2.3.4.1	Structure	41
	2.3.4.2	Theories Based on Interfacial Structure	44
	2.3.5	General Theories	46
	2.4	<u>Transformations Involving Both Compositional and Shape Changes.</u>	51
	2.4.1	Introduction	51
	2.4.2	Definition of Bainite	52
	2.4.3	Kinetics	53
	2.4.4	Morphology	56
	2.4.5	Crystallography	58
	2.4.5.1	Orientation Relationships	58
	2.4.5.2	Habit Planes	60
	2.4.6	Composition	60
	2.4.7	Mechanism	63
	2.4.8	Thermodynamics	65

2.4.9	Application of the Crystallographic Theory of Martensite Transformation	67
CHAPTER 3	THE WIDMANSTATTEN STRUCTURE.	69
3.1	<u>The Genesis - Metallic Meteorites.</u>	69
3.2	<u>Early Experimental Studies.</u>	70
3.3	<u>Theories of Plate Formation.</u>	74
3.3.1	Point Diffusion Effects	74
3.3.2	Strain Energy	74
3.3.3	Interfacial Energy	75
3.3.4	Ledges	78
3.3.5	Martensitic Theories	81
CHAPTER 4	THE NATURE OF THE PROBLEM.	84
<u>PART II - EXPERIMENTAL</u>		
CHAPTER 5	INTRODUCTION.	89
CHAPTER 6	EXPERIMENTAL METHODS.	90
6.1	<u>Specimen Preparation and Heat Treatment.</u>	90
6.2	<u>The Morphology of Widmanstatten Ferrite Plates.</u>	94
6.2.1	Surface Relief Effects	94
6.2.2	Shape of Ferrite Plates	98
6.3	<u>The Crystallographic and Geometric Features of Widmanstatten Ferrite.</u>	99
6.3.1	Introduction	99
6.3.2	The Austenite Lattice Orientation	99
6.3.3	The Habit Plane	101
6.3.4	The Ferrite Lattice Orientation	102
6.3.5	The Orientation Relationship	106
6.3.6	The Shape Strain	113
CHAPTER 7	RESULTS.	115
7.1	<u>Morphology and Nature of the Shape Change.</u>	115
7.2	<u>The Habit Plane.</u>	118

7.3	<u>The Orientation Relationship.</u>	121
7.3.1	Two Independent Experiments	121
7.3.2	The Kossel Technique - Accuracy	122
7.3.3	The Multiple Variant Solutions	125
7.4	<u>The Shape Strain.</u>	130
CHAPTER 8	APPLICATION OF THE CRYSTALLOGRAPHIC THEORY TO THE FORMATION OF WIDMANSTATTEN FERRITE.	132
8.1	<u>Introduction.</u>	132
8.2	<u>The Choice of Transformation Model.</u>	132
8.3	<u>Calculation of the Strains.</u>	136
8.3.1	The Correspondence and Pure Strain	136
8.3.2	The Invariant Line Strain	138
8.3.3	Factorization of the Strain	139
CHAPTER 9	DISCUSSION	154
9.1	<u>Experimental Results.</u>	154
9.2	<u>Comparison of Experiment and Predictions of the Martensite Crystallographic Theory.</u>	163
APPENDICES		167
1	Twin Trace Analysis	167
2	A Quick Method of Locating the Vector $[hkl]$	168
3	The Least Squares Analysis	170
4	Determination of the Shear Component of $d_1$	173
REFERENCES		175

## SYNOPSIS

This thesis presents a study of the crystallographic and morphological properties of Widmanstätten ferrite precipitates in a hypoeutectoid iron/carbon alloy and the text is divided into two parts.

In Part I the literature on solid state phase transformations in metals is briefly reviewed with particular reference being given to the formation of plate morphologies. The structure of the interphase boundary is considered to be a significant factor determining the mechanism of crystal growth and the coherent, semicoherent and incoherent boundaries are discussed. A classification, which distinguishes martensitic transformations from diffusional or nucleation and growth transformations, is followed. The basis of the distinction is an inferred degree of coherence of the interface in the case of martensitic transformations, which allows a mode of interface migration that leads to a change of shape of the transformed region, and the postulation of a lattice correspondence. The properties of both types of transformation are reviewed and the crystallographic theories of martensitic transformations are described.

The possibility that this theory could also describe the features of transformations involving long range diffusion is examined. It is shown that consideration of the consequences of diffusion leads to the belief that a change of shape should only be observed in the case where the diffusing species occupy interstitial positions in the respective lattices. The significance of the observation that substitutional solid solutions may decompose to form Widmanstätten precipitates exhibiting

a change of shape is not resolved. Other theories which attempt to explain the Widmanstätten morphology are shown to be incompatible with the observation of a change of shape.

Part II describes the experimental work undertaken to test the theory that the geometric and crystallographic features of plates of proeutectoid ferrite may be accounted for by the crystallographic theory of martensitic transformations, since these reportedly exhibit the defining characteristic of a change of shape. Measurements of the habit plane, the austenite/ferrite lattice orientation relationship and the shear component of the shape strain were made on ferrite laths formed isothermally at 700°C in an iron/0.45% carbon alloy.

The results of two-surface trace and tilt determinations show that the habit plane is approximately 12° from  $\{111\}_F$  and that the magnitude of the shear component of the shape strain is 0.47. Both single laths tilted in opposite senses and double laths tilted about a central "mid-rib" were observed to form with similar habit planes, suggesting the possibility that two directions of the shape strain are associated with a single habit plane.

Measurement of the orientation relationship was carried out using two methods both of which involved the determination of the ferrite orientation using the Kossel technique. Both methods yielded essentially similar results which showed that the orientation relationship was approximately, but significantly different from, that of Kurdjumov Sachs. One of the methods, which involves determining only the orientation of two or more variants of the ferrite in order to obtain an austenite/ferrite orientation relationship, has not been previously reported and is considered to yield highly accurate results when the Kossel data is first

subjected to a least squares refinement.

Following the approach of previous work, the crystallographic theory has been applied to the ferrite transformation using the assumption that the complementary strain is a single shear of the systems  $(110)\langle uvw \rangle_F$  or  $\{hkl\}[\bar{1}10]_F$ . This is shown to yield predictions of the orientation relationship and strain magnitudes inconsistent with the experimental observations. Alternatively by using the experimental habit plane, orientation relationship and shape strain, it is shown that the transformation can not be achieved by an invariant plane strain on the habit plane, and a complementary strain that is a simple shear.

These results suggest that either the transformation is martensitic in nature, but that the complementary strain is not a simple shear, or that the theory, with the usual assumptions about the nature of the strains, cannot account for the observed features. It is felt that the former possibility is most plausible in view of the close similarity of many of the observed properties to those of classic martensite, but the lack of evidence on the possible nature of the complementary strain and the imprecise value of the shape strain obtained, does not allow this view to be fully justified.

The possibility remains that the crystallographic and geometric properties of the laths examined were affected by the specimen free surface. No attempt was made to compare the present results on surface laths with those of laths formed in the bulk of the specimen, mainly because there is no known method of determining the shape strain in fully transformed material remote from a specimen surface.

PART I

LITERATURE REVIEW

CHAPTER 1

GENERAL INTRODUCTION.

It has become customary to divide solid state transformations in metallic systems into two groups, with transformations belonging to the same group being identified by the existence of certain defining features (1). The validity of this division depends upon the selected feature or features being manifestations of a particular transformation mechanism.

Bilby and Christian (2) proposed that one class, the martensitic transformations, could be distinguished by the macroscopic change of shape which accompanies the transformation and which is revealed as a characteristic relief effect on a prepolished surface of the parent material. The atom movements that give rise to this shape change are regarded as being systematic and co-operative, as a result of which there is a unique association of any lattice point of the initial structure with the lattice point it becomes in the final structure (3). Formally, a correspondence of lattice sites is said to exist. The particular mechanisms by which these atom movements may be achieved must be such as to allow the interface to retain a high degree of coherency and, because each atom undergoes a similar displacement, the identity of the interface is unique and is retained as the transformation proceeds.

The adoption of this single geometrical feature of the shape change, with the implied existence of a correspondence, as the defining feature of the martensitic class of phase transformation means that other properties commonly possessed by the transformations in quenched steels are no longer regarded as essential to the classification, (see for

example Greninger and Troiano (4)). In particular, transformations which require compositional changes may be considered formally to be martensitic if they possess a change of shape of the correct form.\*

Diffusion controlled nucleation and growth transformations on the other hand, are envisaged as proceeding slowly at a rate governed by long range atom migration and thermally activated atom-by-atom transfer across the interphase boundary. A process of this sort does not involve any correspondence of lattice sites, not any change of shape of the transformed region (apart from volume changes) and in general the boundary will have no particular identity.

Christian (5) proposed that transformations of the first type be termed "military" and he aptly summarised the differences between the two modes by sustaining the metaphor: "... complete regimentation is found only in martensite itself, where (in principle) none of the atoms changes place with its neighbours." The atom movements are pictured as orderly, disciplined and military. Contrasted with this were the "civilian", diffusion controlled transformations, where no co-ordination is involved and "... each atom obeys the well-known civilian principle of every atom for itself." The individual atom movements in this case are then independent of each other and apparently random.

Strict adherence to the above view leads to several transformations being classed as martensitic even although they require some diffusional

---

\* Christian (6), Wayman (7) and Clark and Wayman (8) have pointed out that the shape change must be more than simply a surface rumpling and experiment must be detailed enough to show that the shape change represents an invariant plane strain on the habit plane, as required by the crystallographic theory (Section 2.3).

atom movement. This occurs because they also exhibit the defining characteristic of a change of shape. The transformation of austenite to bainite or Widmanstätten ferrite in ferrous alloys (8), and the transformation of metastable  $\beta$  phase to Widmanstätten  $\alpha$  in copper base alloys (8, 10), are two examples where this occurs. Since the atom movements which give rise to the shape change cannot be those which give rise to the compositional change, it is necessary in these cases to propose that both possible kinds of atom movements are involved in the transformation. In the case of an interstitial solid solution this is particularly easy to visualize, for the compositional change may be effected by diffusion of the small, highly mobile solute atoms, while the correspondence (and therefore the shape change) is maintained by a homogeneous strain of the larger, less mobile solvent atoms. This is essentially the model proposed for bainite and represents a viewpoint which has been developed by a number of workers over some period (1-3, 5, 6, 8, 13, 14, 23). However, a difficulty is encountered when similar reasoning is applied to substitutional solid solutions, where the diffusional atom movements could be expected to destroy the correspondence (6), and the view has not yet gained universal acceptance.

Aaronson (11) for example, has criticised the use of surface relief as a criterion indicating a martensitic mechanism in cases where diffusion is also involved. Aaronson believes that the tilting of the surface is an incidental feature, being an accompanying characteristic of ledge movement, the mechanism by which he proposes growth of plates in a supersaturated matrix takes place. Alternatively Geisler (12) has suggested that relief can be produced by accommodation slip where

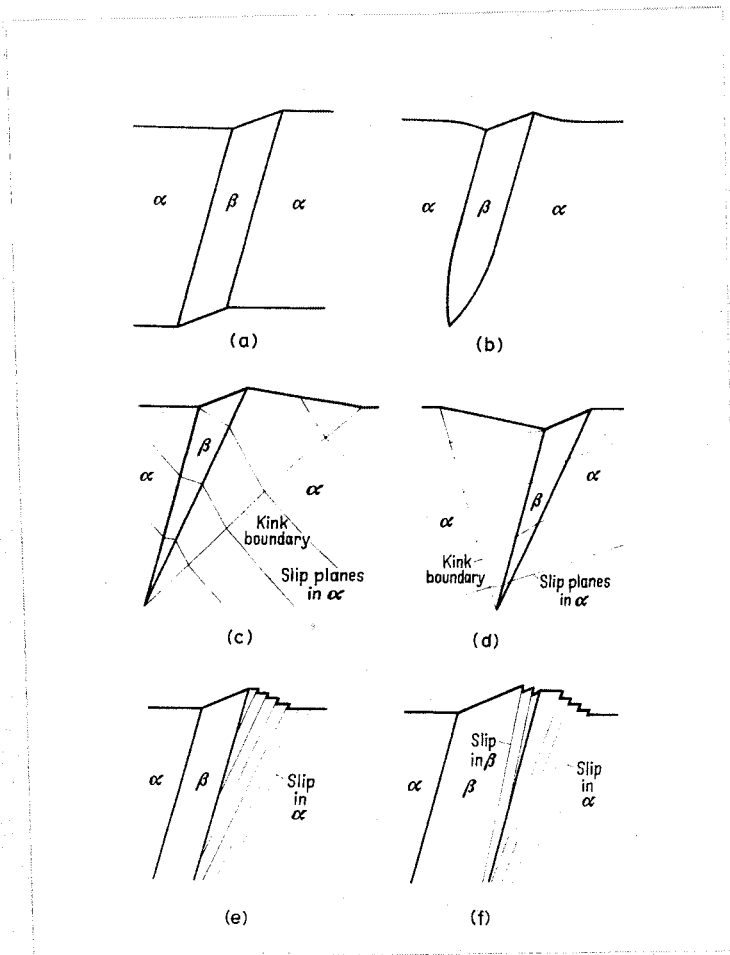


**Fig. 1.1** Shape changes resulting from transformation and accompanying plastic deformation.  
 (a) Unconstrained transformation in a single crystal producing ideal shape change.  
 (b) Lenticular plate with elastic accommodation.  
 (c-f) Possible ways in which slip and kinking may accommodate a transformation shape change. If the slip occurs on a sufficiently fine scale the true shape change may be modified, but it is unlikely that slip alone will produce the change of shape.

Christian (6).

large volume changes are involved.

Christian (6) however, has pointed out that a shape change necessarily leads to a higher strain energy than the same transformation without a change of shape; it is therefore highly improbable that changes of shape will be produced wholly by accommodation slip, although slip may accompany a transformation shape change as shown in Figure 1.1. Bowles and Tegart (13) have also pointed out that slip is most unlikely to produce relief effects of the correct nature.

The ledge model encounters equally fundamental objections since it proposes that growth essentially takes place by the migration of disordered facets of the interphase boundary. Although Aaronson claims that ledges will produce "geometric" shape changes when they intersect a free surface, it is difficult to see how. The advance of the disordered edge of a ledge involves no correspondence and, if at all similar to other disordered interphase boundaries, will not produce a shape change. Furthermore, the presence of accommodation effects, often produced in transformations involving a shape change, should never be sustained by an incoherent or disordered boundary. It is usually argued therefore, that if the shape change is described by an invariant plane strain (as in martensite) then the inference of at least partial coherence and the existence of a correspondence, is justified (5); conversely if there is no change of shape it is unlikely that the interface will possess any degree of coherence, and the growth should be accomplished by diffusional processes.

The suggestion made over fifteen years ago by Bowles and Barrett

(14), that coherent nuclei may initiate transformations other than the martensitic type, has recently been revived in essence by Pitsch et al (15, 16), who have suggested that coherence at nucleation may be inferred from the orientation relationship. Their observation that in iron/cobalt alloys the lattice orientation relationship between grain boundary allotriomorphs of ferrite and the matrix phase, falls within a region expected from considerations of the Bain correspondence, (which holds for all diffusionless transformations in ferrous martensites), may be of direct importance to a general theory of solid state phase transformations. Many of the ideas however, are controversial and are not yet adequately supported by experiment.

The foregoing considerations briefly introduce some of the difficulties which have so far prevented a criterion for classifying solid state transformations being universally accepted and agreed upon. One view which has emerged (3, 8), and which will be followed in this thesis, is that all martensitic transformations possess a uniquely related set of crystallographic and geometric properties, as a result of which a particular kind of transformation mechanism has been invoked. A test of this proposal is that the features of a transformation be in accordance with the predictions of the crystallographic theory of martensite transformation developed originally by Bowles and Mackenzie (34, 35) and Wechsler, Lieberman and Read (33).

In the chapters which follow a detailed account of diffusional phase transformations in metals is given, with particular attention being paid to the role of interfacial structure and its relevance to the formation of Widmanstätten precipitates. The crystallographic theory of martensite

is presented and discussed and its application to other than diffusionless transformations is considered. Finally, by way of introduction to the experimental work, an outline of the problems confronting an analysis of the Widmanstätten transformations is given.

---

CHAPTER 2SOLID STATE PHASE TRANSFORMATIONS.2.1 Introduction

The types of reactions which metallic solid solutions undergo on cooling may be described in terms of a combination of the structural and compositional changes required to achieve a given transformation. For example, a change of crystal structure without a change of composition can take place in pure metals which exhibit polymorphism and in the quenching of solid solutions to form martensite, while superlattice formation may involve neither overall composition change nor any change of crystal symmetry, so that the reaction is simply a rearrangement of atoms on the lattice sites. Precipitation and eutectoidal reactions, on the other hand, require both long range diffusion and a change of crystal symmetry. The latter is a special case since two phases grow from the single, metastable parent and will not be considered in great detail in this thesis. The present work is concerned principally with precipitation of one solid solution from another where changes of both composition and crystal structure are involved.

In terms of the classical nucleation theory the appearance of an embryo of a new crystalline phase is accomplished by thermally activated fluctuations of composition and structure within the metastable parent crystal. Below a critical temperature where the increase in energy due to the presence of an embryo of given size (surface energy, strain energy, etc.) is sustained by the decrease in chemical free energy, then the embryo (now nucleus) can grow. In classifying solid state transformations

attention is often focussed on the growth characteristics (rather than the nucleation event), or the ways in which atoms are transferred across the interface, these being deduced from the properties accompanying subsequent growth of the nucleus. The following sections of this chapter examine the main properties of the different types of solid state transformations and the tenets of the existing classifications are reviewed in some detail.

## 2.2 Diffusional Precipitation Reactions

### 2.2.1 General

In diffusional transformations the product grows from a nucleus by the relatively slow migration of the interphase boundary. As the nomenclature implies, the rate of movement of the boundary is limited by the ability of the atoms to rearrange themselves by diffusive processes, and the mechanism is therefore envisaged as the thermally activated transfer of individual atoms across and/or to this boundary. Except in special circumstances, the structure of the boundary is regarded as being disordered, and apart from being an interphase boundary, is analogous to a high angle grain boundary.

This type of transformation is both time and temperature dependent and generally exhibits characteristic C-curve kinetics when reaction time is plotted versus isothermal reaction temperature. Complete transformation may be achieved isothermally.

Although the volume of transformed material may differ from the volume of parent wherein it originated, the mode of atom transfer within the boundary is such that strain energy is not accumulated (apart from that arising out of the transformation volume change), and there is no definable shape change. Most notably, the homogeneous, macroscopic shape change that characterises martensite transformations is absent.

### 2.2.2 Nucleation

According to the classical theory of nucleation as applied to super-saturated vapours, the appearance of a small volume of a new phase with the correct atomic configuration can occur by a fluctuation process. The model suffers from the limitation that bulk properties are given to

very small volumes but within this limitation it is demonstrative of the principles involved (17).

By considering a small spherical region (for lowest surface energy), with radius  $r$ , the total free energy change is usually given by:

$$\Delta G = -\frac{4}{3} \pi r^3 \Delta G_v + 4\pi r^2 \sigma \quad \dots 2.1$$

where  $\Delta G_v$  is the change in chemical free energy/unit volume, and  $\sigma$  is the specific surface energy/unit volume. In solid state phase transformations, using simplifying assumptions, values for  $\Delta G_v$  can be estimated or measured, but in such transformations an additional term is added to equation 2.1 to take into account strain energy, so that:

$$\Delta G = -\frac{4}{3} \pi r^3 \Delta G_v + 4\pi r^2 \sigma + \frac{4}{3} \pi r^3 \epsilon \quad \dots 2.2$$

where  $\epsilon$  is the strain energy/unit of volume of transformed material.

This function exhibits a maximum value of  $\Delta G$ , ( $\Delta G_c$ ) at a limiting value of  $r$ , ( $r_c$ ) called the critical size. Any configuration of atoms (embryo) smaller than the critical size spontaneously shrinks while any of greater size (nucleus) will spontaneously grow. The critical size is obviously temperature dependent, decreasing as the temperature is reduced below the equilibrium value.

The probability that an embryo will reach the critical size is:

$$P_N \propto \exp \left( \frac{-\Delta G_c}{RT} \right) \quad \dots 2.3$$

and the probability, and therefore the nucleation rate, are dependent on the degree of undercooling, down to a temperature where the decreased diffusivity inhibits the transient formation of embryos. Considering the probability that an atom will make a diffusive type "jump" to be given by:

$$P_G \propto \exp \left( \frac{-Q}{RT} \right) \quad \dots 2.4$$

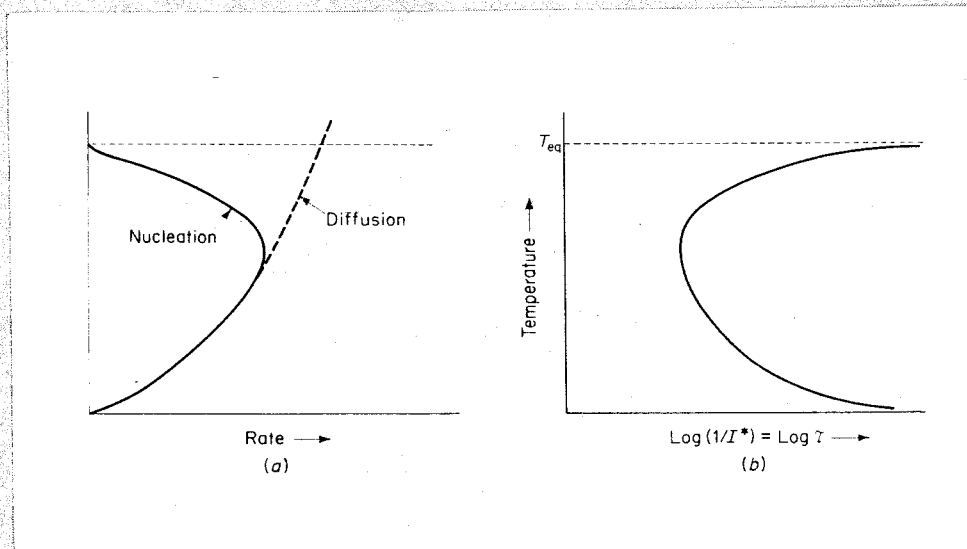


Fig. 2.1 The dependence of the nucleation rate ( $I^*$ ) on temperature below the equilibrium temperature. Below the "nose" of the curve nucleation rate is proportional to the rate of diffusion and the usual C-curve results.

Hobstetter (17).

where  $Q$  is the activation energy for diffusion, the overall nucleation rate ( $I^*$ ) can be considered as the combination of the probabilities represented by equations 2.3 and 2.4, giving:

$$I^* = K \exp \left[ -(\Delta G_c + Q) / RT \right] \quad \dots 2.5$$

By differentiating equation 2.5 with respect to reciprocal temperature, a function is obtained which is able to account for the observed dependence of nucleation rate on temperature. At high temperatures  $Q$  is small and the nucleation rate depends on  $\Delta G_c$ . At low temperatures  $\Delta G_c$  is small and the rate is governed by diffusion. The resulting C-shaped time-temperature-transformation curve, typical of many nucleation and growth transformations, is shown in Figure 2.1.

The calculations of Nabarro (18) show that the strain energy arising from differences in specific volume may be lowest for plate and needle morphologies and, if this term is important during nucleation, it should manifest itself by encouraging lenticular nuclei. The previous assumption of a spherical volume becomes inappropriate under these conditions. However, if an equation of the form of 2.2 describes nucleation, then it is the balance of surface and strain energy which is the factor limiting the nucleation event and two cases can be recognised.

In the first case there is total or partial registry of the two phases across the interface, the interface is said to possess a degree of coherency, and the surface energy term  $\sigma$  tends to be lowered, becoming zero in the case of perfect matching of atom sites at the interface. This latter situation, which corresponds to there being no dislocations in the interface, is physically improbable because of the restrictions on the lattice parameters. Forced coherency therefore leads to high

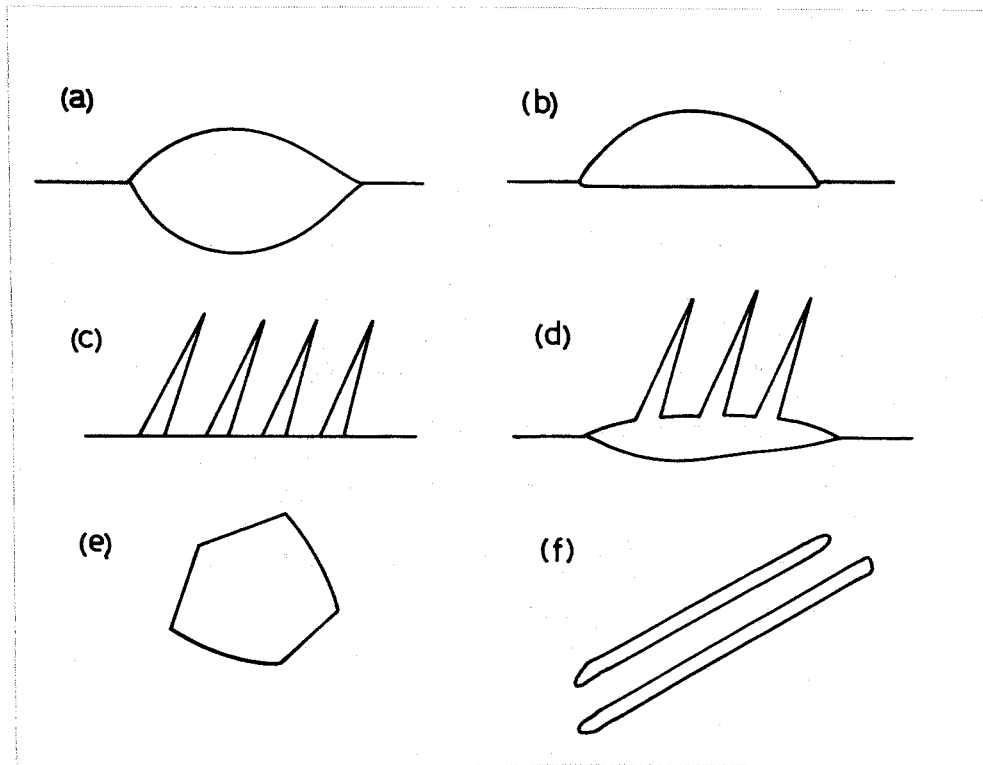


Fig. 2.2 The classification of precipitate morphologies.  
 (a-b) Grain boundary allotriomorphs. In (a) the allotriomorph presents disordered boundaries to both parent grains while in (b) the coherent segment allows fast growth to occur into only one grain.  
 (c-d) Primary and secondary Widmanstätten sideplates. Whereas the primary plates nucleate directly on twin or grain boundaries the secondary plates result from the development of preferred directions of growth from other morphologies.  
 (e) Idiormorph.  
 (f) Intragranular Widmanstätten plates.

after Aaronson (20)

values of elastic strain, ie.  $\epsilon$  is high. Alternatively, if there is complete absence of coherence at the interface the only strain energy involved is that associated with the specific volume change, but the surface energy term is then correspondingly high, ie.  $\sigma$  is high.

The familiar role of grain boundaries and lattice defects, acting as preferred sites for nucleation, can be rationalised in terms of their influence on the total free energy change. This is lowered if the formation of the embryo involves destruction of part of the existing surface or lattice defect. Aaronson (19) believes that grain boundary allotriomorphs are the first morphology to appear in many nucleation and growth transformations and suggests that the nature of the nucleation site is a major factor influencing the final shape of the precipitate. Aaronson (20) outlined the following classification of morphologies based on nucleation site and the final shape of the precipitate:

1. Grain boundary allotriomorphs.
2. Widmanstätten sideplates.
3. Widmanstätten plates (intragranular).
4. (Widmanstätten) sawteeth.
5. Idiormorphs.
6. Massive structures.

Sawteeth appear to be a transient form which predominate at high reaction temperatures and which are converted to sideplates by both decreasing temperature and increasing time (20). They therefore appear to be Widmanstätten plates which have had insufficient time to grow and are not included in Figure 2.2.

The massive structure is also not regarded as a fundamental morph-

ology as it results from the coalescence of the other morphologies at long reaction times.

The major morphologies are diagrammatically represented in Figure 2.2 and in the following sections their modes of formation and growth are discussed with reference to interfacial structure and crystallographic properties.

### 2.2.3 Growth

#### 2.2.3.1 Time Dependence

The thermally activated growth of a nucleus into a crystal of macroscopic dimensions may be (i) interface, or (ii) diffusion controlled. In the first case the kinetics reflect the rate at which atoms can transfer or "react" at the phase interface, while in the second it is the volume diffusion of atoms to or away from the (equilibrium) interface which is rate controlling. An example of the former is the growth of the new phase in pure metals during polymorphic transformation, where a linear growth law is observed (1). The second type typically exhibits parabolic growth rates when the interphase boundary is disordered, as in the growth of allotriomorphs normal to the grain boundary. In circumstances where the diffusion path is constant, eg. the precipitation of duplex structures (pearlite) or the lengthwise growth of needle morphologies, a linear time dependence of growth is again possible.

The growth of anisotropic shapes such as plates, has proven to be far more complicated than the diffusion-controlled growth of disordered boundaries, as is exemplified by the results reported for the bainite and Widmanstätten ferrite transformations in steels. These are given in Section 2.4, where the bainitic transformations are considered in

detail. The view which has emerged however, is that the growth kinetics depend markedly on the structure of the various segments of the interphase boundary, and the considerations which lead to a theory of precipitate morphology based on interface structure are discussed in the following section.

#### 2.2.3.2 The Role of the Interface Structure

The most general form of interphase boundary is similar in structure to a high angle grain boundary and will be referred to as a disordered or incoherent interphase boundary throughout this thesis. The diffuse nature and lack of atom matching at this type of interface gives rise to a high surface energy (20), and therefore to difficulty of nucleation through the term  $\sigma$  in equation 2.2. Once established however, disordered boundaries readily allow relaxation of both strain and composition gradients and growth of a new phase of different composition takes place by individual atom migration, at a rate controlled by the volume diffusion of atoms to or away from the advancing interface. When duplex structures are formed the boundary may act as a diffusion short circuit, thus allowing rapid atom transfer between the parent and the two product phases.

Following the considerations of Smith (21) there are two other types of interphase boundaries which warrant consideration, these are:

- (i) the coherent boundary.
- (ii) the partially coherent boundary.

The distinction between these two types of boundaries is made on the basis of complete or partial matching of the atomic configuration of each phase at a planar interface. Depending upon the degree of coherence, the latter type can be represented by various forms of dislocation arrays

which accommodate the mismatch between the two lattices. Because of their dislocation structure they are usually associated with anisotropic properties and, at high temperatures, are comparatively slow moving relative to disordered boundaries. If a boundary of the semi-coherent type advances, producing the product phase in its wake, under certain conditions a correspondence of lattice sites is implicit and a macroscopically homogeneous change of shape accompanies the transformation (6). In solid state transformations it is rare to have fully coherent interfaces, for this requires a relationship between the lattice parameters that can only be satisfied coincidentally, but semi-coherent boundaries are not uncommon, especially in the formation of metastable precipitates in ageing type reactions.

The simplest model of a semi-coherent interface comprises a set of parallel edge dislocations, with a common Burgers vector which does not lie in the interface, and which can glide into either phase. The structure of this type of interphase boundary is equivalent to that of a symmetric low angle tilt boundary. Under these conditions the dislocations are glissile and the structural change produced by movement of the interface is diffusionless. This model describes the martensitic type of interface (6) and will be discussed in Section 2.3.4.

Another type of semi-coherent boundary can be envisaged where the Burgers vectors of the interface dislocations lie in the plane of the interface. In this case the propagation of the boundary can take place only by climb of the dislocations, so that the process becomes dependent on thermal activation, and the displacement of the boundary is non-conservative. A schematic representation of this situation is the

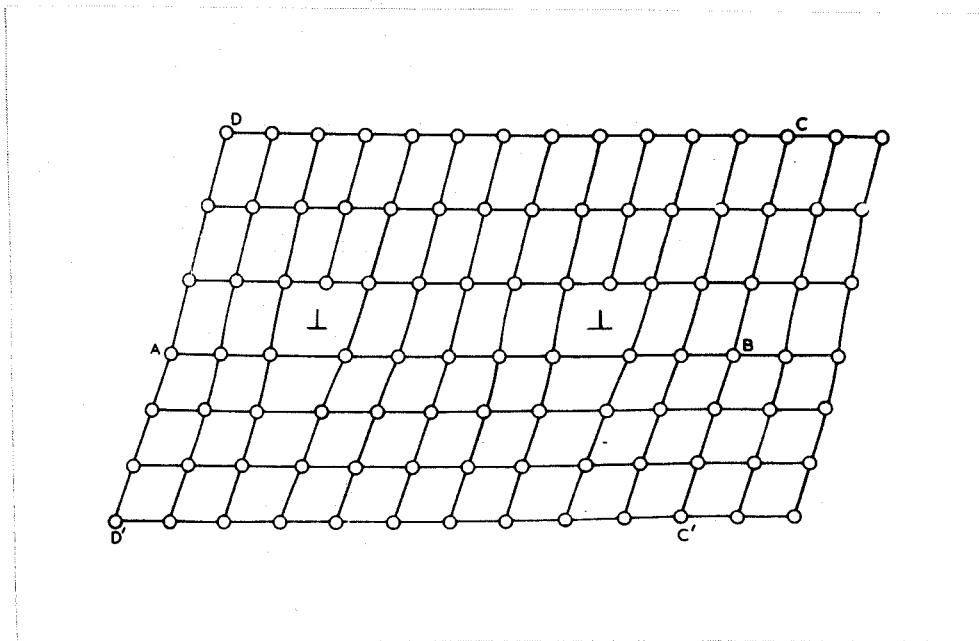


Fig. 2.3 A simple epitaxial semi-coherent boundary containing edge dislocations having a common Burgers vector which lies in the interface. If the interface at AB moves, there is a change of shape, but as the dislocations must climb the motion is non-conservative and a continuous flow of atoms to or from the boundary region is required.

Christian (6).

epitaxial semi-coherent boundary shown in Figure 2.3 (6). Although there are no known examples, the importance of this type of boundary is that, conceptually, it allows for a change of shape to accompany what must be essentially a diffusional process.

As the edge dislocations, shown in Figure 2.3, climb upward, a region of "parent" crystal with shape ABCD is transformed into a region of "product" crystal with shape D'C'BA. This macroscopic shape change results from the combination of the shape change of a unit cell with the uniaxial (lateral) contraction produced by the climb of the dislocations. The removal of the two half planes of atoms, in conjunction with the change of shape of the unit cell, allows the macroscopic shape change to be achieved. Christian (6) has pointed out however, that in the time taken for climb, it should be possible for diffusive flow to destroy, at least partially, the correspondence and hence the associated shape change.

The most general kind of semi-coherent interface which can be proposed is one containing sets of non-parallel dislocations having non-parallel Burgers vectors. This may be considered as a boundary having both glissile and epitaxial components. As in the case of the simple epitaxial boundary, it is difficult to see why the change of shape accompanying propagation of such an interface would not be at least partially removed by atom transport.

Although in the majority of cases recorded (see Section 2.4) the composition of plate-shaped precipitates exhibiting surface relief effects has not been determined, it is implicit from their microstructural appearance and growth kinetics that a change of composition takes place at some stage of their formation. The question which therefore

arises is what is the relationship between the atom movements producing the change of shape and those which achieve the composition change. The former kind of atom movement is usually considered (2, 5, 6) to be co-operative and to involve an interface that is at least semi-coherent, while the latter is regarded as essentially individual, and the boundary is of the disordered type.

A possible explanation is that the displacive atom movements result from the movement of a glissile martensitic type of interface, while the composition changes takes place quite independently by diffusion. A model of this kind can readily be applied to the transformation of one interstitial solid solution to another where only the solute atoms need undergo place exchange. This is the model commonly associated with the bainite transformation in iron/carbon alloys (1) where it is envisaged that the high mobility of the interstitial carbon atoms allows the composition to be adjusted quite independent of the species occupying lattice sites.

When this reasoning is extended to substitutional solid solutions, the postulate of two distinct types of atom movements introduces difficulties similar to those already described for the epitaxial boundary, namely the need for the transitory formation of non-equilibrium structures, followed by long range diffusion of atoms occupying lattice sites. Following the reasoning used earlier, the latter should destroy the shape change, a postulate which is contrary to observation. These difficulties have not been resolved in any published account of the problem.

In the case of ordering reactions, where the rearrangement of atoms

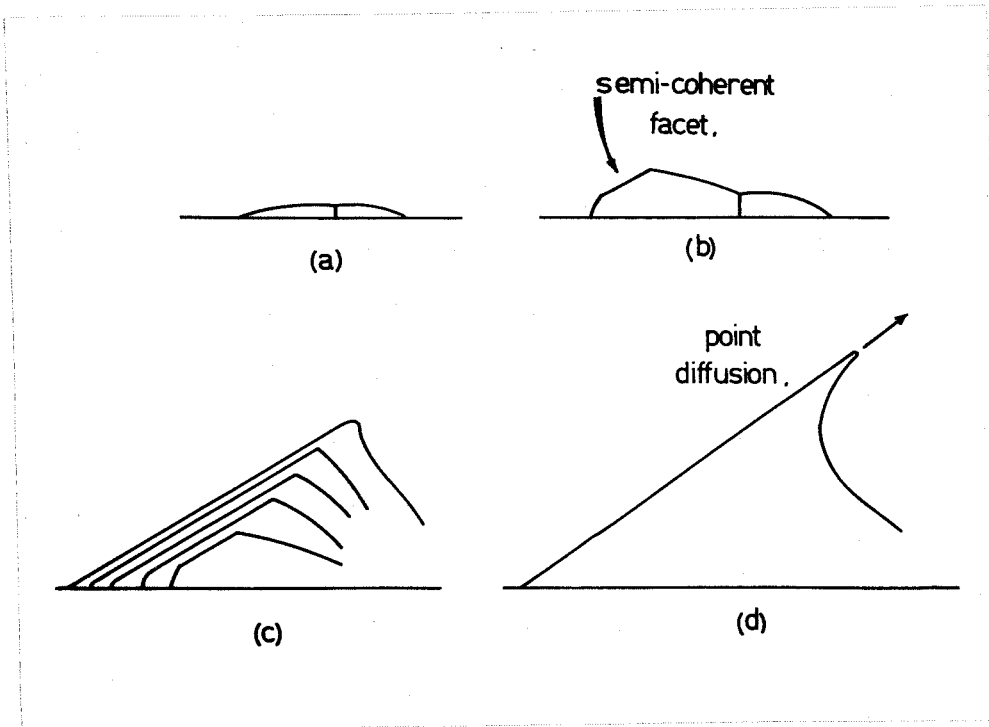


Fig. 2.4 Schematic representation of the development of a grain boundary allotriomorph into a sideplate by the formation of semi-coherent facets on the disordered allotriomorph boundary.

after Aaronson (20).

can occur locally in the immediate vicinity of the interface the problem is slightly simplified, and the only question that arises is the sequence of the symmetry change and the local atomic rearrangements producing the ordered configuration.

Following Smith (21), Aaronson (20) has pointed out that, where a precise orientation relationship exists between parent and product phases, the structure of a boundary that completely encloses the product crystal must vary greatly, and for most orientations of the interface it should be of the disordered type. At some orientations relatively good matching may be achieved with resultant lowering of surface energy ( $\sigma$  cusp) and the boundary may be of the dislocation type. Aaronson (20, 24-26) holds the view that in precipitation reactions, plate morphologies grow by the lateral movement of ledges along such semi-coherent boundaries. Small facets of disordered boundary are proposed to be present at the risers on the stepped interface and growth by the advance of the "disordered edges of ledges" takes place in the usual fashion of a disordered boundary. In this model the semi-coherent broad faces are immobile and result from "pinning" of the advancing disordered boundary as it bows out and reaches the stable orientation. Figures 2.4 and 2.5 depict growth by this mechanism.

The overall rate of advance of the interphase boundary normal to itself is slower than the rate of advance of the disordered boundary and is dependent on (i) the step height (ii) the rate of step formation and (iii) the rate of lateral step migration. Aaronson claims that the ledge mechanism can account for the observed kinetics of plate formation

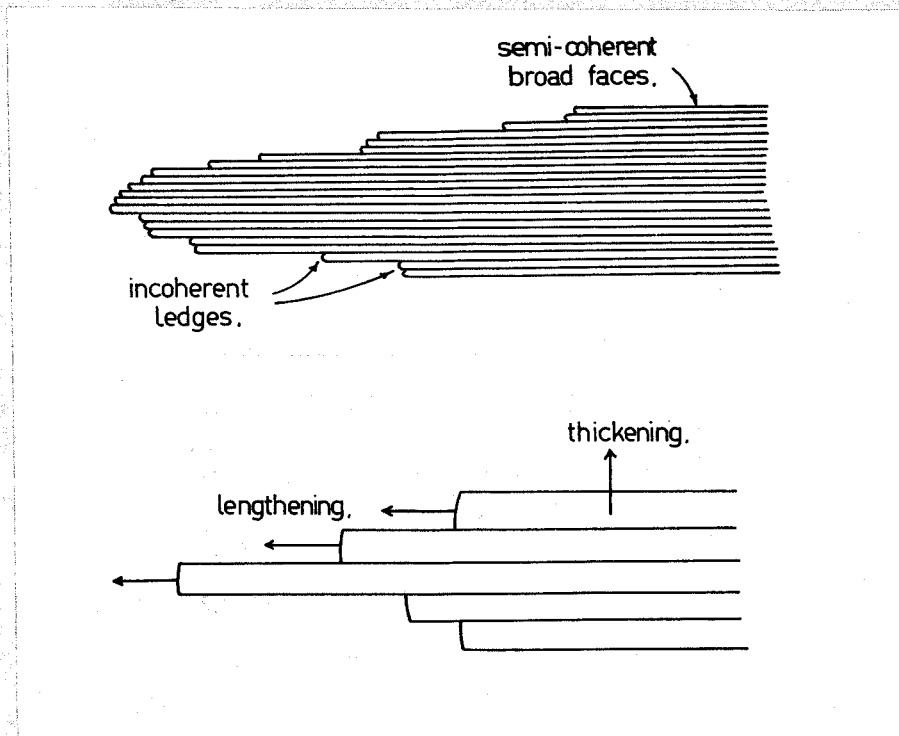


Fig. 2.5 The structure and mode of growth of Widmanstätten plates proposed by Aaronson. The kinetics of lengthening are controlled by the movement of the small disordered steps, aided possibly by point diffusion, while the thickening kinetics depend on the density of the ledges.

(where length growth is observed to be very much faster than width growth - Section 2.4), as well as providing a means of explaining the shape change. At present there is very little practical evidence supporting these claims for the existence of ledges. In addition, it is not at all clear how a ledge mechanism, which involves the advance of a disordered boundary, can produce a macroscopically homogeneous change of shape of the transformed region.

A further detailed discussion of those transformations which involve diffusion, and also produce relief effects, is given in Section 2.4.

#### 2.2.4 The Temperature Dependence of Morphology

The shapes of precipitates commonly found in transformations involving diffusion have been classified according to the nature of the nucleating site and subsequent growth characteristics, as outlined in Sections 2.2.2 and 2.2.3. These growth characteristics have been shown to be closely related to the structure of the interphase boundary. One of the prime factors influencing the structure of the interphase boundary is the degree to which the reaction is undercooled.

At low degrees of undercooling the driving force for nucleation is small and precipitates with the lowest sum of strain and surface energies should be preferentially nucleated, as indicated by equation 2.2. According to Smith (21), although precipitates with coherent or semi-coherent boundaries may be nucleated at temperatures near the equilibrium temperature, growth of these nuclei is limited because the level of accumulated lattice strain cannot be supported by the comparatively small amount of volume free energy available. It is pointed out that

a grain boundary may provide both a site for easy nucleation as well as an existing segment of incoherent boundary which can be inherited by the precipitating phase, so that growth can then take place by the diffusional transport of atoms across this disordered boundary. At higher degrees of undercooling it is proposed that interphase boundaries with higher strain and/or surface energies can be tolerated, and that the conditions regulating the motion of dislocation type boundaries may become more favourable. Whereas Smith did not discuss the migrational mechanisms by which the semi-coherent boundary moves, or the properties which accompany its movement, Aaronson's ledge theory has been developed using a realizable model of growth. This theory also attributes a semi-coherent structure to the planar interfaces of Widmanstätten precipitates. Both theories agree on the properties attributed to disordered boundaries, but Aaronson pays closer attention to the migrational mechanisms available to the semi-coherent boundaries and suggests that his model is supported by the observed kinetics of growth. The following account, due to Aaronson (20), describes how the degree of undercooling determines the predominating morphology by influencing the growth kinetics and the structure of the interphase boundary.

(a) Allotriomorphs

At low degrees of undercooling grain boundary allotriomorphs are the first morphology to form during precipitation from solid solution in a wide variety of alloys. In general the interphase boundaries of allotriomorphs are regarded as being disordered, and rapid growth, especially along the matrix grain boundary, can take place. Initially, allotriomorphs tend to be lens-shaped, but because of their slightly

anisotropic growth and high nucleation rate, impingement rapidly takes place and the familiar grain boundary networks finally obliterate the identity of the individual allotriomorphs. Subsequent growth takes place by the movement of the disordered boundary into the adjacent grains, at a rate controlled by volume diffusion. Unlike Smith, Aaronson suggests that at very small degrees of undercooling the dislocation and the disordered boundaries may have comparable rates of migration. Since under these conditions, the rate of migration is more or less independent of the orientation of the boundary, he further suggests that plates cannot develop. As undercooling is increased only the disordered boundaries can take full advantage of the steeper concentration gradients, orientation dependence of migration rate becomes appreciable, and facets may begin to develop as shown in Figure 2.4.

(b) Idiomorphs

Idiomorphs are equiaxed crystals, sometimes with crystallographic facets, which form within grains at intermediate degrees of undercooling. For the formation of ferrite idiomorphs in the iron/carbon system, this is about 25-50°C.

In hypoeutectoid alloys idiomorphs are rarely found in specimens transformed isothermally and they are usually limited to carbon levels well below the eutectoid. Aaronson tentatively suggests that, in the iron/carbon system, the formation of idiomorphs can be explained by a theory of boundary orientation-dependent growth kinetics. Over the critical range of undercooling disordered boundaries have no kinetic advantage over dislocation boundaries and isotropic growth results.

The degree of undercooling required to form idiomorphs depends markedly on the alloy but is usually sufficient to allow intragranular nucleation to take place. In the case of ferrite precipitating from austenite it is suggested that the Kurdjumov-Sachs (KS) orientation relationship holds and that the planar interfaces are usually, but not always, parallel to  $\{111\}_F$ . The irregularities of shape of these idiomorphs arise from the fact that the precipitate cannot be completely enclosed by equivalent pairs of planes chosen from the low index planes of the austenite and ferrite lattices.

(c) Plates

The plate morphology becomes predominant at high degrees of undercooling (approximately  $100^\circ\text{C}$  in hypoeutectoid iron/carbon alloys) resulting in Widmanstätten microstructures. Growth of secondary side-plates (Figure 2.2 (d)) may take place by the development of dislocation facets on disordered boundaries as shown in Figure 2.4. Primary plates and intragranular plates (Figures 2.2 (c) and (f) respectively) are envisaged as being developed from plate-shaped nuclei having the KS relationship to the parent grain.

These proposals describe the change of morphology with temperature which is experimentally observed, and gain further support from the agreement between the predicted and measured growth kinetics. In addition, Aaronson (20) has accumulated a large volume of indirect evidence to support his theory. However, in the sense that many of the crystallographic properties (such as the lattice orientation relationships and the identity of both the dislocation and disordered facets of the interphase boundaries) have not been examined in a

majority of cases, it is felt that many of Aaronson's ideas go unsupported. This is especially true of the proposed ledge structure of the plate boundaries.

Other plate producing reactions occur which are also dependent on high levels of undercooling. In the diffusionless martensitic transformations a plate shaped product phase results from the migration of a particular type of planar interface and the transformation is characterised by a change of shape. This type of transformation is associated with the highest degrees of undercooling ( $>1000^{\circ}\text{C}$  in some ferrous alloys) and is fully discussed in Section 2.3. Transformations where plate-shaped precipitates are formed with diffusion accompanying a shape change often occur at somewhat lower undercoolings, eg. bainite, and these are discussed in Section 2.4. Chapter 3 contains discussions of the theories of formation of Widmanstätten plates and is an extension of many of the concepts introduced in the present and subsequent sections of this chapter.

#### 2.2.5 Orientation Relationships

In transformations in which both lattice and compositional changes occur, it has become increasingly evident that a crystallographic orientation relationship between the parent and product (or products) obtains in a majority of instances (1, 14). A partial list of such transformations would include ageing reactions, Widmanstätten precipitation, eutectoidal and discontinuous precipitation, as well as grain boundary precipitation (15, 16). The interface controlled polymorphic transformations represent one of the few exceptions to the general rule and there is apparently no orientation relationship in this case (1).

In crystallographic theories of phase transformations, the choice of a particular orientation relationship is explained in terms of the influence of the orientation relationship on the surface and/or the strain energy terms of equation 2.2, thereby reducing the total energy required to establish the nucleus.

In his original hypothesis, Smith (21) proposed that the anisotropic Widmanstätten shape owes its origin to the existence of a specific orientation relationship associated with the formation of low energy interfaces along the conjugate plane. This idea has been generalised by Hillert (22) in his attempts to describe the properties accompanying the formation of pearlite. Smith proposed that oriented nucleation of a proeutectoid constituent takes place so that the interfacial (surface) energy ( $\sigma$ ) is least, and postulated that a degree of coherency exists between the precipitate crystal and the parent grain. If the nucleus forms with a high degree of undercooling a partially coherent interface may be able to grow at a reasonable rate, and Smith regarded this as the origin of the plate morphology. At low degrees of undercooling he proposed that the dislocation boundary is immobile and only in the event of the nucleus developing an incoherent segment can rapid growth take place. This can happen if nucleation occurs at an existing boundary, and the theory has been developed to account for the growth of proeutectoid ferrite and pearlite from austenite grain boundaries, where the incoherent ferrite boundary may grow into the adjacent austenite grain (22). The nucleus in this case is considered to grow only into the grain to which it bears no orientation relationship and to which it presents an incoherent boundary. This mechanism clearly cannot be

used to explain the growth of pearlite nodules nucleated remote from the grain boundaries.

Bowles and Barrett (14) suggested that if a nucleus forms with a high degree of coherency a martensitic mechanism\* may be operative in the early stages of transformation and that there will then be an orientation relationship. Complete coherency is sustained in the initial stages of precipitation by low temperature ageing in many systems, but the sequence of events leading to the appearance of the final equilibrium precipitate often proceeds from these coherent particles through possibly a number of metastable transition phases. At some critical size, where the coherency strains are exchanged for a dislocation array constituting an interface of reduced coherency, the growth mechanism may also change but the orientation relationship to the parent need not necessarily be destroyed unless the "new" phase is renucleated.

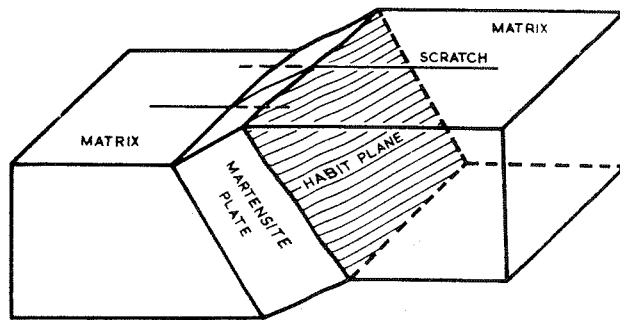
More recently Pitsch et al (15, 26) measured the orientation relationship of grain boundary precipitates to the adjoining austenite grains in an iron/cobalt alloy. They concluded that in all cases examined, the allotriomorphs bore an orientation relationship to at least one of the adjoining grains. Although the measured orientation relationship spread over about  $10^\circ$ , Pitsch et al proposed that there was a correspondence, and therefore, that a martensitic mechanism was operative at the nucleation stage. Aaronson (20), on less direct evidence, has also concluded that ferrite allotriomorphs (in this case in the iron/carbon system) bear the same relationship to the parent grain as do the Widmanstatten plate morphologies, ie. the KS relationship.

---

\* See Section 2.3 esp. subsection 2.3.2.1.

To speculate on the nature of the nucleus and the early growth mechanisms from a knowledge of the orientation relationship is inviting, but as Christian (23) has pointed out, preferred orientations are a necessary but not sufficient condition for the existence of a correspondence, which is presently accepted as the criterion of a martensitic mechanism. If, as in ageing reactions, the orientation relationship of an equilibrium precipitate phase is finally achieved through a prior sequence of metastable transition phases, rather than by a nucleation process involving directly the parent lattice, the measured orientation relationship may give no indication of the mechanism of the transformation.

As is the case for transformation kinetics, a knowledge of an orientation relationship can provide support for a proposed mechanism but cannot, in itself, constitute a basis for classifying transformations.



(a)



(b)

Fig. 2.6 (a) Schematic illustration of the ideal shape change occurring when transformation takes place in a single crystal. Mackenzie (3)  
 (b) A photomicrograph of relief effects in a grain of partially transformed Fe-30% Ni alloy. Bowles and Barrett (14)

## 2.3 Martensitic Transformations.

### 2.3.1 Introduction - The Geometric & Crystallographic Properties

The recognition of the martensitic class of transformations was initiated by observations which indicated a mode of decomposition in quenched steels with kinetics and physical properties vastly different from those of high temperature transformations achieved by diffusional growth. More recently, although the transformation is still accepted as a mode distinct, the term "martensitic" has been applied to cover those transformations which exhibit certain characteristic geometric and crystallographic properties (3). The usage is no longer restricted to steels but is now more general and can refer to any solid state transformation having the required properties.

When one phase forms martensitically from another, the product commonly takes the form of plates with approximately planar interfaces lying along particular crystallographic planes (the habit plane) of the parent lattice. Further, a definite orientation relationship exists between the two lattices, and there is a change of shape of the transformed volume which reveals itself by the tilting of a prepolished surface. Scratches placed on such a surface remain continuous but are deviated (rotated) during transformation. The transformation of planes into planes and directions into directions allows the macroscopic shape change to be described as a homogeneous strain (the shape strain) (28).

The observation that there is little or no plastic deformation of the parent<sup>\*</sup> has been taken to mean that there is no appreciable rotation of the habit plane by the shape strain and in fact, in some theories,

---

\* See however, Section 2.3.5.

apart from <sup>or</sup> small dilatation ( $< 1.5\%$ ), all lines in the habit plane are assumed to be invariant - ie. both unrotated and unchanged in length by this strain.

One final observation which has been made using electron microscopy is the presence of a fine internal structure within the martensite product (29), and this has been taken as direct evidence of part of the transformation mechanism. It will be seen that this is most important in the development of the crystallographic theory of martensitic transformations, and that slip and/or twinning of the martensite are the inhomogeneities involved.

In the crystallographic theories the habit plane, orientation relationship, shape strain and structural inhomogeneity are all inter-related in a unique way. A knowledge of the lattice parameters of the two phases and some additional feature of the transformation, such as the plane of the inhomogeneity, together with an assumption about the direction of displacement of this inhomogeneity, allows the other features to be predicted. The rigid conditions inferred from the existence of these unique geometrical features has led to the development of a theory whereby the transformation is described by a hypothetical sequence of strains.

### 2.3.2 The Strains Involved in Martensite Transformations

#### 2.3.2.1 The Correspondence and the Total Lattice Strain

It is possible to convert any unit cell of one crystal structure into a unit cell of another by means of a homogeneous deformation; depending upon the choice of unit cells additional "shuffles" within this cell may be required to completely describe the transformation (2, 5).

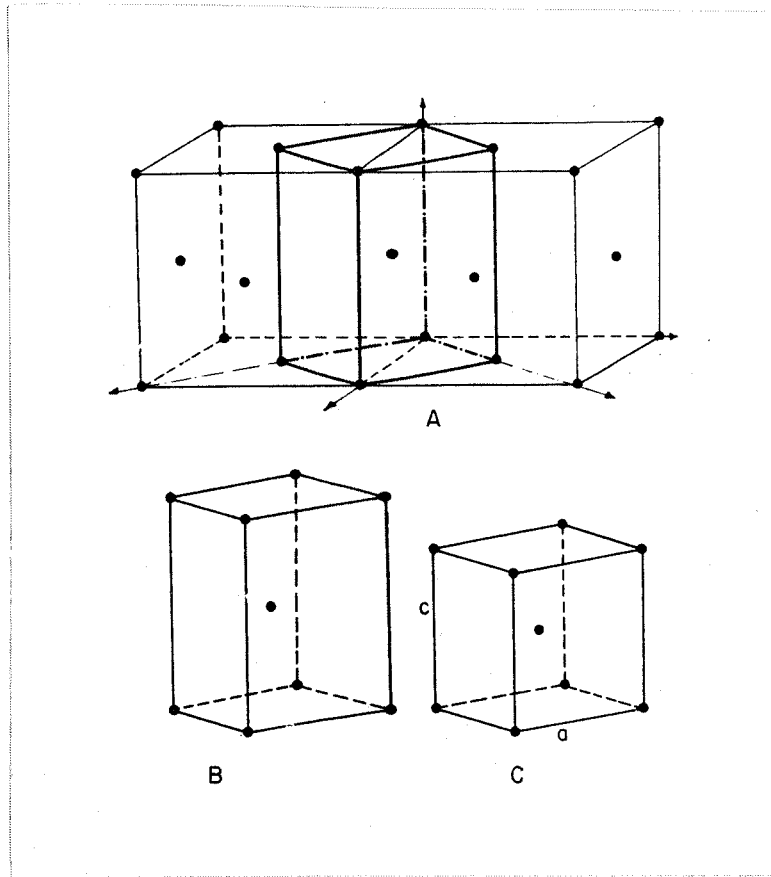


Fig. 2.7 The correspondence between the body centred and face centred cells originally proposed by Bain.

Examination of the possible ways in which an f.c.c. lattice can be transformed to a b.c.t. martensite lattice led Bain to propose a simple mechanism which, although incompatible with many of the observed features, has been retained as part of all subsequent descriptions. Bain proposed that the f.c.c. lattice, regarded as a b.c.t. lattice with a  $(c/a)$  ratio of  $\sqrt{2}$ , can be converted to a b.c.t. lattice of the correct (lower) axial ratio by compression along one (the  $c$ ) axis, and expansion along the other two. Later, Jaswon and Wheeler (30) suggested that the overall atomic displacements, which generate the martensite lattice in the correct orientation, may be described by a homogeneous strain applied to a unit cell of the parent. Although such a strain can always be found it is not unique, for the choice of related unit cells may be made in an infinity of ways. Jaswon and Wheeler assumed that the correct choice of unit cells is determined by the requirement that each atom of the parent lattice moves to the nearest available site in the product lattice, as it does in the Bain model. A more general proposal by Lomer (31), is that the principal strains of the pure strain\* should be minimum.

This reasoning leads to the concept of a unique relationship between the atom sites in the two lattices - a correspondence - and it is this which is regarded as the unifying characteristic of all martensitic transformations, and serves to distinguish this mode from other transformation modes. Because of the correspondence, rows and planes of

---

\* A homogeneous strain relating two lattices may be factorized into a pure strain which distorts one lattice into the other and a rotation which brings about the required coincidence. The axes of the pure strain are referred to as the principal axes and the respective strains as the principal strains. The principal axes are distorted to their final lengths by the principal strains without rotation.

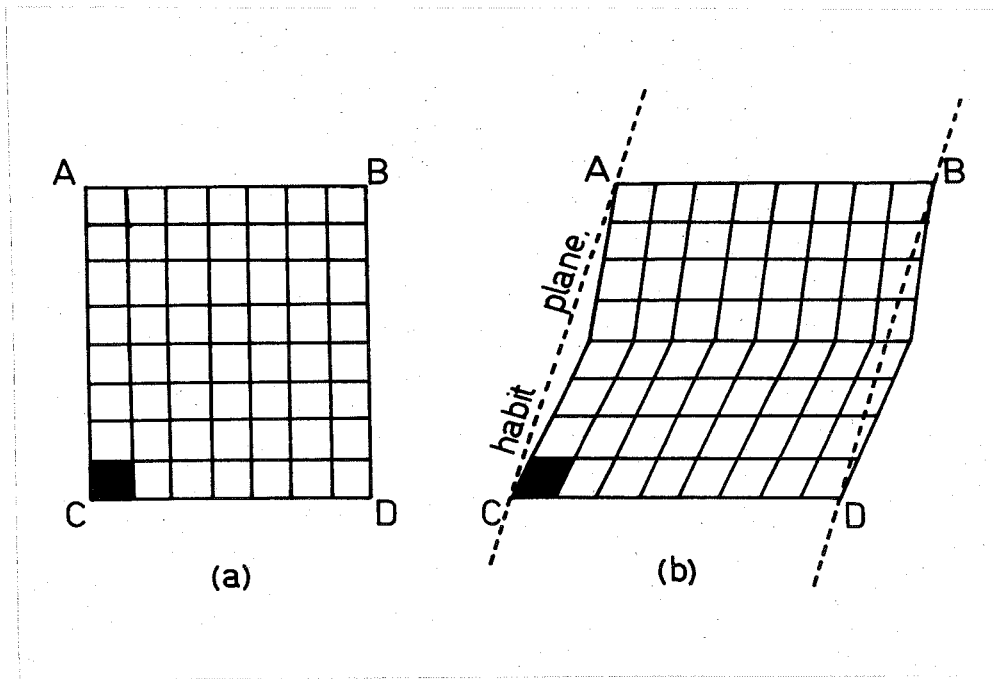


Fig. 2.8 Schematic illustration of the inequality of the shape strain, which relates the cells ABCD, and the total lattice strain, which relates the small filled unit cells.

atoms in the parent and product phases are related in a manner closely analogous to that produced by mechanical twinning.

By choosing a very large unit cell, a homogeneous strain relating some fraction of atom sites may be defined, which involves low values of the principal strains. Christian (5) points out however, that the large amount of additional atom movements required to bring all the intermediate atoms to their correct positions precludes the possibility of such a strain accomplishing the transformation (Figure 2.8). The correspondence then usually relates atoms in a small unit cell, in fact the unit cells so related are nominated as being the smallest consistent with the condition that they contain equal numbers of atoms (2).

#### 2.3.2.2 The Shape Strain

By reference to Figure 2.8 it may be seen that the homogeneous strain relating the large unit cell ABCD is not the same as the homogeneous strain relating the small filled unit cell. These strains, diagrammatically represented, may be identified with the macroscopic shape strain and the total lattice strain respectively. The inequality of these strains was first observed by Greninger and Troiano (32), who showed that the measured shape strain, when applied to the parent lattice, did not produce the martensite lattice in the correct orientation.

Bowles and Mackenzie (28) proposed that the total atomic displacements be resolved into component "homogeneous" and "inhomogeneous" strains. The homogeneous component is regarded as producing the observed macroscopic shape change, while the inhomogeneous component achieves the additional atomic displacements required to form the product lattice in its observed orientation without further change of

shape. This strain will be discussed in detail in the next section. The combination of these two component strains defines a strain which is locally homogeneous and can be identified with the total lattice strain, but which is inhomogeneous on a larger scale of the order of the plate dimensions (28).

Since plates of up to several millimeters in length can be traversed on a relief surface with an optical microscope and still remain in focus (3), it has generally been accepted that rotation of lines in the habit plane does not occur. Similar observations can be made using interferometric techniques. The shape strain then, since it does not rotate the habit plane or any line within the habit plane, has been described as an invariant plane strain by Bowles and Mackenzie (28) and also by Wechsler, Lieberman and Read (33).

In an invariant plane strain (IPS) the vectors representing the displacement of all lattice points are in a common direction and have magnitudes proportional to their distances from a fixed reference plane (the invariant plane, which is unrotated and undistorted by the strain). An IPS can generate the correct product lattice from a parent only in the exceptional circumstance where the atomic configuration of the habit plane is the same in both structures (1), so that, in general, there must be additional lattice strains involved.

Alternatively it can be shown (1, 2) that the total lattice strain will only be an invariant plane strain under certain circumstances involving relative values of the lattice parameters of the two lattices, which can be satisfied only fortuitously. In general then, the total lattice strain is distinct from the shape strain which is at least

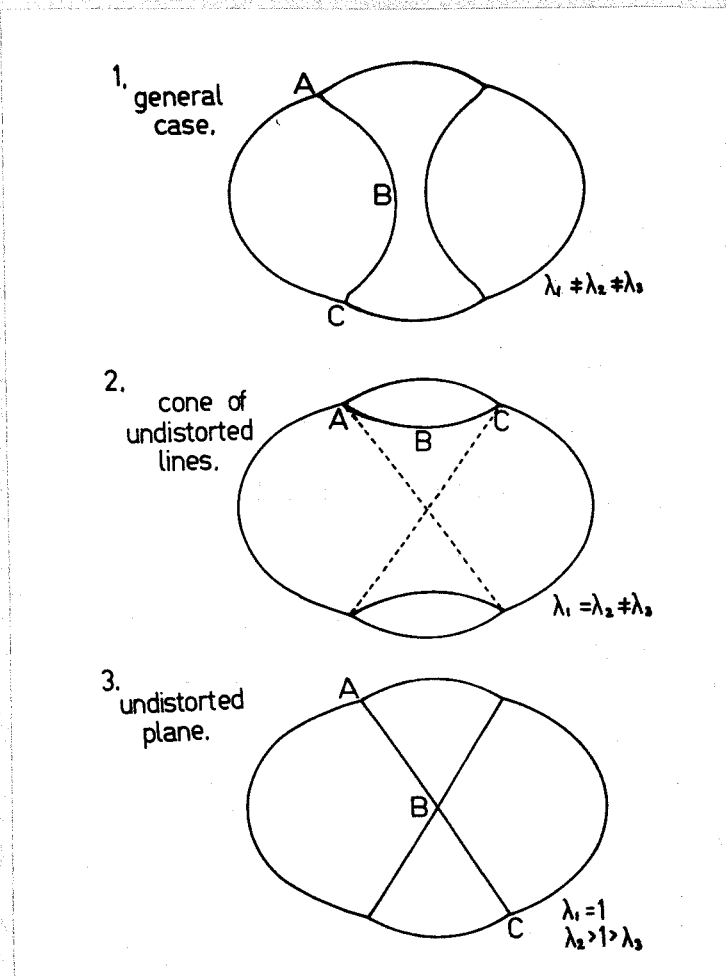


Fig. 2.9 The loci of interpenetration, ABC, for unit sphere with the strain ellipsoids, for different values of the principal strains (ellipsoid axes).

approximately an IPS. Bilby and Christian (2) pointed out, that in order for a portion of a crystal to undergo a homogeneous plane strain deformation and yet remain in contact with the undeformed region, that these special circumstances are: one of the principal strains must be unity and the other two must be either (i) of opposite sign or (ii) at least one must be also unity. To illustrate this, Figure 2.9 has been constructed to show the strain ellipsoids generated from unit sphere by different relative values of the principal strains.

### 2.3.2.3 The Complementary Strain

The additional atomic displacements, which, in conjunction with the shape strain, define the total lattice strain, have been called the complementary strain by Bowles and Mackenzie (28). Since the complementary strain cannot produce any further change of shape it must be a shear and must occur inhomogeneously on macroscopic dimensions. The inhomogeneity ensures that the change of shape produced by the simple shear does not accumulate over macroscopic dimensions and, in general, it is assumed to be either slip or twinning within the product lattice. The manner in which a lattice strain may be combined with a lattice invariant strain to accomplish a given shape deformation, is illustrated in Figure 2.10.

An alternative approach is to consider the strain which must be removed from the total lattice strain in order to account for the shape change. The amount of the complementary shear must be just sufficient to ensure that the shape strain is an invariant plane strain in accordance with the observation that lines within the habit plane are unrotated and unextended (3). This condition, in effect, ensures that the strain

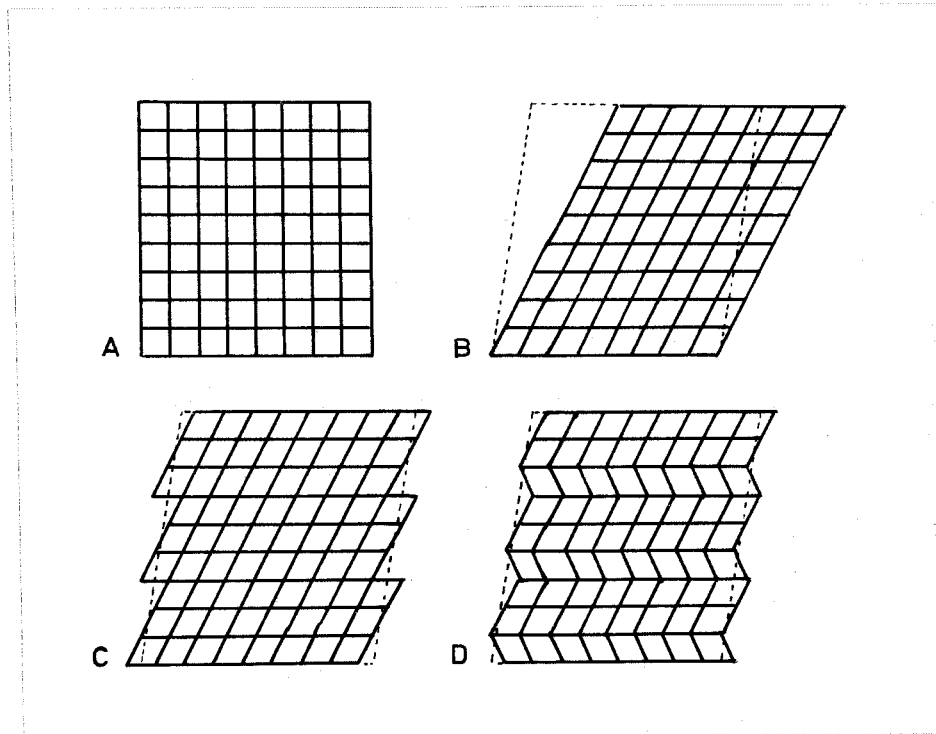


Fig. 2.10 Schematic illustration showing how a macroscopic shape change (dotted) can be produced from an original lattice (A) by means of a lattice strain (B) followed by either lattice invariant slip (C) or lattice invariant twinning (D).

after Bilby and Christian (2).

ellipsoid meets the initial sphere along a plane without any restriction being placed on the lattice parameters.

A fractional twinning shear, equal to a given slip shear, can easily be envisaged by varying the volume proportions of the two twin related regions. This may be deduced from Figure 2.10 (D), so that in terms of the theory the two cases are equivalent. In a physical sense, the slip transformation involves only one lattice strain and one partially compensating lattice invariant strain, whereas in twinned martensite the two twin-related lattices are generated from a common, hypothetical intermediate lattice, by equal and opposite shears requiring two lattice deformations. Bowles and Mackenzie have shown that if the twinning shear, relating the two resulting product lattices, is to be a combination of two other shears, then it must have either a shear plane or shear direction in common, implying that the complementary strain must be a simple shear occurring on either the twin plane or in the twinning direction of the product lattice (28).

### 2.3.3 The Phenomenological Theories

#### 2.3.3.1 Wechsler, Lieberman and Read (WLR)

In considering the transformation of austenite to martensite in steels (33) WLR proposed that the strain describing the shape change is exactly an IPS and is composed of a total lattice strain, consisting of a pure strain and a rigid body rotation, and a lattice invariant strain which is either a slip or fractional twinning shear in the product. In matrix form this is written:

$$P_1 = R B P_2^{-1} \quad \dots 2.6$$

or

$$P_1 = S_t P_2^{-1} \quad \dots 2.7$$

where  $P_1$ ,  $R$ ,  $B$ ,  $P_2$  and  $S_t$  are (3x3) matrices representing the shape strain, a rigid body rotation, the pure (Bain) strain, a lattice invariant shear and the total lattice strain respectively.

The pure strain converts a unit cell of austenite into a unit cell having the dimensions of the final martensite cell, the rotation ensures that the habit plane is unrotated and the lattice invariant strain achieves the macroscopic requirement of an undistorted plane. The elements of the lattice invariant strain thus ensure that the strain ellipsoid produced from the unit sphere by the pure strain, intersects the sphere along a plane, the undistorted plane (Figure 2.9).

Knowing the correspondence and the lattice parameters allows the strain  $B$  to be determined. The further assumption that the lattice invariant strain is a simple shear on a known plane in a known direction, determines  $P_2$ , or its inverse  $P_2^{-1}$ , in terms of an unknown strain magnitude  $m_2$ .

$$\text{defining } F = B P_2^{-1} \quad \dots 2.8$$

it was shown that two critical amounts of shear could be found which satisfy the condition for the existence of an undistorted plane, the condition being that one of the principal strains,  $\lambda$ , of the strain  $F$ , is unity.

Thus, by solving the determinantal equation:

$$\det \left| F'F - \lambda^2 I \right| = 0 \quad \dots 2.9$$

it can be shown that the resulting cubic equation in  $\lambda^2$  reduces to a quadratic in terms of the unknown magnitude  $m_2$ , and that the two values of  $m_2$  can be determined. Lines in the undistorted plane are rotated by the operation of the strain  $F = B P_2^{-1}$  and the rigid body rotation  $R$  must carry all vectors in this plane back to their initial positions without distortion, and so the strain  $P_1$  is fully determined.

The strain  $P_1$  therefore has an invariant plane, which is identified as the habit plane. In general four distinct solutions arise because there are two critical values for the shear magnitude. In order for there to be a solution at all however, it is seen that the cone of normals unextended by the pure strain must intersect the zone of the proposed shear direction, while the cone of unextended lines must intersect the proposed shear plane.

#### 2.3.3.2 Bowles and Mackenzie (BM)

Completely independently of the WLR work, Bowles and Mackenzie (BM) (28, 34, 35) developed a general theory to account for the crystallographic features of martensite transformations. Although arrived at by different reasoning their theory can be shown to be mathematically equivalent to the former theory (1, 7). By careful examination of all the geometric and crystallographic features of the transformation BM proposed that the homogeneous strain relating the lattices in their observed orientation relationship could be resolved into "homogeneous" and "inhomogeneous" components. The "homogeneous" component defines the macroscopic shape change and the "inhomogeneous" component the additional displacements required to generate the martensite lattice in the observed orientation. The conclusion that the additional displacements are

"inhomogeneous" follows from the requirement that they must produce no change of shape, since this must all be accomplished by the homogeneous component.

The combination of these two strains defines a strain which is locally homogeneous and is identified with the total lattice strain, but which is macroscopically inhomogeneous, ie. over dimensions of the order of the plate size.

Thus:

$$S_t = P_1 P_2 = R B \quad \dots 2.10$$

which is the same as equation 2.6, where the symbols have their previous significance.

The shape strain is assumed to differ only from an invariant plane strain by a uniform dilatation, so that

$$P_1 = \frac{I}{\delta} (I + m_1 d_1 p'_1) \quad \dots 2.11$$

where  $m_1$ ,  $d_1$  and  $p'_1$  are the magnitude, direction and plane respectively of the IPS, and  $I$  is the identity matrix. The term  $\delta$  is included as an adjustable parameter in the BM theory. By allowing the shape strain to deviate by small amounts ( $< 2\%$ ) from an IPS, an extra degree of freedom in application of the theory is provided and this distinguishes the theory from that of WLR. Consideration of the properties of the complementary strain  $P_2$ , led BM to the conclusion that it could only be a simple shear in which periodic inhomogeneities (slip) counteracted the change of shape accompanying the shear displacements describing the additional atom movements. Alternatively, a fractional twinning shear producing twin related orientations in the product, was postulated.

Therefore:

$$P_2 = (I + m_2 d_2 p'_2) \quad \dots 2.12$$

A schematic illustration of these two modes of complementary strains is given in Figure 2.10.

It follows:

$$S_t = \frac{I}{\xi} (I + m_1 d_1 p'_1) (I + m_2 d_2 p'_2) \quad \dots 2.13$$

The strain  $S$ , derived from  $S_t$  by removal of the small dilatation is an invariant line strain — the invariant line  $x_1$  being the direction of intersection of the two invariant planes,  $p'_1, p'_2$ . There is also a plane with an invariant normal which contains the two directions of displacement  $d_1$  and  $d_2$ .

In the original formulation of the theory (28, 34, 35),  $S_t$  was found from a knowledge of the correspondence and the lattice parameters (determining the pure strain), and the assumption that the complementary strain was a shear on the known twinning plane in the known twinning direction. The (known) shear plane must therefore contain the invariant line and the plane with the invariant normal must contain the (known) shear direction.

In the BM theory the elements of the invariant line strain  $S$  are given ultimately in terms of the elements  $g_{rs}$  of another matrix  $G$ , and the  $g_{rs}$  are determined from the values of the lattice parameters ( $a'$  and  $a$ ), the axial ratio of the martensite ( $\gamma$ ), the plane and direction of the complementary strain, and the single variable parameter  $\theta$ , where  $\theta = \xi (a'/a)$ . For a given transformation, the strain  $S$  depends on the value of  $\xi$ , and for a selected value of  $\xi$  there are four solutions

for S and hence four predicted habit planes. When the transformation involves twinning, and the twins are generated with crystallographically equivalent correspondences the four solutions reduce to two pairs, the pairs being simply variants. This implies that the twinning plane is a mirror plane of the parent lattice (34).

Factorization of the strain S can be carried out using the following reasoning (28). Since the direction  $d_2$  and the normal  $p'_2$  (twinning elements) are invariant to the strain  $P_2$ , they must be displaced to their final position solely by the strain  $P_1$ .

thus:

$$P_1 d_2 = S d_2 \quad \dots 2.14$$

$$\text{and } p'_2 P_1^{-1} = p'_2 S^{-1} \quad \dots 2.15$$

or

$$d_1 \parallel S d_2 - d_2 \quad \dots 2.16$$

$$\text{and } p'_1 \parallel p'_2 S^{-1} - p'_2 \quad \dots 2.17$$

Simple expressions for the elements of the two strains  $P_1$  and  $P_2$  are given in terms of the parameters of the transformation in references (28), (34) and (35).

An alternative approach was developed by BM (36) which allows the elements of the complementary strain to be predicted from a knowledge of the orientation relationship, the habit plane and the lattice parameters. This "reverse" approach was applied specifically to the  $\{225\}_F$  transformation in steels and the elements of the two component strains  $P_1$  and  $P_2$  were expressed in terms of a single parameter, x. The value

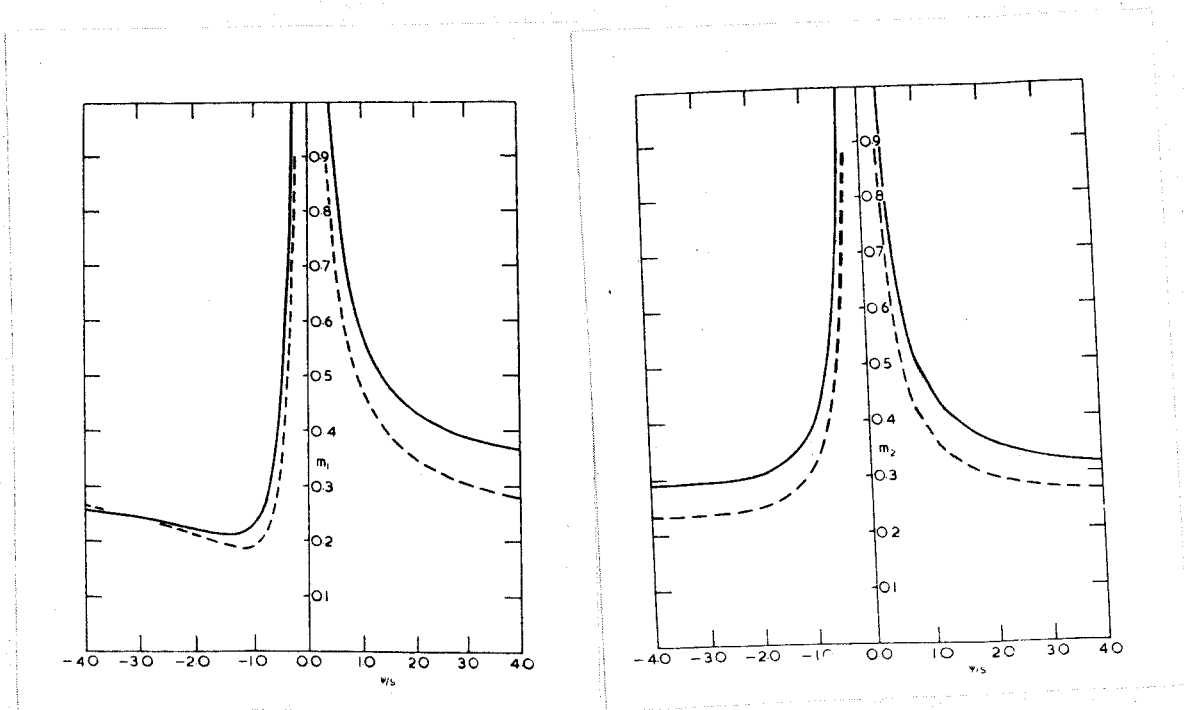


Fig. 2.11 Diagrams showing the variations of the strain magnitudes  $m_1$  and  $m_2$  as functions of the parameter  $x = \psi/s$ . The dashed curve represents the variation for a value of  $\theta^2 = 0.62$ .

Bowles and Mackenzie (36)

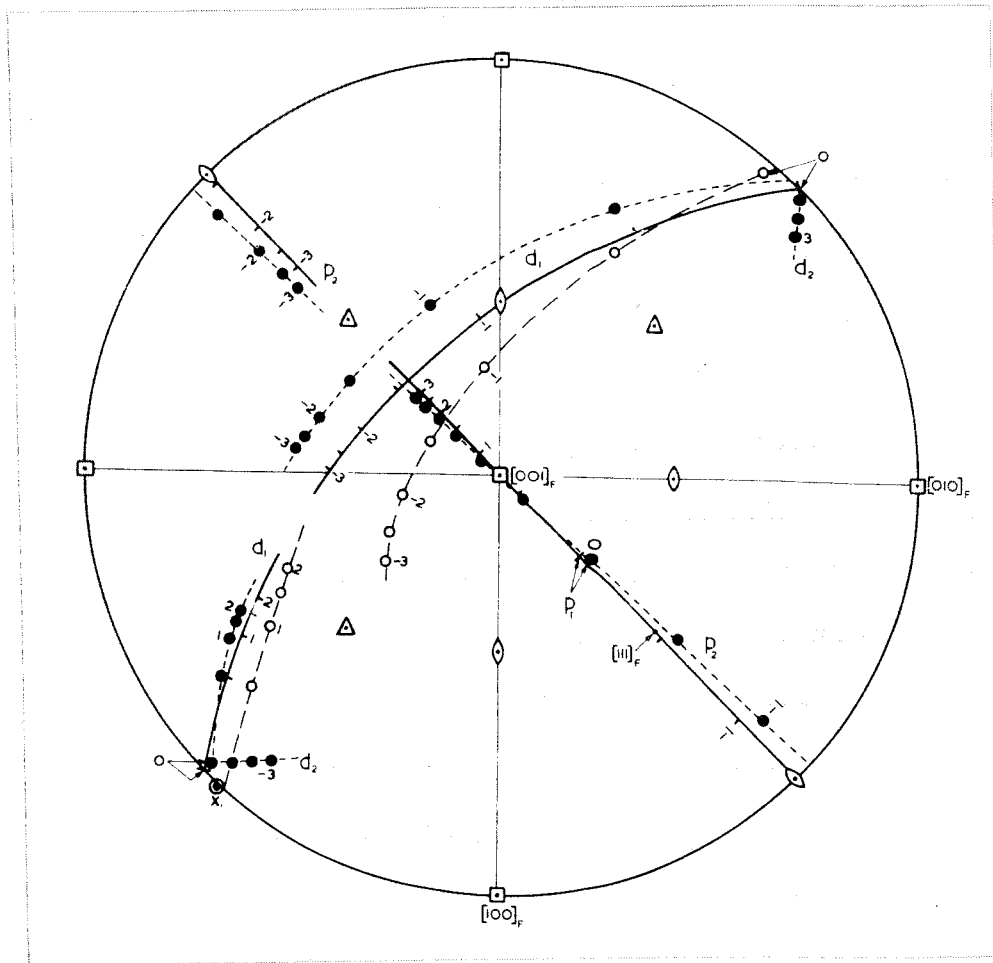


Fig. 2.12 Stereographic projection showing the predicted variation of the elements  $p'_2$ ,  $d_1$  and  $d_2$  with  $x = \psi/s$  for habit planes near  $(225)_F$

-----  $\theta^2 = 0.62$

- - - -  $\theta^2 = 0.65$

———— zero order approximation.

Bowles and Mackenzie (36)

of  $x$  is determined from

$$x = \psi/s \quad \dots 2.18$$

where  $\psi$  is a small rotation about  $x_1$  which brings the martensite lattice into the observed orientation,

$$\text{and} \quad s = g g_{22}^{* \frac{1}{2}} \quad \dots 2.19$$

$$\text{where} \quad g = 2 \gamma \theta^3 \quad \dots 2.20$$

$$g_{22}^* = [\gamma^2 + (2 - \gamma^2) m^2] / 2 \theta^2 \gamma^2 \quad \dots 2.21$$

Figures 2.11 and 2.12 show diagrammatically the variation of  $m_1$ ,  $m_2$ ,  $d_1$ ,  $p'_1$ ,  $d_2$  and  $p'_2$  with  $x$  for the  $\{225\}_F$  transformation.\*

### 2.3.3.3 Applications of the Theories.

The WLR theory has been successfully applied to the martensitic transformation in iron/22% nickel/0.8% carbon studied by Greninger and Troiano (32). This alloy exhibits an irrational habit plane very near  $\{3,10,15\}_F$  and the predictions of the theory for a range of lattice parameters are shown as a grid, in Figure 2.13, which encloses the experimentally observed poles. Because of the relative insensitivity of the solutions to the actual values of the lattice parameters, the WLR theory essentially predicts the same habit plane for all steels and therefore cannot adequately explain the various other habits observed in ferrous alloys. In carbon steels for example, there is a discontinuous change of habit with carbon content, and the near  $\{259\}_F$  habit plane characteristic of compositions  $>1.4\%C$  gives way to near  $\{225\}_F$

---

\* The subscripts F and B are used throughout this thesis to refer to the face centred and body centred lattices respectively.

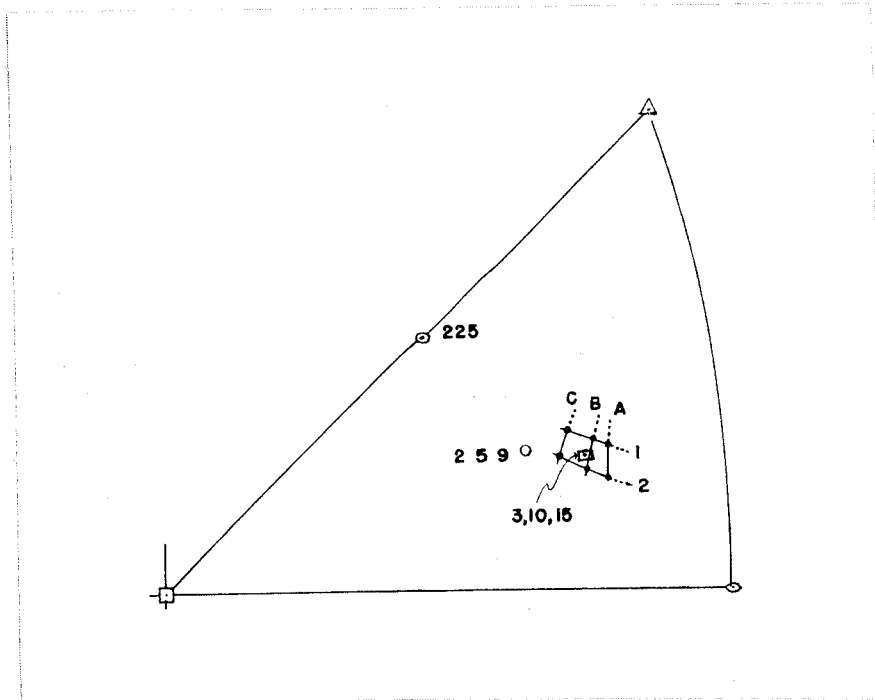


Fig. 2.13 Stereographic projection showing the grid of habit planes predicted by the WLR theory for a range of lattice parameters incorporating most iron base martensites.

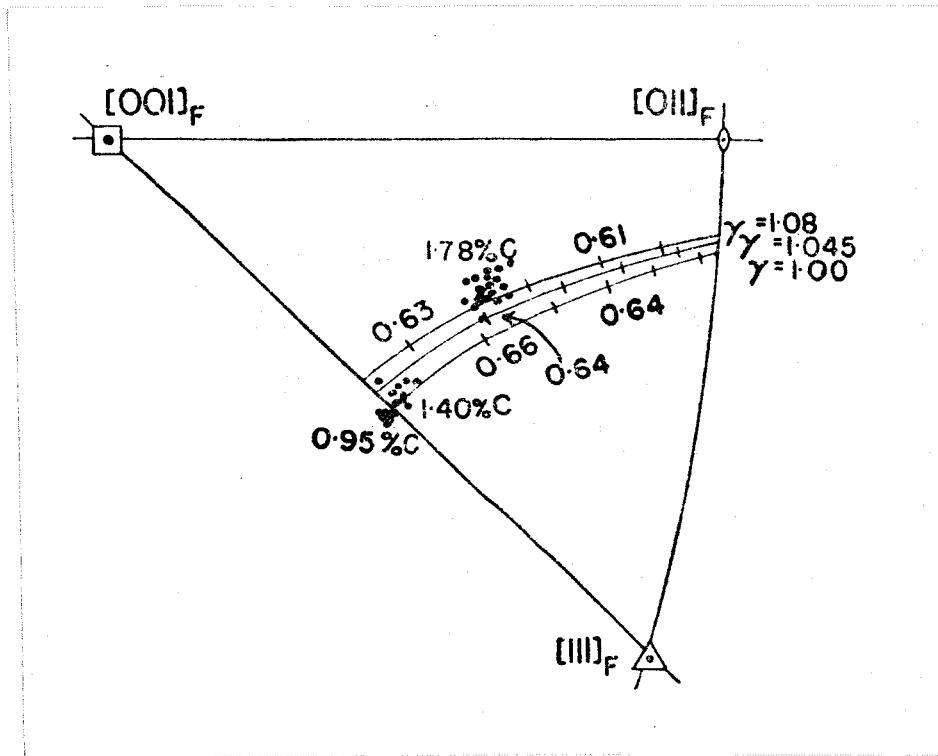


Fig. 2.14 Stereographic projection comparing the measured habit planes for carbon steels with the predictions of the BM theory for different  $\gamma = (c/a)$  ratios as a function of the parameter  $\theta = \delta(a'/a)$ .

Bowles and Mackenzie (35)

habit plane for compositions in the range 0.9 - 1.4%C.

The BM theory, with the added flexibility of the parameter  $\theta = \xi(a'/a)$ , predicts a locus of possible habits, for any given axial ratio, which passes near both  $\{225\}_F$  and  $\{259\}_F$ , as shown in Figure 2.14. BM concluded that their theory was in reasonable agreement with the experimental results of both Greninger and Troiano (32) and Machlin and Cohen (37) for the  $\{259\}_F$  transformation, and by choosing a suitable value for  $\xi$ , was also capable of predicting habits near  $\{225\}_F$ .

Using the reverse approach BM (36) showed that the most important parameter to measure in the transformation was the direction of the shape strain. Measurements of  $d_1$  were subsequently made by Bowles and Morton (38), Morton and Wayman (39) and Dunne and Bowles (40) for the  $\{225\}_F$  transformation. The latter concluded that the BM theory, in its original form, cannot simultaneously account for both the observed orientation relationship and the measured shape strain. This must be true of any transformation with habit of the form  $\{hhl\}_F$  and a complementary strain which is a combination of shears in the common direction  $[\bar{1}\bar{1}0]_F$ . In this case the dilatation required to account for the change in atomic spacing when  $[\bar{1}\bar{1}0]_F$  transforms to  $[\bar{1}\bar{1}1]_B$  (which would otherwise be invariant), in conjunction with the IPS describing the shape change, produces a volume change which is not that produced by the transformation. Furthermore, the measurements of both Dunne and Bowles (40) and Krauklis and Bowles (41) indicate that the dilatation accompanying the  $\{225\}_F$  transformation is small and very probably zero, so that its inclusion is questionable and a modified theory has been formulated (60).

In addition to the  $\{259\}_F$  and  $\{225\}_F$  habits some intermediate values have been reported for transformations in alloy steels (42, 43). The unmodified WLR theory is unable to account for these observations and extensions of the theory, which relax the conditions on the lattice invariant shear, have been proposed (Section 2.3.5). The BM theory can account for some of these habits, but not the experimental spread, if a dilatation is included (7).

The WLR theory has been successfully applied to the transformations in gold/cadmium (44) and indium/thallium (45) and BM have analysed the b.c.c. to orthorhombic transformations in copper/aluminium, gold/cadmium, titanium and lithium (46). The agreement between theory and experiment is satisfactory for these transformations. For the transformation in copper/tin alloys, Kennon and Bowles (47) found that the theory could not be reconciled with experiment if the complementary strain is restricted to being a simple shear. Their observation of up to four twin pairs within a single plate strongly suggests a complementary strain of a more complex nature, and this possibility has been the topic of the theoretical investigations reported in Section 2.3.5.

#### 2.3.4 The Martensite Interface

##### 2.3.4.1 Structure

Although the martensite interface is essentially planar, the condition for exact matching in the composition plane is only encountered coincidentally by fortuitous relationships between the lattice parameters. In transformations involving a change from f.c.c. to h.c.p. for example, this condition is sometimes met and the two lattices may be completely coherent across the common, close packed planes  $\{111\}$  f.c.c. and

{0001} h.c.p. (1). Generally the lattices do not match exactly and the mismatch must be periodically corrected by discontinuities such as twin boundaries or dislocations.

The concept of a twinning dislocation, introduced by Cottrell and Bilby (48) as a possible mechanism for the migration of fully coherent mechanical twin boundaries, was extended to the f.c.c. to h.c.p. transformation in cobalt by Bilby (49). The proposal of Cottrell and Bilby, that the coherent twin interface is not a geometrically singular plane, but is composed of crystallographically equivalent segments linked by steps of atomic dimension (the twinning dislocation), draws attention to the physical structure of the interface. It also describes the origin of features accompanying, and provides a mechanism for, interface movement. The propagation of the boundary normal to itself is achieved by the formation of a node around which the twinning dislocation can spiral; for each revolution, provided the Burgers vector of the pole dislocation has a component normal to the boundary, both the twinning dislocation and the node advance into the parent structure producing equivalent atomic displacements on each successively swept plane. In a completely analogous manner Bilby (49) suggested that the more general transformation dislocation can advance the coherent interphase boundary separating regions of different crystal structure, and that the resulting homogeneous strain is an IPS. The transformation dislocation obviously moves in the habit plane and the usual restriction, that motion can only occur in the plane containing the dislocation line and its Burgers vector, is relaxed.

Because of the usual restrictions imposed by the lattice parameters

on the principal strains, most martensitic boundaries are of the semi-coherent rather than the fully coherent type. It is proposed that within the semi-coherent boundary small islands of matching lattice are enclosed by dislocation arrays which accommodate the strain accumulated from the forced coherence and, in general, the plane of the interface is irrational. The simplest model of such an interface is a parallel set of dislocations with a common Burgers vector which can glide on the corresponding planes of either lattice. Other boundaries, which reduce to either sets of parallel dislocations with different Burgers vectors, or sets of dislocations in different directions but with a common Burgers vector, can be envisaged (6). If the properties of such two dimensional arrays of dislocations are reduced to a single entity viz: a surface in which the dislocation structure can be treated as being homogeneous, the resulting surface dislocation (50) can be adapted to account for the properties of martensitic transformations (51).

In the case of fully coherent transformations a correspondence is implicit and the transformed volume necessarily changes shape (6). Furthermore, the lattice deformation and the shape deformation are the same IPS, so that the transformation is completely described by the movement of the transformation dislocations along the interface.

The propagation of semi-coherent boundaries requires the movement of the coherent regions as well as the discontinuities and the shape strain is again an IPS (6), which, in this case, is not equal to the lattice deformation. The total shape deformation is thus made up of a lattice deformation describing the change of shape of a coherent region and a lattice invariant deformation brought about by the motion

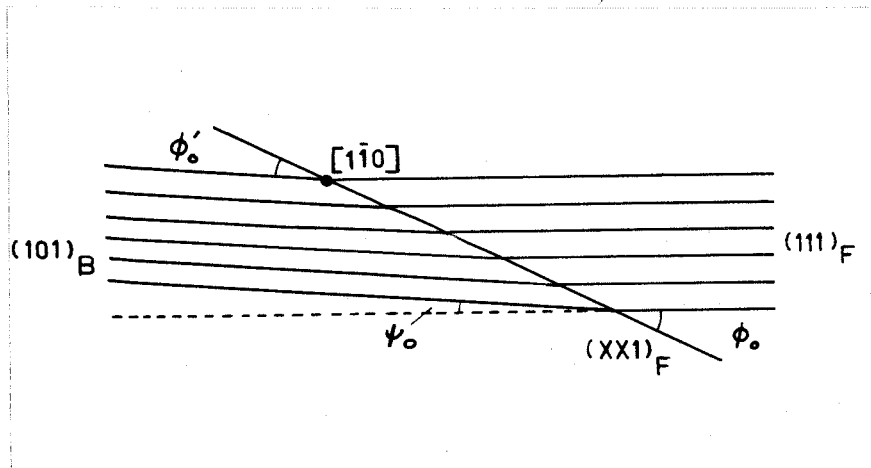


Fig. 2.15 Schematic diagram of Frank's matching interface in which the nearly parallel  $\{111\}_F$  and  $\{110\}_B$  meet in an interface of the form  $\{hkl\}$ . The angle  $\psi_0$  defines the deviation from parallelism of the close packed planes and  $\phi_0$  the identity of the interface.

of the discontinuities.

The theories based on different proposals about the nature of the interface are briefly discussed in the following section.

#### 2.3.4.2 Theories Based on Considerations of Interfacial Structure

Following the observation that the orientation relationships for ferrous martensitic transformations all have the common feature of near parallelism of the close packed planes, and believing the interface to allow some degree of lattice conformity, Frank (52) proposed a matching theory in which a plane of the form  $\{111\}_F$  meets the nearly parallel plane of the form  $\{110\}_B$  edge to edge along the common close packed direction. Because the interplanar spacings are different in the two lattices, exact parallelism of these conjugate planes is not possible, but small deviations from parallelism ( $\approx 1^\circ$ ) allow the planes to meet, at least in the case of near KS relationships, along a direction  $\langle 110 \rangle_F \parallel \langle 111 \rangle_B$ . An adjustment of the interatomic spacings along these rows is then necessary, which is tantamount to postulating a uniaxial distortion of the interface. Two dimensional matching of this kind can only deal with transformations in which the close packed directions are parallel and lie in the habit plane, so that habit planes off the  $\langle 1\bar{1}0 \rangle_F$  zone are not predicted.

In a more general three dimensional analysis Bilby and Frank (53) introduced a different matching model wherein prisms of the two lattices are fitted together at the interface. Two triangular prisms with two base edges of the form  $\langle 211 \rangle_F$ , and one of the form  $\langle 110 \rangle_F$  lying in the zone of the respective prism generators  $\langle 011 \rangle_F$  and  $\langle 111 \rangle_B$ , are truncated to meet along the habit plane. Except in special circumstances the

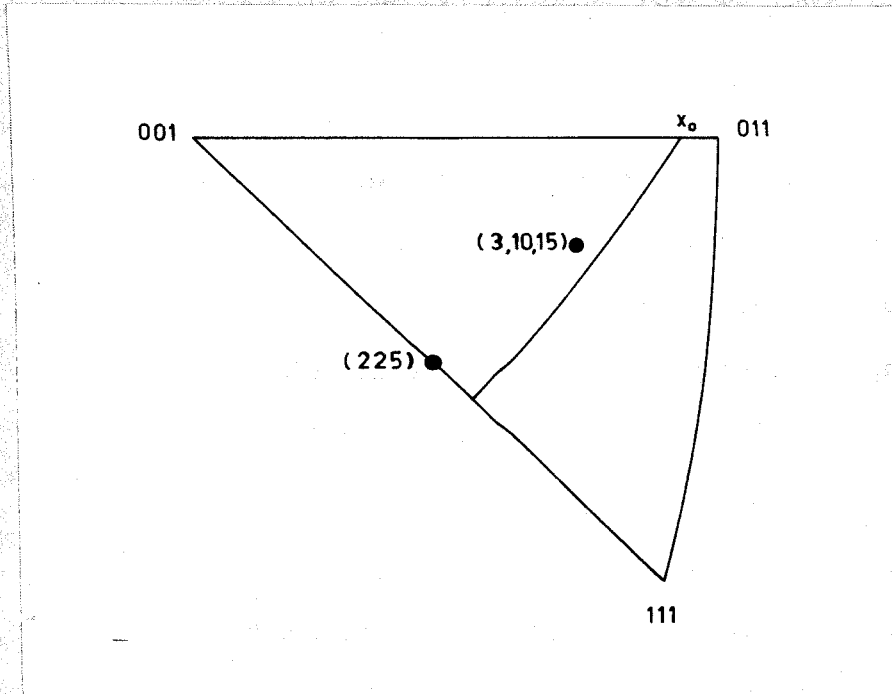


Fig. 2.16 Stereographic projection showing the variation of the habit plane predicted by the prism matching theory as a function of a parameter  $x_0$ .

interface will also contain dislocations. A geometric solution to the problem of matching the prisms is given in terms of a single parameter  $x_0$ , and a locus of predicted habit planes, which passes near  $\{3,10,15\}_F$  and between  $\{225\}_F$  and  $\{112\}_F$  results, and is shown in the Figure 2.16.

As in the WLR theory the habit plane is undistorted and the shape strain, which converts one prism into the other is an IPS. Bullough and Bilby (BB) (51) and Suzuki (121) have drawn attention to the dislocation structures of the martensite interface and have proposed theories based on considerations of the consequences of the movement of suggested dislocation arrays.

Using the concept of a surface dislocation consisting of an array of like, parallel dislocations which are glissile, BB showed that the predicted shape strain is again an IPS. From a knowledge of the correspondence, the lattice parameters and a plane and direction for dislocation movement appropriate to the dislocation array, BB formulated expressions for the habit plane, orientation relationship and direction and magnitude of the shape strain. With glissile interfacial dislocations the theory is equivalent to that of WLR (no dilatation) but, by relaxing this requirement, BB proposed that a dilatation could be incorporated into the theory.

Suzuki treated separately the cases of  $\{225\}_F$  and  $\{259\}_F$  habit planes in the transformation of f.c.c. to b.c.c. lattices by considering transformation to be achieved by transformation dislocations. The observed differences in kinetics of transformations exhibiting these habit planes were attributed to the different ways in which perfect dislocations release the strain energy caused by the transformation.

The crystallographic properties were calculated using the hypothesis that this is achieved by perfect dislocations propagating on planes parallel to  $(112)_B$ .

These dislocation theories effectively provide mechanisms for the transformations described by phenomenological theories and to be correct they depend ultimately on a sound phenomenological description being first achieved.

### 2.3.5 General Theories

The inadequacy of the early theories in accounting for all the observed features of martensitic transformations in steels leads to the belief that in their initial form they lack generality, and several attempts have been made to bring them into better agreement with experiment. The majority of proposals have centred on the nature of the complementary strain and several attempts to predict the observed habit plane variation, by relaxing the condition that the complementary strain is a simple shear on the twinning element of the body centred structure,  $\{112\} \langle 111 \rangle_B$ , have been made.

Wechsler, Read and Lieberman (54) calculated the undistorted planes corresponding to lattice invariant shear on  $\{111\}_F$  in  $\langle 110 \rangle_F$  and  $\langle 112 \rangle_F$  but they did not consider this choice of shear elements resulted in solutions in agreement with the habit planes near  $\{225\}_F$  or  $\{259\}_F$ . Otte (55) extended this analysis by considering shear systems for the complementary strain based on  $\langle 111 \rangle_B$ , and suggested that the reported habits may be accounted for by shear on a plane or combination of planes containing this direction. Bowles and Kennon (56) used a similar postulate in an attempt to explain the observed variation of habit with

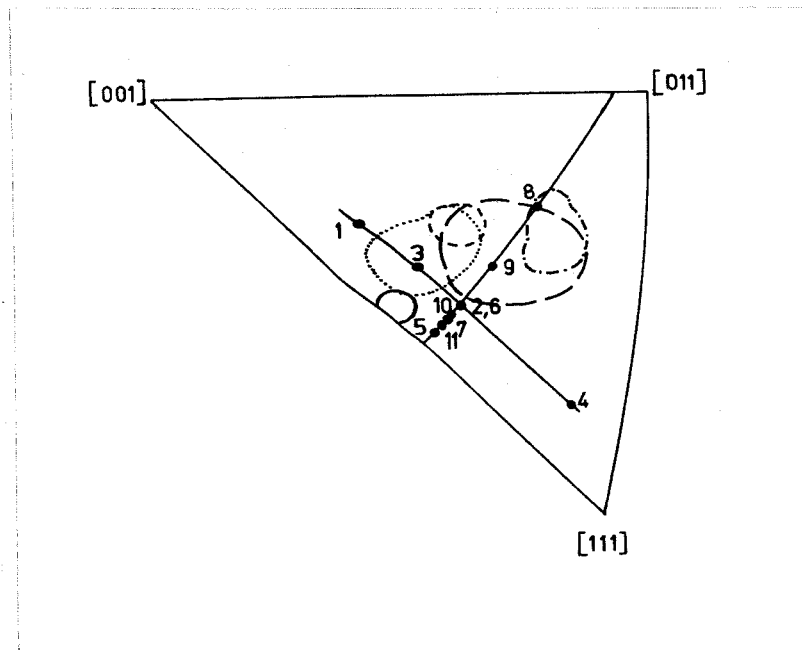


Fig. 2.17 Stereographic projection showing the predicted habit planes for the lattice invariant shear modes shown in Table 2.1, compared with the scatter of experimental habit planes for a number of alloys.

- - - - - Fe - 32% Ni
- - - - - Fe - 30% Ni
- - - - - Fe - 1.8% C
- ..... Fe - 2.8% Cr - 1.5% C
- \_\_\_\_\_ Fe - 0.95% C, Fe - 1.4% C

Crocker and Bilby (57)

TABLE 2.1

## Major Deformation Modes Examined by Crocker and Bilby

(Christian (1))

	(Austenite Modes)	$m_2^*$	$m_1^*$
1	$(11\bar{1})$ $[101]$	0.36 <sup>e</sup>	0.51
2	$(11\bar{1})$ $[1\bar{1}0]$	0.23	0.23
3	$(11\bar{1})$ $[\bar{2}1\bar{1}]$	0.24	0.32
4	$(11\bar{1})$ $[1\bar{2}1]$	0.26	0.18
5	$(00\bar{1})$ $[1\bar{1}0]$	0.43	0.53
6	$(11\bar{1})$ $[1\bar{1}0]$	0.23	0.23
7	$(\bar{1}13)$ $[1\bar{1}0]$	0.27	0.36
8	$(110)$ $[1\bar{1}0]$	0.23	0.18
9	$(331)$ $[1\bar{1}0]$	0.23	0.19
10	$(\bar{1}12)$ $[1\bar{1}0]$	0.25	0.31
11	$(115)$ $[1\bar{1}0]$	0.31	0.40

\*  $m_2$  is the magnitude of the lattice invariant shear and  $m_1$  is the magnitude of the shear component of the shape strain.

<sup>e</sup> In general, each deformation mode results in two solutions for the magnitude of the lattice invariant shear and each solution is associated with two habit plane predictions. The lower magnitude solution is recorded in this table and the corresponding habit plane prediction which is nearer to the observed habit plane range, is plotted in Figure 2.17.

temperature in their analysis of bainite in iron/carbon alloys.

A comprehensive analysis of the solutions obtained by varying the elements of the lattice invariant shear was carried out by Crocker and Bilby (57). Working with the Bullough and Bilby theory, Crocker and Bilby examined over 300 shear systems on the low index planes and directions of the austenite and martensite, by either allowing the shear plane to vary for a fixed shear direction, or by allowing the shear direction to rotate within a fixed shear plane. In order to reduce computation only those modes giving rise to small magnitudes of the shape shear and lattice invariant shear were analysed in detail. It was found that virtually any habit plane could be predicted by suitable choice of the shear elements, so that it became necessary to consider only those modes representing normal mechanical deformation modes of either structure, viz:

$\{111\}_F$	$\langle 110 \rangle_F$	Austenite Modes
$\{111\}_F$	$\langle 112 \rangle_F$	
$\{110\}_B$	$\langle 111 \rangle_B$	Martensite Modes
$\{112\}_B$	$\langle 111 \rangle_B$	
$\{123\}_B$	$\langle 111 \rangle_B$	

resulting in the eleven non-equivalent solutions shown in Table 2.1 and Figure 2.17. Although dilatations of  $\pm \frac{1}{2}\%$  were also allowed, Crocker and Bilby showed that their results did not fall within the normal scatter regions for the commonly observed habits  $\{3,10,15\}_F$ ,  $\{259\}_F$ ,  $\{225\}_F$  and  $\{111\}_F$ . On this basis they concluded, contrary to Otte (55), that a complementary strain, which is a simple shear, cannot explain the

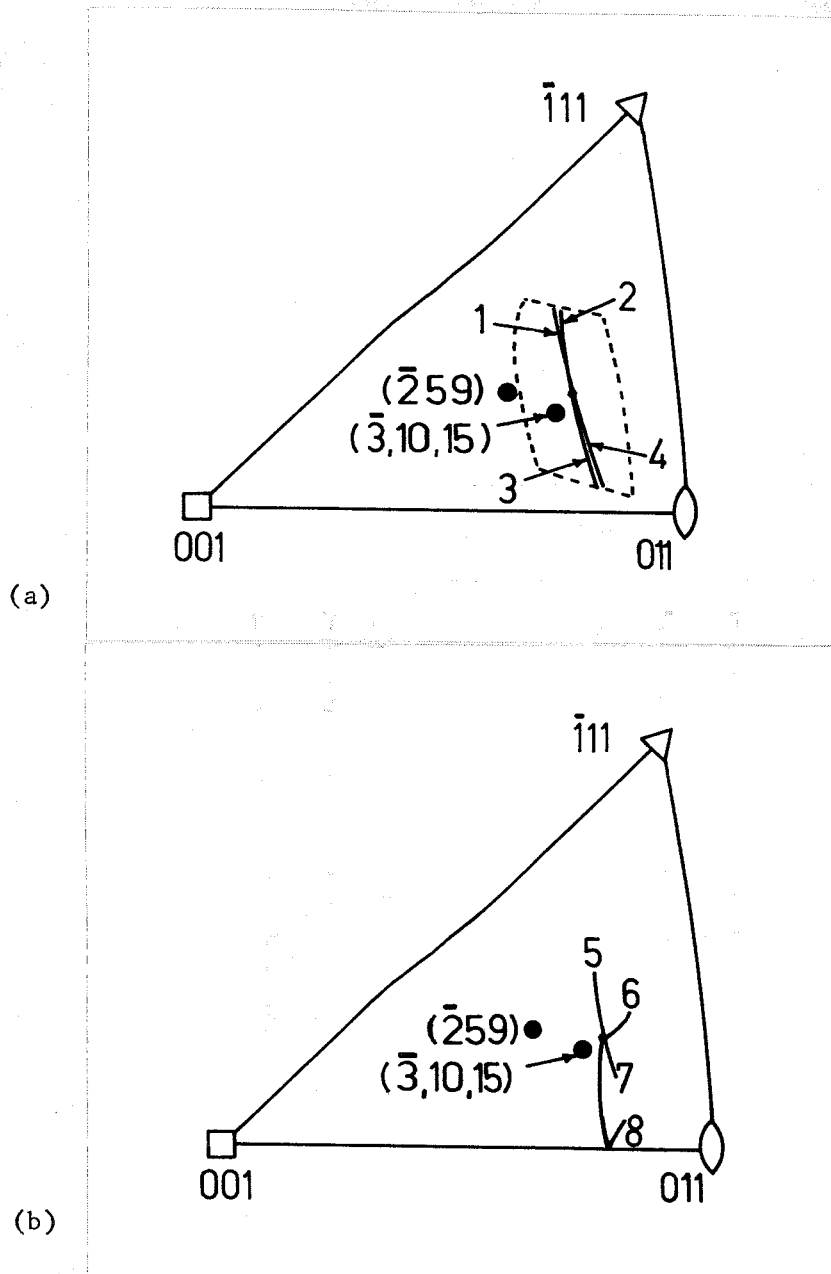


Fig. 2.18 Stereographic projection showing the loci of predicted habit planes for the lattice invariant shear modes shown in Table 2.2.

TABLE 2.2

No.	Lattice Invariant Shears (B)	Habit (F)
1	(112) $[\bar{1}\bar{1}\bar{1}]$ follows (011) $[0\bar{1}\bar{1}]$	(3, $\bar{15}$ , 10)
2	(112) $[\bar{1}\bar{1}\bar{1}]$ preceeds (011) $[0\bar{1}\bar{1}]$	(3, $\bar{15}$ , 10)
3	(112) $[\bar{1}\bar{1}\bar{1}]$ follows (011) $[0\bar{1}\bar{1}]$	(3, 15, 10)
4	(112) $[\bar{1}\bar{1}\bar{1}]$ preceeds (011) $[0\bar{1}\bar{1}]$	(3, 15, 10)
5	(112) $[\bar{1}\bar{1}\bar{1}]$ preceeds (011) $[0\bar{1}\bar{1}]$	(3, $\bar{15}$ , 10)
6	(112) $[\bar{1}\bar{1}\bar{1}]$ follows (011) $[0\bar{1}\bar{1}]$	(3, $\bar{15}$ , 10)
7	(112) $[\bar{1}\bar{1}\bar{1}]$ preceeds (011) $[0\bar{1}\bar{1}]$	(3, 15, 10)
8	(112) $[\bar{1}\bar{1}\bar{1}]$ follows (011) $[0\bar{1}\bar{1}]$	(3, 15, 10)

observed habit planes, satisfactorily.

A generalised theory, which retains the concept of the shape strain being an IPS, but which allows the complementary strain to be the product of two lattice invariant shears, the resultant of which need not be a simple shear, has recently been proposed by Acton and Bevis (58) and Ross and Crocker (59).

In these theories,  $P_2$  of equation 2.6 becomes a combination of two shears  $P_3$  and  $P_4$ , so that:

$$P_1 = RB (P_3 P_4)^{-1}$$

Beginning with the reported co-existence of  $\{112\}_B$  and  $\{110\}_B$  transformation twins in the alloy used by Oka and Wayman (120), Acton and Bevis developed the two shear model using  $\{112\}_B$  and  $\{110\}_B$  as  $p'_3$  and  $p'_4$  respectively.  $P_3$  is taken to be the usual  $(112) [\bar{1}\bar{1}\bar{1}]_B$  twinning mode and  $P_4$  is allowed to take the form either  $(011) [0\bar{1}\bar{1}]_B$  or  $(0\bar{1}\bar{1}) [011]_B$  for the variant of the correspondence used by Oka and Wayman. For zero  $(011)_B$  component the computed results are the same as those of the WLR analysis but as small amounts of the additional shear are introduced a locus of possible habits is produced. These loci, shown in Figure 2.18, are for  $(112)_B$  shear magnitudes in the range .20 - .24, which correspond to  $(011)_B$  shear magnitudes of 0-.077 and shape strain magnitudes from .17 - .21. The introduction of a dilatation allows the predicted habit planes to lie in the area bounded by the dotted line in Figure 2.18 (a).

For  $\{225\}_F$  habits the  $\{110\} \langle 111 \rangle_B$  and  $\{111\} \langle 110 \rangle_B$  systems were considered as accompanying the twinning shear. The loci of predicted

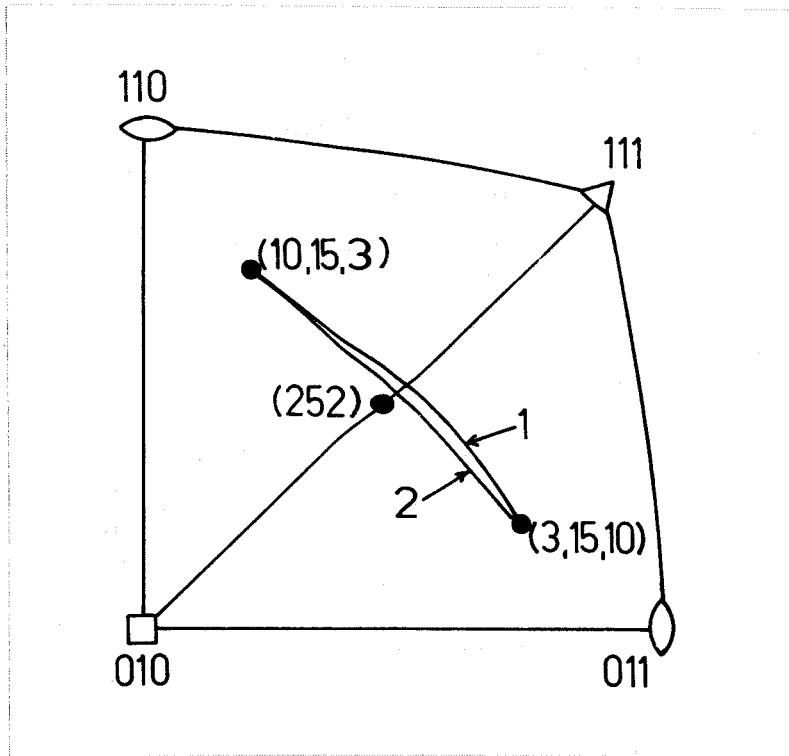


Fig. 2.19 Stereographic projection showing the loci of predicted habit planes for:

1.  $(011) [\bar{1}11]$  preceding  $(112) [\bar{1}11]$ .
2.  $(112) [\bar{1}11]$  preceding  $(112) [\bar{1}11]$ .

Ross and Crocker (59)

habit planes, for reasonable values of the strain magnitudes, were shown to be continuous between  $\{259\}_F$  and  $\{225\}_F$  for the combinations of  $(110) [\bar{1}\bar{1}\bar{1}]_B$  either following  $(112) [\bar{1}\bar{1}\bar{1}]_B$  or preceding it.

Acton and Bevis stressed that if the first shear is a twinning shear, then the second shear, whether it be slip or twinning, must be able to penetrate the first. Within this limitation they tentatively suggested that the two shear mechanism is able to explain the observed martensite habits, but pointed out that the main justification for including a second shear relies on experiment and therefore, that further electron microscopy is required in order to provide direct evidence justifying the use of this shear and to allow further development of the theory.

Ross and Crocker (59) have independently arrived at the same conclusions. In their more comprehensive analysis of the  $\{225\}_F$  and  $\{259\}_F$  transformations they considered combinations of  $\{112\}_B$  twinning preceding slip shears on planes containing  $\langle 111 \rangle_B$ . Once again, the  $\{3,10,15\}_F$  is predicted but none of the loci pass near  $\{225\}_F$ . For either  $(01\bar{1})[\bar{1}\bar{1}\bar{1}]_B$  or  $(\bar{1}12)[\bar{1}\bar{1}\bar{1}]_B$  preceding  $(112) [\bar{1}\bar{1}\bar{1}]_B$ , however, Ross and Crocker produced habit loci continuous between  $\{3,10,15\}_F$  and  $\{225\}_F$  which require only small amounts of the slip shear to precede twinning. They suggested that of the two possibilities, the shear  $(\bar{1}12)[\bar{1}\bar{1}\bar{1}]_B$  is the more attractive.

The inability of the use of a simple twinning shear to explain the results of Dunne and Bowles (40), led these workers (60) to propose a slightly different theory which requires that a lattice invariant accommodation strain, involving slip in the austenite, accompany the

transformation. In terms of the formal analysis this is equivalent to relaxing the condition that the complementary strain is a simple shear, and this condition is formulated by the equation:

$$S_t = P_1 P^{-1} P_2$$

where  $P^{-1}$  is not a simple shear. This proposal is justified by the observation of extensive  $\{111\}_F$  slip accompanying the  $\{225\}_F$  transformation in iron/carbon, iron/chromium/carbon and iron/manganese/carbon alloys (39, 41).

The shape strain  $P_1$  is an invariant plane strain on the habit plane and the complementary strain is a shear in the  $[\bar{1}\bar{1}0]_F$ . The properties of the accommodation strain are determined by considering the remaining part of the total lattice strain:

$$\begin{aligned} P &= S_t^{-1} P_2 P_1 \\ &= (RB)^{-1} P_2 P_1 \end{aligned}$$

Using the hypothesis that the strain in the habit plane is non-uniform and distorts  $[\bar{1}\bar{1}0]_F$  to its final length without rotation while leaving the line  $90^\circ$  from  $[\bar{1}\bar{1}0]_F$  invariant, the accommodation strain is identified as an invariant line strain which may be resolved into slip shears on the four  $\{111\}_F$  in two  $\langle 110 \rangle_F$ .

The results of the analysis are shown to be in good agreement with the experimental results of Dunne and Bowles where exact parallelism of  $[\bar{1}\bar{1}0]_F$  and  $[\bar{1}\bar{1}1]_B$  was assumed. Dautovich (119) has shown however, that for  $\{225\}_F$  martensite in iron/manganese/carbon, neither the close packed planes nor the close packed directions are exactly parallel and concluded that the theory is inadequate to explain these results.

## 2.4 Transformations Involving Both Compositional and Shape Changes.

### 2.4.1 Introduction

The discussion so far has indicated that there are two possible transformation modes in solid state transformations. These are distinguished experimentally by the presence or absence of a change of shape of the transformed region. In the case of martensitic transformations there is a change of shape and usually, although not necessarily, there is no diffusion. In diffusional transformations there is no change of shape. There is a group of transformations, typified by the bainite transformation in steels, in which both a change of shape and long range diffusion are observed to occur concurrently. These transformations have been termed atypical by Kennon (61) or more recently quasi-martensitic by Leiberman (62). Although requiring diffusion, such transformations are formally martensitic if the view is taken that they possess a correspondence.

The observation that Widmanstätten ferrite in the iron/carbon system also exhibits a surface relief effect (63-67) has led to some discussion (11, 82) as to whether this transformation is rightly a form of bainite or whether it is a unique morphology. For this reason it is proposed to discuss the bainite reaction in terms of the classification of solid state transformation which has been outlined in the previous sections.

Davenport and Bain (68) were the first to suggest that the transformation of steels at temperatures intermediate between those required for pearlite formation and  $M_s$  gives rise to a unique microstructure. The so-called bainite reaction was the last of the major modes of austenite decomposition to be discovered and from the very beginning its identity,

and indeed its existence, has been questioned and re-examined several times.\* Many of the observed properties, and therefore the mechanism of the bainite reaction, remain obscure (69).

#### 2.4.2 Definition of Bainite

Perhaps, as has been suggested by Aaronson (11), the current "aura of confusion" surrounding the bainite transformation may stem from definition and terminology (indeed there would appear to have been some confusion in these matters). But Aaronson's proposals themselves raise several difficulties and in many respects are contrary to common terminology.

In their original interpretation of the structure of bainite, Davenport and Bain (68) considered it to be a ferrite/carbide aggregate formed at intermediate temperatures in the decomposition of iron/carbon alloys. It was regarded as being a non-lamellar counterpart of the eutectoid reaction, its formation being essentially diffusion controlled as shown by the typical C-curve kinetics. This definition was accepted by subsequent workers (70) and is retained by Christian (23).

The surface relief effects accompanying bainite formation, observed initially by Ko and Cottrell (71), led to the postulation of a degree of interface coherency and of a shear or displacive mechanism of growth. The crystallographic features of the transformation were subsequently analysed on the basis of the crystallographic theory of martensitic transformations by Bowles and Kennon (47) and Srinivasan and Wayman (72). These results are discussed in Section 2.4.9.

Garwood (10), on the basis of observed surface relief effects,

---

\* See for example conference proceedings (5, 10, 11, 69).

extended the term bainite to include the decomposition of quenched  $\beta$  phase in copper/zinc and copper/aluminium alloys annealed isothermally at about 500°C. In addition McDougall (9) has shown that a Widmanstatten form of  $\alpha$ , exhibiting martensitic like relief, can be formed in these systems by continuous cooling or by isothermal transformation of  $\beta$  phase at temperatures 80 - 100°C below the  $(\alpha + \beta)/\beta$  boundary — a logical extension of the observation that at similar degrees of undercooling a  $W_s$  (Widmanstatten start) temperature exists for proeutectoid ferrite in the iron/carbon system (20). The extension of the term bainite to include these non-ferrous transformations would seem to be misleading since in many respects they are quite different to the aggregate structures formed in ferrous alloys, and for the purpose of this thesis they will be referred to as Widmanstatten transformations.

The difficulties of description as seen by Aaronson (11), arise because of the sometimes conflicting definitions based on morphology, kinetics and shape change and these are discussed in the following sections.

#### 2.4.3 Kinetics

Bainite in steels, microstructurally defined as a non-lamellar ferrite/carbide aggregate, typically exhibits C-curve kinetics. The curve describing bainite formation generally appears below the pearlite curve which in turn is below the various proeutectoid curves. In plain carbon steels the pearlite and bainite curves interpenetrate but in alloy steels they may be well separated, in which case the bainite curve is usually asymptotic to a definite maximum temperature, denoted  $B_s$ . The form and position of these curves relative to the time and

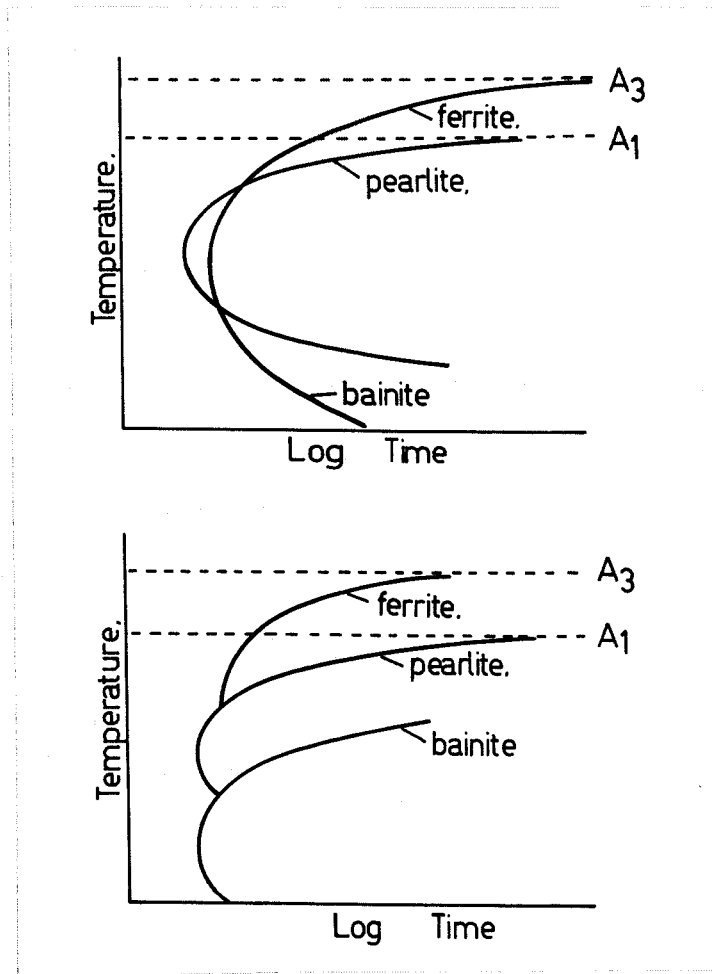


Fig. 2.20 Two possible relationships between the C-curves for alloy steels. The top diagram shows the pearlite curve interpenetrating a continuous ferrite/bainite curve and implies that bainite and Widmanstatten (proeutectoid) ferrite form a continuous series of decomposition products. The lower diagram indicates a  $B_s$  temperature which is not the  $A_3$  temperature, and therefore requires that both kinetically and morphologically the two products must be differentiated.

temperature axes are most important since a knowledge of these may contribute to an understanding of the transformation mechanism — if the mechanism changes then a change of kinetics is not unexpected.

Examination of Hultgren's (73) comprehensive series of C-curves for a wide variety of ferrous alloys containing small quantities of alloying elements, does not yield unequivocal evidence for separate C-curves for proeutectoid ferrite and bainite. The results generally group themselves into figures of the type shown opposite in Figure 2.20. Hultgren postulated that the cases where two distinct C-curves were evident could be explained if it was assumed that in one case both carbon and alloying elements segregate to achieve equilibrium with the austenite (orthoferrite) while in the other case, at lower temperatures, only carbon diffusion is sufficiently rapid and the ferrite inherits the full alloy content of the parent (paraferrite). Aaronson (11) has criticised this hypothesis on the basis of electron probe analysis of ferrite formed above and below the kinetic  $B_s$  temperature, maintaining that there is no evidence for two modes of ferrite precipitation. Aaronson believes that the "bay" observed in the C-curves for some alloys is attributable to the anomalous effect of certain alloying elements, notably molybdenum.

However, Garwood (10) has observed a slight "bay" or discontinuity in the C-curve for isothermally transformed  $\beta$  phase in copper/zinc alloys and this difference he attributes to the morphological change from platelike to rodlike forms of the precipitated  $\alpha$ . Owen and White (74) have reported a similar break in the curve for iron/carbon bainites, at a temperature corresponding to a morphology change around 350°C.

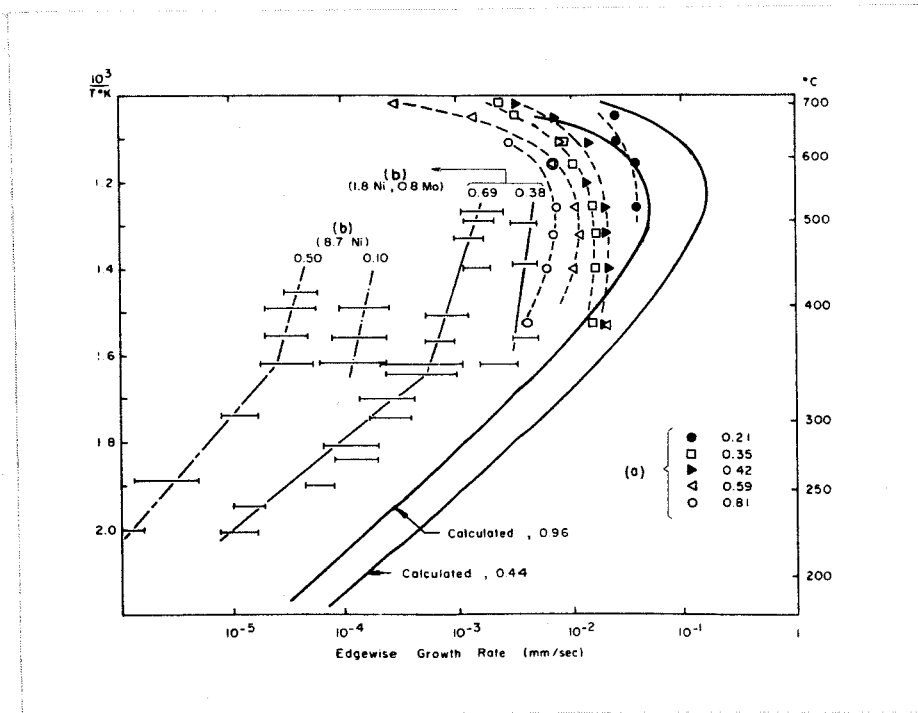


Fig. 2.21 Comparison of the calculated rates of edgewise growth for Fe/C alloys with the experimental rates.  
 (a) Widmanstatten ferrite and bainite in plain carbon steels.  
 (b) Bainite in alloy steels.

Kaufman et al (77)

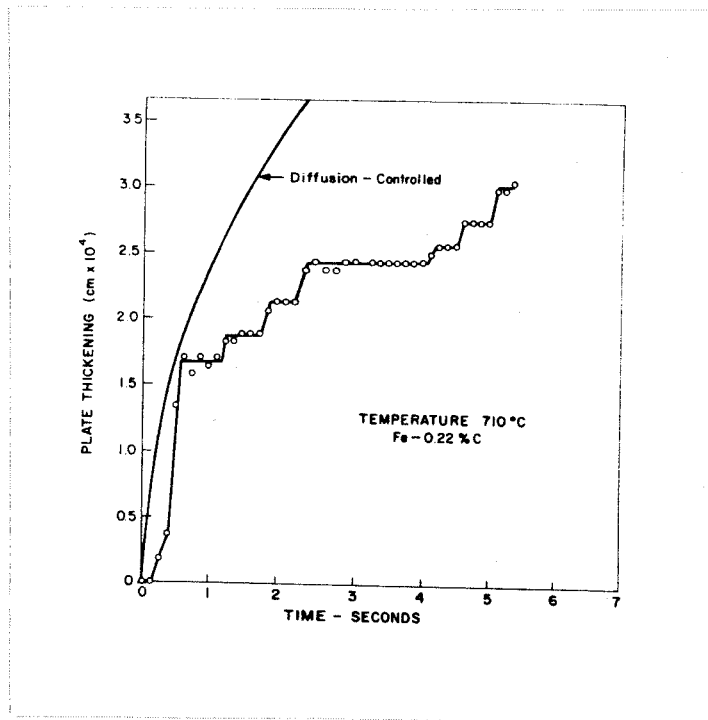


Fig. 2.22 Comparison of the calculated rates of thickening of ferrite sideplates (using a diffusion control model) with the experimental rates determined by Aaronson et al (79).

This observed change in transformation kinetics may be indicative of a change in mechanism.

In the iron/carbon bainites the ferritic component forms characteristically as plates; the rates of both lengthening and thickening of these have been measured experimentally (64, 76, 78) and compared to the overall rate of austenite decomposition. The rates of lengthening shown in Figure 2.21 are taken from Kaufman and Cohen (77) and these show that Widmanstätten ferrite, upper bainite and lower bainite each exhibit growth rates which fall on a single continuous curve. These workers have taken this to mean that the three structures are formed by essentially similar transformation mechanisms.

Both the rate of lengthening and the rate of thickening have been reported as being linear functions of time at constant temperature (76), the rate of lengthening being greater by a factor of approximately twenty. This linear growth law has been analysed by Speich (76) and Aaronson (11) in the following terms:

(a) Lengthening is controlled by the rate of carbon diffusion in austenite as represented by the Zener-Hillert model (see for example Christian (1)).

(b) Thickening cannot be controlled by carbon diffusion away from the planar interfaces as this would require a parabolic growth law.

Recent thermionic emission microscopy on ferrite sideplates has shown however, that thickening actually occurs by discreet jumps separated by repeated arrests (79), as shown in Figure 2.22. The significance of this observation is not yet fully understood but it has been interpreted by Aaronson as evidence of ledge growth.

#### 2.4.4 Morphology

Two major morphologies have been reported for bainite; a third has been nominated but its identity, although distinct, is less certain. Each morphology is characteristic of a definable temperature range for any particular alloy system. Although the forms of bainite were postulated following early optical metallographic work, more recent application of electron microscopy has verified the original morphological distinctions.

a). Lower bainite (80) consists of ferrite plates within which small platelets of carbide are precipitated characteristically at angles of  $55 - 60^{\circ}\text{C}$  to the major growth (long) direction of the plate. This mode is usually formed by isothermal transformation below a temperature of about  $350^{\circ}\text{C}$ . The microstructure observed using electron microscopy is similar to that of martensite found in quenched and tempered high carbon steels — although there is no evidence of internal twinning. There is also evidence of a fine scale substructure within the plates (80-83) as well as a single advancing (growing) interface. Double plates are formed in some instances which exhibit two opposite tilts about a central "midrib" (76). These double plates are characteristic of the Widmanstatten precipitates found in copper/zinc alloys (10).

b). Upper bainite (80) is formed above  $350^{\circ}\text{C}$  in most steels and, although still consisting of lenticular ferrite, the fine scale morphology of the structure changes, with the cementite plates being directed along, rather than across, the ferrite plates. At transformation temperatures near  $500^{\circ}\text{C}$  the ferrite is needlelike or lathlike, with the majority of the carbide being precipitated at the lath boundaries. In

some cases carbide has also been observed within the laths. This type of bainite is more reminiscent of tempered low carbon martensite. A substructure in the form of sheaves (80-83) has been also reported (in association with a high dislocation density) for upper bainite.

c). The identity of the acicular ferrite morphology is not well defined and it has been variously referred to as the X-constituent (84), acicular ferrite (64), Widmanstätten ferrite (82) or simply upper bainite (11). Each of these descriptions appear to relate to carbide free ferrite plates or laths formed at high temperatures within the temperature range of bainite formation ( $< 550^{\circ}\text{C}$ ).

The observation that Widmanstätten ferrite in hypoeutectoid iron/carbon alloys forms with a surface relief effect and has kinetics of formation that are continuous with those of upper bainite, has led to widespread belief that these three morphologies form a continuous series of decomposition products (11, 76). Unlike upper bainite however, the carbide free ferrite does not form sheave structures (82).

The fine scale substructure of bainite has been examined by several workers but the only similar study of proeutectoid ferrite has been that of Heheman (82), who considered this morphology to be a single crystal of b.c.c. material with a low dislocation density. Heheman regarded this structure as evidence typifying growth by movement of a single, diffusion controlled interface.

Upquenching bainite to temperatures in the Widmanstätten range does not remove the high dislocation density and substructure, thus ruling out the possibility that Widmanstätten structures form initially as bainite and then subsequently anneal. Similar upquenching experiments (81) in

the region of the upper to lower bainite transition temperature, have shown that each of these structures is formed only within definable temperature ranges and that they do not continue to grow when the temperature is suddenly changed beyond this range. Such observations imply that each of the morphologies is distinctive, and that the transformation mechanism is different in each case.

#### 2.4.5 Crystallography

##### 2.4.5.1 Orientation Relationships

Using a pole figure technique Mehl et al (70) reported that in upper bainite the orientation relationship between the ferrite and the parent austenite is most closely represented by the Nishiyama relationship\* while for lower bainite it exhibits the Kurdjumov-Sachs relationship.\* These two relationships differ only by a rotation of  $5^{\circ}16'$  and both have been observed in the martensites of quenched steels (1). The Kurdjumov-Sachs relationship has also been assumed to hold for the precipitation of proeutectoid ferrite in iron/carbon alloys by Mehl et al (101), who used an etch pit technique to determine the traces of  $\{110\}_B$  and then compared these with  $\{111\}_F$  traces, in order to justify the assumption.

Kennon (61) reported that the Nishiyama relationship was more nearly approached by bainitic ferrite in his study of lower bainite. Wayman

---

*	Nishiyama Relationship (N)	$\{111\}_F \parallel \{110\}_B$
		$\langle 211 \rangle_F \parallel \langle 110 \rangle_B$
	Kurdjumov-Sachs Relationship (KS)	$\{111\}_F \parallel \{110\}_B$
		$\langle 110 \rangle_F \parallel \langle 111 \rangle_B$

and Srinivasan (72) found  $4^\circ$  between the close packed directions  $[\bar{1}01]_F$  and  $[\bar{1}\bar{1}1]_B$  and  $\frac{1}{2}^\circ$  between the close packed planes  $(111)_F$  and  $(011)_B$  in their study of lower bainite in an iron/chromium/carbon alloy, and noted that this orientation relationship was different from that of martensite in the same alloy. The accuracy of their Laue work is quoted to  $\pm\frac{1}{2}^\circ$ .

The method of orientation determination using selected area diffraction in transmission electron microscopy, was successfully used by Shimizu et al (85) and Shackelton and Kelly (86) to yield further important information on the transformation, especially with regard to the precipitation of carbide within the basic ferrite structure. For lower bainite the relationship (86):

$$\begin{aligned} (001)_{Fe_3C} & \parallel (211)_B \\ [100]_{Fe_3C} & \parallel [0\bar{1}1]_B \\ [010]_{Fe_3C} & \parallel [1\bar{1}\bar{1}]_B \end{aligned}$$

is the same as that observed in tempered martensite.

Shimizu et al (85) proposed the relationship:

$$\begin{aligned} (011)_{Fe_3C} & \parallel (011)_B \\ [100]_{Fe_3C} & \parallel [01\bar{1}]_B \end{aligned}$$

The two relationships differ by  $1^\circ 40'$  in the positions of the close packed direction with the positions of the close packed plane being identical. This difference has been attributed to experimental error.

Shackelton and Kelly found that as the transformation temperature is gradually increased above  $350^\circ C$ , the orientation relationship between the carbide and ferrite of lower bainite gradually disappears, eventually being completely replaced by a new relationship. The following ration-

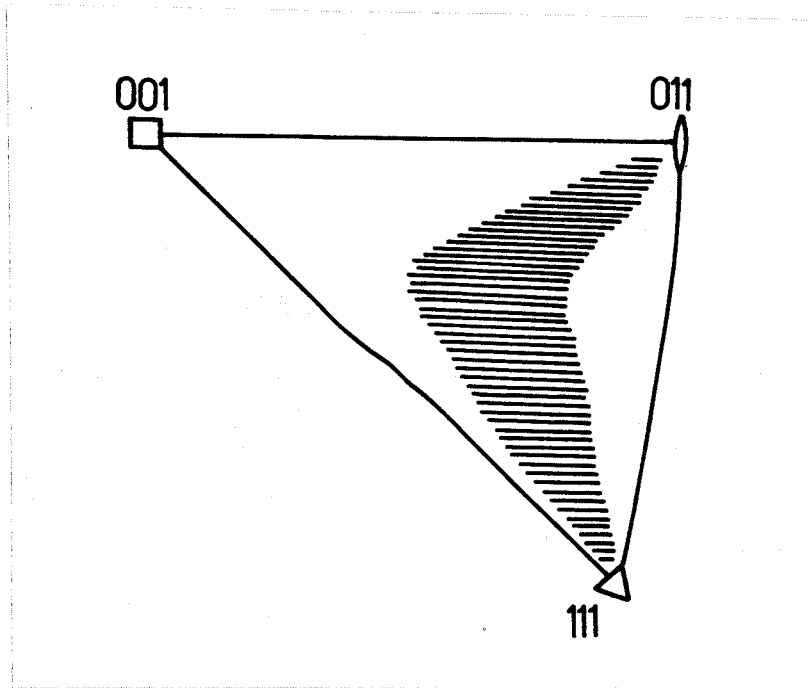


Fig. 2.23 Stereographic projection showing the variation of the bainite habit plane with temperature. The identity of the habit varies from near  $\{110\}_F$  at low temperatures to near  $\{111\}_F$  at high temperatures. The difficulty of measuring the indices exactly is reflected by the wide scatter of results.

after Kennon (61)

alization was made regarding the new orientation relationship.

- (i) The ferrite component was related to the austenite by the Kurdjumov-Sachs relationship.
- (ii) The carbide was related to, not the ferrite, but the austenite, by the Pitsch relationship:

$$\begin{array}{l} (001)_{\text{Fe}_3\text{C}} \parallel (\bar{2}25)_{\text{F}} \\ [100]_{\text{Fe}_3\text{C}} \parallel [\bar{5}54]_{\text{F}} \\ [010]_{\text{Fe}_3\text{C}} \parallel [\bar{1}10]_{\text{F}} \end{array}$$

#### 2.4.5.2 Habit Planes

Measurements by Greninger and Troiano (87), Mehl (70) and Kennon (61) have shown that the habit plane is different for upper and lower bainite and that there is actually a continuous variation of habit plane with transformation temperature as shown in Figure 2.23. The habit plane of Widmanstätten ferrite is often reported as being  $\{111\}_{\text{F}}$  but the evidence on which this is based will be examined in more detail in the next chapter.

#### 2.4.6 Composition

Radcliff and Rollandson (88) have pointed out that one of the principal difficulties in developing a theory for bainite transformations is that, for expediency, the majority of experimental studies have been carried out on alloy steels. The reasons for choosing alloy steels can usually be traced to ostensibly favourable properties (such as lowering of  $M_s$ , decreased reaction rate, and separation of the bainitic from the pearlitic mode of transformation) imparted to the reaction by the alloying elements. The main disadvantage and the objection to the

use of highly alloyed steels in studies of this kind, is that the basic mechanism of the transformation may be obscured by the presence of the alloying elements.

On the basis of experiments on the rate of thickening of ferrite allotriomorphs in alloy steels Aaronson (11) has proposed that some elements have an anomalous effect on the ferrite growth kinetics which leads to the production of a "bay" in the normal TTT curve for the transformation. This he proposes, may explain the evolution of the kinetic definition of bainite in which the decomposition product is identified as occurring only below a definite, maximum temperature, denoted  $B_s$ . According to Aaronson a definite  $B_s$  temperature is only observed in ferrous alloys when alloying elements are present in sufficient quantity to produce a deep bay in the TTT curve. If only the lower half of the curve is distinct from the pearlite curve, then Aaronson suggests it is possible to misinterpret this as a separate curve asymptotic to the temperature  $B_s$ .

This view, like that of Kaufman et al (see Section 2.4.8), envisages proeutectoid ferrite and bainitic ferrite as forming by the same process. Such a view is reasonable only if it can be shown that the mechanism of the transformation does not change as the reaction temperature is decreased. The evidence summarised so far, however, shows that the change of shape may be the only common feature of the different modes and that the morphology, crystallography and internal structure of the ferrite may change significantly as the temperature is reduced.

The effect of carbon content on the transformation characteristics has recently been studied by Pickering (83) who showed that increasing

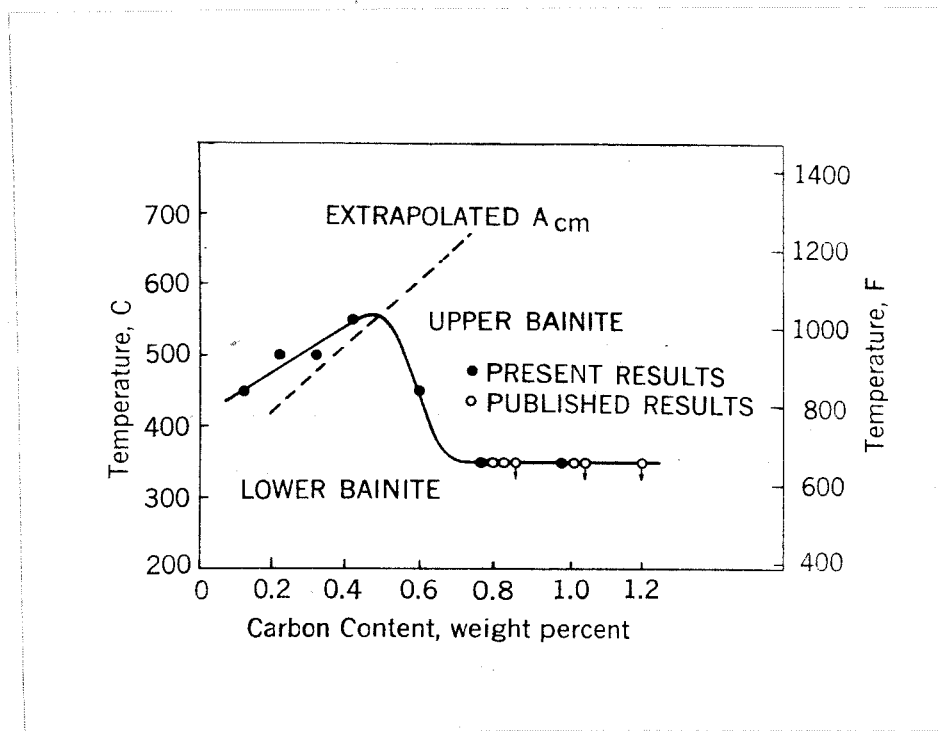


Fig. 2.24 Graph showing the maximum temperature above which lower bainite is never observed, as a function of carbon content.

Pickering (83)

the carbon content of  $\frac{1}{2}\%$  molybdenum/boron steels not only increased the amount of carbide in lower bainite, but that it also affected the temperature of transition from upper to lower bainite. Pickering proposed that the temperature at which upper bainite gives way to lower bainite is that at which the rate of carbon diffusion becomes so slow that it can no longer drain away in advance of the growing austenite/ferrite interface. The observed temperature dependence of this transition was explained by proposing that at low carbon levels ( $< 0.1\%$ ) there is a steep concentration gradient ahead of the advancing austenite/ferrite interface which allows rapid carbon diffusion at temperatures above about  $450^{\circ}\text{C}$ . Below this temperature diffusion can no longer keep up with the interface and carbon is incorporated into the ferrite, leading to the formation of lower bainite. If the carbon concentration of the alloy is increased, the concentration gradient ahead of a growing ferrite plate is reduced, diffusion is slower, and the transition temperature increases as shown in Figure 2.24. The observed dependence of the transition corresponds fairly well with the extrapolated  $A_{cm}$  line up to carbon levels of  $0.5\%$ . At  $0.5\%C$  the  $A_{cm}$  line intersects the observed transition line, and at higher concentrations it is suggested that primary cementite becomes capable of nucleating and precipitating directly from the austenite, resulting in upper bainite. Consequently there is a sharp decrease in the upper temperature limit for the formation of lower bainite at this point.

Pickering's view seems to suggest that the rate of advance of the austenite/ferrite boundary is temperature dependent and that if the rate of carbon diffusion cannot equal the former then a degree of super-

saturation results. If this suggestion is allied with the previous proposal of a semicoherent austenite/ferrite interface, it is possible, in principle, to see how the incorporation of carbon into the ferrite in increasing proportions could influence the characteristics of the advancing boundary. At present, such a theory is merely speculation, but the concepts are not inconsistent with the observation that the isothermal transformation of supersaturated  $\beta$  phase in copper alloys also shows a dependence of morphology on temperature and composition (114-116).

#### 2.4.7 Mechanism

The experimental observations so far described amount to a comprehensive description of the transformation in carbon steels below about 500°C from which certain proposals on the transformation mechanism have been enunciated. The status of acicular ferrite is less certain, the information being incomplete rather than ambiguous.

The break in kinetics, activation energy,\* morphology and crystallography at temperatures in the vicinity of 350°C, in conjunction with the implications of the upquenching experiments of Goodenow et al (81), inevitably lead to the conclusion that a change of growth mechanism takes place in the vicinity of this temperature. The proposals are:

- (i) Ferrite is the nucleating phase.
- (ii) Below 350°C cementite precipitates from supersaturated ferrite which forms an acicular structure similar to martensite. The trans-

---

\* The activation energy data in itself is not conclusive as has been pointed out by Christian (1) but when read in conjunction with the other data some credence is lent to its significance.

formation sequence is envisaged as: austenite transforms to supersaturated ferrite by the advance of a semi-coherent interface behind which strain energy is released by the precipitation of the excess carbon as  $\text{Fe}_3\text{C}$ . The crystallographic relationships support this view.

(iii) Above  $350^\circ\text{C}$  ( $\%C < 0.5\%$ ) the diffusivity of carbon is sufficiently high to allow the excess carbon, or part thereof, to move ahead of the advancing ferrite interface and an essentially carbide free lath grows until the austenite immediately ahead of the interface becomes supersaturated and precipitates carbide. Again the crystallography strongly supports the mechanism and there have been several reports of carbon gradients measured in the parent austenite ahead of the advancing austenite/ferrite interface (82, 83, 89). Notwithstanding this observation, there is evidence that some slight supersaturation accompanies upper bainite formation (92), so that it is not inconceivable that there is a continuous variation in the degree of supersaturation of the precipitating ferrite which is dependent upon the transformation temperature.

Consideration of these diffusional aspects of the transformation however, tends to place too little emphasis on the correspondence implied by the shape change (6), and the many similarities of crystallography and morphology to martensitic transformations in quenched steels (72). Following the considerations given in Section 2.2.3.2, wherein it was suggested that a shape change could be regarded as indicative of an interface of the glissile martensitic type, it would seem that the bainite reaction comes within the classification of a martensitic transformation, since a change of shape has been observed in many instances (61, 64, 71, 72, 76). To test this reasoning fully it is appropriate

TABLE 2.3

The free energy difference between austenite and martensite of the same composition at  $M_s$ , and the temperature ( $T_o$ ) at which the austenite and martensite can exist in stress free equilibrium.

Kaufman et al (77)

Atom fraction of carbon	Zener (90)		Fisher (91)		Kaufman (77)	
	$T_o$ °K	$\Delta F$ cal/mole	$T_o$ °K	$\Delta F$ cal/mole	$T_o$ °K	$\Delta F$ cal/mole
0.02	890	-290	920	-320	910	-270
0.04	725	-290	800	-365	750	-260
0.06	590	-290	725	-445	640	-265

to apply the crystallographic theory of martensite transformations to bainitic ferrite. Although still far short of describing the mechanism of a transformation, in the sense of proposing a discrete dislocation model, an agreement of the crystallographic theory with experiment would suggest limitations on the allowable nature of the interface and the overall strains which any dislocation model would have to achieve. Before reviewing the application of the crystallographic theory to bainite, an outline of the thermodynamic argument which has been advanced against the proposal that bainite forms as supersaturated ferrite, will first be given.

#### 2.4.8 Thermodynamics

The acicular mode in the decomposition of austenite encompasses Widmanstätten ferrite, upper and lower bainite and martensite, each of which exhibits surface relief effects on a prepolished and transformed surface. The question arises as to the significant differences between these structures.

The proposal that the body centred cubic matrix phase of lower bainite precipitates initially with the same carbon content as the parent (ie. as supersaturated ferrite) has been analysed by Zener (90), Fisher (91) and Kaufman et al (77) who calculated the temperature  $T_0$  at which austenite and martensite of the same composition could co-exist in stress free equilibrium. The results of these calculations have been summarised by Kaufman et al and are shown in Table 2.3 together with the calculated free energy changes associated with the austenite to martensite transformation. Kaufman et al also calculated the free energy changes associated with the decomposition of austenite to ferrite

of equilibrium carbon concentration, and to supersaturated ferrite.

They found that the driving force for decomposition decreased in the order:

equilibrium ferrite  $\longrightarrow$  martensite  $\longrightarrow$  supersaturated ferrite,

and concluded that it was most unlikely that supersaturated ferrite should ever form. In addition, on the basis of continuity of kinetics (Figure 2.21), they also concluded that Widmanstätten ferrite is properly a form of bainite and that  $B_s$  is therefore equatable to  $W_s$ . (By analogy to  $M_s$ , the upper temperature limits for the formation of bainite and Widmanstätten ferrite are denoted respectively  $B_s$  and  $W_s$ ).

Since  $W_s$  is less than  $100^\circ\text{C}$  below the  $\delta/(\delta+\alpha)$  boundary in carbon steels (20), it is much higher than the calculated  $T_0$  temperature and, using the above interpretation, so too is  $B_s$ . It is therefore clear that the condition that the free energy change in going from austenite to martensite be zero, does not define an upper temperature limit for the formation of bainite, and Kaufman et al suggest that  $B_s$  is simply the temperature at which austenite can decompose by a mechanism involving the acicular growth of ferrite. Although these calculations have shown that it is unlikely that bainite will retain the full carbon content of the transforming austenite the same conclusion could have been reached by analysis of the experimental data, where it has been found that in upper bainite carbon segregates ahead of the interface, as it also must in Widmanstätten ferrite. The prime assumptions of the calculation are clearly inconsistent with this observation.

Furthermore, the equating of  $B_s$  and  $W_s$  is not substantiated beyond a degree of kinetic continuity for the two morphologies and it

seems preemptive to make such a suggestion on these grounds.

#### 2.4.9 The Application of the Crystallographic Theory of Martensite Transformation

The existence of similarities in the crystallographic and geometric features of many transformations involving diffusion, to those of the classical martensitic transformations, leads to the belief that the former may be analysed on the basis of the crystallographic theory. Some transformations in pure metals have been examined and considered to be martensitic (46) but these will not be discussed here; attention will only be paid to transformations exhibiting the aforementioned dichotomy.

Bowles and Tegart (13), who applied the theory to the precipitate formed in aged copper/beryllium alloys, found that the early stages of (coherent) growth produced surface relief effects in conjunction with a definable habit plane and orientation relationship. They proposed that the crystallography agreed with the predictions of the phenomenological theory of martensitic transformations.

Subsequently Bowles and Smith (93) extended the concept further by showing that the cubic to orthorhombic ordering transformation in copper/gold alloys, which exhibits the kinetics of a diffusion controlled transformation, also conforms with the theory.

Following this, Bowles and Kennon (47) proposed that the bainite reaction in steels is probably quite well accounted for by the theory if the lattice invariant strain is allowed to take place on any plane containing the  $[\bar{1}\bar{1}0]_F$  direction. A complete analysis was precluded because of the inability of these workers to nominate the specific

variants of the habit plane and orientation relationship which were related. This was an experimental difficulty inherent in the extremely small size of the bainite plates and the absence of retained austenite in their iron/carbon alloys. Wayman and Srinivasan (72) overcame this difficulty in their study of lower bainite formed in an iron/chromium/carbon alloy and, apart from a discrepancy in the calculated value of the shape strain magnitude, they maintained that the transformation crystallography was consistent with the predictions of the theory. The lattice invariant strain proposed in this case, was slip in the  $[\bar{1}11]_B$  twinning direction on a plane about  $20^\circ$  from the  $(112)_B$ . An important observation arising from their work is that bainite and martensite formed in the same material have quite different crystallographic characteristics so that bainite cannot be regarded as being a form of autotempered martensite as has sometimes been suggested.

The conclusion, that some transformations exhibiting the crystallography typical of martensitic transformations may be kinetically restricted by the need for accompanying diffusion, seems inescapable. Under the conditions where the atomic species have different mobilities, and where reasonably high degrees of undercooling can support the movement of a partially coherent martensitic type of interface ( and thence the maintenance of a correspondence), such transformations should be possible. Perhaps the best known example of this type of transformation is the bainite reaction in steels but the observation that Widmanstätten structures in brass also exhibit these properties leads to the belief that the mode may be quite general.

---



Fig. 3.1 A photograph of the original "nature print" of the Elbogen meteorite made by Von Widmanstätten about 1808. The meteorite contains approximately 7% Ni and the section shows a single crystal of taenite (austenite) which has almost completely transformed to kamacite (ferrite) in classic "Widmanstätten" fashion.

## CHAPTER 3

THE WIDMANSTATTEN STRUCTURE3.1 The Gensis - Metallic Meteorites

In 1804 William Thompson, doctor of medicine turned naturalist, when attempting to remove polishing powder from the lapped surface of the Pallas meteorite with dilute nitric acid, revealed an extremely regular and geometric pattern on the polished section (94). This event represents the real discovery of the now familiar patterns and anticipates the beautiful nature prints of Alois Joseph Franz Von Widmanstätten recorded in 1808 but not published until 1820 by his colleague Carl Von Schreibers. It was the work of the Austrians however, which preempted the fame (95). Although the plate-like pattern was subsequently found in steels and artificial iron/nickel alloys the significance of the microstructure was not deduced until over one hundred years after its discovery when Young (96), aptly enough experimenting with iron/nickel meteorites, interpreted the results of an X-ray analysis in crystallographic terms.

Young's now classic experiments on the Carlton meteorite ( $\approx 13\%Ni$ ) in 1926, showed that not only was the plane of the Widmanstätten pattern approximately parallel to a  $\{111\}_F$  ie. an octahedral plane of the taenite, but that a  $\{110\}_B$  (where the B subscript refers to the kamacite) was also mutually parallel (approximately) to this "Widmanstätten plane". The relevant  $\langle 110 \rangle_F$  and  $\langle 111 \rangle_B$  directions, lying respectively in the parallel  $\{111\}_F$  and  $\{110\}_B$ , were found to be almost parallel, differing only by  $1.5^\circ - 2^\circ$ . Similar results were reported for the Canon Diablo meteorite

( $\approx 7\%$  Ni), where the determined orientation relationship was also shown to approach that represented by the exact KS relationship.

In a second paper (97) Young made a further, more detailed contribution. By carefully measuring the traces of the Widmanstätten plates on adjacent cut and polished faces of three meteorites, ranging in composition from 7% to 13% Ni, Young found that the angles between the planes defined by the traces differed by up to  $3.9^\circ$  from the angle of  $70^\circ 32'$  required by a  $\{111\}_F$  habit. X-ray analysis of the crystal orientations showed that in one case a  $\{111\}_F$  (taenite) was approximately  $1^\circ$  from  $\{110\}_B$  (kamacite) while in the other two cases these planes were essentially parallel. As in the earlier work, the angles between the corresponding directions  $\langle 110 \rangle_F$  and  $\langle 111 \rangle_B$ , respectively in the near parallel  $\{111\}_F$  and  $\{110\}_B$ , were found to be between  $1.2^\circ$  and  $1.5^\circ$ .

Whereas no errors were given in the first paper the deviations quoted in the second were considered to be significant by Young (97), and it may be taken therefore, that the orientation relationships involved are not exactly KS. Nevertheless, it should be noted that these early, experimentally determined relationships for Widmanstätten plates are well within the range of orientation relationships which have been subsequently reported for the decomposition of austenite to either martensite or bainite in a wide number of ferrous alloys (7).

### 3.2 Early Experimental Studies of Widmanstätten Transformations

In a series of papers appearing between 1931-1937 Mehl and his co-workers (98-102) examined Widmanstätten precipitates in a variety of ferrous and non-ferrous alloys. On the basis of many similarities in

the observed features of the different iron based materials it was concluded that the Widmanstatten transformations in these alloys had as their origin a mechanism inherent in the common allotropic transition (101, 102, 105). The crystallographic properties reported for these alloys, and the evidence from which these properties were deduced, may be summarised as follows:

(a) From a single surface trace analysis, foils of drastically quenched pure iron were proposed to exhibit a "Widmanstatten figure with an octahedral habit". The orientation relationship was nominated to be that of KS, the latter being inferred from a widely spread  $\{110\}_B$  pole figure which included the KS relationship.

(b) In the hypoeutectoid iron/carbon alloy studied (101), the habit plane was not determined but, following Bellaiew (106), it was assumed to be  $\{111\}_F$ .<sup>\*</sup> An austenite orientation was determined by measuring the habit plane traces and, assuming these to define  $\{111\}_F$ , the lattice orientation was then plotted stereographically. The  $\{110\}_B$  traces were then approximately located using an etch pit technique and these were plotted on the same stereographic projection. From this stereogram the positions of the matching close packed planes and directions in the two lattices were estimated and, despite the approximate nature of the results, the orientation relationship was reported as being consistent with that of KS.

---

\* Bellaiew's conclusions are based on the observation that on random sections taken through twenty grains of a hypoeutectoid alloy containing a well-formed Widmanstatten figure, no more than four variants of the habit plane were ever encountered.

(c) Mehl and Derge (105) examined the iron/nickel system using the Canon Diablo meteorite previously studied by Young, and a series of laboratory prepared iron/nickel alloys. In the meteoric iron the habit plane was assumed to be  $\{111\}_F$  and Mehl and Derge proposed that their  $\{110\}_B$  pole figure, determined using X-rays, could be accounted for if the orientation relationship was that of KS. The orientation relationship of the plate-like transformation product found in the laboratory prepared alloys, on the other hand, was reported to change continuously from that of KS to N, as the transformation temperature was decreased from above room temperature to  $-190^\circ\text{C}$ .

The most obvious criticism of the above work is that no distinction was drawn between the meteoric kamacite, presumably formed at high temperatures by a diffusional mechanism, and the products formed at low temperatures by quenching the iron/nickel alloys. This shortcoming also appears in Young's second paper where reference is made to work on laboratory prepared alloys. There would seem to be little doubt that Mehl's photomicrograph (105), which also appears in Barrett's text (107), is martensite, while the quenched pure iron specimens (102) previously mentioned, may also have been martensitic.

In another series of tests, a hypoeutectoid, a eutectoid and a hypereutectoid series of iron/carbon alloys were quenched to produce martensite (70). By carrying out single surface trace analyses on polished sections of these specimens, Mehl et al found only four predominant trace directions in each case and concluded that the habit plane of martensite must be  $\{111\}_F$ . Since it is now recognised that, for carbon contents greater than 0.5%, the habit plane of martensite is

not  $\{111\}_F$ , it appears that the correctness of habit plane determinations made from such limited experimentation must be questionable. This leads to the second criticism for, as described above, it was on this sort of observation that the habit plane of Widmanstätten ferrite plates was reported to be  $\{111\}_F$  by Bellaiew.

Finally, the tendency of these workers to look for and report simple, rational crystallographic relationships must be mentioned. Young (97) for example, has shown that when the data of Mehl et al (105) is treated statistically, the nomination of the exact KS orientation relationship is actually invalid.

Despite the limited nature of the data available on the crystallographic features of the Widmanstätten transformation, and especially the sparsity of recent experimental work, these early results are often quoted in even the more modern literature (20, 107) as being well documented and unquestionably rational relationships. In the section which follows the theories that have been forwarded to explain the phenomenon of Widmanstätten precipitation are reviewed, but in light of the above-mentioned uncertainty surrounding many of the observed features, critical evaluation of these theories is not always possible. In general terms, the features of Widmanstätten precipitates are not questioned; they undoubtedly exist as plates (and therefore possess a definable habit plane) and there would seem to be a relationship between the orientation of the parent and precipitate lattices. But the significance of the more recently reported change of shape (9, 10, 63-67) is not generally agreed upon, and in some cases even the kinetics of growth (77, 79) and the composition and internal structure (114-116)

have not been unequivocally determined. It would appear therefore, that if a valid theory is to emerge then the properties of the transformation must first be examined more carefully.

### 3.3 The Theories of Plate Formation

#### 3.3.1 Point Diffusion Effects

In considering the reasons for the development of plate-shaped precipitates in diffusional transformations it was pointed out by Zener and Wert (108) that any anisotropic shape such as a plate, a disc, or a needle, can grow more quickly at its edges by virtue of the higher concentration gradients present at these sites. These shapes also have the highest surface / volume ratios. Mehl et al (101) viewed the plate morphology as a perpetuation of the nuclear shape by such "point effects" of diffusion. In their view the orientation of the precipitate was somehow regarded as fundamental, being determined at nucleation, with the morphology following from growth of these oriented nuclei, aided possibly by the point effect. Although possibly an important factor in the development of the anisotropic shapes, the point effect alone cannot adequately explain the occurrence of a crystallographically definable habit plane and orientation relationship. Nor can it account for the macroscopic change of shape which accompanies the transformation, and an alternative theory must be sought.

#### 3.3.2 Strain Energy - Nabarro (18)

Following his calculations of the strain energy associated with precipitate particles of different shapes, Nabarro proposed that the lenticular morphologies arise from the ability of these particular shapes to achieve minimum of elastic strain in the surrounding parent

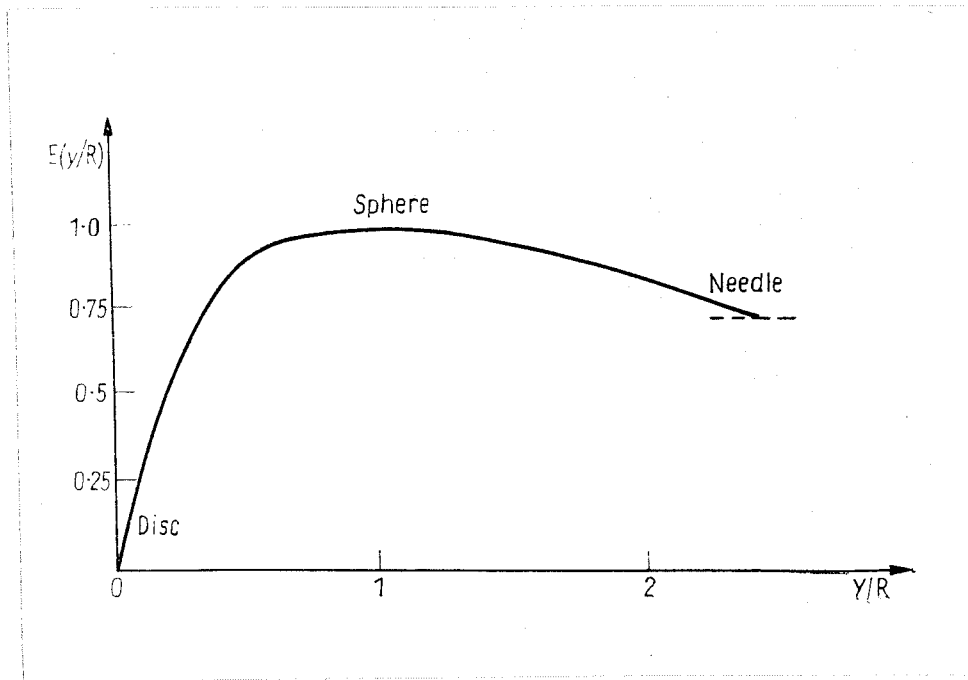


Fig. 3.2 The variation of strain energy of an incoherent nucleus as a function of its shape. The parameter  $y/R$  is related to the axial ratios of the particles.

after Nabarro (18)

lattice. Assuming the precipitate to be incompressible, Nabarro showed that when an incoherent precipitate is formed in sufficiently flat sheets, the total strain energy can be reduced significantly. Figure 3.2 shows the variation of total strain energy as a function of particle shape, as calculated by Nabarro. Laszlo (109) extended this concept further by considering the additional cases of:

- (i) elastic stressing of both precipitate and matrix.
- (ii) plastic deformation accompanying precipitation.

Aaronson (20) however, has criticised these strain energy theories, pointing to the microstructural changes which take place when Widmanstatten structures are deformed and annealed (21). These changes, he suggests, are strongly indicative of surface energy being the fundamental factor controlling the nucleation and growth of the Widmanstatten morphology.

### 3.3.3 Interfacial Energy - Smith (21)

In a comprehensive study of the effect of surface tension on the form of microstructures, Smith (21) proposed that the nature of the interphase boundary, and its surface energy, are major factors influencing the shapes of precipitates. This theory has already been discussed in some detail in Section 2.2. Disordered, high energy or incoherent boundaries are formed with difficulty but once established may grow rapidly at a rate governed by the diffusivities of the atom species involved. Coherent and semi-coherent interfaces, although nucleated more easily, are limited in their growth by the accumulation of strain energy associated with the "matching" of the lattices at the interface. The implication is that a grain boundary allotriomorph will nucleate

coherently in one grain, but will grow more easily into the adjacent grain by the advance of the incoherent segment of the boundary, as was discussed in Section 2.2.5.

This proposal further predicts that at high degrees of undercooling the higher driving force and decreased volume diffusivity should favour the growth of the partially coherent type of boundary. This prediction is in agreement with the observation that Widmanstätten structures, the planar interfaces of which are assumed to be semi-coherent, are only formed at relatively large degrees undercooling (20). The most convincing support however, comes from the rather special case of discontinuous precipitation where the incoherent cell boundary sweeps through the grain adjacent to the grain to which the cell bears an orientation relationship (20). Equivalent evidence for general precipitation does not appear to be available, although Hillert's observation (22) that the planar Widmanstätten interfaces do not propagate across annealing twin boundaries, but rather degenerate into forms microstructurally more typical of incoherent interfaces, lends some indirect support to Smith's theory.

The difficulty of determining in which grain a grain boundary allotriomorph is nucleated and into which grain it grows has hampered experimental studies aimed at clarifying growth mechanisms using theories based on interfacial structure. Pitsch and Ryder (15, 16) for example, measured the orientation relationship between ferrite allotriomorphs and the austenite grains with which they shared a common interface. These workers attempted to relate this orientation data to the growth characteristics by nominating into which grain the allotrio-

morphs were growing. This was done from considerations of the allotriomorph shapes and their disposition to the original austenite grain boundaries. Although it was claimed that an orientation relationship does exist, the results of this analysis were not sufficiently comprehensive to allow an evaluation of the possible relationship between the orientation of a precipitate crystal and its growth characteristics. It should be noted however, that the use of micro-focus Laue and Kossel techniques to examine orientation relationships much more rigorously than has been done in the past, may allow some of Smith's ideas to be tested more fully. There are reports that such work is underway (27).

Although Smith's theory hinges on the proposal that dislocation boundaries are immobile at low degrees of undercooling, no real discussion of the possible structure or the migrational mechanisms available to the interface, was given. If, following Christian (6), the boundary is proposed to contain both glissile and non-glissile dislocations, motion of the boundary should produce a shape change. As this shape change would produce a higher strain energy than that of the transformation of the same volume without a change of shape (6), the low surface energy term of equation 2.2 may be outweighed by the strain energy, thus suggesting a reason for the undercooling required to form Widmanstatten plates. As was the case for the simple epitaxial boundary however, (with non-glissile interface dislocations) it is hard to see why this shape change should not be at least partially removed by the diffusional atom movements accompanying growth.

### 3.3.4 Ledges - Aaronson (20, 24-26)

Another approach based on considerations of interfacial structure and a possible growth mechanism for semi-coherent boundaries, has been proposed by Aaronson. From the observation that precipitate lattices are always oriented with respect to the parent (and essentially following Smith (21)), Aaronson believes that at least portion of the enclosing interphase boundary must consist of areas of relatively good atomic matching, and that, within such areas, the interface consists of elastically strained coherent regions separated by rows of dislocations. The Widmanstätten morphologies are envisaged as arising from a kinetic and geometric advantage given to these boundaries, by the incorporation of small steps or ledges, at high degrees of undercooling. Allotriomorphs, on the other hand, develop from the movement of the large incoherent segments of interphase boundary and this case has already been discussed.

Considering the austenite to proeutectoid ferrite transformation to exhibit the exact KS relationship, with the close-packed  $\{111\}_F$  as the plane of the interface, or habit plane, Aaronson proposed that, in this case, the lattices match well only along  $\langle 110 \rangle_F$  and accordingly that the boundary is more likely to consist of incoherent regions separated by semi-coherent strips. The semi-coherent portion is assumed to exert a dominant influence on the migrational characteristics of the boundary and is considered in some detail.

In adopting the view that the interface plane is a plane achieving good atomic matching of the two lattices, Aaronson's theory would seem to be limited to rational low index habits and, in the two cases which

he has examined in detail (20), he has nominated the parallel low index planes (given by the experimentally determined orientation relationship), as habit planes. Any small changes in orientation of the boundary, brought about by, say, transformation strains, are proposed to lead to the development of small disordered ledges on the initially planar interface, as was shown in Figure 2.5, and this is the general structure of Aaronson's semi-coherent boundary.

In the sense that they can grow only by the lateral movement of these ledges (neglecting climb) the broad faces of a semi-coherent boundary advance discontinuously with time. The boundary remains stationary until swept by a ledge whence it advances an amount equal to the step height. Aaronson (79) has measured the rate of thickening of ferrite plates and suggested that the results are consistent with a ledge growth model.

Using transmission electron microscopy Laird and Aaronson (25, 26) made a dynamic study of the ageing of thin foils of aluminium/15% silver heated by the electron beam. In this work they identified the dislocations present at the broad faces of the platelike precipitates and were also able to measure the precipitate growth kinetics. They concluded that the kinetics and morphology were best accounted for by assuming the broad faces to be of the semi-coherent dislocation type of interface which grew by the lateral movement of ledges. Observations of precipitate behaviour in thin foils however, may not be representative of the events taking place in bulk specimens; this view is enhanced by Laird and Aaronson's earlier observation (24) that the morphology, crystallography and kinetics of transformation of copper/aluminium precipitates

depend on the nature of the specimen (viz: foil or bulk aged samples). In other transformations the evidence for ledges is scant and Aaronson merely extrapolates the concept of a ledge to include all Widmanstätten transformations. In the iron/carbon system for example, the single photomicrograph depicting "superledges" on a proeutectoid ferrite plate is quite unconvincing (20). Thus although most of the evidence for ledges is of an indirect nature, Malcolm and Purdy (110) have found that the faces of Widmanstätten  $\alpha$ , precipitated from  $\beta$  in a copper/39.6% zinc alloy, consisted of equal areas of nearly orthogonal planar segments of  $\{231\}_\beta$  near  $\{335\}_\alpha$ . These steps appear to be different from the incoherent ledges of Aaronson's theory, but the possibility of incoherent lateral ledge motion on a submicroscopic scale was not discounted by these workers.

In a discussion of Laird and Aaronson's interpretations of the aluminium/silver transformation, Christian (23) has pointed out that no clear distinction is drawn between atomic steps or ledges (transformation dislocations) and regions of misfit on a planar interface (interface dislocations), and that if Aaronson's ledges are in fact the former, the usual restrictions on dislocation climb may not apply. The fairly specialised nature of the f.c.c. to h.c.p. transformation, which possesses a rational habit plane and can be achieved by a homogeneous shear on alternate atomic planes on a parallel set of  $\{111\}_F$ , renders extension of the proposed mechanism to other transformations rather tenuous. Equally well, the rigid "diffusional" approach used by Aaronson in the disordered edges-of-ledges model would seem to be limited, especially in view of some similarities of the proposed structure

of the interface to that of a martensitic boundary (49). Furthermore it is not at all clear how the disordered ledges can produce a shape change (as has been proposed) because migration of disordered boundaries does not allow the existence of a correspondence.

### 3.3.5 Martensitic Theories

In all cases, martensite is observed to form as plates, laths or lenses, the latter usually being considered as plates which have been modified by the accumulation of elastic and plastic strain of the lattice. Also, it is implicit in the hypothesis that the change of shape can be described as an IPS, that the product forms as plates, with the habit plane as the unrotated plane of the IPS. Plate morphologies therefore, are an essential characteristic of martensitic transformations and it is of interest to examine the application of martensite theory to Widmanstatten transformations.

Surface relief effects accompanying the transformation of Widmanstatten ferrite in steels were first reported by Miodownik (63) who suggested the possibility of growth by a martensitic mechanism. There have been numerous subsequent verifications that the relief effects exist and that they are very similar to those produced by martensite (8, 64-68), as well as observations (66) that the proeutectoid cementite reaction exhibits similar characteristics when the product is Widmanstatten. Furthermore, there is now evidence (9) that the Widmanstatten  $\alpha$  transformation occurring in brasses on either isothermal transformation or on slow cooling (as differentiated from the ageing type experiments of Garwood (10)) also shows relief of the correct form. Laird and Aaronson (25) reported "martensite like" relief effects accompanying

their f.c.c. to h.c.p. transformations in an aluminium/silver alloy although, as Clark and Wayman (8) have emphasised, their work was not rigorous and no indication was given of how nearly the relief effects are described by an IPS. In all of these examples composition changes accompany the transformation suggesting that they have the dual characteristics of bainitic transformations already considered.

Following the reasoning of Mehl et al, Spretnak and Speiser (111) hypothesised, mainly from conclusions drawn from the nature of orientation relationships and kinetics, that the  $\delta \rightarrow \alpha$  transformation proceeds by shear. To substantiate this claim, Eichen and Spretnak (112) examined the movement of the  $\delta/\alpha$  interface in pure iron using thermionic emission microscopy and pointed to the observed discontinuous propagation with time as evidence of the proposed shear mechanism. Christian (in a discussion of reference (112)) criticised the criterion used by Eichen and Spretnak, maintaining that discontinuous boundary movements can be explained by several alternatives (eg. ledges). However, he supported the general concept of a change from the nucleation and growth mode, characteristic at high temperatures, to a martensitic or shear mode at lower temperatures.

Otte and Massalski (113) claimed that the habit planes of some nucleation and growth transformations (Widmanstätten) could be approximately predicted by using the theory of WLR. No attempts have been made to apply the theory in detail to such transformations but the significance of the similarities of so many of the crystallographic properties to martensite has recently been a topic of controversy (8, 6, 11, 20). In particular, the significance of the geometric

and crystallographic features, especially the change of shape, has been questioned.

Aaronson's objections (11, 20) to shear mechanisms describing "diffusion controlled" transformations in iron/carbon alloys are two-fold:

- a) the thickening kinetics of plates cannot be described by the rate of carbon diffusion away from the interface.
- b) the reaction: austenite to supersaturated ferrite, at the temperature involved, appears to be thermodynamically impossible.

However, the crystallographic theories, being phenomenological, make no attempt to describe the mechanism, and hence the kinetics, of the transformations they describe and any success achieved by application of the theory to a particular transformation must be regarded as the most significant test of the various proposals relating to the mode of transformation.

---

CHAPTER 4THE NATURE OF THE PROBLEM.

Normally the concept of a lattice correspondence is associated with a diffusionless mode of transformation, since each atom occupying a lattice site in the parent crystal moves to a "corresponding" lattice site in the product crystal as it is transferred across the interface. The observation that a change of shape, and therefore a correspondence, occurs in several Widmanstätten precipitation reactions, suggests that in this case at least some of the atoms do not undergo displacement as a result of the homogeneous strain during transformation, but rather are transported over distances of the order of the precipitate dimensions by diffusional processes. These transformations then, seem to require atom movements of the kind that distinguish martensitic transformations as well as those which are characteristic of diffusional transformations. The view which is to be tested in this thesis is that the crystallographic and morphological properties result from the movement of a semi-coherent interface of the martensitic type, while the kinetics result from the need for accompanying diffusion.

In interstitial solid solutions this model is realizable and has already been applied to the formation of bainite (56, 72). The solvent atoms are regarded as being relatively immobile and are homogeneously strained during transformation, while the highly mobile solute atoms may effect the composition change by diffusion, without destroying the correspondence (6).

The question of segregation prior to or following the passage of the interface is most important in developing a model for these trans-

formations and has been partially discussed following different proposals for the bainite reaction in steels. In lower bainite the "intermediate" transformation product is usually taken to be supersaturated ferrite, in which case the interface must separate regions of identical composition and is, in a sense, like the boundary of diffusionless martensitic reactions. Carbide precipitation takes place behind the interface and presumably only influences the interface indirectly through the release of lattice strain.

The formation of a ferrite nucleus with a different composition to that of the parent austenite eg. Widmanstätten ferrite or upper bainite, immediately leads to an increase in the carbon content to the austenite adjacent to the interface and interpretation of the events leading to the propagation of the boundary is not simple. The possible sequence of events could be:

(i) Supersaturated ferrite is formed by a martensitic mechanism followed by draining of the carbon back through the interface to the austenite.

ie. displacement followed by diffusion.

(ii) Segregation of carbon ahead of the interface takes place to produce a carbon depleted austenite which then transforms martensitically to ferrite.

ie. diffusion followed by displacement.

(iii) Simultaneous displacive and diffusive atom movements occur within the interface.

The first model is similar to the proposal for lower bainite except

that the carbon escapes by diffusion to the austenite rather than by precipitation as carbide behind the interface. The second model is essentially that proposed by Entin (89) and Spretnak and Speiser (111) and, although requiring diffusion up a concentration gradient may not necessarily represent diffusion up an activity gradient, as suggested by Aaronson (20), since there are both shape and volume changes associated with the austenite to supersaturated ferrite transition which may affect the carbon activity.

The third model envisages co-operative straining of the iron atoms and diffusion of the carbon within the boundary. The possibility of interface control, by reaction of the carbon atoms with the interface dislocations, could account for the rate of thickening being slower than that expected using a simple diffusion control model. A ledge type mechanism (although not of the disordered type proposed by Aaronson) may not be precluded by the postulation of a martensitic interface, and could also possibly be adapted to this model.

There is no a priori reason for preferring any of these models and indeed, it may be that none of them describes the events actually taking place at the interface. This presents a major difficulty in formal application of the crystallographic theory of martensite formation to the ferrite reaction because the lattice parameters of the phases related across the interface are required in order to determine the elements of the pure strain. Thus, although the concept of both displacive and diffusive atom movements seems in principle to be possible, there are numerous difficulties associated with interpreting the identity of the transitory non-equilibrium phases which must

necessarily be invoked when constructing a model.

An even greater difficulty arises when it is attempted to apply similar reasoning to the case of substitutional solid solutions, for, according to Christian (6) compositional changes involving long range diffusion should continually destroy the correspondence and the shape change. As has already been pointed out, this conclusion is not in agreement with the reports of shape changes accompanying the diffusional transformation in copper/zinc alloys (9, 10). The available evidence indicates that at low temperatures the product is plate-like with an irrational habit plane, faulted and highly supersaturated, while at higher temperatures rods of almost equilibrium composition and with no internal structure, are formed (10, 114-116). Both morphologies exhibit surface relief effects (10, 114) and upquenching from the lower temperature causes a change of morphology (116) just as is the case for bainite (81). The sequence is therefore almost exactly analogous in both cases despite the lack of precipitation in the non-ferrous alloys. Garwood (10) in fact, proposes that the atom movements leading to the change of composition do not take place at the advancing coherent interface but proceed fairly rapidly close behind (similar to model (i)). If Christian's view is correct however, these additional movements should destroy the correspondence.

Whereas the present argument hinges on the belief that the shape change, with its appreciable shear component, indicates a lattice correspondence, Aaronson (118) stated that this need not be generally true. Aaronson believes that the "incoherent edges of ledges" model can simulate a martensitic transformation by producing "geometric"

relief effects even though the unit process is an unco-ordinated diffusive exchange of atoms at the ledge riser. He suggests that in transformations involving diffusion martensitic growth is improbable, if not impossible.

Wayman et al (8, 117) have taken the view that the crystallographic properties cannot be dispensed with so lightly. They support the philosophy that if a unique relationship between all the crystallographic observables can be shown to hold, in accordance with the predictions of the crystallographic theories, then the transformation must be martensitic. This view requires that the shape change, habit plane, orientation relationship and the inhomogeneity be determined experimentally and compared rigorously with the predictions of the theory.

Such an analysis has as yet not been attempted for the Widmanstätten transformations and it is the purpose of the second part of this thesis to report the results of work directed to this end.

An agreement between the predictions of the crystallographic theory and experiment would serve to justify the proposal that the change of shape is indicative of a lattice correspondence, but it is pointed out that this would still leave open the question of the transformation kinetics, for as Aaronson has shown, the kinetics cannot be explained in terms of volume diffusion away from a planar interface.

---

PART II

EXPERIMENTAL

CHAPTER 5INTRODUCTION

The experimental work described in this part was undertaken in an attempt to gain a description of the geometric and crystallographic features of the transformation of austenite to Widmanstätten ferrite in iron carbon alloys, and to determine whether these features could be accounted for using the crystallographic theory of martensitic transformations.

Although not without disadvantages (see Section 6.3.2) the Widmanstätten transformation in iron/carbon alloys recommended itself for several reasons. On purely theoretical grounds, the concept of a lattice correspondence and the accompanying change of shape, observed in conjunction with a composition change, is easily envisaged in the case of interstitial solid solutions (6). The decomposition of austenite by various modes has been well documented, providing a large volume of theoretical and experimental information on which to draw and finally, a change of shape has been reported for this system (64-67).

An alloy of iron/0.45% carbon was used for this investigation and Chapter 6 describes the experimental techniques of alloy preparation and heat treatment adopted, as well as the methods used to study the features of the transformation. The results of experimental investigations of the general morphology and the determinations of habit plane, orientation relationship and shape strain are presented in Chapter 7. An analysis of these results in terms of the Bowles Mackenzie crystallographic theory is given in Chapter 8. Finally, in Chapter 9 the experimental results and conclusions are discussed.

---

CHAPTER 6

EXPERIMENTAL METHODS.

	Page
6.1 Specimen Preparation and Heat Treatment.	90
6.2 The Morphology of Widmanstatten Ferrite.	94
6.3 The Crystallographic and Geometric Features of Widmanstatten Ferrite.	99

6.1 Specimen Preparation and Heat Treatment

Initially two alloys, of 0.38% and 0.45% carbon, were prepared. In both cases 5 k.g. of soft magnetic iron and pure carbon granules were melted and cast in an Hereaus vacuum induction furnace. The ingots were hot rolled to 1 cm. plate and the surface was then ground to remove oxide scale and any decarburised layer.

Ferrite plates isolated from the other morphologies could be prepared more readily in the 0.45% carbon alloy and all the subsequent studies were carried out using this material.

TABLE 6.1

The Composition of the Iron/0.45% Carbon Alloy

C	P	Mn	Si	S	Al
0.45	0.0009	0.15	0.075	0.019	0.05

The formation of Widmanstatten structures requires higher degrees of undercooling than the allotriomorphic and idiomorphic forms and for

an iron/0.45% carbon alloy the  $W_s$  temperature is at least  $80^{\circ}\text{C}$  below the  $\delta/(\alpha+\delta)$  boundary and is approximately  $680-700^{\circ}\text{C}$  (20). Following this, two methods of heat treatment were employed and found satisfactory.

Specimens were cut from the hot rolled plate and surface ground to regular geometric shapes. These were then prepared metallographically on all faces using standard mechanical polishing techniques. In the first method specimens measuring  $0.5 \times 0.5 \times 1.0$  cm. were enclosed in a small "box" made from thin sheet of the same alloy and placed in a 13 mm. bore translucent silica tube. This was then evacuated to  $0.1 \mu$  and back filled with  $1/3$  atm. of dry argon before sealing to form a closed capsule. The silica tubes were baked under high vacuum to remove adsorbed gases prior to introduction of the specimen and container. Austenitizing was carried out for four days at  $1200^{\circ}\text{C}$  and a small amount of titanium turning located in the tube near the container ensured a continual low oxygen partial pressure. The "box" served the purpose of keeping the specimens out of contact with the silica and the titanium turnings. In addition it provided an environment for the specimen of essentially its own composition, and it was hoped that any decarburization, contamination, or thermal etching of the surface would be minimised. Transformation was carried out by transferring the tube and contents to a second furnace which was maintained continuously at  $690^{\circ}\text{C} \pm 10^{\circ}\text{C}$ . It was estimated that the specimen reached the transformation temperature in less than two minutes and isothermal treatment for  $\frac{1}{2} - \frac{3}{4}$  hour was allowed before the tube was withdrawn and cooled to room temperature. Extremely smooth, clean surfaces exhibiting

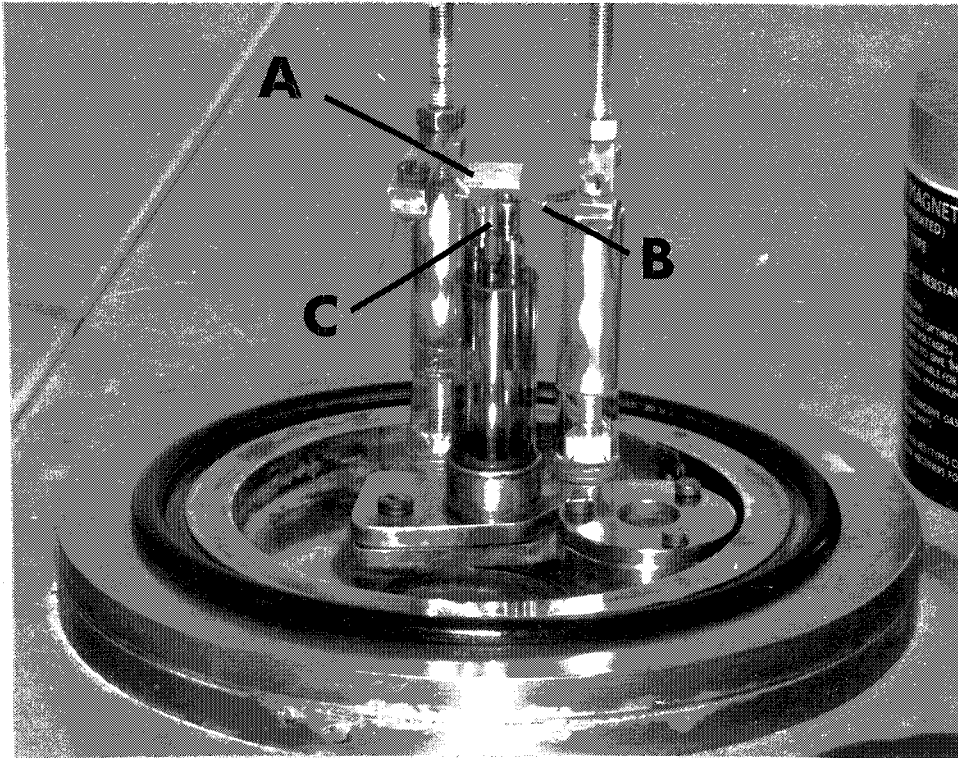


Fig. 6.1 The emission heater with the vacuum bell removed showing:  
Specimen (A) located on thermocouple wires and high tension lead (C) in position to be heated by electrons emitted from filament (B).

fine detail were produced in this way.

The second method employed an electron emission furnace in which the specimen was heated, under vacuum (pressure  $< 0.1\mu$ ), by a current of electrons emitted from a hot tungsten filament at a potential of 1200 volts. Specimens measuring approximately  $1.0 \times 1.0 \times 0.2$  cm. were spot welded directly onto chromel-alumel thermocouple wires and a high tension lead as shown in Figure 6.1. The temperature was indicated continuously and could be varied by adjusting the filament current by means of a variable transformer. Using this apparatus it was found that treatments at lower temperatures ( $1100 - 1150^{\circ}\text{C}$ ) for times of the order of 1 hour produced austenite grains several millimetres in diameter, comparable in size with those produced in the silica capsules. There was, however, some loss of surface perfection due to evaporation and/or crystallographic thermal etching, but the slightly rougher surface in no way impaired the observation of surface phenomena. Quenching was achieved by turning off the filament so that the specimen cooled by radiation to the transformation temperature. The cooling rate was  $20 - 30^{\circ}\text{C}$  per second and the isothermal temperature was reached in less than 20 seconds. The quench was arrested by turning the filament on at a pre-determined current chosen to maintain the specimen at the selected isothermal transformation temperature.

The temperature range over which Widmanstätten structures are the dominant morphology was found to be quite small. At higher reaction temperatures grain boundary and massive morphologies predominated, while at lower temperatures, because of the eutectoid reaction, decomposition to pearlite or bainite occurs with complete suppression of the proeutectoid

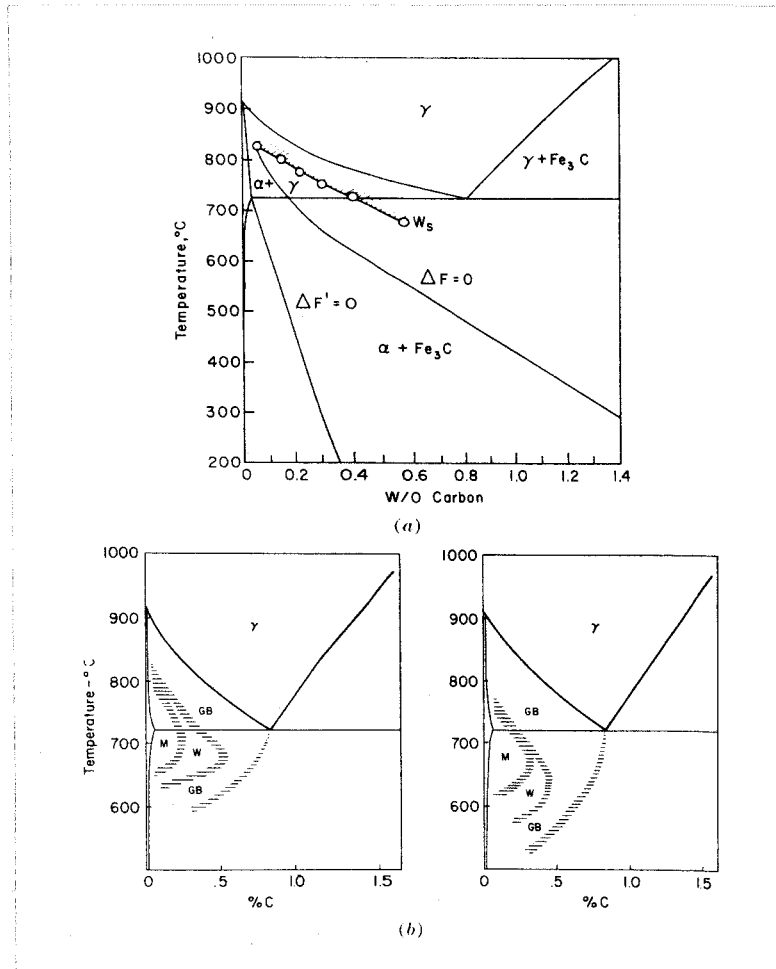


Fig. 6.2 (a) Composition dependence of the  $W_s$  (Widmanstatten start) temperature.  
 (b) Temperature-composition ranges over which grain boundary allotriomorphs (G.B.), Widmanstatten plates (W) and massive ferrite (M) are dominant in specimens with a large austenite grain size (L.H.S.) and a small austenite grain size (R.H.S.).

Aaronson (20)

reaction.

The temperature range over which plates were observed was  $660^{\circ}$  -  $720^{\circ}\text{C}$  and this is consistent with the findings of Aaronson (20), as shown in Figure 6.2.

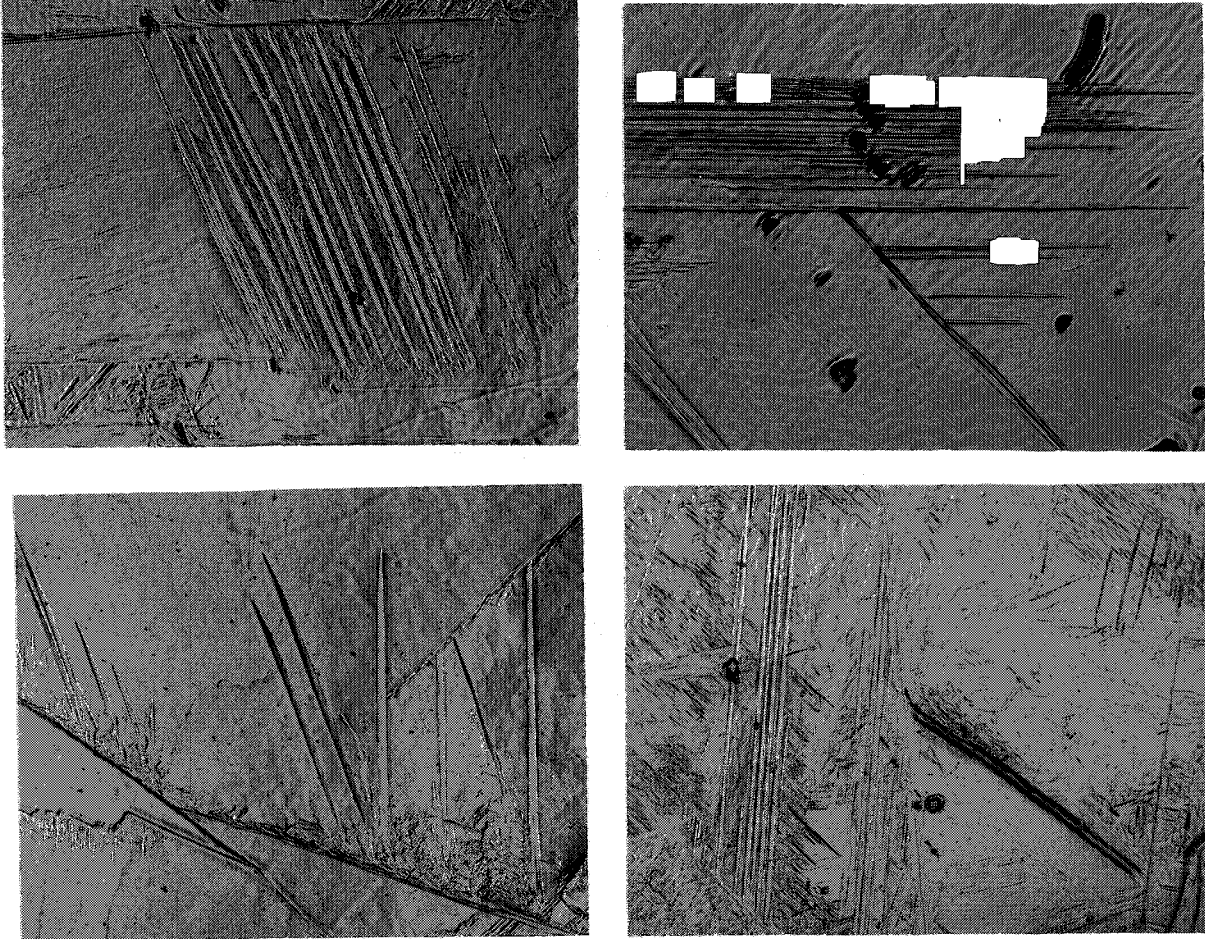


Fig. 6.3 Typical photomicrograph of the surface effects produced in the iron/0.45% carbon alloy isothermally heat-treated at 700°C.

Oblique illumination X 50.

## 6.2 The Morphology of Widmanstatten Ferrite Plates

### 6.2.1 Surface Relief Effects

The observation that Widmanstatten precipitation gives rise to relief effects on pre-polished surfaces has been reported previously for several transformations (8, 63-67). These observations were of a qualitative nature and no attempt has been made to determine the exact nature of the shape change. A study of the shape change accompanying the formation of Widmanstatten ferrite was made therefore, to determine whether the shape change possesses the characteristics definitive of martensitic transformations (1, 8, 35).

Both the methods of heat treatment described in the previous section produced surfaces of high quality and the features of the microstructure could be recognized without etching or any further preparation as shown in Figure 6.3. Thermal grooving of the prior austenite twin and grain boundaries defined clearly these features and the Widmanstatten ferrite plates, especially those formed at lower temperatures, produced easily recognizable relief effects which could be viewed readily using oblique illumination. The other ferrite morphologies produced a smooth flat surface, while in some cases the pearlite could actually be discerned as surface roughness due possibly to small dilatational changes taking place during the formation of the lamellae. Confirmation that the relief effects were associated with Widmanstatten ferrite was obtained by removing the relief surface with light polishing on a diamond polishing pad and then etching in nital, (Figure 6.4).

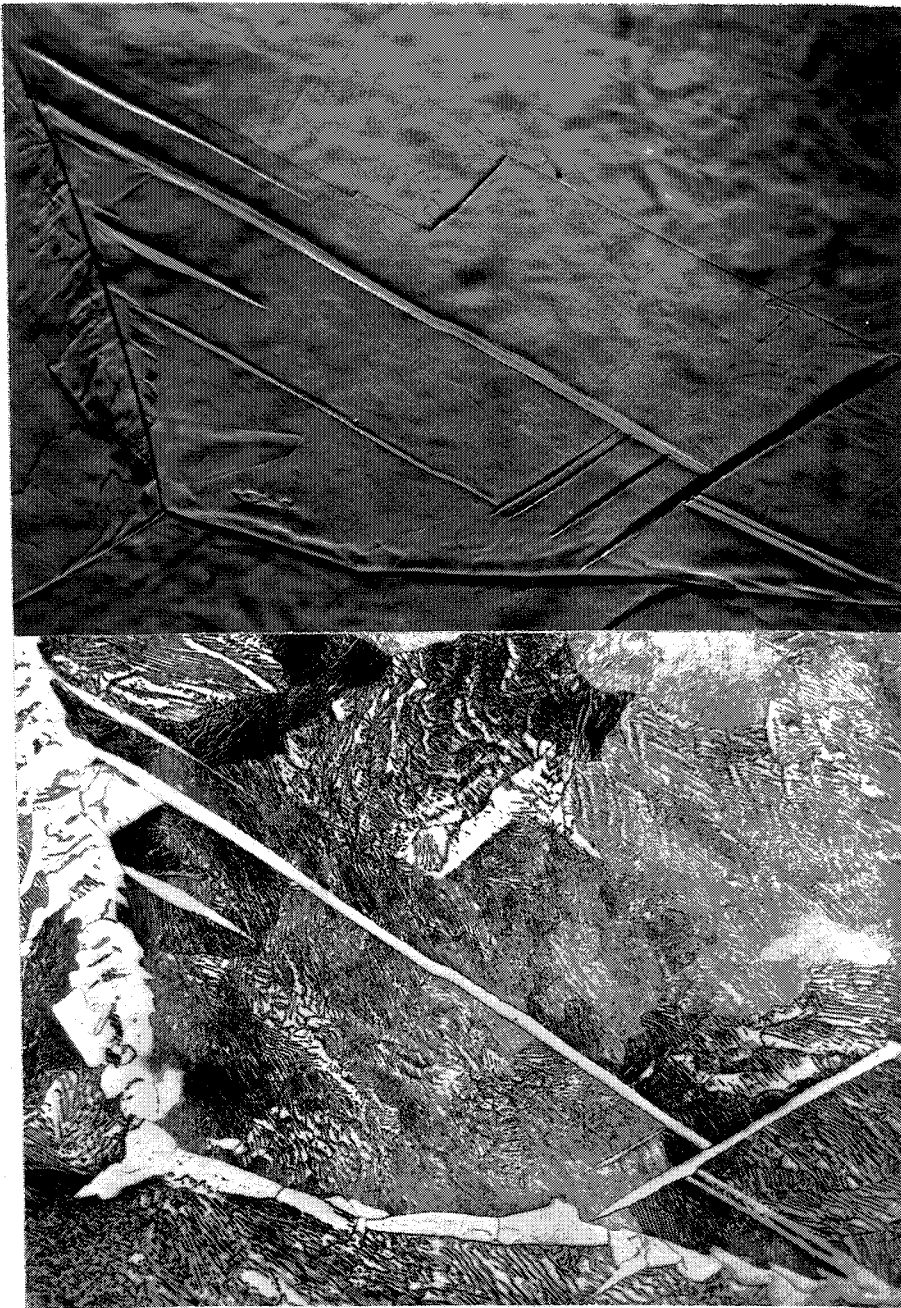


Fig. 6.4 (a) Widmanstätten sideplates exhibiting surface relief effects. Oblique illumination X 500  
(b) Same field after polishing and etching in nital.

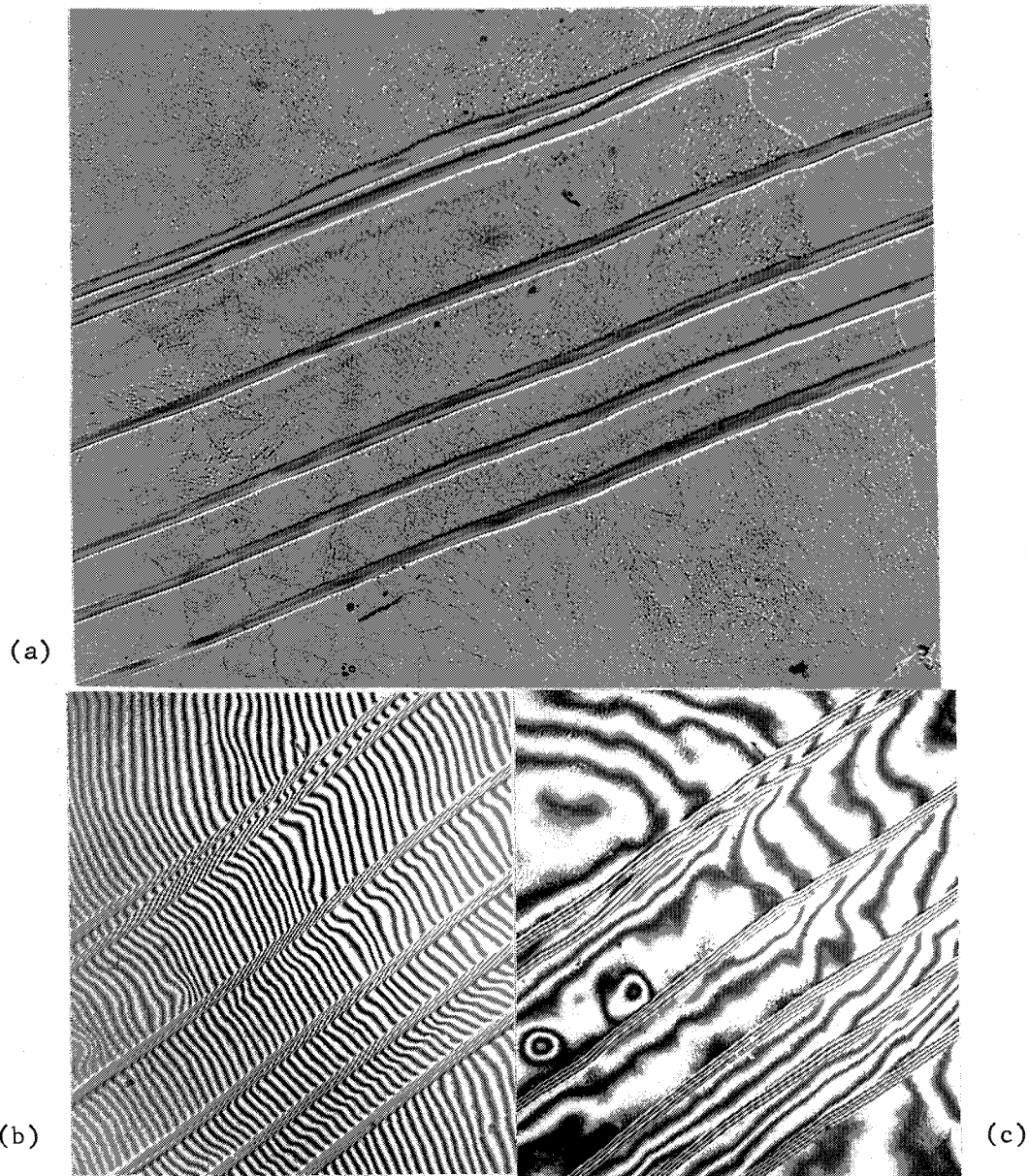


Fig. 6.5 (a) Photomicrograph of a group of parallel plates in pearlite matrix. Oblique illumination X 250  
 (b) Interferogram of same field with the optical flat uniformly inclined to the specimen surface. The deviation of the parallel fringes, where they cross the plates, indicates that the surface remains plane but is tilted with respect to the pearlite matrix. approx. X250  
 (c) As for (b) with the optical flat parallel to the specimen surface. Adjacent fringes now represent vertical height differences on the specimen of  $\lambda/2$  and are seen to be parallel to the plate trace indicating a simple rotation of the surface about this direction. approx. X250

(a) Interferometry

A Leitz Wetzlar two beam interferometer with monochromatic light ( $\lambda = 5,500 \text{ \AA}$ ) was used to study the form of the relief effects. This instrument combines light rays reflected from an optical flat with rays reflected from a specimen surface, to produce a pattern of interference fringes which allows the topography of surface features to be examined quantitatively, since each fringe represents an optical path difference of  $\lambda/2$ .

By adjusting the optical flat to be parallel to the pearlitic areas adjacent to a ferrite plate, a series of fringes mounting the tilted region can be produced. Under these conditions the fringe spacing on the pearlite should be a maximum and, if in the region transformed to ferrite, the original surface remains plane and is simply tilted about the trace of the habit plane in the surface, then the fringes should be parallel to one another and to both traces of the plate. Although this condition is almost satisfied, Figure 6.5 (c), the general rumpling of the surface produced during heat treatment rendered it impossible to determine whether it was satisfied exactly. The interferograms show that the change of shape can be described, at least approximately, by a simple rotation of the transformed region about its surface trace, but small rotations of this trace out of the specimen surface may not have been detected.

The angle of tilt was calculated from the relationship:

$$\text{Angle of tilt} = \tan^{-1} (\lambda/2d)$$

using the setting of the optical flat described above, where d is then the projected, magnified distance between adjacent parallel fringes.

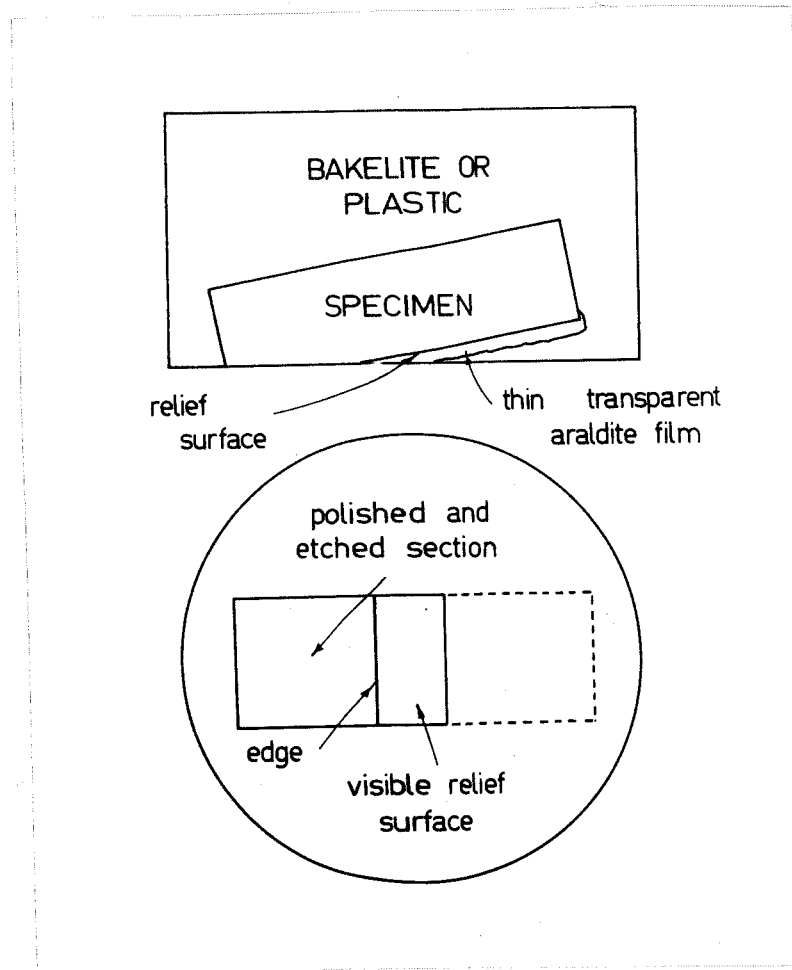


Fig. 6.6 Showing the method for taper sectioning which allows the relief surface to be directly correlated with the microstructure, as well as permitting the nature and sense of the tilt to be recognised.

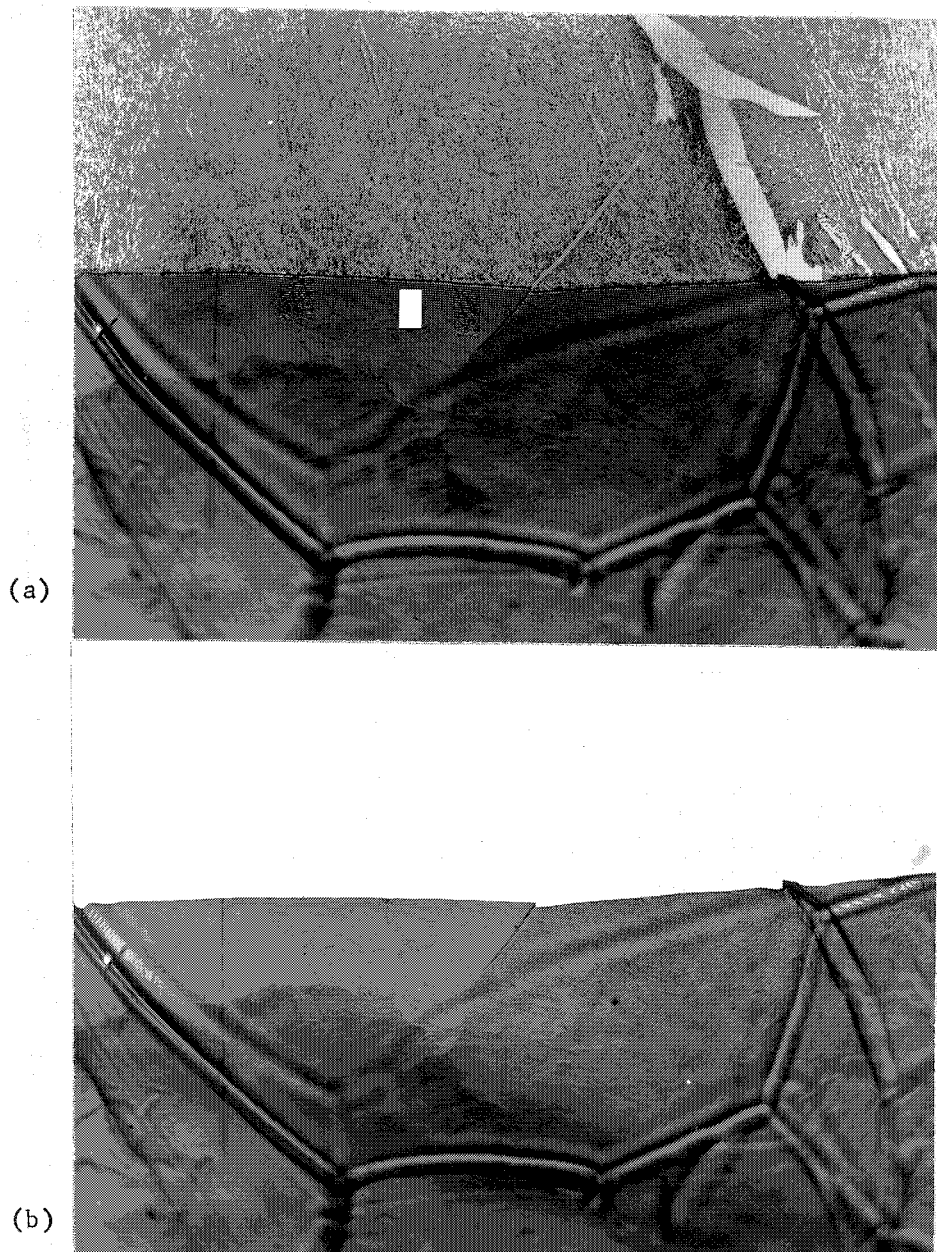


Fig. 6.7 Taper sections showing a thermally etched prior austenite grain boundary and a small Widmanstatten plate in both relief surface and polished section, (a) etched and (b) unetched. X 250  
Note the interference fringes visible at the thin edge of the plastic wedge. The tilting of the surface by the plate and the grooved grain boundary are revealed by the edge contour.

The fringe spacing was measured on a 35 mm. negative of calibrated magnification, using a Cambridge Universal Measuring Machine.

(b) Taper Sectioning

Taper sectioning, to reveal small surface details and microstructure simultaneously, is a standard technique in which the surface to be examined is usually electroplated with a metal of similar hardness in order to retain a sharp edge during cutting and polishing. Using this method the original surface is revealed at an edge in section, with the surface contours being effectively magnified by the lateral displacement to an extent that depends on the angle of section. The remaining unexposed surface is completely hidden by the electroplated material.

In order to overcome this limitation a modified technique (9) using a hard, adherent, transparent plastic, in place of the electrodeposited metal, was developed to protect the edge. This method allows the original surface to be viewed through the thin wedge of plastic (Figure 6.6). Unidirectional micropolishing with the thin edge of the plastic wedge "trailing" was used to retain a sharp interface. The surface, the nature of the tilt and the corresponding microstructure could be viewed together, with the relief surface running off into an "out-of-focus" position because of its inclination to the polished surface as shown in Figure 6.7. The use of high magnification microscopy is restricted because of the limited depth of focus in viewing the relief surface.

This method was found to be superior to sectioning normal to the surface since it allowed effective magnification of the relief effects, superior edge retention, and simultaneous observation of the surface



(a)

(b)

Fig. 6.8 Microstructure of a heat treated specimens after scratching, obtained by light polishing to remove the relief surface and etching in nital. X 50  
(a) Directly beneath the scratches.  
(b) Remote from scratched area.

relief effects and the corresponding microstructure. The photomicrographs in Figure 6.7 confirm the interferometric observation that Widmanstätten plates of ferrite give rise to relief effects similar to those of martensite.

(c) Scratch Rotations

In order to carry out shape strain determinations on iron/carbon and iron/manganese/carbon martensites, which have an  $M_s$  above room temperature, Dunne (122) designed a modification for the emission heater which allowed the specimen surface to be scratched at high temperatures prior to transformation. A small brush of aluminosilicate rope, mounted on a rod introduced to the vacuum chamber through a Wilson Seal, enabled scratches in several directions to be produced on the prepolished surface while the specimen was continuously heated from below.

In the present study specimens were scratched at temperatures near  $1000^{\circ}\text{C}$  just before quenching to the isothermal transformation temperature of  $680^{\circ}$ .

Microscopic examination of the surface showed that copious nucleation of unwanted morphologies was induced by the scratching and their presence precluded the method being used for this alloy.

By searching the relief surfaces for plates intersected by scratches, a few examples were obtained, which showed qualitatively that scratches are simply rotated by the macroscopic transformation strain (see Section 7).

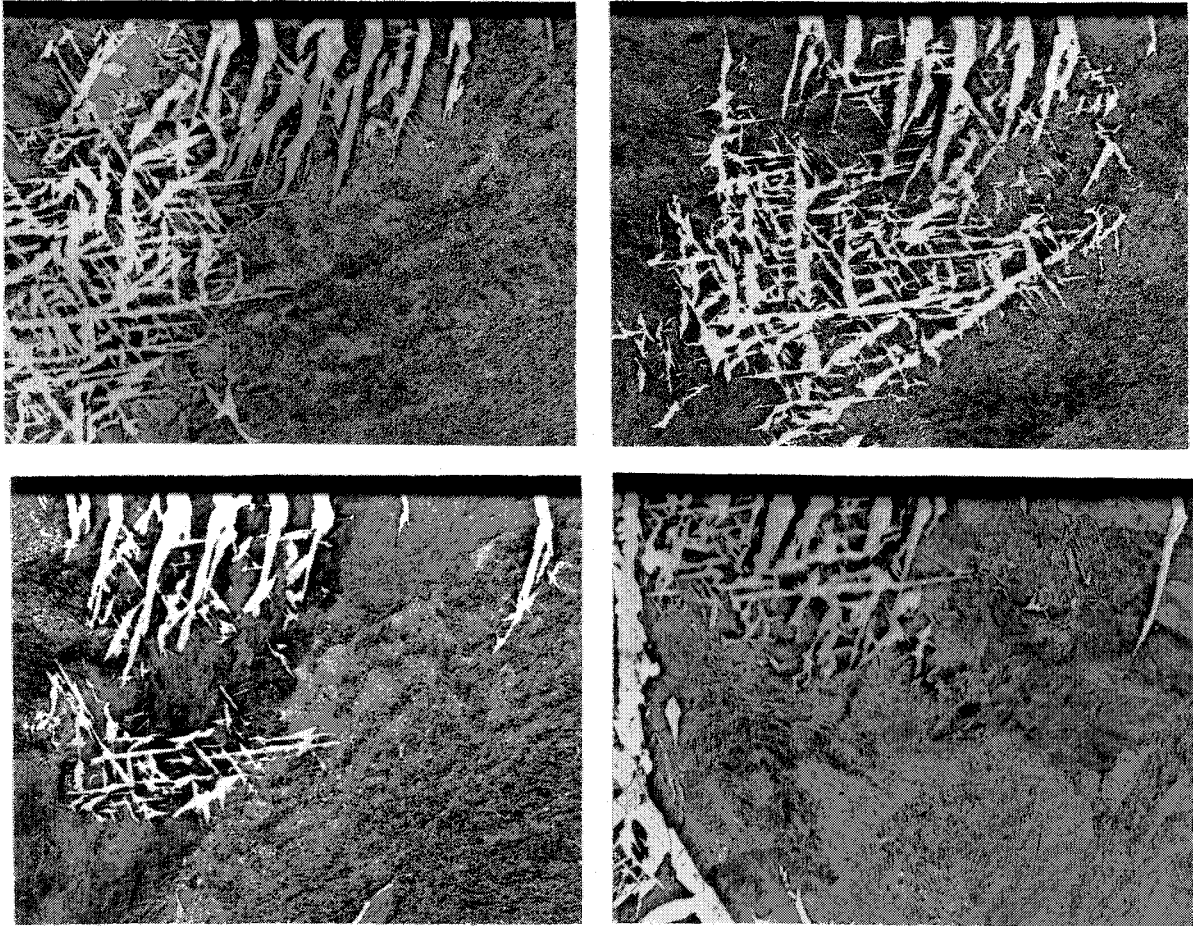


Fig. 6.9 Micrographs of successive parallel sections taken through a group of Widmanstätten plates. The specimen free surface coincides with the top edge of the micrographs. X 100

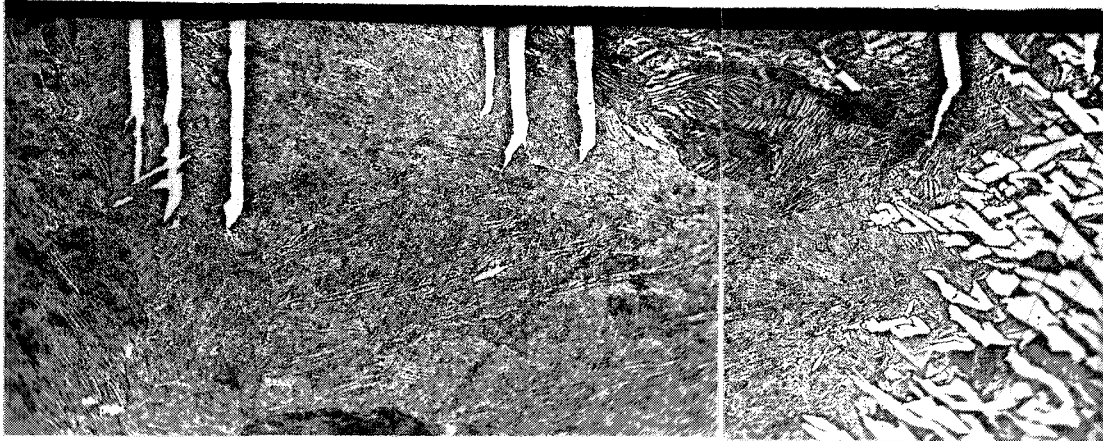


Fig. 6.10 Normal section through a group of parallel plates showing surface tilting and change from simple lath morphology at some depth below the surface. X 250

### 6.2.2 The Shape of Ferrite Plates

By successive sectioning perpendicular to the relief surface at a number of positions along the length of a tilted region, it was possible to gain a full description of the morphology of the underlying micro-constituent, Figure 6.9. In order not to damage the original relief surface during the cutting and polishing it was painted with a transparent laquer. The preliminary cutting was carried out using a surface grinding machine, followed by abrasion on wet silicon carbide papers, again with the edge containing the detail always "trailing".  $30\mu$  and  $8\mu$  diamond impregnated bakelite laps were used as an intermediate stage before final polishing on  $1\mu$  diamond napless cloth. It was found that the techniques produced a sharp edge only at the expense of surface finish and for the photomicrographs shown, the specimens were finished by careful polishing on a  $1\mu$  napped cloth for just sufficient time to remove the heavy scratches, accepting that this inevitably resulted in some edge rounding.

The appearance in section of a typical specimen is shown in Figure 6.10. In view of the length / depth ratio, the best description of the shape of the precipitate is probably that suggested by Wayman and Clark (8), namely a lath. These narrow plates or laths were found to have lengths in the relief surface often of the order of the parent grain size ( $\approx 1$  mm.) while their thickness was usually in the range  $5 - 25\mu$ . The shape of the laths in section will be discussed in detail in the results.

### 6.3 The Crystallographic and Geometric Features of Widmanstätten

#### Ferrite

##### 6.3.1 Introduction

The results of the preliminary studies of precipitate morphology described in the previous sections show that Widmanstätten ferrite has a lath shape with a recognizable habit plane and an accompanying change of shape that is described closely, if not exactly, by an invariant plane strain.

The remaining sections of this chapter describe the experiments made to determine the crystallographic indices of the habit plane and the austenite/ferrite lattice orientation relationship, and the magnitude and direction of the macroscopic shape strain.

##### 6.3.2 The Austenite Lattice Orientation

One of the major experimental limitations of the use of iron/carbon alloys as a system for investigation was that, because of the eutectoid reaction, the parent austenite is not retained at room temperature and the orientation of any prior grain must be determined from  $\{111\}_F$  annealing twin boundary traces. The twin vestiges method often used in studies of martensite and bainite reactions where 100% transformation may occur was of limited use in the present studies since twin vestiges cannot be detected in etched pearlitic microstructures. The thermally etched twin traces in the original relief surfaces, however, could be readily recognized and measured.

When an austenite grain containing suitable ferrite laths and annealing twins can be observed on two non-parallel relief surfaces, measurement of the traces of two non-parallel twins in the two surfaces is sufficient

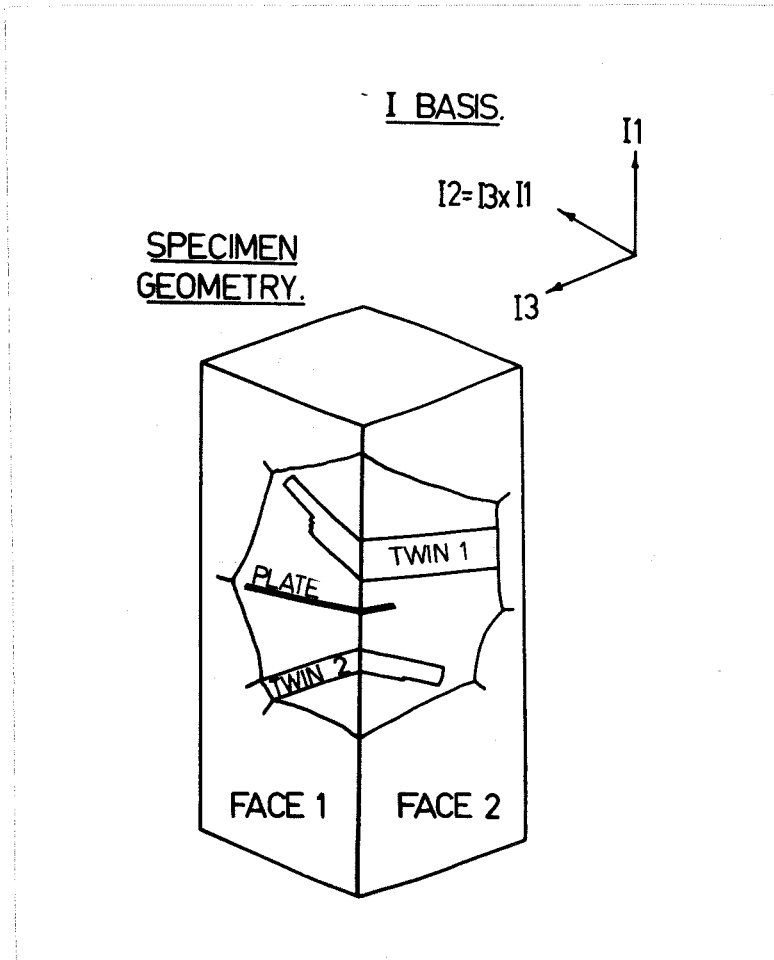


Fig. 6.11 The specimen geometry and the orthonormal I basis defined by:

$I_1$  = Positive direction of the edge between faces 1 and 2.

$I_2$  =  $(I_3 \times I_1)$

$I_3$  = Normal to face 1.

to define two  $\{111\}_F$ , and therefore, to define the orientation of the austenite lattice. Any additional information, such as other twin traces or thermally etched lines, provides a check of internal consistency of a determination based on the minimum data.\* If only traces from one surface are used then a minimum of three of the possible four must be observed and the orientation may be determined using the tables computed and compiled by Otte and Drazin (123).

All trace measurements were made on a Bausch and Lomb research metallograph with a rotating stage calibrated to  $0.1^\circ$ . The angle between adjacent faces of the specimen was determined with a two circle goniometer graduated in minutes of arc.

Trace measurements need to be referred to a selected basis and an obvious choice is that of the specimen geometry, hereinafter to be called the I basis. This is shown in Figure 6.11.

Because of experimental error the twin poles determined from trace measurements will usually be in error and the angle between them will deviate from the exact  $70^\circ 32'$  by a small amount, so that some method of adjustment is necessary if these are to be used to define a cubic lattice. One way of doing this is to assume arbitrarily, or from the confidence of the observation, that one of the poles, say  $T_1$  and the vector product  $(T_1 \times T_2)$ , are positioned correctly and then to adjust the second pole in the zone  $(T_1 \times T_2)$  by fixing it at the correct angle to  $T_1$ . The three  $\langle 100 \rangle$  of the austenite so determined can then be used to define an orthogonal set of base vectors, the F basis, which is

---

\* The minimum data is actually the traces of a single twin in two surfaces and one other twin trace, giving two possible (twin-related) solutions.

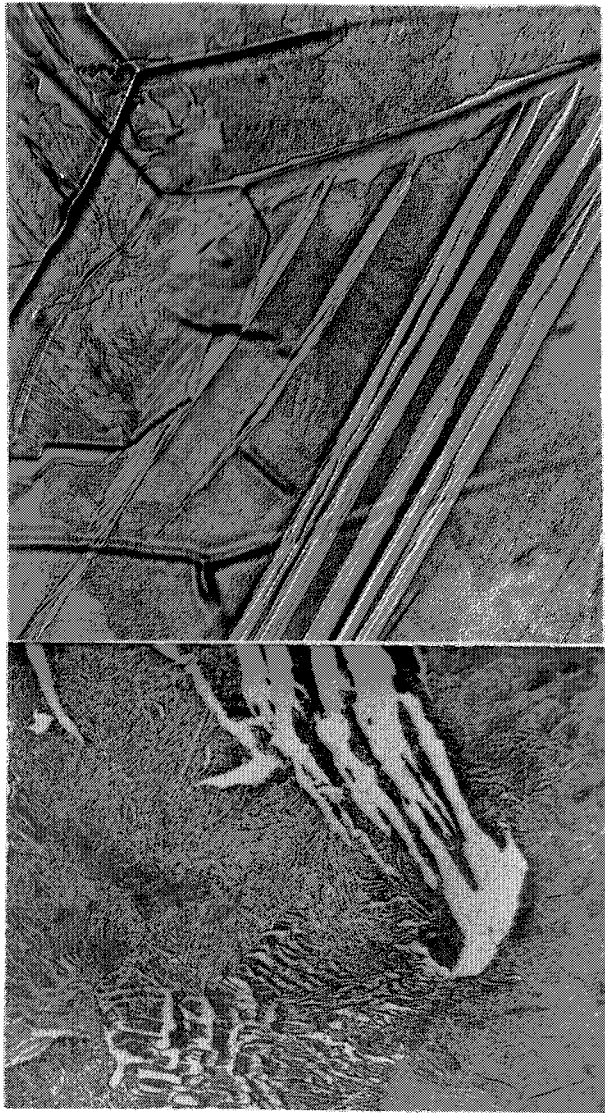


Fig. 6.12 A specimen prepared for two surface habit plane trace analysis. X 250

related to the specimen (I) basis through the (3 x 3) transformation matrix:

$$R = \mathbb{I}F$$

where the successive columns of R are the base vectors  $[100]_F$ ,  $[010]_F$ ,  $[001]_F$ , referred to the I basis.

This matrix reportedly (122) varies only slightly from a rotation matrix derived by a much more complicated least squares analysis of trace data and this method of adjustment was considered adequate for many of the numerical methods used in later sections. In most cases stereographic methods using the initial trace data were used for the habit plane determinations and for preliminary, approximate determinations of the orientation relationship.

In addition to non-systematic errors accumulated in measurements, systematic errors, incurred through the possibility of submicroscopic stepping of the twin boundaries, usually limit the overall accuracy of the twin trace method to about  $1^\circ$  (122).

### 6.3.3 The Habit Plane

To determine the habit plane of Widmanstätten laths exhibiting surface relief effects, the parent austenite orientation was first determined using twin trace methods and then the grain sectioned so as to allow the habit plane of the plate to be determined from its traces in two nearly perpendicular surfaces, as shown in Figure 6.12. This was usually achieved by polishing parallel to, or normal to, face 2 until a cross section of the plate was exposed. The traces of the plate in the two surfaces define a plane, the habit plane, which can be expressed in the crystallographic F basis through the common basis I.

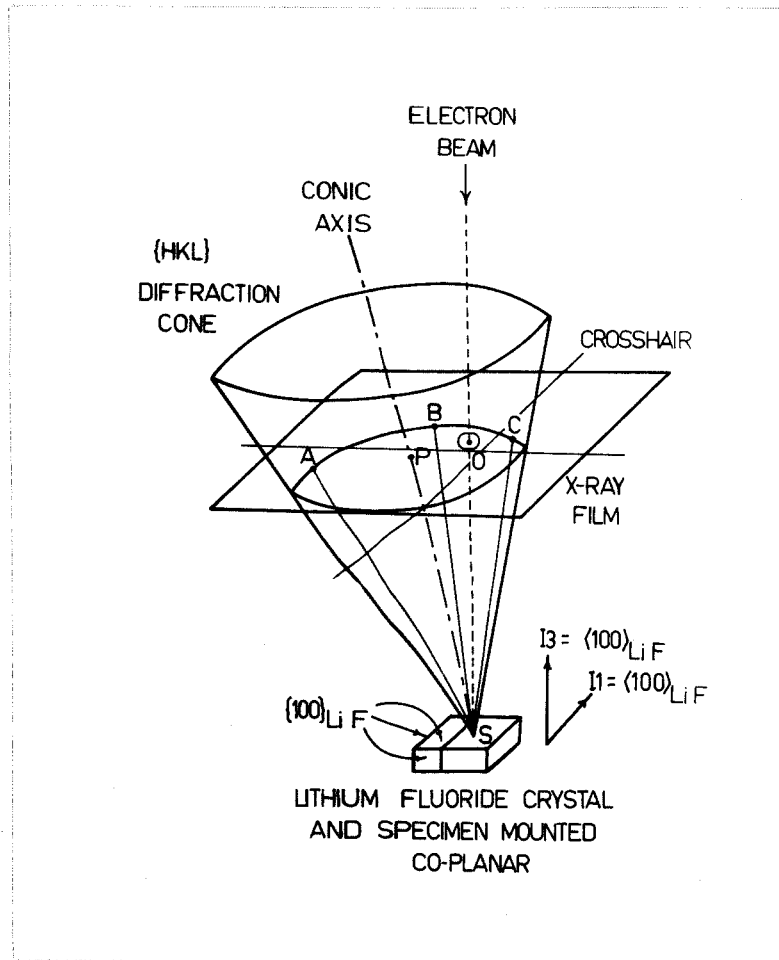


Fig. 6.13 The geometry of the Kossel camera. The three points A, B and C define the conic on the film and allow the conic axis SP to be determined, with reference to the M basis. Lithium fluoride reflections allow the I basis to be represented on the film and so the positions of conic axes can be related to the specimen geometry.

It was found that the traces of the laths in the relief surface were long, straight and well defined and could be measured accurately (as evinced by least squares deviations on several measurements of the same trace; these were usually of the order of  $\pm 0.5^\circ$ ). The trace in the second surface was usually far less well defined, especially if the plates had limited depth, or rounding of the surface corner occurred during polishing. The "plate-with-tail" effect shown in Figure 6.10 made more difficult the recognition of a habit "plane", but it was found that, with careful polishing, the largest laths consisted a parallel-sided portion adjoining the tilted surface. In this region trace measurements were easily made in both surfaces. For the "tail", which was tapered, only an average or median direction was measured in the second surface.

#### 6.3.4 The Ferrite Lattice Orientation

An obvious problem in determining the lattice orientation of a chosen ferrite lath is the lath size. Two possible methods presented themselves, the microfocus Laue and the Kossel techniques. After preliminary considerations the latter method appeared to hold the most promise and the Laue technique was not pursued.

An A.R.L. electron probe microanalyser, fitted with facilities for back reflection Kossel analysis, provided a means of determining the orientation of selected ferrite laths in the relief surface. An optical system on this instrument allowed continuous viewing of the part of the specimen exposed to the electron beam. The geometry of the apparatus is shown in Figure 6.13.

In the microanalyser, a focussed electron beam excites a divergent cone of characteristic X-rays from a point source ( $\approx 5\mu$  dia.) on the

specimen surface, which, when diffracted by the lattice, give rise to characteristic patterns where the diffracted cones intersect the film. Operating at the maximum voltage of 30 k.v. and sample currents of  $1\mu$  amp. required exposure times of approximately one minute using double-sided, high contrast X-ray film.

The contrast between the Kossel lines and the background is the principal limiting factor of this method. In general the contrast is low for back reflection conditions because of the high background produced by the X-ray continuous spectrum. Contrast is decreased further by decreasing crystal size, decreasing crystal perfection and increasing alloy content, so that the technique is somewhat limited in its possible applications. For example, Dautovich (119) obtained no patterns from  $\{225\}_F$  martensite plates of similar size to the present Widmanstätten precipitates, while McGirr and Malin (124) showed that deformation of more than 10% in annealed copper crystals prevented reflections.

The method of analysing the Kossel patterns was that used by McGirr and Malin (125). These workers devised a general method for determining the orientation of crystals with cubic symmetry from the positions of the conics on the film. It is essentially a geometric solution, which is analytically inexact since it assumes that the centre of the system is the centre of the punched hole carrying the aperture for the electron beam. Their analysis also requires that the specimen to film distance be known but, because of the complicated geometry of the camera, this cannot be measured precisely.

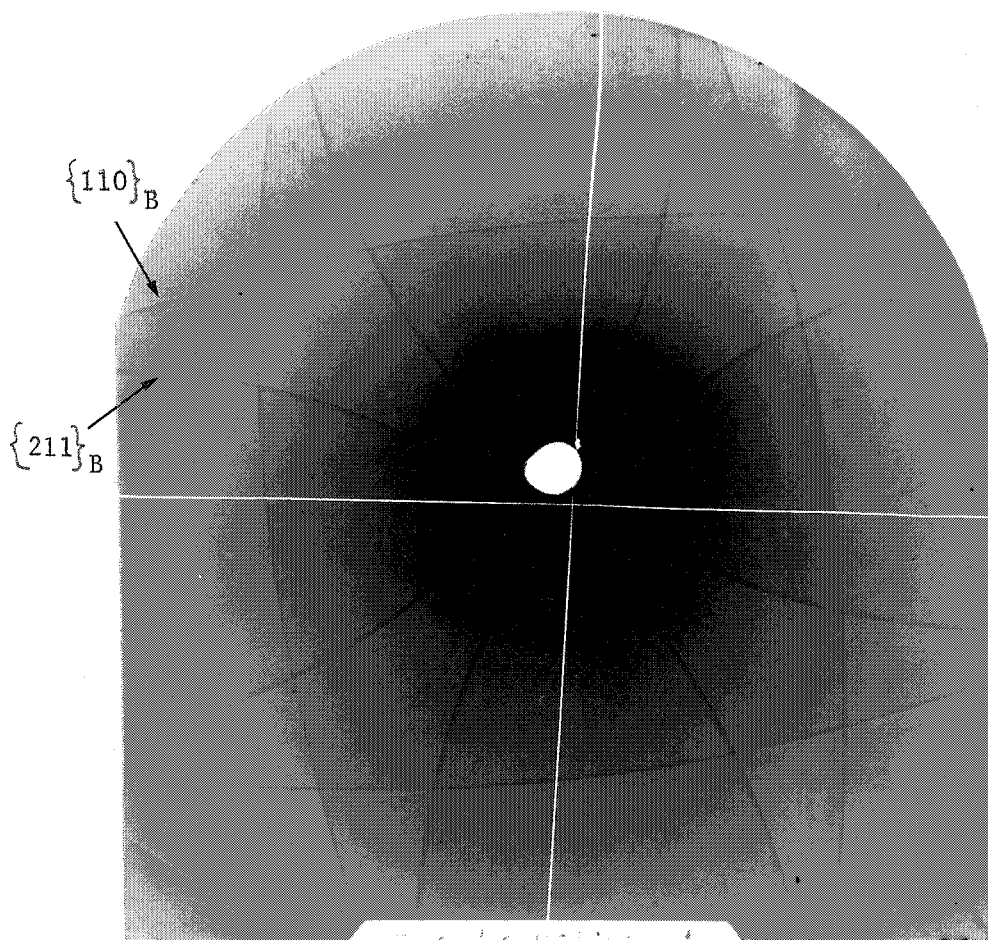


Fig. 6.14 A typical back reflection Kossel pattern obtained from a large grain of electropolished ferrite.  $K_1$  and  $K_2$  doublets are resolved on each of the symmetrically disposed  $\{110\}$  and  $\{211\}$  diffraction cones. The cross wires imaged on the film, provide a reference for measuring the spatial position of the conics.

The method consists of marking each conic at three widely spaced points, A, B, C, as shown in Figure 6.13 and measuring the cartesian co-ordinates of these with respect to the assumed centre, O. Two fine wire crosshairs imaged on the film during exposure (Figure 6.14) allowed each film to be placed in a Cambridge X-Y measuring machine in a standardized fashion with a high degree of reproducibility. In this way an arbitrary, orthogonal X-Y-Z measuring basis, M, was established with the X direction parallel to the horizontal crosshair, the Y direction in the plane of the film and perpendicular to X, and Z the direction  $(X \times Y)$ , or the film plane normal. Referring to Figure 6.13, S is the origin of the X-rays on the specimen, SP is the axis of the cone of diffracted X-rays, and the directions SA, SB and SC make equal angles with SP. P therefore lies at the intersection of two planes, one of which is the locus of directions equiangular to SA and SB and one of which is the locus of directions equiangular to SB and SC. Knowing the wave-length of the characteristic radiation giving rise to the reflections and an approximate lattice parameter for the specimen (in conjunction with the above geometry), the direction cosines of the cone axes (in arbitrary M basis), as well as the indices of the reflecting plane (hkl), can be determined for each conic. The calculations were programmed on an IBM 1620 computer and a working copy of the programme was kindly supplied by McGirr and Malin.

The exact geometrical analysis requires a knowledge of the position of the origin and the specimen to film distance, neither of which is known with certainty. Furthermore, the precision with which the three points can be defined upon the conic is limited, and it is the precision

of their location that is thought to be the main factor limiting the accuracy of the technique. Experimentally these points were marked by lightly puncturing the film with the point of a fine needle.

The films obtained by McGirr and Malin, for large recrystallized grains of copper, were of high contrast with negligible line broadening and, despite the inexact nature of the method, it was estimated that the axes (plane normals) of the best conics (highest contrast and curvature) could be located within  $0.1^{\circ}$  of their true positions, as evinced by the consistency of the measured interaxis angles. McGirr and Malin found that varying the position of the origin and the specimen to film distance over small limits did not lead to significant changes in this order of accuracy (124). Apart from the criterion of internal consistency however, no information was available on the overall accuracy of the method so that it was necessary to carry out additional work in order to estimate what this was for the present experimental conditions.

The method outlined for determining the direction of a conic axis requires a minimum of three points, defining the conic, to be marked on the film. By placing say thirty points on the conic, ten independent assessments of direction of the conic axis can be made and a mean value, with statistical limits, computed. This gives an estimate of the reproducibility of the marking technique and a measure of the expected internal consistency. Several films were analysed in this way.

While the error associated with the positioning of any axis is calculable in this way, a knowledge of the individual errors does not lead simply to a specification of the accuracy of an actual crystal orientation determined from a number of these axes. In the present

studies the accuracy of an orientation determination was estimated by using a least squares method to define the position of a cubic lattice best fitting a given number of experimental poles of known indices (this method is described in Section 6.3.5). By computing the orientation of a cubic lattice for which the sum of the squares of the angular differences between the experimentally determined poles and their "true" position is least, a quantity related to the standard deviation of these angles can be calculated (Appendix 3). When the results of McGirr and Malin were reprocessed using this procedure the quantity ( $\approx$  std. dev.) was found to be  $\pm 0.05^\circ$  which confirms the estimated value of the internal consistency figure for interplanar angles of  $0.1^\circ$  quoted by these authors.

As an additional check two completely independent assessments of the orientation relationship between two ferrite crystals were also made. These results and those of the other analyses referred to above are described fully in Section 7.3.2.

#### 6.3.5 The Austenite-Ferrite Lattice Orientation Relationship

The aim of the work described in this section was to determine the orientation relationship between the crystal lattices of the parent and the product phases for a particular, known variant of the habit plane. In general the most accurate determination of an orientation relationship is obtained when X-ray reflections from both lattices can be observed on the same film, thus allowing measurement of the angles between plane normals to be made directly. The results of Dautovich (119) from iron/manganese/carbon martensite plates using the oscillating crystal method, for example, showed small deviations from parallelism

of the close packed planes in the two lattices and the error of the determinations was estimated to be approximately  $\pm 0.05^\circ$ .

In the present case the parent phase decomposes finally to pearlite, so that direct X-ray analysis of both austenite and ferrite lattices simultaneously, was not possible. Indeed, direct observations of the parent phase cannot be made at all and its orientation must be determined indirectly, as for example from thermally etched twin vestiges as described in Section 6.3.2. For these reasons it seemed at first that the orientation relationship between the parent austenite and the ferrite could only be determined by combining the results of two independent experiments — one to determine the austenite orientation and the other to determine that of the ferrite. This constituted a major disadvantage of the iron/carbon alloy and one of the major experimental difficulties of the project. Two methods for calculating the austenite/ferrite lattice orientation relationship were developed and these are outlined in the following sections.

#### Method A - Two Independent Experiments

In order to be able to relate the position of a ferrite lattice determined from the Kossel patterns with the orientation of the parent austenite lattice determined from twin vestige analysis, a common system of reference must be used for the two determinations. The basis selected was that of the specimen geometry (ie. the I basis). However, the crystallographic information recorded on the films bears an unknown spatial relationship to the specimen geometry, and this is, in essence, what has to be determined. Positioning of the specimen, by

setting some recognizable geometric feature such as a specimen edge parallel to the crosshairs in the Kossel camera, is not possible since the crosshairs imaged on the film are not imaged on the optic system.

In order to overcome this difficulty a link between the position of the specimen and the position of the film was devised. This was achieved by mounting a cleaved prism of lithium fluoride single crystal, with faces parallel to  $\{100\}$ , and the specimen face down on a sheet of glass, with one edge of the single crystal abutting the reference direction,  $I_1$ . After setting in resin, the mount was removed from the glass and portion of the lithium fluoride crystal coated with approximately  $1\mu$  of chromium, by vapour deposition. When the coating is excited by the electron beam, characteristic chromium X-rays are diffracted by the lithium fluoride crystal and the positions of the  $\{100\}$  lithium fluoride reflections define the positions of the I base vectors on the film. The use of this pseudo-Kossel technique allowed the relationship between the M and I bases to be determined, since the set of vectors  $\langle 100 \rangle$  lithium fluoride represent the  $\langle 100 \rangle_I$  expressed in the M basis. The  $(3 \times 3)$  transformation matrix  $M^T I$  relating the two bases is constructed by writing as its successive columns the measured direction cosines of the  $\{100\}$  lithium fluoride reflections. Because of experimental error the measured vectors are not orthogonal and some adjustment of their position is required; the method adopted was that described on page 100 for adjusting measured twin poles. It was found that only small deviations from the measured value, typically less than  $0.1^\circ$ , resulted using this method. In this way it was possible to express the determined ferrite poles in the I basis regardless of the orientation in which the

specimen was initially placed in the camera.

The level of precision required by the crystallographic theory means that analytical rather than stereographic projection methods must be used to define the lattice orientations. The method used to determine the austenite orientation from twin trace measurements, relative to the I basis, is described in Appendix 1. The direction cosines of the ferrite poles, in the same basis, were calculated from their measured positions in the M basis using the transformation matrix  $M^T I$ . When a ferrite plane of interest did not give rise to reflections on the film the direction cosines of its pole were calculated using a geometric method outlined in Appendix 2. For convenience of calculation this method was programmed on a computer.

The precision of the orientation relationship determined in this way, from two independent determinations of the orientations of the respective lattices, was thought to be limited mainly by the uncertainty in the austenite orientation and also, but to a lesser extent, by the corrections applied to the elements of the matrix  $M^T I$ . Because of the inherently greater precision of the orientation determinations made using the Kossel technique a method for determining the austenite/ferrite orientation relationship using only the ferrite orientations determined using this technique, was developed.

#### Method B - Using Crystallographic Variants of the Precipitate

Bowles (126) has proposed a method whereby a prominent crystal direction in a parent lattice may be determined from a knowledge of the orientations of two product lattices which are variants. The orientation relationship between the parent and product lattices need not be

rational or even known. The basis of the method is that the orientations of the two variants can be made crystallographically coincident by a rigid body rotation about an axis that is an axis of symmetry of the parent lattice.

In general, two different orientations of a lattice can be brought into crystallographic coincidence by a number of different rotations, each rotation bringing a selected vector of one lattice into parallelism with a crystallographically equivalent vector of the other. The number of possible rotations depends upon the symmetry of the crystal lattices involved. For the case where the two lattices are precipitate variants at least one of these rotations defines an axis and angle of rotation that represents a symmetry operation of the parent lattice.

In the present case, involving lattices of cubic symmetry, the method consists of determining experimentally the orientations of the lattices of two non-parallel ferrite laths with respect to a common measuring basis, and then calculating the twenty four rigid body rotations which can bring the experimentally determined lattices into coincidence. The twenty four solutions, represented as  $(3 \times 3)$  rotation matrices, result from considering the twenty four crystallographically equivalent but physically distinct ways in which  $\langle 100 \rangle_B$  can be chosen as right handed sets of base vectors for one ferrite lattice, once a particular set has been arbitrarily assigned to the other lattice.

The rigid body rotation which most closely represents a symmetry operation of a cubic lattice is found by comparing the twenty four calculated angles of rotation with the actual angles of rotation of the

twenty four symmetry operations (see Table 6.2). The axis of rotation, (expressed either in the measuring basis or the ferrite basis), corresponding to the correct angle of rotation, is identified as the relevant low index direction (axis of symmetry) of the parent austenite.

TABLE 6.2

The Symmetry Operations of a Cubic Lattice

Rotation Axis	Multiplicity	Angles of Rotation	Number of Equivalent Rotations
Identity Rotation		$0^\circ, 360^\circ$ etc.	1
$\langle 100 \rangle_F$	3	$90^\circ, 180^\circ, 270^\circ$	9
$\langle 110 \rangle_F$	6	$180^\circ$	6
$\langle 111 \rangle_F$	4	$120^\circ, 240^\circ$	8
		Total	24

Since a combination of at least two and sometimes three vectors of the types shown in the first column of Table 6.2 are required in order to uniquely define the orientation of a cubic lattice, orientation determinations on at least three variants of the precipitate in a single parent grain are necessary to allow three axes of rotation, and hence three austenite vectors, to be determined.

In the specimens studied, three analysable variants of ferrite within a single austenite grain occurred only rarely, while the case of two variants occurred quite regularly and so a method of treating this case was developed. The results of a number of determinations of a single rotation axis in different specimens may be combined to

give a number of parent lattice vectors sufficient to define a parent orientation, and therefore the orientation relationship, when the habit plane is also known. For each pair of variants the rotation axis was referred to the ferrite basis, with the base vectors being identified by their relationship to the habit plane. The use of this relationship is equivalent to expressing each solution in terms of the same variant of the lattice correspondence.

For the above methods to be valid there must be an exact orientation relationship obtaining in the transformation and the orientations of the product lattices must be known exactly. In practice the latter condition can never be true because of experimental error in the orientation determinations. The presence of this error means that, for the case of three variants, the angles between the three determined rotation axes will in general not be equal to the angles between the crystal directions they represent. Similarly, when a number of axes from the two variant cases are combined they will not define exactly a cubic lattice. Thus in each case an orientation has to be fitted to the experimentally determined set of vectors in order to allow the orientation relationship to be determined. Accordingly some measure of the degree of fit of this determination is required to distinguish between the possibilities:

- (a) that an exact orientation relationship exists but is not observed because of experimental error.
- (b) that the product lattices are not exact variants and so there is some real spread of values in the orientation relationship.

The method used to fit an exact cubic lattice to both the ferrite poles determined from the Kossel patterns, and the rotation axes representing austenite poles, was based on the least squares analysis of Mackenzie (127). For the ferrite orientation the poles of the five best conics from each film were used to define the orientation of a cubic lattice for which the sum of the squares of the angular deviations between each experimental pole and its true position was least. The mathematical basis of this method, which was programmed for processing on an IBM 360/50 computer, is given in Appendix 3.

In the programme the least squares analysis was coupled to the multiple variant calculation allowing the correct rotation matrix, representing the rotation relating the variants, to be computed. From the elements of this matrix the direction cosines of the axis and the angle of the symmetry operation in the parent lattice were calculated. In order to retain accuracy all the calculations were done using "double precision" which means that the computer worked with 8 byte digits or 16 decimal places.

#### 6.3.6 The Shape Strain

Bowles and Mackenzie (36) showed that in martensitic transformations the direction of the shape strain is the most important parameter to measure, since it varies sensitively with changes in  $x = \psi/s$ . This direction can be determined experimentally by analysing the change of direction of at least three arbitrary vectors (eg. scratches) in the initial prepolished surface (38-40). As mentioned in Section 6.2.1 (c) the techniques used by Dunne (122) failed to produce analysable results for it was found to be almost impossible to produce ferrite plates

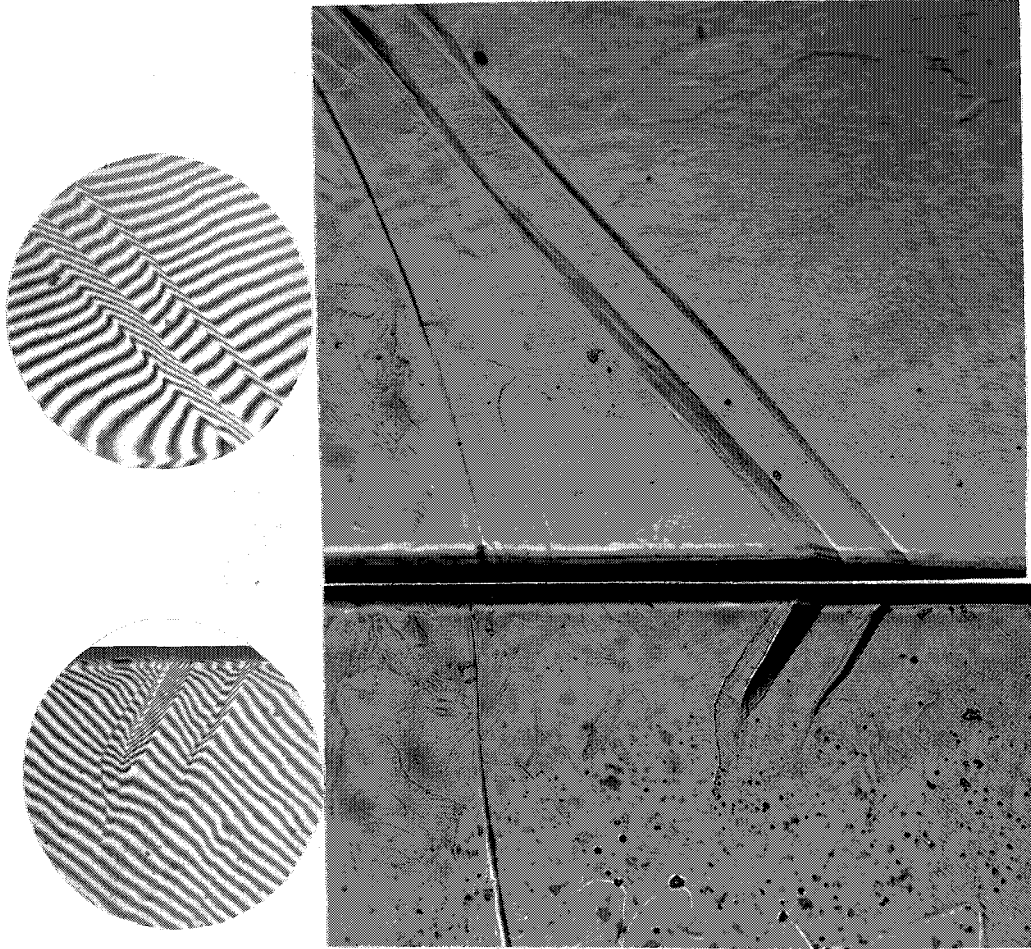


Fig. 6.15 Two ferrite laths producing relief on two surfaces at right angles, with corresponding interferograms.

X 500

subsequent to scratching the surface of the specimen. The decomposition of the matrix phase to pearlite precluded the method developed by Krauklis and Bowles (41) from being used for the present transformation.

Two cases presented themselves where the relief effect produced by a lath appeared on two perpendicular surfaces. The tilts on the two surfaces were measured using interferometry, the angle between the faces was measured with a two circle goniometer and the sense of the tilts was determined by observing the displacement of the specimen edge. From this data, the direction and magnitude of the shear component of the shape strain was determined with respect to the specimen geometry. Analyses of austenite twin traces and Kossel patterns, from the austenite and ferrite lattices respectively, then allowed the shape shear to be expressed with respect to the crystallography of the participating phases. An example of the numerical methods used to calculate this shear component from the experimental results, is shown in Appendix 4.

---

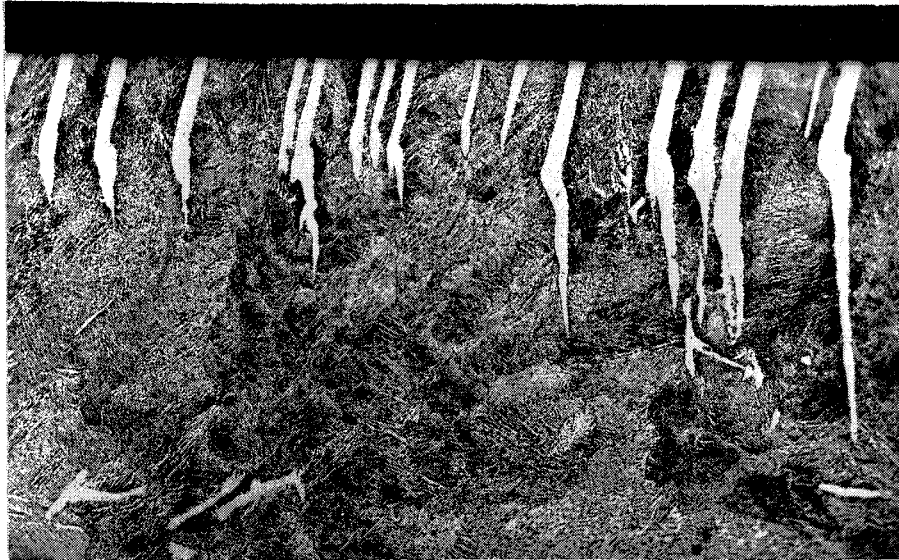


Fig. 7.1 A cross section through a group of parallel laths showing the platelike region extending from the free surface and the marked change of morphology at about 0.1 mm. below the surface. X 250

CHAPTER 7RESULTS.

	Page
7.1 Morphology and Nature of the Shape Change.	115
7.2 The Habit Plane.	118
7.3 The Orientation Relationship.	121
7.4 The Shear Component of the Shape Strain.	130

7.1 Morphology and Nature of the Shape Change

Widmanstätten ferrite formed at a free surface was found to have a narrow plate or lath shape, with the dimension in the surface (length) being very much larger than the width or depth. The dimensions of the laths varied with the transformation temperature, becoming smaller as the temperature was reduced because of competitive growth of pearlite, but in general their size was similar to  $\{225\}_F$  martensite plates (119, 122). The typical appearance of ferrite laths in section is shown in Figure 7.1 in which a parallel-sided, distinctly platelike portion immediately below the surface, extending into the bulk a distance of the order of several plate widths, can be seen. At a depth generally not exceeding approximately 0.1 mm., the shape and direction of the laths were observed to change, becoming ragged, less characteristically platelike and finally tapering off to a tip resembling a "comet tail" attached to the original lath. No interface was ever observed between the two segments, suggesting that the whole morphology is possibly the product of a single continuous growth process.

The platelike section, which extended to the free surface gave rise to surface relief effects similar in appearance to those of martensitic

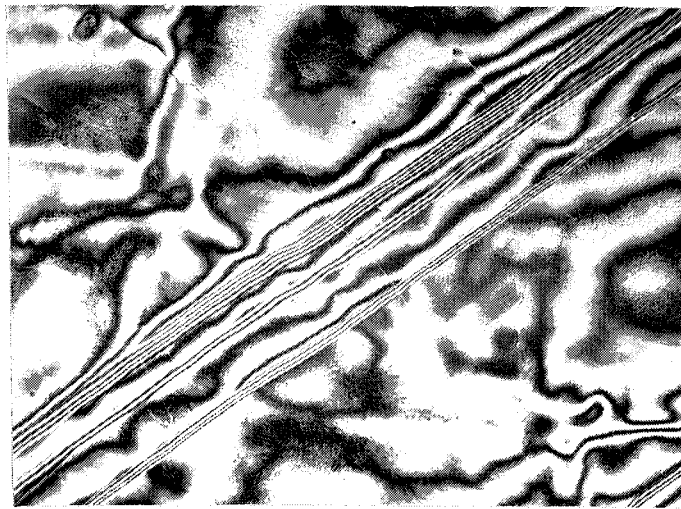
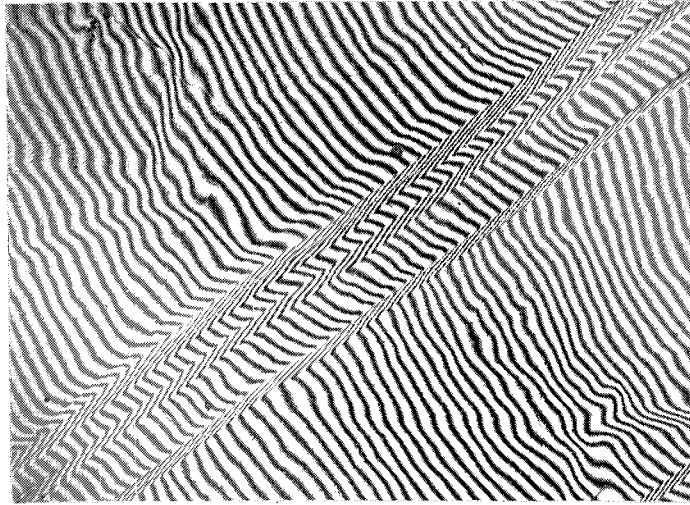


Fig. 7.2 Interferograms showing that the form of the surface relief effect is indicative of an invariant plane strain. approx. X 250

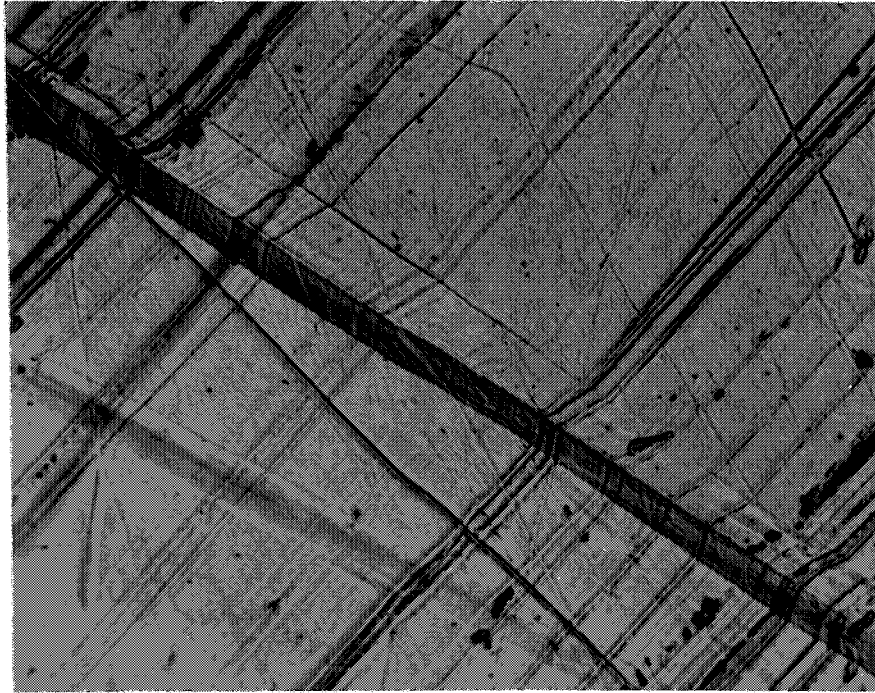


Fig. 7.3 A photomicrograph of a small V-shaped Widmanstätten plate formed after the surface had been scratched at 1000°C. Tilts and large scratch displacements are apparent. Oblique illumination X 1000

transformations. Examination of these relief effects, using interferometry and taper sectioning techniques, showed that the original surface remained essentially plane and was simply tilted during the transformation. The interferograms, typified by those shown in Figure 7.2, strongly suggest that the original surface is simply rotated about the trace of the habit plane, but the presence of surface rumpling prevented confident determination of whether the surface traces of the habit planes are unrotated and remain in the original surface.

Examination of Figure 7.3, which shows a double plate (in relief) intersected by scratches placed on the surface prior to transformation, shows that vectors (scratches) remain straight and continuous but are deviated by the transformation. The displacements of the scratches in Figure 7.3 are of the order of  $15^\circ$  and  $25^\circ$ , suggesting that a large component of the shape strain lies in the surface.

These results indicate that the macroscopic strain giving rise to the shape change is a homogeneous strain that can be described approximately, if not exactly, by an invariant plane strain in which the plane of the lath is the invariant plane.

Taper sectioning and interferometry yielded several additional observations on the shape change, the first of which was that double or v-shaped tilts, similar to those reported for the copper/zinc alloys (8, 10), were not uncommon. V-shaped relief effects have also been recorded by Dunne (122) for  $\{225\}_F$  martensite in iron/carbon and iron/manganese/carbon alloys and by Speich (76) for iron/carbon bainites. In such cases only one ferrite lattice orientation was

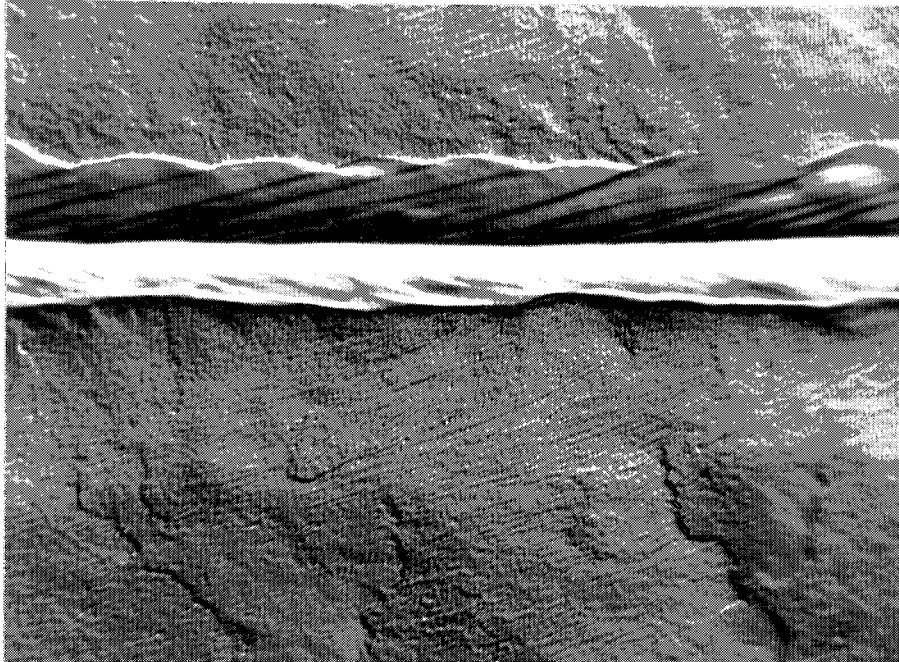


Fig. 7.4 Photomicrograph showing irregular lath/matrix interface and possibly evidence of an inhomogeneity of the transformation strain. The lath shows a straight "mid-rib" and lack of plastic accommodation in the matrix, which is characteristic of many double sided laths.

Interference contrast X 1000

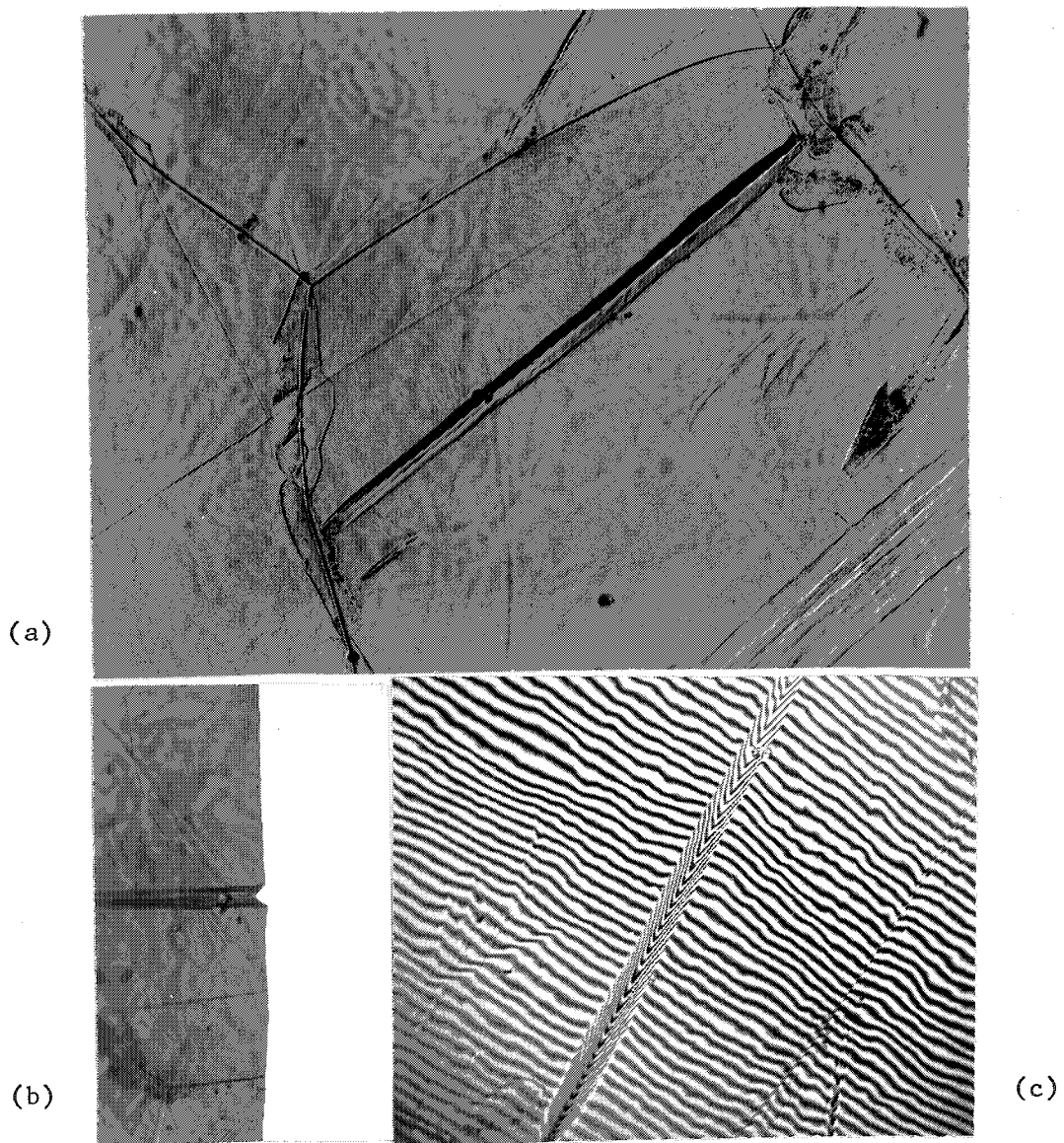
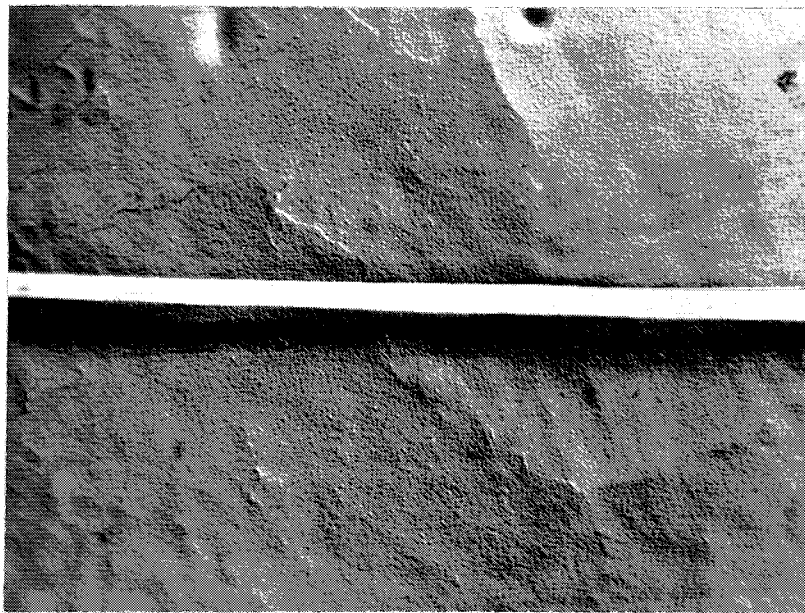
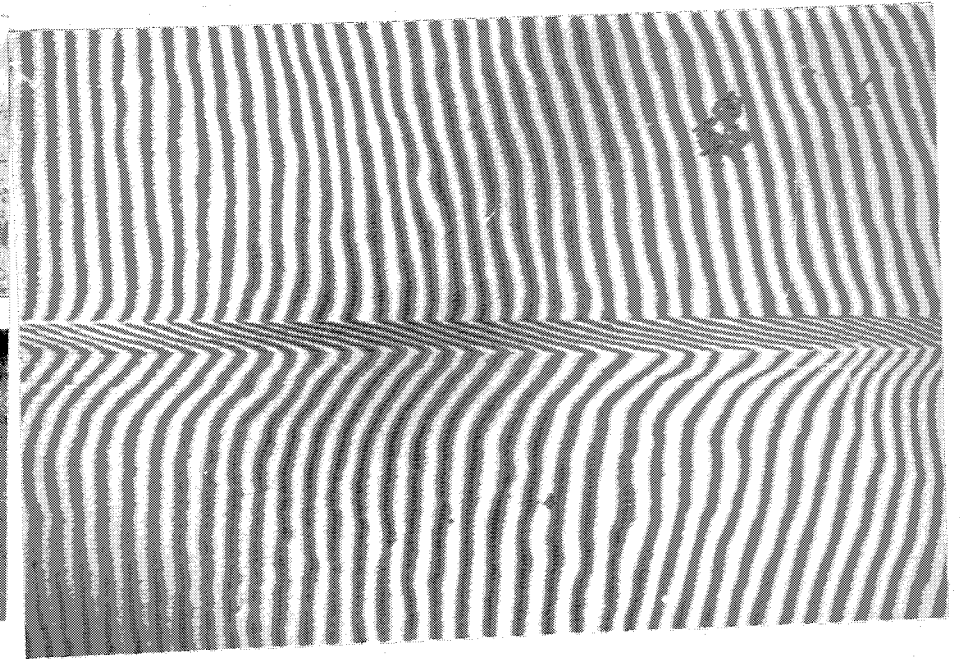


Fig. 7.5 (a) A photomicrograph of a double sided lath completely traversing the parent austenite grain. X 250.  
 (b) Taper section through the lath showing that the sense of the tilt is "out" of the specimen surface.  
 (c) Interferogram of the same lath. Note that there is no significant plastic accommodation in the matrix.



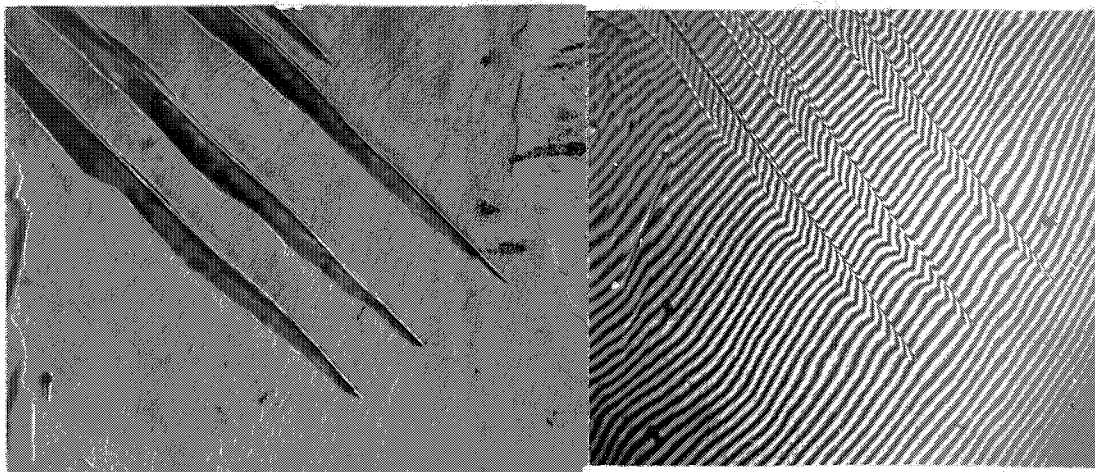
(a)



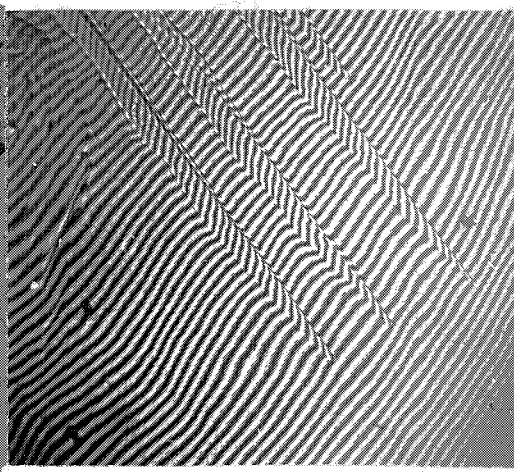
(b)

Fig. 7.6 A parallel sided, single tilt lath showing significant accommodation on only one side.  
(a) Interference contrast X 500.  
(b) Interferogram of same field.

(a)



(b)



(c)

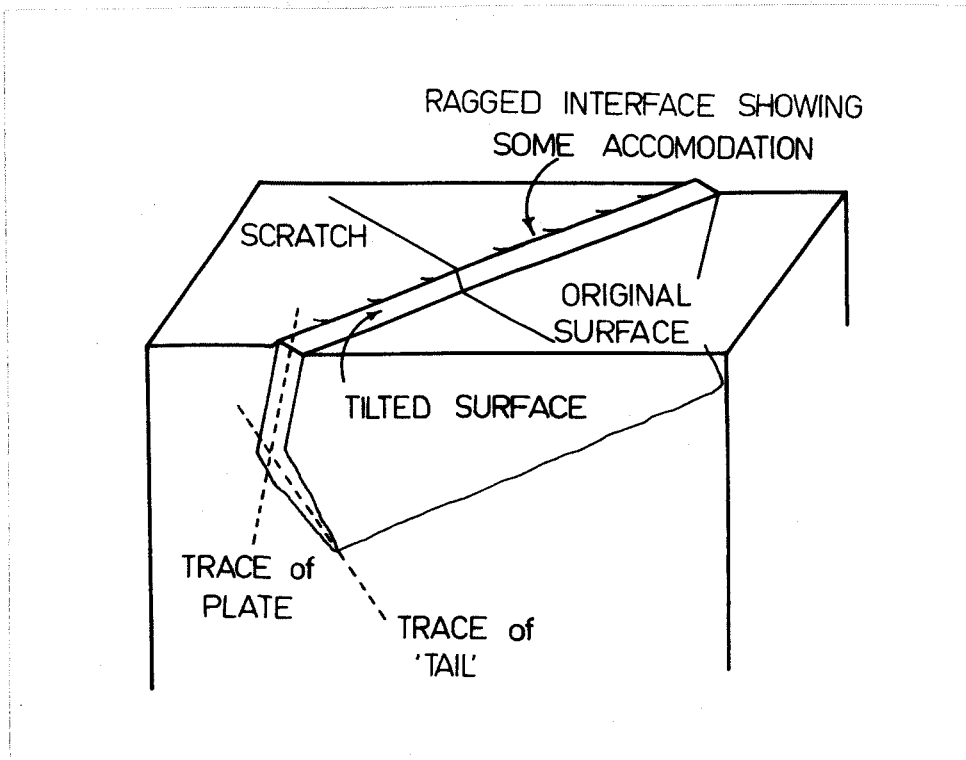


Fig. 7.7 (a) Photomicrograph of Widmanstätten sideplates exhibiting one distinctly ragged interface. Oblique illumination X 250  
(b) Interferogram of same field showing slight accommodation at the ragged edge.  
(c) Schematic representation of the growth of a ferrite plate.

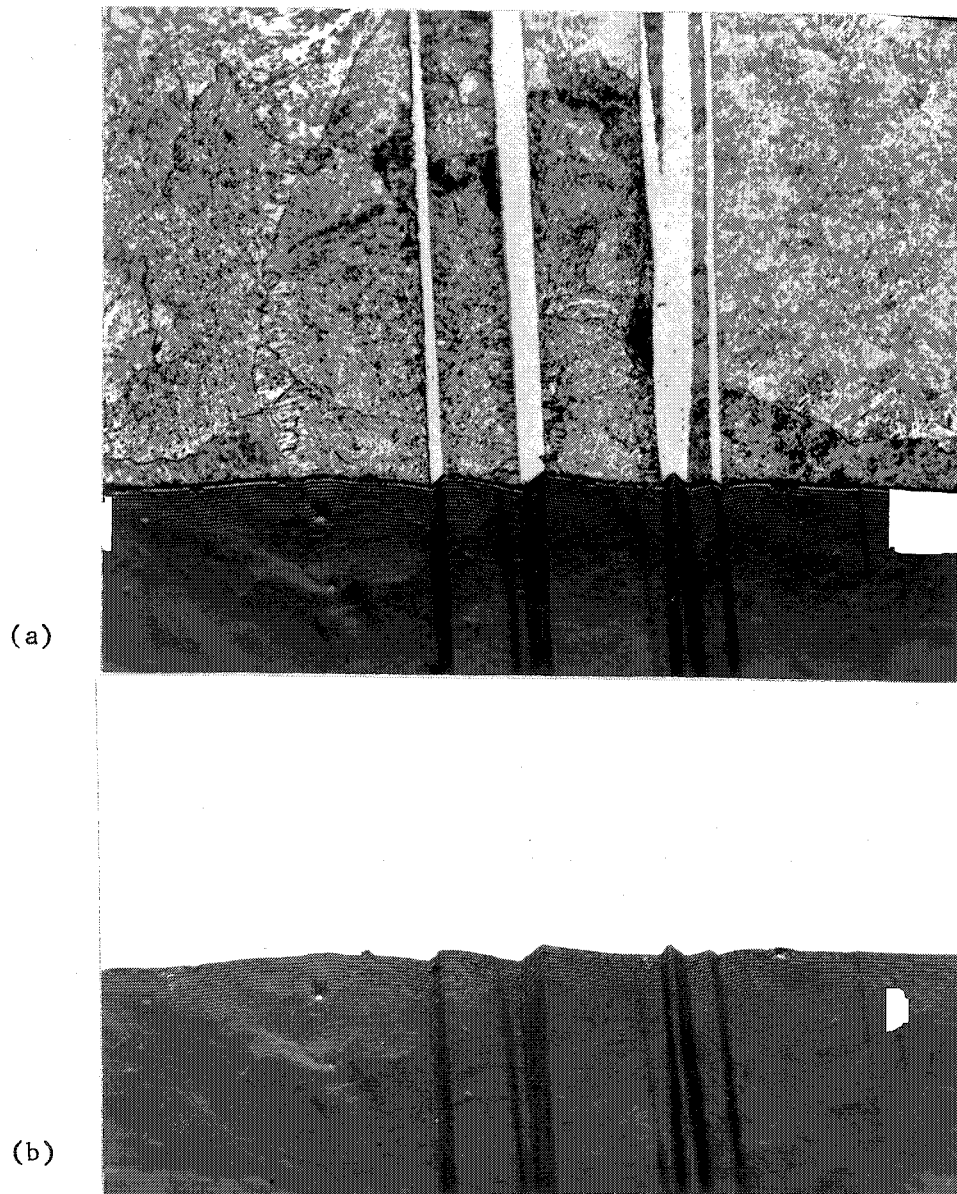


Fig. 7.8 Photomicrographs of taper section of adjacent single and double tilt laths. X 500

(a) Etched in nital.

(b) Unetched.

The figures show that parallel laths may have opposite senses of tilt and that there may be significant accommodation strain in the matrix.

detected by the Kossel technique and etched taper sections, similar to that shown in Figure 7.5, revealed no observable boundary between the two halves of the lath.

Single tilt laths were often found to be accompanied by significant plastic accommodation of the matrix (Figures 7.6, 7.7, 7.8) which was localised to the side of the lath having the ragged interface (Figure 7.7 (a)). The plastic accommodation was appreciably less (and possibly zero) for the double tilt laths, which appear to be "self accommodating" (refer to Figures 7.4 and 7.5).

Another feature shown in Figure 7.8 is that single laths, tilted in opposite senses, can be seen associated with the double lath (which incidentally is tilted into the surface rather than out of the surface, as is the lath of Figure 7.5). The effect of the two outside laths of Figure 7.8 abutting together would be to produce a double lath similar to the one shown. Accommodation effects in the parent phase may also be observed associated with only one edge of two oppositely tilted single laths in this field, notably those edges which would be the outer edges of a composite or double lath formed by their coalescence.

TABLE 7.1

{111} twin trace data defining the austenite lattice in the I basis for preliminary habit plane determinations shown in Figure 7.9. All of the angles defining the position of a trace are measured from the direction  $I_1$ .

Specimen No.	Traces of Twin 1		Traces of Twin 2		Angle Between Faces	Traces of Plates in Face 1*
	Face 1	Face 2	Face 1	Face 2		
1	178.0	175.7	68.6	162.0	87°55'	62.2- 64.0 (17)
2	106.4	93.9	160.8	163.1	91°	15.9- 16.8 (3)
3	80.7	38.7	142.0	148.5	89°20'	40.0- 40.5 (8)
4	112.3	71.1	93.5	142.2	92°30'	72.0- 77.0 (8)
5	31.2	160.0	118.2	112.9	89°30'	40.3- 41.1 (5)
6	151.9	76.8	80.2	58.9	88°	4.5 (1)
	"	"	"	"	"	8.3 (1)
	"	"	"	"	"	144.0-148.8 (4)
	"	"	"	"	"	154.4 (2)

\* Trace measurements in section plane not shown.  
The number in brackets indicates the number of plates measured.

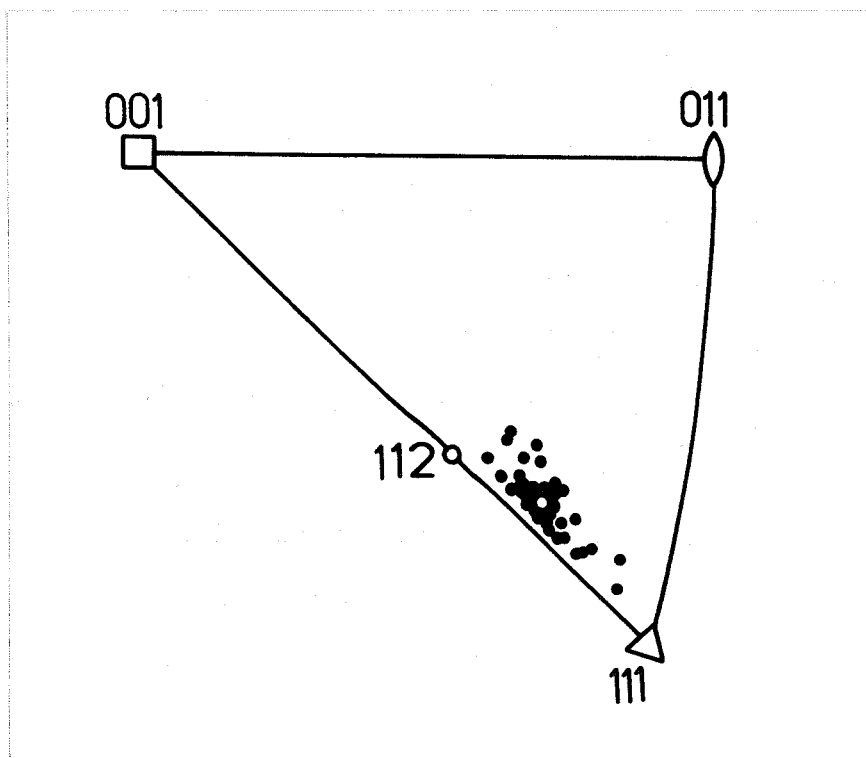


Fig. 7.9 The habit planes of forty nine laths referred to the austenite lattice. The open circle represents the mean of these determinations and is approximately  $12^\circ$  from  $(111)_F$ .

## 7.2 The Habit Plane

As a preliminary part of the investigation the habit planes of forty nine laths selected from six grains of determinable orientation, in six different specimens, were measured using two surface trace analysis. The relatively large number of laths arises because of their tendency to form groups and determinations were often made on parallel laths of the same variant as well as on different variants within the same grain. The results, referred to the I basis, are summarised in Table 7.1 and are shown plotted stereographically, with the austenite in standard projection, in Figure 7.9.

The scatter of results parallel to the  $[\bar{1}10]_F$  zone is attributable, at least in part, to the difficulty of measuring the trace of the lath in the second surface, but some scatter is certainly real and does not arise from experimental errors. A mean value of the results for the laths was estimated and was found to have direction cosines:

$$\begin{pmatrix} .4523468 \\ .5057018 \\ .7346080 \end{pmatrix}_F$$

which is a plane displaced  $12^\circ$  from  $(111)_F$ ,  $8\frac{1}{2}^\circ$  from  $(112)_F$  and approximately  $3^\circ$  from the  $[\bar{1}10]_F$  zone. Because of their tapering shape it was not possible to accurately define a habit "plane" for the "tails". By measuring their mean trace in the second surface, as indicated in Figure 7.7, and combining this with the trace in the original relief surface, approximate habit planes, which scattered around  $(111)_F$ , were obtained. When these were plotted on the same projection, with the plates in the standard triangle bounded by  $[001]_F$ ,  $[011]_F$ ,  $[111]_F$ , the "tails" appeared to be disposed in a regular way to the plates, as

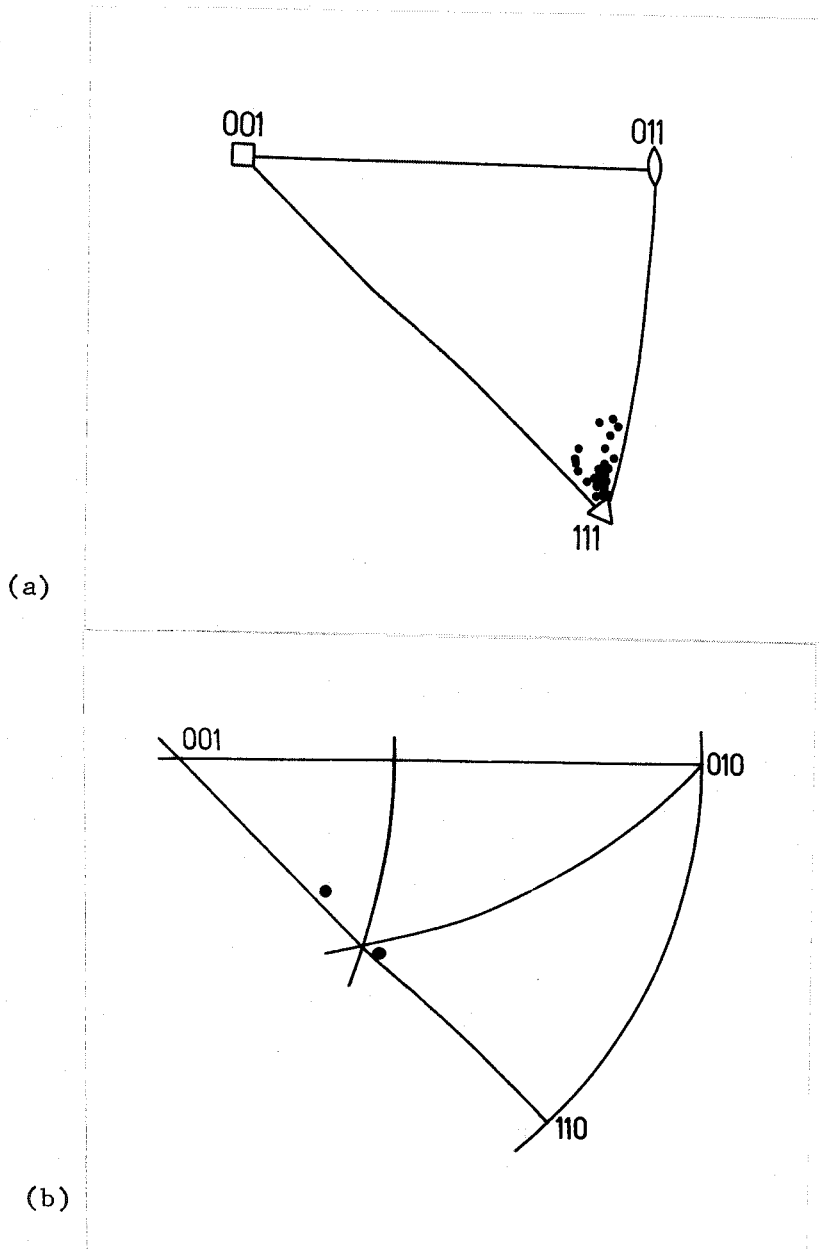


Fig. 7.10 (a) Stereographic projection of the indices of the "plane" defined by the "tails" of the laths shown in Figure 7.9.  
 (b) Stereographic projection of the relationship between the habit planes of two portions of a lath. The two poles lie on a common zone, and axis of which is the long direction of the lath, but differ in position on this zone by virtue of their different trace in the second surface. (Figure 7.7 (c)).

shown in Figure 7.10.

Although these determined habit planes deviate markedly from values reported in the literature, and are therefore significant results in themselves, a far more complete description of the crystallography of the laths is necessary for the purpose of analysing the transformation in terms of the crystallographic theory. In particular, the lattice orientation relationship for a known variant of the habit plane, is required.

Accordingly, a further eleven specimens were carefully analysed, each twin and lath trace being measured a number of times in order to allow standard deviations and a measure of overall accuracy to be determined. The orientation of the lattice for each lath was then obtained from Kossel analysis and finally the specimen was sectioned to determine a second trace of the lath. When the results of these determinations, shown in Table 7.2, were plotted stereographically, it was evident that the two-surface method allowed an unambiguous estimate of the habit plane to be made in the I, and thence in the F, basis. The most accurate (long) traces of twenty three laths showed standard deviations of about  $\pm \frac{1}{2}^\circ$  and, when the trace normals of these were plotted as a single surface analysis, they did not pass through  $(111)_F$ . Furthermore, they were displaced far enough from the  $[\bar{1}10]_F$  zone, in the region of  $(111)_F$ , to prevent any ambiguity arising as to which stereographic triangle contained the habit plane. This occurs because the long directions of the plates are invariably near  $[\bar{1}10]_F$  and the zones of these directions (trace normals) lie almost parallel to  $[\bar{1}10]_F$  zone.

TABLE 7.2

Two surface trace data, in the I basis, for orientation and habit plane determinations. The standard deviation of all measurements are shown.

Spec. No.	Twin Traces (T1)		Twin Traces (T2)		Angle Between Faces	Angle Between $\{111\}_F$	Plate Traces, Face 1*
	Face 1	Face 2	Face 1	Face 2			
7	62.9 $\pm$ 0.19	132.7 $\pm$ 0.30	6.5 $\pm$ 0.38	40.2 $\pm$ 0.35	89°50' $\pm$ 4'	70°40'	58.9 $\pm$ 0.55 67.0 $\pm$ 0.77 141.2 $\pm$ 0.29
8	68.1 $\pm$ 0.22	51.1 $\pm$ 0.19	133.9 $\pm$ 0.26	108.5 $\pm$ 0.39	87°54' $\pm$ 5'	70°39'	84.6 $\pm$ 0.56
9	45.7 $\pm$ 0.26	126.3 $\pm$ 0.22	9.2 $\pm$ 0.33	†	89°03' $\pm$ 3'	70°44'	119.2 $\pm$ 0.30 32.0 $\pm$ 0.34
10	37.8 $\pm$ 0.22	147.1 $\pm$ 0.10	161.8 $\pm$ 0.27	105.2 $\pm$ 0.14	91°50' $\pm$ 5'	70°42'	43.0 $\pm$ 0.38 28.1 $\pm$ 0.38
11	21.6 $\pm$ 0.40	29.0 $\pm$ 0.25	58.7 $\pm$ 0.33	†	89°22' $\pm$ 2'	70°36'	95.4 $\pm$ 0.26 105.3 $\pm$ 0.37
12	170.4 $\pm$ 0.26	163.4 $\pm$ 0.20	111.1 $\pm$ 0.28	77.1 $\pm$ 0.46	89°45' $\pm$ 3'	70°27'	52.2 $\pm$ 0.57 169.4 $\pm$ 0.34
13	109.1 $\pm$ 0.35	102.0 $\pm$ 0.17	170.5 $\pm$ 0.25	176.9 $\pm$ 0.26	92°01' $\pm$ 2'	70°	45.0 $\pm$ 0.18
14		CALCULATED	FROM SINGLE	SURFACE ANALYSIS	(122)		
15	24.0 $\pm$ 0.40	32.0 $\pm$ 0.22	127.9 $\pm$ 0.36	107.9 $\pm$ 0.43	88°50'	70°46'	130.9 $\pm$ 0.57 84.0 $\pm$ 0.14
16	81.0 $\pm$ 0.10	94.1 $\pm$ 0.10	16.6 $\pm$ 0.25	24.3 $\pm$ 0.32	89°19'	70°48'	13.1 $\pm$ 0.67 155.7 $\pm$ 0.11
17	159.1 $\pm$ 0.41	101.9 $\pm$ 0.28	92.2 $\pm$ 0.32	70.5 $\pm$ 0.37	90°43'	69°32'	44.7 $\pm$ 0.12

\* Traces of plate in section not listed.

† Additional traces in face 1.

Measurement of the trace in the second surface locates the habit plane exactly but experimental error in the trace measurements, commonly observed to spread by about  $\pm 1^\circ$ , but reaching  $\pm 2^\circ$  in the worst case, contributes to the scatter of habit planes along the  $[\bar{1}10]_F$  zone. The extent of this scatter is approximately equal to the scatter in the trace measurements in the second surface.

It was this ability to unambiguously determine the indices of the habit plane which allowed the associated variant of the correspondence to be consistently selected.

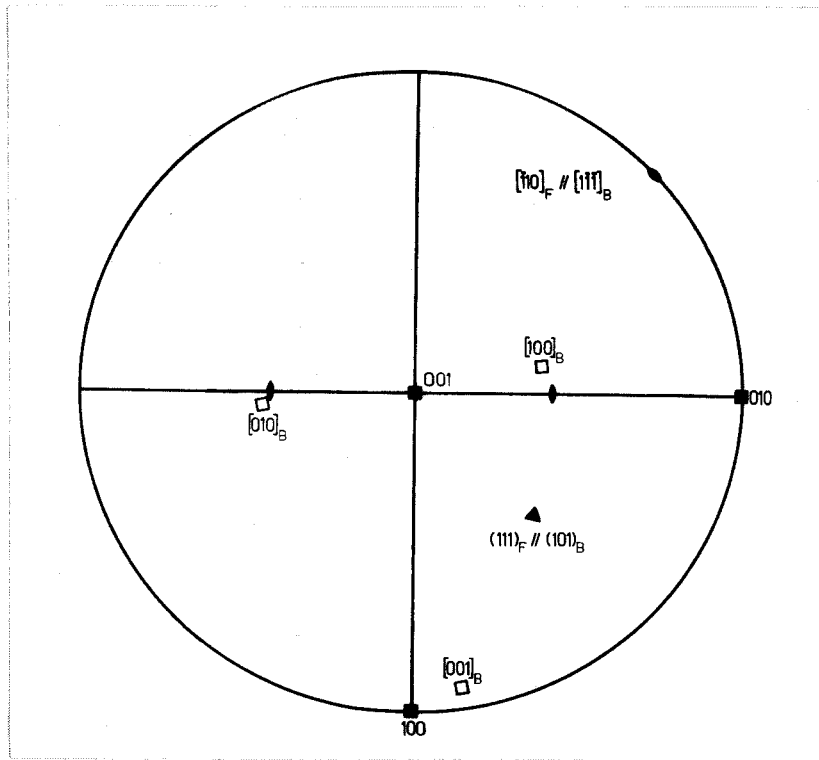


Fig. 7.11 Stereographic projection showing the particular variant of the Kurdjumov-Sachs relationship most closely representing the present results for the habit plane being in the triangle  $[001]_F$   $[011]_F$   $[111]_F$ . The austenite lattice is drawn in standard projection and the B subscripts refer to the ferrite lattice.

### 7.3 The Orientation Relationship

#### 7.3.1 Method A : Two Independent Experiments

When the lattice orientations for the same twenty three laths were determined and plotted stereographically it was found that, within the limits of the graphical technique, a  $\{110\}_B$  lay near a  $\{111\}_F$  and a  $\langle 111 \rangle_B$  near  $\langle 110 \rangle_F$ , viz: a near Kurdjumov-Sachs relationship. In addition, with the austenite rotated into standard projection and with the habit plane in the triangle bounded by  $[100]_F$ ,  $[110]_F$  and  $[111]_F$ , the  $(111)_F$  and  $[\bar{1}10]_F$  were the matching close packed plane and direction respectively. Two twin-related variants of the ferrite lattice can satisfy the Kurdjumov-Sachs relationship with a single variant of the austenite lattice, but only the one represented by the correspondence shown in Figure 7.11 was observed experimentally for the specimens examined. This correspondence may be written:

$$B^C_F = \begin{pmatrix} 0 & 1 & 1 \\ 0 & \bar{1} & 1 \\ 1 & 0 & 0 \end{pmatrix}$$

The experimentally measured indices of the corresponding close packed planes and directions for both lattices, expressed in the I basis, are shown in Tables 7.3 and 7.4; the deviation from exact Kurdjumov-Sachs relationship indicated by these figures has been calculated and is shown in the extreme right hand column of each table. Because in most cases the experimentally determined vectors do not appear to be in error by more than  $\frac{1}{4}^\circ$ , (as evinced only by internal consistency) no attempt has been made, in these tables, to adjust the experimental vectors to fit a cubic lattice exactly.

TABLE 7.3

Measured direction cosines of the corresponding close packed directions expressed in the I basis. The austenite vectors were determined from twin traces, Table 7.2, and the ferrite from Kossel patterns.

Spec. No.	Variant No.	MEASURED DIRECTION COSINES IN I BASIS						Plate No.	Deviation from KS.
		<110> AUSTENITE			<111> FERRITE				
7*	1	+ .4765442	+ .8786686	+ .0291032	+ .4545911	+ .8902652	+ .0278369	1	1°25'
		As above			+ .4668801	+ .8838832	+ .0278147	2	0°38'
	2	As above			+ .4626647	+ .8859964	+ .0308536	3	0°55'
8	1	+ .1987259	+ .9778432	+ .0658083	+ .2110020	+ .9759142	+ .0554624	1	0°55'
	2	- .7056964	+ .6346498	+ .3149799	- .7310888	+ .6227124	+ .2788150	2	2°37'
		As above			- .7240398	+ .6314138	+ .2776366	3	2°24'
9	1	- .4489511	+ .8928033	+ .0366737	- .4679241	+ .8823674	+ .0429324	1	1°56'
		As above			- .4696306	+ .8812882	+ .0458127	2	2°5'
		As above			- .4675019	+ .8833262	+ .0279527	3	1°44'
10	1	- .7966652	- .6043098	+ .0115788	- .7982248	- .6020738	+ .0185032	1	0°26'
	2	As above			- .7995780	- .5995780	+ .0344731	2	1°21'
11	1	- .6419690	- .6122751	+ .4615136	- .6640904	- .5933941	+ .4548265	1	0°32'
	2	- .1526216	+ .9880303	+ .0224209	- .1185248	+ .9922331	+ .0377525	2	1°24'
12	1	- .3332147	+ .9350427	+ .1210907	- .3425149	+ .9312589	+ .1242590	1	0°36'
	2	+ .6473519	+ .7433767	+ .1683051	+ .6143742	+ .7685219	+ .1786566	2	2°27'
13*	1	+ .9650388	- .2601842	+ .0316883	+ .9652085	- .2613609	+ .0079250	1	1°40'
	2	- .7104845	- .6585507	+ .2480384	- .6965814	- .6778393	+ .2451761	2	1°33'
14*	1	+ .9995998	- .0243627	+ .0143797	+ .9927538	- .1168637	+ .0280150	1	5°22'
15	1	+ .6173023	- .7866980	+ .0066372	+ .6754354	- .7364960	+ .0368868	1	5°12'
16	1	+ .1492827	+ .9843513	+ .0936329	+ .1298269	+ .9848448	+ .1149984	1	1°39'
	2	- .9037941	- .3867118	+ .1833341	- .8986138	- .3991805	+ .1820680	2	0°47'
17(a)	1	+ .9239115	- .3629026	+ .1211968	+ .9129873	- .3885284	+ .1244981	1	1°37'
	2	- .7909974	- .5891779	+ .1649013	- .8054893	- .5737153	+ .1484521	2	1°31'
17(b)	1	+ .9239115	- .3629026	+ .1211968	+ .9123771	- .3893089	+ .1265160	1	1°39'
	2	- .7909974	- .5891779	+ .1649013	- .8074164	- .5701268	+ .1517683	2	1°38'

TABLE 7.4

Measured direction cosines of the corresponding close packed planes expressed in the I basis. The Austenite vectors were determined from twin traces, Table 7.2, and the ferrite from Kossel patterns.

Spec. No.	Variant No.	MEASURED DIRECTION COSINES IN I BASIS						Plate No.	Deviation from KS.
		{111} AUSTENITE			{110} FERRITE				
7*	1	+ .6873523	- .3517360	+ .6354749	+ .6853622	- .3695810	+ .6274459	1	1°08'
		As above			+ .6667977	- .3725233	+ .6454508	2	1°46'
		As above			+ .6683027	- .3570617	+ .6525932	3	1°30'
8	1	- .7759481	+ .1159663	+ .6200453	- .7379537	+ .1215707	+ .6638117	1	3°20'
	2	+ .7041291	+ .6775985	+ .2122789	+ .6817325	+ .6831197	+ .2618896	2	3°08'
		As above			+ .6926209	+ .6803377	+ .2396152	3	1°43'
9	1	+ .8912780	+ .4443747	+ .0903026	+ .8797952	+ .4628585	+ .1081834	1	1°38'
		As above			+ .8826295	+ .4568264	+ .1107828	2	1°28'
		As above			+ .8806831	+ .4605695	+ .1107358	3	1°38'
10	1	+ .4505752	- .5810090	+ .6777984	+ .4367200	- .5605516	+ .7036031	1	2°01'
	2	As above			+ .4589646	- .5752121	+ .6771133	2	0°35'
11	1	- .3085961	+ .7787629	+ .5461636	- .3289160	+ .7625484	+ .5570763	1	1°37'
	2	- .9663838	- .1159468	+ .2294756	- .9698494	- .1198188	+ .2122157	2	1°02'
12	1	- .9120194	- .3522238	+ .2101402	- .9037074	- .3598925	+ .2317326	1	1°30'
	2	+ .0789007	- .1542705	+ .9848733	+ .0080989	- .2199310	+ .9754828	2	5°33'
13*	1	- .2334132	- .7607991	+ .6055598	- .2207539	- .8162478	+ .5338879	1	5°12'
	2	- .6506297	+ .7450140	+ .1470858	- .6412287	+ .7320621	+ .2300227	2	4°50'
14†	1	- .0266171	- .9834355	+ .1793020	- .1310371	- .9785421	+ .1590355	1	6°05'
15	1	+ .7649418	+ .5951337	+ .2463330	+ .7036673	+ .6587389	+ .2663009	1	4°48'
16	1	+ .9850245	- .1563063	+ .0727648	+ .9874758	- .1366853	+ .0787948	1	1°11'
	2	- .2431577	+ .8165236	+ .5236061	- .2457933	+ .8017156	+ .5472991	2	1°21'
17(a)	1	+ .3576471	+ .9317026	+ .0633934	+ .3820302	+ .9193251	+ .0943114	1	2°22'
	2	+ .5709289	- .6139348	+ .5450911	+ .5419948	- .6079980	+ .5801548	2	2°39'
17(b)	1	+ .3576471	+ .9317026	+ .0633934	+ .3807425	+ .9188907	+ .1033211	1	2°44'
	2	+ .5709289	- .6139348	+ .5450911	+ .5420478	- .6157138	+ .5719095	2	2°15'

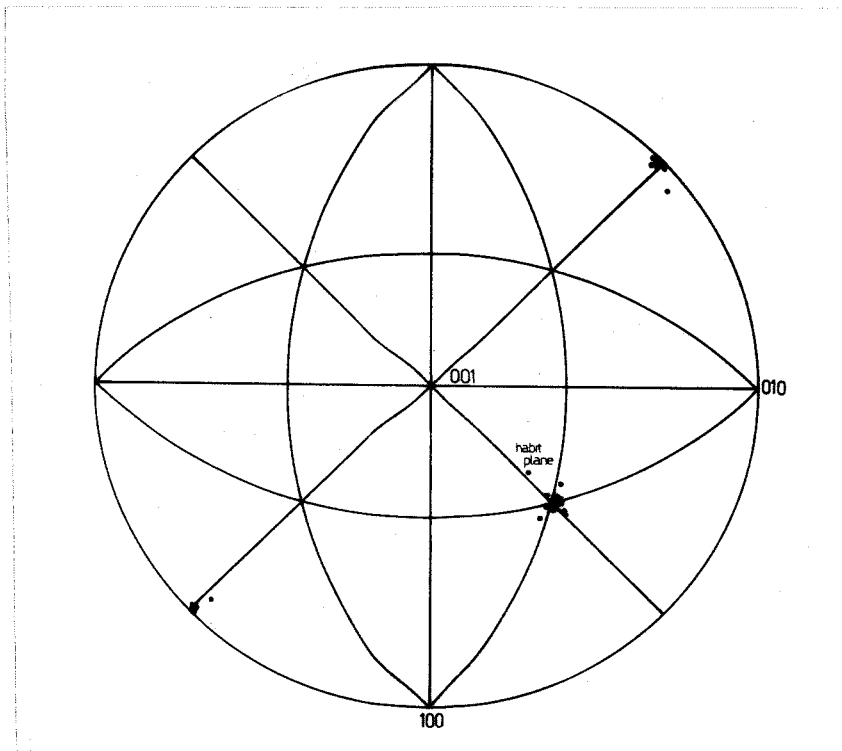


Fig. 7.12 Stereographic projection showing the experimentally determined close packed ferrite planes and directions given in Tables 7.3 and 7.4 and their relationship to the habit plane, drawn with respect to a standard austenite lattice. The austenite lattice was determined from twin traces and the ferrite, from Kossel analysis. The orientation relationship is seen to scatter around that of Kurdjumov-Sachs.

For example, if two measured planes of the type  $\{111\}_F$  happened to represent the close packed planes for the variants of the orientation relationship examined, the experimental vectors have been used with their small attendant error and the angle between them will be, not exactly  $70^{\circ}32'$ , but the value shown in column seven of Table 7.2. Similarly, for the  $\{110\}_B$  determinations, where these were observed directly as reflections on the film, they were taken to be best represented by the experimental value. The results are shown stereographically in Figure 7.12.

With the exception of specimen Nos. 13 and 17 the twin trace method allowed two  $\{111\}_F$  to be determined which were within  $\frac{1}{2}^{\circ}$  of the correct angle to one another. Under these circumstances the essentially arbitrary method of adjustment proposed on page 100 or the more complicated least squares refinement (127), should require only small changes in the locations of these crystallographic poles. Since both the lithium fluoride and the ferrite orientations can be determined to about  $\pm 0.1^{\circ}$  using the Kossel technique, the total experimental error of  $\pm \frac{1}{2}^{\circ}$  in the orientation relationship determination is probably incurred using this method.

### 7.3.2 The Kossel Technique - Accuracy

The method of determining the austenite orientation described in Section 6.3.5 (B) obviates the need for austenite twin trace measurements and allows the parent orientation to be defined using only ferrite lattice orientations determined by the Kossel technique. In order to determine the potential accuracy of this method the precision of the Kossel technique was examined experimentally and the

results of this analysis are now reported.

The angular consistency of ferrite crystallographic poles determined using the method described in Section 6.3.4 was found to vary with the quality of the conics on the film. For large equiaxed grains of ferrite, metallographically polished to  $1\mu$  diamond finish and etched in nital, the conics were more diffuse than those obtained from the same grains when electropolished. Although as-transformed specimens were examined without metallographic polishing, a size effect was observed and analysable patterns were not obtained from ferrite plates having a width less than about  $5\mu$ .

From the method of analysing the conics, those of higher curvature would be expected to yield the more accurately determined poles, and since this is a property of the crystallographic identity and the order of the reflection observed, the accuracy also depends on the crystal orientation (for a given camera geometry).

As a first test, two completely independent determinations of the orientation of two variants in specimen No. 17 were made and these results appear in the tables as 17 (a) and 17 (b) respectively. The two results differ by a rotation of only  $4'$  of arc.

Secondly, although the average consistency of interplanar angles observed in a set of experimentally measured poles was of the order of  $0.1^\circ$  for the large, electropolished ferrite grains, for the Widmanstätten plates it ranged from  $0.1^\circ$  in the best to over  $0.25^\circ$  in the worst cases.

To enable an estimate of the order of accuracy attainable, a number of conics on a typical film were multiply marked and a number

TABLE 7.5

Internal consistency and statistical analysis of  
selected conics from three plates in Specimen No.7.

Plate	Reflect -ing Plane	Average Direction Cosines	Std. Dev.	Conic Curv- ature	Angle Between Poles
1	{110} {110}	+ .1619457   - .0724696   + .9841350 - .6688240   + .3651021   + .6475905	+ 3' + 7'	High Low	59°50'
2	{110} {110}	+ .1652149   - .0923548   + .9819237 - .6702574   + .3498107   + .6545132	+ 3' + 6'	High Low	60°02'
3	{110} {110}	+ .1422686   - .0595292   + .9880359 - .6850756   + .3620534   + .6321303	+ 5' + 6'	High Low	59°39'

of independent determinations were made of each conic axis. A summary of the results is shown in Table 7.5. The standard deviations for the high curvature conics are seen to be about one half those for low curvature conics and for the former this deviation ( $\pm 3'$ ) compares well with the observed internal consistency range of  $0.1^\circ - 0.25^\circ$  ( $6' - 15'$ ). On the basis of these results it seemed that ferrite poles could be determined, in the majority of cases, to much better than  $0.25^\circ$  if a method of defining the position of a cubic (ferrite) lattice using only the better conics was devised.

The method chosen was that described by Mackenzie (127), which is essentially a least squares analysis. By selecting five conics, on the basis of high contrast, curvature, and good internal angular consistency, the orientation was determined by finding a (3 x 3) matrix which rotated a cubic lattice from standard orientation to a position best fitting the experimental data. This position of best fit was taken as the determined orientation. A quantity related to the standard deviation of the experimental poles from their true position was also calculated.

When the data for specimen Nos. 7 - 17 was analysed deviations ranging from  $\pm 0.04^\circ$  to  $\pm 0.25^\circ$  were found, with the majority near  $\pm 0.15^\circ$  ( $9'$ ). By multiply marking the conics and using mean values of the conic axes in the least squares program, deviations consistently below  $\pm 0.1^\circ$  were obtained. The potential precision of crystal orientations determined using this technique therefore seemed extremely high and, if the transformation being studied allows Kossel patterns from both parent and product phases to be obtained on the same film with

TABLE 7.6

Computed ferrite data for the cases where two variants were present in a common parent grain.  
 $\Delta$  = Deviation from exact KS. relationship.

Spec. No.	Variant No.	Std. Deviation*	CLOSE PACKED PLANES			CLOSE PACKED DIRECTIONS				
			DIRECTION COSINES			$\Delta$	DIRECTION COSINES			$\Delta$
7	1	+ 6'	+ .6846168	-.3639249	+ .6315525	1°46'	-.4623680	-.8866352	+ .0096962	0°54'
	2	- 5'	+ .6701407	-.3494947	+ .6548014		-.4663972	-.8845602	+ .0051964	
8	1	+ 12'	-.7425348	+ .1069063	+ .6612209	4°57'	+ .1797507	+ .9827737	+ .0429605	2°06'
	2	- 12'	+ .6585906	+ .7112487	+ .2457311		-.7509458	+ .6002125	+ .3023193	
9			ONE VARIANT ONLY							
10	1	+ 8'	+ .4679462	-.5443784	+ .6961885	0°41'	-.7720627	-.6358895	+ .0213293	1°32'
	2	- 6'	+ .4780812	-.5430114	+ .6903455		-.7723108	-.6342254	+ .0359757	
11	1	+ 14'	-.3296023	+ .7661019	+ .5517702	1°03'	-.6344149	-.6125301	+ .6386152	0°28'
	2	- 6'	-.9649335	-.1551885	+ .2117073		-.1539427	+ .9878245	+ .0224580	
12	1	+ 6'	-.8804711	-.4028102	+ .2500293	0°51'	-.3828479	+ .9152013	+ .1261734	2°56'
	2	- 2'	+ .0125932	-.2133302	+ .9768990		+ .5779945	+ .7987739	+ .1669812	
13	1	+ 14'	-.1871147	-.8227198	+ .5367684	0°39'	-.9750260	+ .2220906	+ .0005155	0°33'
	2	- 9'	-.6793180	+ .7051326	+ .2032611		-.6659298	-.7087056	+ .2329679	
14			ONE VARIANT ONLY							
15			ONE VARIANT ONLY							
16	1	+ 11'	+ .9603336	+ .2691152	+ .0730507	1°31'	-.2762728	+ .9537767	+ .1182511	0°27'
	2	- 5'	-.5396189	+ .6287750	+ .5598662		-.6565061	-.7305834	+ .1877436	
17(a)	1	+ 5'	+ .3238549	+ .9416635	+ .0915396	1°38'	+ .9347378	-.3334278	+ .1228464	0°26'
	2	- 4'	+ .5790033	-.5800977	+ .5729239		-.7691097	-.6218257	+ .1476589	
17(b)	1	+ 9'	+ .3261412	+ .9399216	+ .1008922	1°35'	+ .9321182	-.3375245	+ .1312738	0°15'
	2	- 7'	+ .5728445	-.5868322	+ .5722563		-.7753931	-.6143152	+ .1462276	

\* The standard deviation refers to the least square fitting of a cubic lattice to the experimental poles determined using the Kossel technique.  
 ... of the absolute accuracy of the method.

sufficient contrast, then an orientation relationship, accurate to limits of  $\pm 0.1^\circ$ , should be determinable.

In the present case this was not possible because of the eutectoid reaction. Provided however, that three or more variants of the precipitated ferrite could be found in any prior austenite grain, this difficulty was overcome by using the method described in Section 6.3.5 (B). Because it requires only a knowledge of the ferrite orientations an orientation relationship determined by this method should retain the precision of the individual ferrite orientations as determined by the Kossel technique. The validity of this method requires that the ferrite crystals be exact crystallographic variants. That this condition is satisfied can be judged by the accuracy with which an austenite lattice can be fitted to the determined axes of rotation; for exact variants the least squares deviation should be of the order of  $\pm 0.1^\circ$ .

### 7.3.3 Method B : The Multiple Variant Solutions

The results reported in this section are divided into two parts according to whether there were two or three ferrite plate variants present in one austenite grain. The method of analysis varies slightly in the two cases and only the latter case provides a unique solution if a single grain is examined.

#### (a) Two Variants

Eight of the eleven grains analysed contained two Widmanstätten plate variants, and the calculated close packed ferrite planes and directions which were nearly parallel to  $\{111\}_F$  planes and  $\langle 110 \rangle_F$  directions respectively for these eight cases, are shown in Table 7.6.

TABLE 7.7

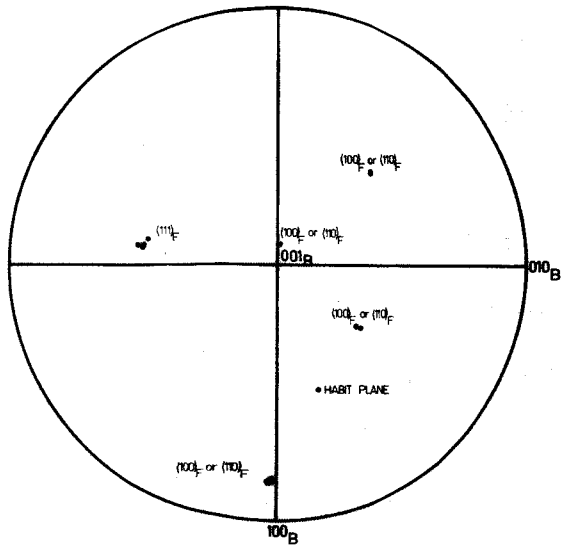
Computed axes of rotation for the  
specimens containing two variants.

Specimen No.	ROTATION AXIS Direction cosines in ferrite basis
7	+.5652703 -.5877167 +.5788424
8	-.6609452 +.1172519 +.7412175
9	ONE VARIANT ONLY
10	+.5677101 -.5882992 +.5758553
11	-.6357706 +.1439258 +.7583410
12	+.9887025 -.1492127 +.0142466
13	-.6019905 +.1559912 +.7831182
14	ONE VARIANT ONLY
15	ONE VARIANT ONLY
16	+.7382703 +.4054520 +.5390413
17(a)	+.7369172 +.4059613 +.5405077
17(b)	+.7357612 +.4074709 +.5409463

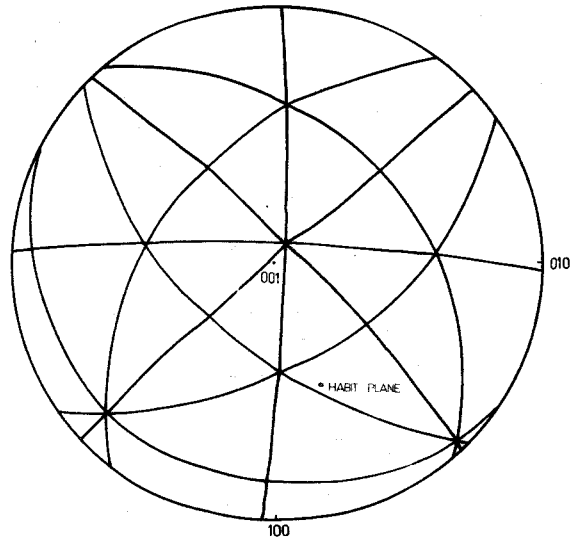
The identities of the matching  $\{101\}_B$  planes and  $\langle 111 \rangle_B$  directions were found by plotting stereographically the austenite orientation determined from twin trace measurements and the ferrite orientations determined from Kossel analysis. Since, in each case the habit plane was known, once the required ferrite planes and directions were identified the direction cosines of these vectors (in the I basis) could be easily calculated using the orientation defining matrix determined by the least squares programme. Whereas the numbers in Tables 7.3 and 7.4 show unadjusted, experimentally determined poles, the values in Table 7.6 are obtained from the least square analysis and the deviation, shown in column three, is included as a measure of the confidence of these results.

If the orientation relationship is exactly that of Kurdjumov-Sachs the angle between the relevant  $\{101\}_B$  of the respective variants (ie. matching  $\{111\}_F$ ) must be  $70^{\circ}32'$  or zero, while the angle between the  $\langle 111 \rangle_B$  must be  $60^{\circ}$ ,  $90^{\circ}$  or zero, within the limits of experimental error. The results show that, for 95% confidence (2 standard deviations), either the planes or directions, or both, deviate significantly from exact parallelism in five of the eight cases. Variations from specimen to specimen are also apparent and this may be observed in Figure 7.12, where the ferrite poles are indicated on a standard austenite projection.

The computed axes of the rotation required to bring the two ferrite lattices into coincidence are shown in Table 7.7. If each of the pairs of laths studied are exactly variants these calculated rotation axes represent low index (symmetry) planes of the parent lattice.



(a)



(b)

Fig. 7.13 The method of calculating the orientation relationship using two variants.  
 (a) The "pole figure" of the rotation axes with their form relative to the austenite axes, plotted with the ferrite in standard projection and the habit plane in the triangle bounded by  $[100]_B$ ,  $[101]_B$  and  $[111]_B$ .  
 (b) Full stereographic projection of the austenite lattice which fits the rotation axes shown in (a) with least squares deviation. The ferrite lattice is in standard projection.

By plotting the ferrite lattice in standard projection, with the habit plane in the triangle bounded by  $[100]_B$ ,  $[101]_B$  and  $[111]_B$ , the experimentally determined axes of rotation were located with respect to the ferrite base vectors, as shown in Figure 7.13 (a), for each case. Because each axis represents a prominent austenite lattice direction, by selecting (in groups of five) sets of these axes for processing with the least squares programme, it was possible to define a number of austenite orientations best fitting the different groups of selected axes.

Reference to Figure 7.13 (a) shows that the rotation axes for which there was more than one determination exhibited some scatter and the computed austenite orientations were found to have corresponding varying degrees of fit, with standard deviations ranging from  $0.13^\circ$  -  $0.78^\circ$ . While the larger figure is at least four times that expected by considering the ferrite lattices to be exactly variants (with the precision of each orientation determination being  $\pm 0.1^\circ$ ), the smaller figure is almost exactly of the expected magnitude. Although these differences suggest that in at least the former case, the ferrite lattices in the group were not variants, the agreement in the best cases strongly suggests that they were.

The orientation of the austenite lattice defined by the set of rotation axes giving the smallest value of the standard deviation is shown plotted stereographically in Figure 7.13 (b) with the ferrite in standard projection.

The direction cosines of the corresponding close packed planes and directions, referred to the standard austenite basis, were

respectively:

$$(101)_B \parallel \begin{pmatrix} +.5766404 \\ +.5894468 \\ +.5657193 \end{pmatrix}_F$$

$$[\bar{1}\bar{1}\bar{1}]_B \parallel \begin{bmatrix} -.7156742 \\ +.6984321 \\ +.0017642 \end{bmatrix}_F$$

The close packed ferrite plane is  $0^\circ 58'$  from  $(111)_F$  and the close packed direction  $0^\circ 42'$  from  $[\bar{1}\bar{1}\bar{0}]_F$ .

Many additional specimens were produced using the emission heater and searched for grains containing three Widmanstätten laths with different habit planes. One such specimen, suitable for analysis, was produced together with several more two variant cases. When analysed, the two variant specimens were found to have rotation axes very close to those already found and these have also been included in Figure 7.13.

#### (b) Three Variants

The analysis for the case of the three ferrite variants was carried out as follows:

- (i) The three axes of rotation, found by combining one variant with the other two in turn, were determined.
- (ii) These axes were referred to the common I basis and the vector cross products of two pairs of these axes were also determined.
- (iii) The best-fit cubic (austenite) lattice defined by these five vectors was computed using the least squares analysis.
- (iv) The orientation relationship between each of the ferrite lattices and the common austenite was then calculated.

(a)

(b)

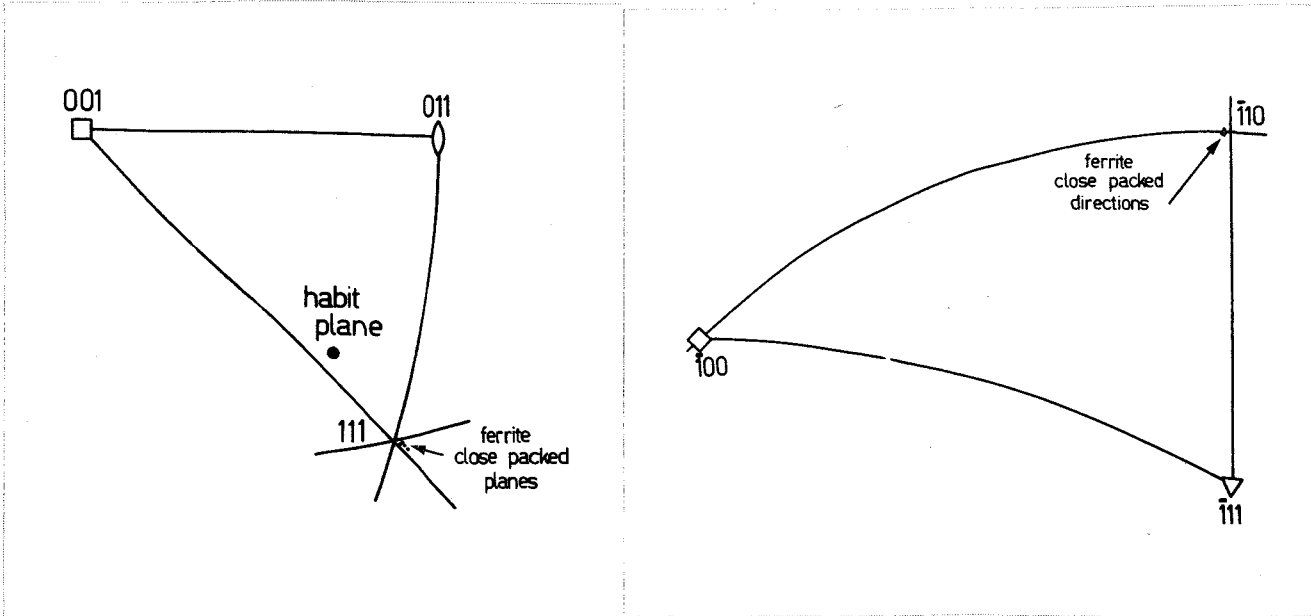
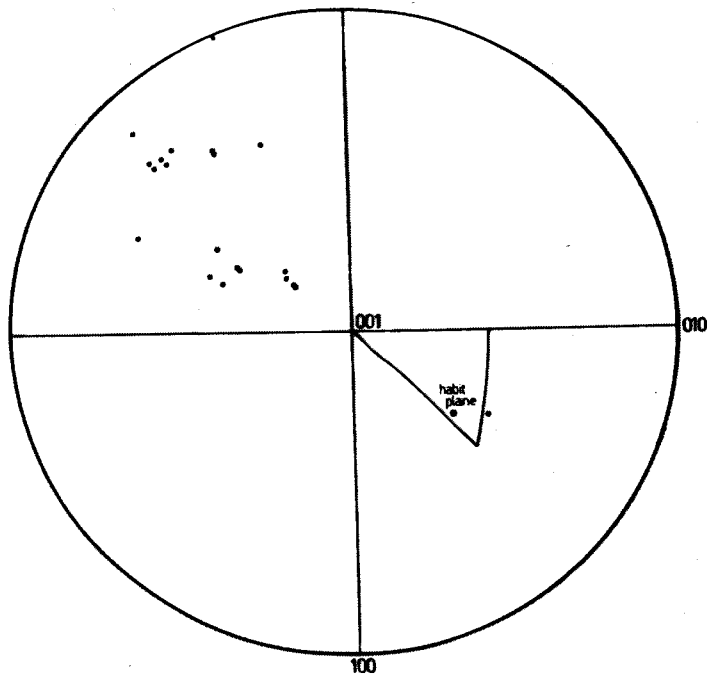


Fig. 7.14 The orientation relationships for the single three variant case examined.  
(a) Stereographic projection of the three  $\{101\}_B$  with the austenite in standard projection.  
(b) Stereographic projection of the three  $\langle 111 \rangle_B$  with the austenite in standard projection.

(a)



(b)

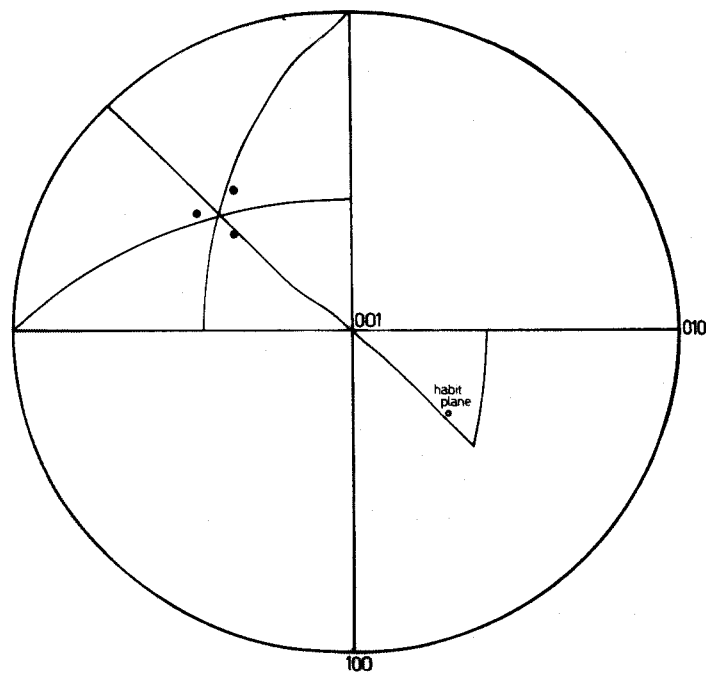


Fig. 7.15 Stereographic projection of the specimen surface normals with respect to the habit plane and the standard austenite lattice.  
(a) The two variant case.  
(b) The three variant case.

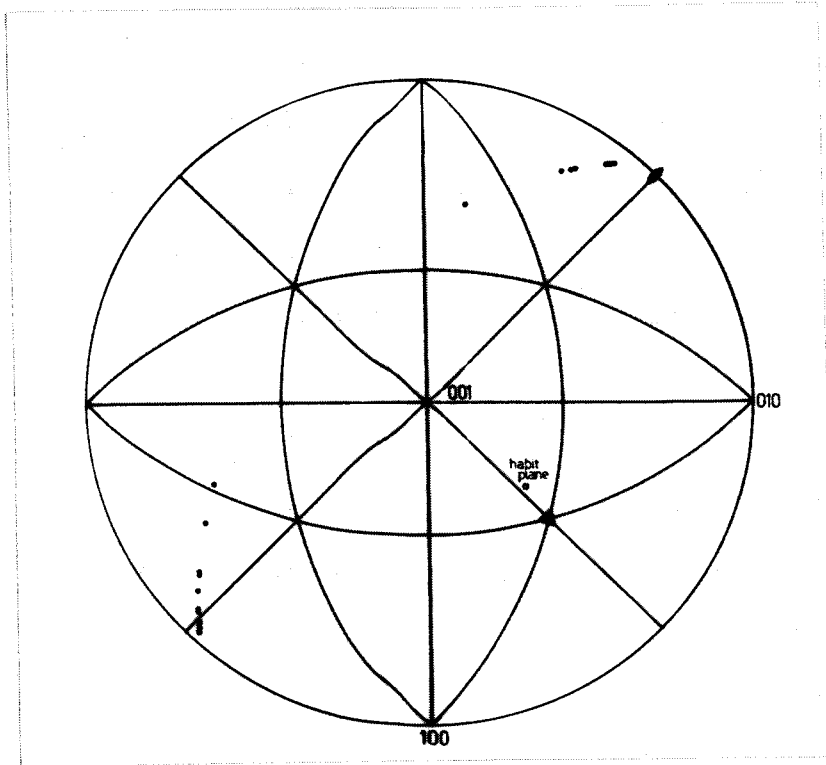


Fig. 7.16 Stereographic projection of the long directions of the ferrite plates in specimen Nos. 7 - 17 (filled circles).

It was found that an austenite orientation could be fitted to the experimental rotation axes with a standard deviation of  $\pm 0.17^\circ$  and this was taken as reasonable confirmation that the ferrite lattices were variants and therefore that the method was valid. Table 7.8 summarises the data obtained for the two variant cases previously described, and the three relationships defined by the three variant cases. For both sets of results it is seen that the sense and magnitude of the deviations from exact Kurdjumov-Sachs relationship are comparable, as shown in Figure 7.14, and are not incompatible with the results obtained using the twin trace data (Figure 7.12).

It is worth noting that the distribution of the specimen surface normals, when plotted with respect to the standard austenite variant, were not randomly distributed but congregated over the area shown on Figure 7.15. In addition to this preferred distribution was the accompanying preferred directionality of the surface trace of the ferrite laths shown in Figure 7.16, where it is seen that the long direction is usually near  $[\bar{1}10]_F$ , the close packed direction.

Since it was customary to select only the largest laths for study it appears that the growth of this morphology is enhanced when certain geometric and physical conditions are satisfied. These conditions appear to be related to the crystallographic identity of the specimen surface. In conjunction with the previously mentioned change of habit below the surface, these observations point to the possibility that the transformation may take place under conditions of low opposing constraint.

TABLE 7.9

Data for shape strain determinations.

No	I BASIS				HABIT PLANE TRACE		PLATE TILT		ANGLE BETWEEN FACES
	Twin 1		Twin 2		Face 1	Face 2	Face 1	Face 2	
	Face 1	Face 2	Face 1	Face 2					
9a	45.7°	126.3°	9.2°	-	119.3°	118.3°	7°30'	14°	89°03'
9b	"	"	"	-	119.2°	117.9°	7°30'	10°38'	"
9c	"	"	"	-	119.1°	114.3°	6°51'	15°19'	"
9d	"	"	"	-	119.8°	116.4°	7°30'	12°21'	"
15	24.0°	32.0°	127.9°	107.9°	130.9°	123.9°	6°27'	14°18'	88°50'

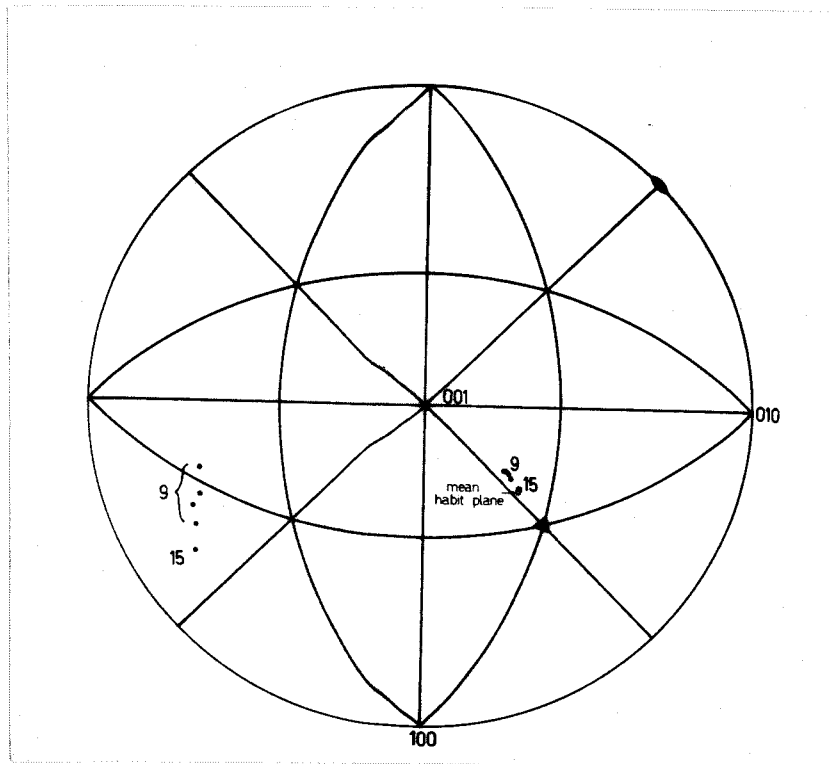


Fig. 7.17 Stereographic projection of the habit planes and corresponding shear components of the shape strain for specimen Nos. 9 (4 laths) and 15 (1 lath). The filled symbols represent the matching planes and directions for the variant of the KS orientation relationship involved.

#### 7.4 The Shape Strain

One grain containing four parallel laths and one containing a single lath, where relief effects could be observed on two surfaces (and where the austenite orientation was determinable) were produced during the course of the experimentation, Figure 6.15. The tilts in two surfaces were measured by interferometry, the habit planes were determined by two surface twin trace analysis (without sectioning) and the orientation relationships were found in the usual way. The results have already been tabulated as specimen Nos. 9 and 15 respectively. The complete experimental results are summarised in Table 7.9.

The initial and final positions of the vector defined by  $I_1$  (ie. the edge of the specimen) were calculable from the measurements in two surfaces of the plate traces and surface tilts. These allowed the direction  $d_1^*$  and magnitude  $m_1^*$  of the shear component of the strain giving rise to the shape change to be determined. These calculations were carried out algebraically using the method described in Appendix 4 and the results are shown in Figure 7.17. The habit plane for specimen No. 15 was much nearer the average value of the earlier determinations than those for specimen No. 9 and the results for this specimen were:

$$d_1^* \text{ (shear component)} = \begin{bmatrix} .5609865 \\ -.8001226 \\ .2123629 \end{bmatrix}$$

$$m_1^* \text{ (magnitude)} = 0.47$$

$$p_1' \text{ (habit plane)} = \begin{pmatrix} .4402022 \\ .5055815 \\ .7420305 \end{pmatrix}$$

These values were used in the calculations described in the next chapter.

For this specimen, the twin trace analysis allowed the austenite orientation to be determined to within the limits of  $\pm\frac{1}{4}^\circ$ , while the measured traces of the habit plane showed standard deviations of  $\pm\frac{1}{2}^\circ$ , suggesting a maximum error of about  $1\frac{1}{2}^\circ$  for the habit plane determination.

Although this lath was actually v-shaped, only one side was well enough developed to allow tilt measurements to be made (Figure 6.15). When tilt determinations were made at different positions along its length considerable scatter was evident (up to  $\pm 1^\circ$ ). This scatter was partially attributable to surface rumpling introduced during austenitization and to the narrowness of the lath, and also to an inhomogeneity in the tilt. The variation of tilt along the length of the plate is in evidence in Figure 6.15 as shown by the presence of striations parallel to the habit plane trace. It was unlikely therefore, that the direction of the shear component of  $d_1$  in the I basis was determined with an accuracy of better than between  $\pm 2^\circ$  and  $\pm 3^\circ$ .

The interfereograms in Figure 6.15 also show that the "tail" of the lath does not produce a change of shape, substantiating the previous suggestion that the platelike portion immediately below the surface may result from a mode of transformation, possible only because of the proximity of the specimen surface. Despite the previous observation that the "tail" appears to be continuous with the lath, the absence of a shape change points to a possible change in the transformation mechanism below the specimen surface.

CHAPTER 8APPLICATION OF THE CRYSTALLOGRAPHICTHEORY TO THE FORMATION OF WIDMANSTATTEN FERRITE.

	Page
8.1 Introduction.	132
8.2 The Choice of a Transformation Model.	132
8.3 Calculation of the Strains.	136

8.1 Introduction

The experimental results reported in the previous section show that Widmanstätten ferrite, precipitated from austenite at a free surface, has geometric and crystallographic features that appear to be analogous to those accompanying martensitic transformations. In this chapter an analysis of the transformation is made to determine whether these features can be accounted for by the crystallographic theory of martensitic transformations. A successful account would provide the strongest evidence that the atom displacements are martensitic in nature, and so substantiate that the existence of a correspondence is implied by the change of shape.

8.2 The Choice of a Transformation Model

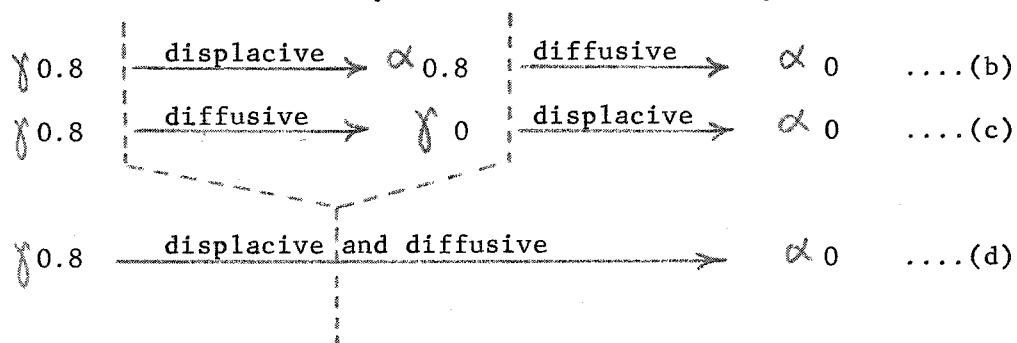
Application of the crystallographic theory to a transformation requires a knowledge of the initial and final structures and the correspondence relating them. In diffusionless transformations there is no difficulty in recognizing these structures. When a phase transformation is observed to be accompanied both by long range diffusion and a change of shape, however, it is not necessarily clear at what stage of the transformation the martensitic characteristics apply. In the case

of ferrite forming from austenite no details of the transformation mechanism are available from experiments nor is its exact nature immediately evident from considerations of phase equilibria.

For the iron/0.45% carbon alloy, the reaction



cannot be sustained because the austenite at the  $\gamma/\alpha$  interface must become rapidly enriched with carbon and will almost immediately reach the composition that is in equilibrium with ferrite at the transformation temperature, viz: 0.8% at 700°C. Thus for continued growth the possible interface reactions may be one of the following:



where the dotted lines represent schematically "interfaces" separating regions of different crystal structure and/or composition. Models (b) and (c) represent extreme cases, where transition structures having complete carbon supersaturation and complete carbon depletion are formed as hypothetical intermediate products. In model (d) there is no transition structure and the initial and final states are taken to be the equilibrium phases of the transformation, with both the diffusive and displacive atom movements taking place within a single interface. It should be noted that model (d) is only likely to be applicable to the case of an interstitial solute where diffusion does not destroy the correspondence.

TABLE 8.1

The lattice parameters for ferrite and austenite used in the calculations.

Phase	Lattice Parameter (A°)	Volume of Unit Cell (A <sup>3</sup> )
0	2.897	24.313
0.8	2.920*	24.897
0	3.633	47.950
0.45	3.648	48.547
0.80	3.659	48.988

\* Supersaturated ferrite.

Since the transformation was carried out isothermally at 700°C the lattice parameters required are those characteristic of this temperature. The lattice parameter of ferrite was taken from high temperature data tabulated by Pearson (128), while that of supersaturated ferrite was estimated by assuming the body centred cell to have a volume equal to that of a martensite cell of the same composition. The latter calculation was made using the room temperature martensite parameters tabulated by Pearson (128) and extrapolating these to 700°C using the coefficient of thermal expansion of pure  $\alpha$ -iron implied by his plot of lattice parameter versus temperature.

The parameters of the equilibrium and transition austenite lattices at room temperature were calculated using the empirical equation of Ridley et al (129), and the high temperature values were found by extrapolating these to 700°C, assuming the coefficient of thermal expansion to be independent of carbon concentration and equal to that of pure  $\gamma$ -iron.\* Table 8.1 shows the lattice parameters and the corresponding cell volumes for each of these phases.

Oblak and Heheman (82) have suggested that in upper bainite the bainitic ferrite may form with some supersaturation, and it is possible that the degree of supersaturation is temperature dependent. If this is so, then Widmanstätten ferrite may precipitate with some initial supersaturation and the compositions of the phases will not be those corresponding to phase equilibrium, model (d), but will be intermediate between models (b) and (d). On this basis there is an unlimited

---

\* The calculated values were found to differ by less than 0.2% from recent experimental values communicated privately by Dr. Ridley.

number of possible transition states that could be proposed by assuming a different degree of supersaturation of the precipitating phase, but in the absence of experimental evidence any attempt to nominate one value must be purely speculative. For this reason the present analysis considers in detail only the two extreme cases of equilibrium, model (d), and complete supersaturation of the ferrite, model (b). As will be seen the changes in the lattice parameters result in only minor changes in the predictions of the theory and it was reasoned that the two cases considered cover the range of possible situations.

The relative merits of these models are considered on the basis of the agreement between the observed geometric and crystallographic features and the predictions of the crystallographic theory and no attempt is made to account for the role of the diffusional atom movements which give rise to the composition change (and therefore the kinetics of the transformation). The analysis is an attempt to determine whether the crystallographic and geometric features can be accounted for by a martensitic mode of transformation involving a correspondence of lattice sites. The justification for the adoption of one of these models would be agreement between the experimental observations and the predictions of the theory.

\_\_\_\_\_

\_\_\_\_\_

### 8.3 Calculation of the Strains

#### 8.3.1 The Correspondence and the Pure Strain

With the habit plane located in the stereographic triangle defined by  $[001]_F$ ,  $[111]_F$  and  $[011]_F$  the particular variant of the observed orientation relationship is described by the correspondence matrix:

$${}^C_B F = \begin{pmatrix} 0 & 1 & 1 \\ 0 & \bar{1} & 1 \\ 1 & 0 & 0 \end{pmatrix}$$

The mutually orthogonal set of vectors  $[100]_F$ ,  $[011]_F$  and  $[0\bar{1}1]_F$  correspond to the mutually orthogonal vectors  $[001]_B$ ,  $[100]_B$  and  $[010]_B$  respectively, and can therefore be taken as the principal axes of the pure strain component of the total lattice strain.

The transformation of one set of mutually orthogonal vectors into another by a lattice strain implies that the strain is homogeneous, and such a strain can always be factorized into a pure strain, B, and a rigid body rotation, R. The principal strains of the pure strain are respectively  $(a'/a)$ ,  $(\sqrt{2}a'/a)$  and  $(\sqrt{2}a'/a)$ . Written in matrix form the pure strain becomes:

$${}^B_P P = \begin{pmatrix} (a'/a) & 0 & 0 \\ 0 & (\sqrt{2}a'/a) & 0 \\ 0 & 0 & (\sqrt{2}a'/a) \end{pmatrix} \quad \dots 9.1$$

where P is the orthogonal basis defined by the principal axes. It can be shown (7) that this matrix takes the same form relative to the F basis because

$${}^B_F F = (F^T P) (P^B P) (P^T F) \quad \dots 9.2$$

Since the strain B produces no rotation of the principal axes, R is the

rotation that must accompany B in order to produce the final lattice in its correct orientation.

$$S_T = RB$$

which is equation 2.10.

For convenience the BM analysis (36) uses a slightly different pure strain. By considering the invariant line strain, S, obtained from  $S_T$  by removal of the small dilatation, the relationship defining the pure strain is given by:

$$S = RM \quad \dots 9.3$$

and

$$M = \begin{pmatrix} \theta & 0 & 0 \\ 0 & \sqrt{2}\theta & 0 \\ 0 & 0 & \sqrt{2}\theta \end{pmatrix} \quad \dots 9.4$$

where

$$\theta = \delta (a'/a)$$

The pure strain M depends on the lattice parameters of the initial and final structures and therefore on the model chosen for the transformation.

The vectors unextended by the pure strain are given by the solutions to the equations:

$$x' {}_F M_F^2 x = 1 \quad \dots 9.5$$

$$p' {}_F M_F^{-2} p = 1 \quad \dots 9.6$$

The loci of all vectors satisfying these two equations are circular cones with an axis parallel to  $[100]_F$  and with semi-apex angles equal to:

$$\phi_i = \cos^{-1} ((2\theta^2 - 1)/\theta^2)^{\frac{1}{2}} \quad \dots 9.7$$

$$\phi_- = \cos^{-1} (2\theta^2 - 1)^{\frac{1}{2}} \quad \dots 9.8$$

$\Phi_i$  defines the initial positions of all directions and the final position of all normals unchanged in length by M, and therefore by S. Similarly,  $\Phi_f$  defines the final positions of all directions and the initial positions of all normals unchanged in length by S.

### 8.3.2 The Invariant Line Strain

The strain S is composed of an IPS and a shear so that the line of intersection of the two invariant planes is also invariant, ie. S is an invariant line strain. A corollary of this is that the two directions of displacement define a plane which is unrotated and the spacing of which is unchanged, ie. a plane with an invariant normal.

The only potential positions of the invariant line,  $x_i$ , and the invariant normal,  $n_i$ , are along the cone generators defined by  $\Phi_i$  and  $\Phi_f$  respectively. The additional conditions that locate  $x_i$  and  $n_i$  uniquely are a knowledge of either the elements of the complementary strain (7, 35), or the habit plane and the orientation relationship (36).

Since  $x_i$  and  $n_i$  are rotated by M, R is the rigid body rotation that restores both  $Mx_i$  and  $n_i M^{-1}$  to their initial positions, thus leaving them invariant. The axis (U) and amount ( $\epsilon$ ) of this rotation can be determined by making use of the following conditions. U is the direction of intersection of two planes, one of which is the locus of directions equiangular to  $x_i$  and  $Mx_i$  and the other of which contains directions equiangular to  $n_i$  and  $n_i M^{-1}$ . The angle,  $\epsilon$ , between the planes defined by either  $(U \times x_i)$  and  $(U \times Mx_i)$  or  $(U \times n_i)$  and  $(U \times n_i M^{-1})$ , determines the amount of the rotation R.

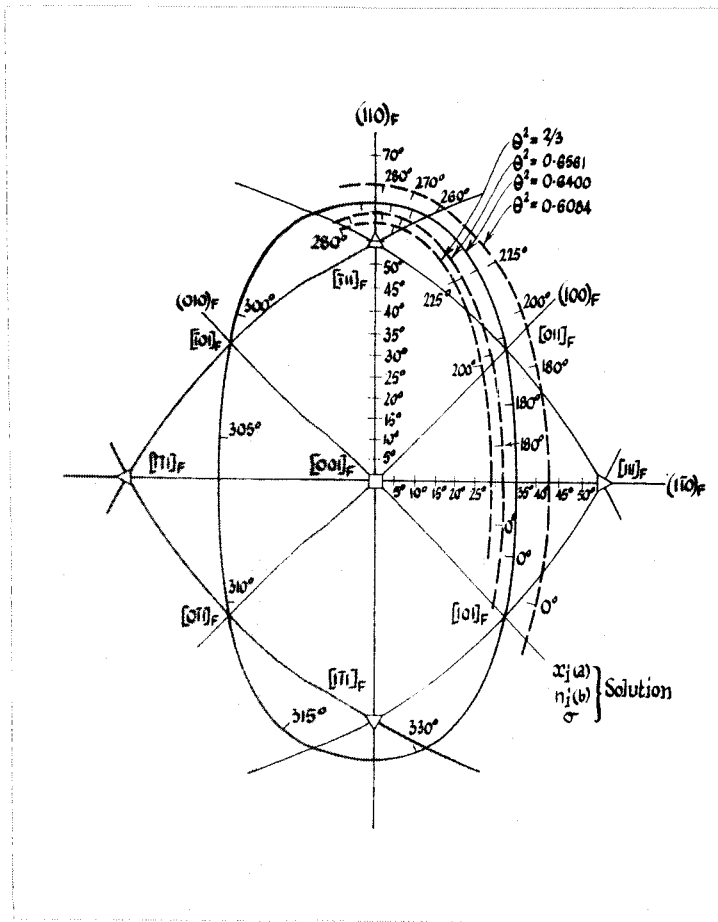


Fig. 8.1 Stereographic projection showing the variation of the bainite habit plane as a function of the parameters  $\theta$  and  $\sigma$ , where  $\theta = (a'/a)$  and  $\sigma$  is the angular distance of the shear plane normal from  $(110)_F$  along the  $[\bar{1}10]_F$  zone.

after Bowles and Kennon (56)

### 8.3.3 Factorization of the Strain

#### (a) Predicting the Habit Plane from a Knowledge of the Complementary Strain

The original or "forward" analysis of martensitic transformations (35) requires that the elements of the complementary strain be known, and this, in conjunction with the lattice parameters, allows the remaining characteristics of the transformation to be found in terms of the variable parameter,  $\theta$ .

No direct experimental evidence of the possible nature of the complementary strain was available for the present case, but inspection of the calculations of Bowles and Kennon (56) for the bainite transformation in steels, shows that for  $\theta^2 \approx 0.60$  and for a complementary shear in the  $[\bar{1}10]_F$  on a plane defined by  $\sigma \approx 40^\circ$ , solutions with habit planes about  $10^\circ$  from  $(111)_F$  are obtained.  $\sigma$  is the angular distance of  $p_2'$  from  $[110]_F$  measured along the  $[\bar{1}10]_F$  zone, and the solutions calculated by Bowles and Kennon are shown in Figure 8.1.

Using the physically realizable  $(111) [\bar{1}10]_F$  shear (for which  $\sigma = 35^\circ 16'$ ) as the complementary strain the following results were calculated:

for

$$d_2 = [\bar{1}10]_F$$

$$p_2' = (111)_F$$

$$\theta^2 = 0.605$$

then

$$\phi_i = \cos^{-1} (.5891582) = 53^{\circ}54'$$

$$\phi_f = \cos^{-1} (.4582576) = 62^{\circ}44'$$

$$x_i = \begin{bmatrix} .5891582 & -.7841396 & .1949813 \end{bmatrix}$$

$$n_i = (.4582576 \quad .4582576 \quad .7615773)$$

which corresponds to the  $x_i(a)$ ,  $n_i(b)$  solution of the Bowles-Kennon analysis.

$$M = \begin{pmatrix} .7778175 & 0 & 0 \\ 0 & 1.0999999 & 0 \\ 0 & 0 & 1.0999999 \end{pmatrix}$$

$$R = \begin{pmatrix} .9817879 & -.1779670 & -.0664847 \\ .1728535 & .9820040 & -.0760911 \\ .0788299 & .0632132 & .9948819 \end{pmatrix}$$

$$S = RM = \begin{pmatrix} .7636518 & -.1957637 & -.0731331 \\ .1344484 & 1.0802044 & -.0837002 \\ .0613153 & .0695346 & 1.0943700 \end{pmatrix}$$

Model (b),  $\delta = .9746693$  for  $(a'/a) = .7980322$

Model (d),  $\delta = .9824074$  for  $(a'/a) = .7917464$

the predicted habit plane is

$$p'_1 = \begin{pmatrix} .4559758 \\ .5218594 \\ .7209361 \end{pmatrix}$$

This is a plane  $1^{\circ}13'$  from the mean experimental habit plane.

The orientation relationship, defined by the rotation of the close packed plane and direction is approximately  $\frac{1}{2}^\circ$  from exact KS relationship being:

$$(101)_B \parallel \begin{pmatrix} .5720031 \\ .5751823 \\ .5847887 \end{pmatrix}_F$$

$$[\overline{111}]_B \parallel \begin{bmatrix} -.7121450 \\ .7020059 \\ .0061009 \end{bmatrix}_F$$

The calculated close packed direction lies near that observed experimentally and is within the range of experimental error, but the close packed plane is  $1\frac{1}{2}^\circ$  from the mean experimental value and lies on the opposite side of  $(111)_F$ , ie. towards rather than away from the habit plane normal. The components of the macroscopic shape change are determined as:

$$d_1 = \begin{bmatrix} .5947076 \\ -.7948689 \\ .1204420 \end{bmatrix}_F$$

$$m_1 \approx 1.0$$

Although  $d_1$  is only  $5^\circ - 10^\circ$  from the direction of the measured shear component of the shape strain, the value of the strain magnitude of the shear component is too high, being approximately twice that observed. The values of the dilatation were also high, being 1.2% and 2.5% contractions for the equilibrium and supersaturated models respectively.

It is concluded that a simple shear on the slip system  $(111) [\bar{1}10]_F$  is unlikely to be the complementary strain in this transformation. The only other solutions compatible with the observed habit plane occur for a small range of irrational shear planes in the zone of  $[\bar{1}10]_F$  near  $(111)_F$ , but these would all have correspondingly high value of the strain magnitudes and are therefore unreasonable alternatives.

Further inspection of Kennon's (61) calculations shows that varying  $d_2$  in the zone of  $p'_2 = (110)_F$  cannot predict the observed habit plane and other possibilities for the complementary strain must be considered.

(b) Predicting the Complementary Strain from a Knowledge of the Habit Plane

The "reverse" approach permits the complementary shear elements to be predicted from a knowledge of the habit plane and the orientation relationship. In general, because of the errors associated with the experimentally determined orientation relationship, the orientation-defining rotation is not known exactly and the factorization of  $S_T$  is not possible. Either a method of adjusting the orientation relationship, or alternatively, of calculating  $S_T$  without using the experimental orientation relationship is therefore required (3). By retaining the postulate that the complementary strain is a simple shear, then the IPS may be determined as follows, using the method of BM (36).

From equation 9.4 the pure strain  $M$  may be determined if  $\theta$  is known. Evaluation of  $\theta$  requires nominating a value for  $\delta$  and hence proposing a model for the reaction in order that the lattice parameters can be defined. For the purpose of the present analysis calculations

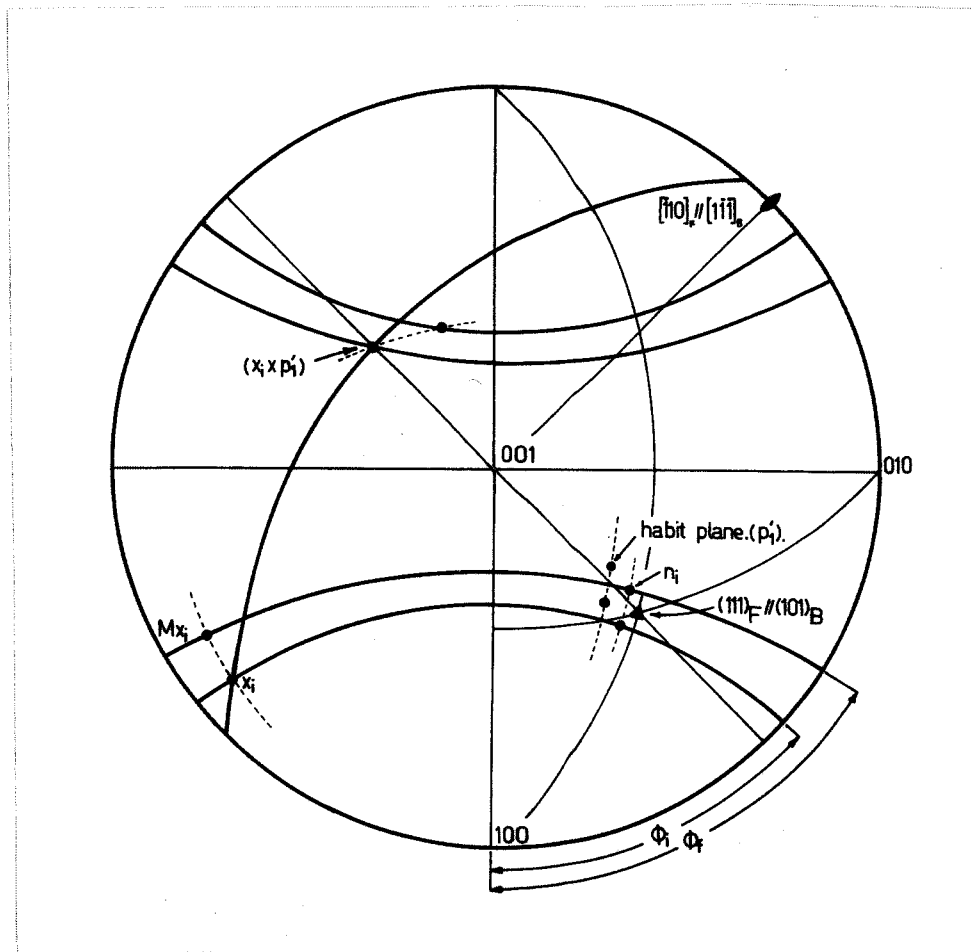


Fig. 8.2 Stereographic projection showing the initial and final positions of the invariant line  $x_i$  and the invariant normal  $n_i$  on the initial and final cones defined by  $\phi_i$  and  $\phi_f$  respectively, for the variant of the correspondence previously described. The austenite lattice is drawn in standard projection.

were made using the parameters for both the reactions:



and



with  $\delta$  set initially equal to unity.

The intersections of the known habit plane with the cones defined by equations 9.7 and 9.8 locate two possible positions for  $x_i$ . Only the intersection labelled  $x_i$  in Figure 8.2 leads to strains compatible with the observed orientation relationship and complete solutions using the other intersection will not be considered further.

The orthogonal basis defined by  $x_i$ ,  $p'_1$  and  $(x_i \times p'_1)$  is related to the F basis by a rigid body rotation  $R_1$ .  $R_1$  may be written as a (3 x 3) matrix, the respective columns of which are the vectors  $x_i$ ,  $p'_1$  and  $(x_i \times p'_1)$  referred to the F basis. Another basis, defined by the positions of  $x_i$  and  $p'_1$  after the strain M and their cross product, is related to the F basis by a second rigid body rotation  $R_2$  the columns of which are derived in a similar way to  $R_1$ .

The rotation which carries the displaced vectors  $M x_i$  and  $p'_1 M^{-1} / (p'_1 M^{-2} p_1)^{\frac{1}{2}}$  back to their initial positions  $x_i$  and  $p'_1$  is:

$$R_o = R_1 R'_2 \quad \dots 9.9$$

and

$$S_o = R_o M \quad \dots 9.10$$

$S_o$  is therefore a strain which leaves  $x_i$  invariant and the plane  $p'_1$  unrotated. The most general strain compatible with the observed habit plane can differ from  $S_o$  only by a small rotation  $R_w$  about the invariant line (36).

thus:

$$\begin{aligned} S &= R_{\psi} R_0 M && \dots 9.11 \\ &= R M \end{aligned}$$

$R_0$  is determined uniquely using only the observed habit plane and lattice parameters. The rotation  $R_{\psi}$  can be determined explicitly by using a value of  $\psi$  chosen to give best possible agreement with the observed orientation relationship. Values of  $\psi = 45^\circ$  and  $\psi = 60^\circ$  were chosen and solutions for these cases were determined.

The factorization of  $S$  is achieved using the relationships:

$$p'_2 \parallel (p'_1 S - g p'_1) \quad \dots 9.12$$

where  $g$  is the determinant of  $S$ . Also  $d_2$  must lie in the zones of

$p'_2$  and  $n_i$ ,

therefore

$$d_2 \parallel (p'_2 \times n_i) \quad \dots 9.13$$

and

$$d_1 \parallel (S d_2 - d_2) \quad \dots 9.14$$

These equations show that, since  $d_2$  is invariant to  $P_2$ , its total displacement must be due to  $P_1$  and parallel to  $d_1$ . It can be shown that:

$$d_1 = (S d_2 - d_2) p'_1 d_2 \quad \dots 9.15$$

which is not a unit vector. The factor required to normalize  $d_1$  gives the magnitude,  $m_1$ , of the IPS.

(a) Calculations for equilibrium ferrite (model d)

$$(a'/a) = .7917464, \quad \delta = 1$$

$$\theta^2 = .6268623$$

$$\phi_i = \cos^{-1} (.6362023)$$

$$\phi_f = \cos^{-1} (.5037108)$$

$$P'_1 = (.4402022 \quad .5055816 \quad .7420305)$$

$$x_i = [ .6362023 \quad -.7587911 \quad .1395807 ]$$

$$M = \begin{pmatrix} .7917464 & 0 & 0 \\ 0 & 1.1196985 & 0 \\ 0 & 0 & 1.1196985 \end{pmatrix}$$

$$R_o = \begin{pmatrix} .9827046 & -.1765020 & -.0560235 \\ .1724970 & .9825389 & -.0697285 \\ .0673525 & .0588586 & .9959916 \end{pmatrix}$$

Case (i)  $\psi = 45'$ ,

$$R_\psi = \begin{pmatrix} .9999490 & .0017857 & .0099399 \\ -.0018684 & .9999637 & .0083186 \\ -.0099247 & -.0083367 & .9999160 \end{pmatrix}$$

$$S = \begin{pmatrix} .7787871 & -.1949993 & -.0517806 \\ .1355588 & 1.1010248 & -.0686779 \\ .0444611 & .0586882 & 1.1163901 \end{pmatrix}$$

for which

$$n_i = (.5037109 \quad .6271180 \quad .5941366)$$

$$P'_2 = (.1983728 \quad .3357138 \quad .9208390)$$

$$d_2 = [ -.7348859 \quad .6726004 \quad -.0868989 ]$$

$$d_1 = [ .8108806 \quad -.5804063 \quad -.0748413 ]$$

$$m_1 \approx 0.9$$

Case (ii)  $\psi = 1^\circ$

$$R_\psi = \begin{pmatrix} .9999093 & .0023625 & .0132563 \\ -.0025095 & .9999354 & .0110871 \\ -.0132292 & -.0111194 & .9998507 \end{pmatrix}$$

$$S = \begin{pmatrix} .7790119 & -.1941383 & -.0481247 \\ .1352038 & 1.1013029 & -.0655479 \\ .0415065 & .0562756 & 1.1167418 \end{pmatrix}$$

for which

$$n_i = (.5037107 \quad .6478853 \quad .5714194)$$

$$p'_2 = (.1288363 \quad .2828626 \quad .9504684)$$

$$d_2 = [-.7453786 \quad .6603154 \quad -.0916200]$$

$$d_1 = [ .8231628 \quad -.5606321 \quad -.0899701 ]$$

$$m_1 = 0.8$$

(b) Calculations for saturated ferrite (model b)

$$(a'/a) = .7980322, \quad \delta = 1$$

$$\theta^2 = .6368555$$

$$\phi_i = \cos^{-1} (.6555799)$$

$$\phi_f = \cos^{-1} (.5231739)$$

$$p'_1 = (.4402022 \quad .5055816 \quad .7420305)$$

$$x_i = [ .6555799 \quad -.7456674 \quad .1191434 ]$$

$$M = \begin{pmatrix} .7980322 & 0 & 0 \\ 0 & 1.1285880 & 0 \\ 0 & 0 & 1.1285880 \end{pmatrix}$$

$$R_o = \begin{pmatrix} .9826352 & -.1770170 & -.0556143 \\ .1730124 & .9824231 & -.0700820 \\ .0670425 & .0592431 & .9959897 \end{pmatrix}$$

Case (i)  $\psi = 45'$

$$R_\psi = \begin{pmatrix} .9999512 & .0015176 & .0097672 \\ -.0016014 & .9999620 & .0085737 \\ -.0097538 & -.0085889 & .9999155 \end{pmatrix}$$

$$S = \begin{pmatrix} .7848684 & -.1974338 & -.0519037 \\ .1372671 & 1.1096020 & -.0693528 \\ .0446630 & .0592810 & 1.1252587 \end{pmatrix}$$

for which

$$n_i = (.5231738 \quad .6350082 \quad .5683782)$$

$$p'_2 = (.0255513 \quad .1795939 \quad .9834090)$$

$$d_2 = [-.7183041 \quad .6874699 \quad -.1068851]$$

$$d_1 = [.8274107 \quad -.5382448 \quad -.1602637]$$

$$m_1 \approx 0.6$$

Case (ii)  $\psi = 1^\circ$

$$R_\psi = \begin{pmatrix} .9999132 & .0020049 & .0130256 \\ -.0021538 & .9999324 & .0114279 \\ -.0130018 & .0114550 & .9998499 \end{pmatrix}$$

$$S = \begin{pmatrix} .7850802 & -.1966681 & -.0482772 \\ .1369826 & 1.1098704 & -.0661075 \\ .0417168 & .0567477 & 1.1256154 \end{pmatrix}$$

for which

$$\begin{aligned}
 n_1 &= (.5231739 \quad .6546780 \quad .5456059) \\
 p'_2 &= (-.0619975 \quad .1040962 \quad .9926331) \\
 d_2 &= [-.7263153 \quad .6774333 \quad -.1164055] \\
 d_1 &= [.8381978 \quad -.5109678 \quad -.1906210] \\
 m_1 &\approx 0.5
 \end{aligned}$$

These results have been plotted graphically in Figure 8.3 where it can be seen that in none of the cases considered does the calculated shear component of  $d_1$  come within about  $30^\circ$  of the experimentally observed value. (The shear components are obtained graphically by the intersection of the zone ( $d_1 \times p'_1$ ) with the habit plane). With the exception of the case which considers the supersaturated model with  $\psi = 1^\circ$ , the magnitudes of the shear components of the shape strain are higher than that observed. This case however, corresponds to the direction of  $d_1$  farthest from the measured shear direction (solution 1 on the figure).

By introducing non unit values for the dilatation and using the lattice parameters for the supersaturated model with  $\psi = 0^\circ 45'$ , simultaneous agreement of the shear components of  $m_1$  and  $d_1$  with the experimentally measured value could not be obtained, as shown by the following summary of the calculations:

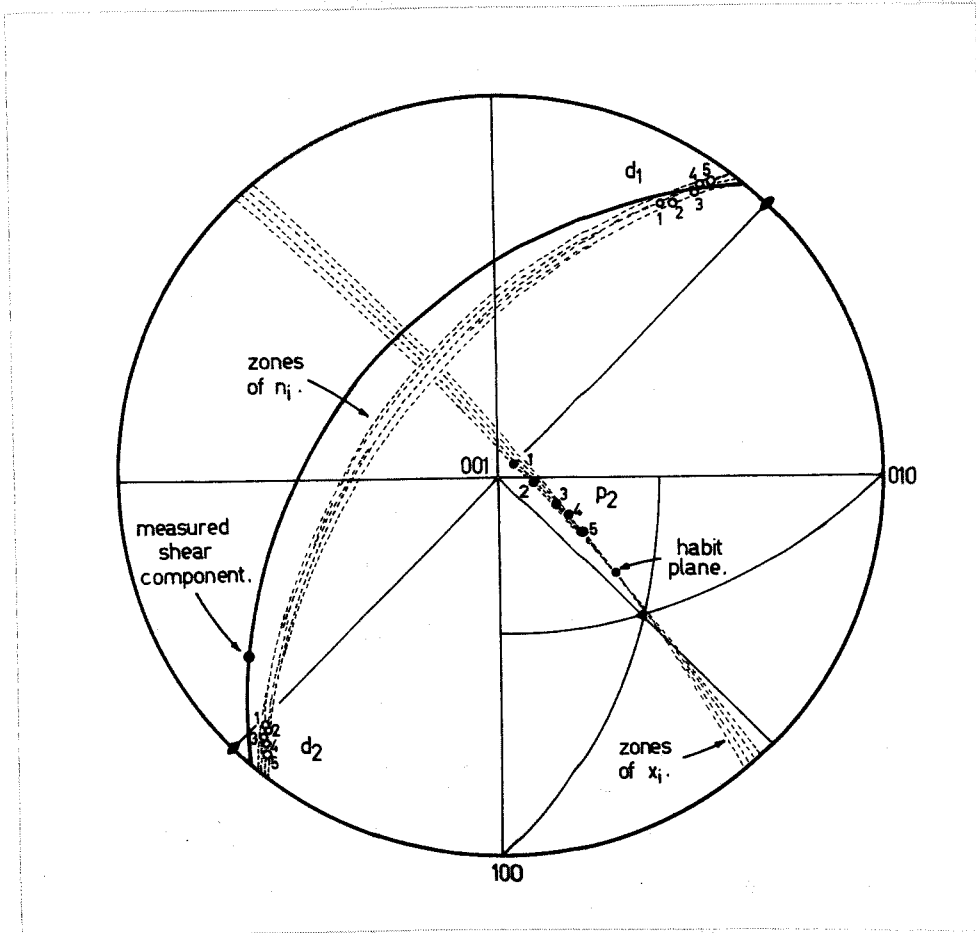


Fig. 8.3 Stereographic projection showing graphically the calculated positions of  $d_1$ ,  $d_2$  and  $p_2$  for five of the six models considered in the text. The austenite is drawn in standard projection and the negative senses of  $d_1$  and  $d_2$  are shown.

Key: 1.	Supersaturated ferrite,	$\psi = 1^\circ$ ,	$\delta = 1.0$
2.	" "	$\psi = 45'$ ,	"
3.	Equilibrium ferrite,	$\psi = 1^\circ$ ,	"
4.	" "	$\psi = 45'$ ,	"
5.	Supersaturated ferrite,	$\psi = 45'$ ,	$\delta = 0.985$

for	$\delta$	=	1.015		
	$x_i$	=	[ .6898205	- .7194395	.08096001 ]
	$n_i$	=	( .5587566	.6424620	.5244365)
	$p'_2$	=	( -.7221728	-.6916797	.0067606)
	$d_2$	=	[ .6851293	- .7139200	.1446238 ]
	$d_1$	=	[ -.3277500	-.4098216	.8512498 ]
	$m_1$	$\approx$	0.22		
for	$\delta$	=	.985		
	$x_i$	=	[ .6177354	- .7702757	.1583611 ]
	$n_i$	=	( .4855782	.6171684	.6191262)
	$p'_2$	=	( .2653397	.3937325	.8800963)
	$d_2$	=	[ -.7494297	.6585144	-.0686574 ]
	$d_1$	=	[ .8065253	-.5894899	-.0449286 ]
	$m_1$	$\approx$	1.2		

The solution for  $\delta = .985$  is also shown on Figure 8.3. From these results it can be seen that with  $\delta = 1.015$ ,  $m_1$  is significantly reduced but the direction of  $d_1$ , and hence the direction of its shear component, is remote from the measured value, and it has not been included on the figure.

Although  $\delta = 1.015$  gives better agreement for the direction of  $d_1$  the magnitude is too high, being approximately three times that observed.

Thus, using the measured habit plane, and the assumption that the total lattice strain which most closely agrees with the observed orientation relationship is an invariant line strain, the observed magnitude and direction of the shear components of the shape strain cannot be

predicted simultaneously.

If as has been proposed (58, 59) the complementary strain is composed of two or more shears which do not reduce to a single shear, then the assumption that the total lattice strain is approximately an invariant line strain is incorrect and the previous analysis is invalid. In the present case, where the initial and final states are not clearly defined but have only been nominated from considerations of the possible reaction paths, analysis of the transformation becomes extremely difficult if the invariant line strain proposal is abandoned. Hence the following analysis, which although an approximation, is presented as a means by which the possible nature of the complementary strain can be estimated. The method involves calculating the IPS capable of producing the observed relief effects.

Reference to the previous calculations or to Figure 8.3, shows that for all the invariant line strains (S) considered, the zones of  $n_i$  intersect the zone containing the measured shear component of the shape strain and the habit plane at approximately the same position. By calculating the direction of this intersection for the supersaturated ferrite model, with  $\delta = 1$  and  $\psi = 45'$ , and using this direction as  $d_1$ , an IPS consistent with the observed  $m_1^*$  and  $d_1^*$  can be determined from the relationship

$$\text{IPS} = (I + m_1 d_1 p'_1)$$

using the values

$$m_1 = .472$$

$$d_1 = \begin{bmatrix} .6006693 \\ -.747869 \\ .282644 \end{bmatrix}$$

The volume change represented by this strain is

$$\det | \text{IPS} | = 1.0453472$$

Since this must also be the volume change produced by the pure strain

$$\begin{aligned} \det | M | &= 2 \theta^3 \\ &= 1.0453472 \end{aligned}$$

from which  $\delta = 1.0093842$ , when the supersaturated ferrite parameters are substituted into this equation, through the term  $\theta$ .

If the strain S is recalculated using this value for the dilatation the strain becomes:

$$S = \begin{pmatrix} .7921611 & -.1998458 & -.0524541 \\ .1389551 & 1.1199262 & -.0698309 \\ .0451262 & .0596242 & 1.1358259 \end{pmatrix}$$

for which

$$\begin{aligned} x_i &= \begin{bmatrix} .6773811 & -.7294513 & .0951612 \end{bmatrix} \\ n_i &= (.5456446 \quad .6407261 \quad .5401314) \end{aligned}$$

The new intersection of the zone of  $n_i$  with  $(d_1 * x p'_1)$  is within  $10'$  of the arbitrarily selected trial value of  $d_1$  and the latter value was used in the calculation.

Removal of the calculated IPS representing the shape strain from the invariant line strain S, leaves another invariant line strain which is identifiable with the complementary strain. Since the volume change of the remaining strain is zero it can only be a combination of shears.

$$P_2 = \begin{pmatrix} .6694017 & -.3416073 & -.2652849 \\ .2917978 & 1.2964278 & .1951562 \\ -.0126381 & -.0070814 & 1.0356786 \end{pmatrix}$$

By expanding the general equation of a shear to give:

$$\text{Shear} = I + m \begin{pmatrix} d_1 p_1 & d_1 p_2 & d_1 p_3 \\ d_2 p_1 & d_2 p_2 & d_2 p_3 \\ d_3 p_1 & d_3 p_2 & d_3 p_3 \end{pmatrix}$$

(where  $d_1, d_2, d_3$  are the components of the shear direction and  $p_1, p_2, p_3$  are the components of the shear plane normal), and equating the terms of this matrix with those of the numerical matrix above, it can be shown that  $P_2$  is not consistent with a single shear. For example when 1.0 is subtracted from the terms of the leading diagonal of the numerical matrix for  $P_2$  the ratios of the terms of any column are:

$$m p d_1 : m p d_2 : m p d_3$$

For the respective columns these are:

Column 1,	-.3306983	:	.2917978	:	-.0126381
Column 2,	-.3416073	:	.2964278	:	-.0070814
Column 3,	-.2652849	:	.1951562	:	.0356786

Similarly for the rows

$$m d p_1 : m d p_2 : m d p_3$$

giving:

Row 1,	-.3306983	:	-.3416073	:	-.2652849
Row 2,	.2917978	:	.2964278	:	.1951562
Row 3,	-.0126281	:	-.0070814	:	.0356786

Although three different values for  $d$  and  $p'$  are obtained, the first and second rows and columns yield solutions near  $(111) [\bar{1}10]_F$  suggesting that this may constitute at least part of the complementary strain.

The foregoing analysis is admittedly an approximation and possibly of limited value, since it assumes that the total lattice strain is, apart from the dilatation, an invariant line strain. This is not necessarily true when the complementary strain is more complex than a simple shear. It is therefore not surprising that the calculated complementary strain is not a simple shear since the "reverse" calculations previously described have already considered the possible factorizations of  $S$  using this assumption.

Furthermore, the elements of the complementary strain are sensitive to the magnitude and direction of the shape strain so that in the absence of accurate experimental values for these quantities, any attempt to predict the complementary strain using other than the most accurately measured values can only be approximate.

Within these limitations the results of the calculations suggest that either the experimentally determined quantities of the orientation relationship and shape strain are in error, or that the complementary strain is not a simple shear and therefore that  $S$  is not an invariant line strain.

---

CHAPTER 9DISCUSSION.

	Page
9.1 Experimental Results.	154
9.2 Comparison of Experiment with the Predictions of Martensite Crystallographic Theory.	163

9.1 Experimental Results

In previous studies of the Widmanstätten ferrite transformation in iron/carbon alloys the habit plane has been reported as  $\{111\}_F$  and the orientation relationship as:

$$\begin{aligned} \{111\}_F & \parallel \{110\}_B \\ \langle 110 \rangle_F & \parallel \langle 111 \rangle_B \end{aligned}$$

which is the Kurdjumov-Sachs relationship. The present results have shown that, for transformation at a free surface, the precipitate has a plate or lath shape with a definite habit plane that is irrational and about  $12^\circ$  from  $\{111\}_F$ . The orientation relationship was also found to be irrational and significantly different from the exact KS relationship. The macroscopic change of shape has been shown to be described approximately, if not exactly, by an invariant plane strain on the habit plane.

For the habit plane being  $\{111\}_F$  and the orientation relationship exactly KS, crystal symmetry results in there being six possible lattice orientations for each of the four variants of the habit plane, giving a total of twenty four crystallographically equivalent orientation relationships that are twin-related in pairs. Experimentally this was not

observed. The position of the habit plane was found to be displaced significantly from the  $[\bar{1}10]_F$  zone and in all cases a particular variant of the orientation relationship was found to be associated with a particular variant of the habit plane.

For a long time the  $\{111\}_F$  habit plane has been regarded as characteristic of martensite and Widmanstätten ferrite in a range of iron/nickel and iron/carbon alloys. The present work and the recent results reported by Marder and Krauss (130), show for the first time that this is not true. Marder and Krauss have determined habit planes  $7^\circ - 10^\circ$  from  $\{111\}_F$  for martensite formed in iron/12% nickel and iron/0.2 - 0.6% carbon alloys. Their near  $\{557\}_F$  habit planes are within  $5^\circ$  of the mean

$$\begin{pmatrix} .4523468 \\ .5057018 \\ .7346080 \end{pmatrix}_F$$

found for Widmanstätten ferrite. It is probably significant that the measured departure from the established octahedral habit should be similar in both cases and substantiates the earlier criticisms of habit planes determined indirectly from single surface observations.

The initial orientation relationship determinations, made using thermally etched twin traces to define the  $\{111\}_F$ , in conjunction with the ferrite orientations determined using the Kossel technique, showed relatively large scatters of up to several degrees. It was originally thought that this scatter could be attributed to the inaccuracies involved in the twin trace method, but reference to the calculated angles between twin poles, shown in Table 7.2, indicates that in most cases

these poles were within  $\frac{1}{4}^{\circ}$  of the correct value of  $70^{\circ}32'$ . It was possible that errors accumulated because of the need to combine three essentially independent orientation determinations in order to define the orientation relationship (ie. those of the austenite, lithium fluoride and ferrite). Despite the large experimental scatter, the distribution of the ferrite poles and directions about the corresponding austenite poles and directions, indicated that there was a statistically significant deviation from exact parallelism of both the close packed planes and directions of the two phases.

The method whereby the parent austenite orientation was determined from a knowledge of the orientations of two or more variants of the precipitated product is new and has not been reported previously. The overall accuracy of this technique depends on obtaining accurate measurements of the orientations of at least two, but preferably three or more, variants of the product lattice and on there being an exact and reproducible orientation relationship. Providing the latter condition holds, the limits of accuracy of this method can be estimated by carefully examining the precision of the individual orientation determinations made using the back reflection Kossel technique.

By using a least squares method of fitting an exact orientation to five experimentally determined plane normals, it was found that crystal orientations could be determined within the limits of  $\pm 0.05^{\circ}$  under the best experimental conditions. For very small precipitate crystals ( $< 15 - 20\mu$ ), or for imperfect crystals, the accuracy is lower and on average, for the present analysis, was of the order of

$\pm 0.1^\circ$ .

Potentially then, highly accurate orientation determinations are possible under conditions which permit good quality Kossel patterns to be obtained. When the parent and product phases co-exist at room temperature and patterns from both phases can be obtained, orientation relationship determinations of the highest accuracy should be possible.

Several attempts were made to obtain Kossel patterns from an iron/nickel meteorite containing a well developed Widmanstätten structure and small amounts of retained austenite. The microstructure of this specimen was ideal for testing the Kossel method but unfortunately the presence of strain in the sample prevented X-ray reflections being obtained.

Despite the relatively small number of physically distinct situations which were examined in the present work, and the lack of experimental situations where more than two non-parallel ferrite laths appeared, the validity of the multiple variant method has been substantially verified by the results. The orientation relationships determined from the average of the two variant cases and the single three variant case, agreed well with one another, and were well within the scatter of results obtained using the twin trace method to determine the austenite orientation. The results have been interpreted as meaning that there is an orientation relationship in which  $(101)_B$  is  $0^\circ 58' \pm 15'$  from  $(111)_F$  and  $[\bar{1}\bar{1}\bar{1}]_B$  is  $0^\circ 42' \pm 0^\circ 15'$  from  $[\bar{1}10]_F$ , and that the scatter of the earlier results using two independent experiments are due to experimental error rather than to the laths not being exact crystallographic variants. The error limits of  $\pm 15'$  are only approximate and are found by simply

adding the standard deviations of the ferrite and indirectly determined austenite orientations.

Attempts to identify the exact nature of the transformation shape change have also been described. The scratch rotation method proved impracticable because of the nucleating effect of the scratching operation but, within the limitations of the method, interferometry showed that locally the relief effects could be described very closely by an IPS on the habit plane. Because of surface rumpling the tilt measurements used to determine the shear component of the shape change exhibited considerable scatter. Measurements made on the face containing the long direction of the plates showed high standard deviations, which in the worst case was  $\pm 15\%$ , while the higher tilts on the second face showed much smaller deviations of the order of  $\pm 5\%$ . If, as an approximation, an error of  $\pm 10\%$  is assigned to the tilt measurements, the calculated shear direction and shear magnitude scatter by  $\pm 2^\circ$  and  $\pm 0.03^\circ$  respectively. On these figures experimental error seems to be an unlikely explanation for the discrepancy between the predictions of the crystallographic theory, described in Chapter 8, and the experimental results.

Several morphological features of the precipitate deserve comment. The product phase at the free surface has been described as platelike and it has been shown to possess a definable habit plane. Below the surface there is a change in the degree of planarity of the interface and also an apparent change of habit.\* This observation suggests the

---

\* The difficulty of assigning a "habit plane" to a feature the shape of the lath "tail" has already been described.

possibility that the presence of the free surface affects the transformation mode and that in some way, laths formed in the surface may differ from those formed in the grain interiors. The degree of perfection of the lath interface also suggests a strong influence of the presence of the specimen free surface on the transformation. Apart from the Widmanstätten patterns of the iron/nickel meteorites, intragranular ferrite plates, comparable in length and perfection with the present surface laths, are found only rarely.

Significant plastic accommodation effects were observed in the austenite adjacent to many of the ferrite laths. Generally this accommodation was present on only one side of the lath, and a possible interpretation is that growth takes place by the movement of this interface. Slip accompanying the propagation of martensitic interfaces has been reported previously (119, 122) and the observation of plastic accommodation in the parent phase, at the austenite/ferrite boundary, supports the idea that the interface must possess at least some degree of coherency.

If, as Aaronson (20) has suggested, ferrite plates (or laths) grow by the lateral movement of non-coherent edges of ledges across the broad faces, it is very difficult to see how significant plastic accommodation can accumulate ahead of the advancing interface. Since in this theory the atoms join the product at the disordered part of the boundary, and the coherent part results only from immobile facets developing on the former, accumulation of strain does not seem possible. Equally difficult to explain is the nature of the macroscopic change of shape, which cannot be accounted for if the ledge risers have the

usual properties of disordered boundaries.

The volume changes for the transformation of austenite to both equilibrium and supersaturated ferrite were calculated from the lattice parameters and were found to be less than 2% in both cases, so that no significant plastic strain would be expected from this source.

Double tilt laths, similar to those often found in bainite (76) and copper/zinc alloys (8 - 10), also appeared occasionally. In these cases, the plastic accommodation effects which accompany the single tilt laths were notably absent, the opposing tilts appearing to annul the accumulation of lattice strain. A significant feature of the double laths was that in no case examined were X-ray reflections obtained from two lattices. This result implies that the two parts of the lath have the same orientation. Some instances of apparently parallel single laths, tilted in opposite senses, were also observed but unfortunately the habit planes and lattice orientations of these laths were not measured. Both of these observations lead to the suggestion that there may be two possible directions of the shape strain.

Morton (131), attempting to explain the occurrence of parallel martensite plates tilted in opposite senses, proposed that two different values of  $d_1$  could be associated with essentially similar habit planes. Dunne's results (122) showed however, that if the habit plane lies exactly on the  $[\bar{1}10]_F$  zone, the two apparent  $d_1$  values are crystallographic variants related by reflection across the zone. The present results cannot be explained on this basis, for as has been shown, the habit plane is sufficiently far from the  $[\bar{1}10]_F$  zone to allow the twin-related variants to be distinguished experimentally.

Thus the present results do not allow the following possibilities to be differentiated:

(a) Single laths with identical habit planes, but having opposite tilts, result from the operation of two different shape strains.

(b) Apparently parallel single laths of opposite tilt do not have the same habit plane but are actually twin-related variants.

(c) Double laths are formed by the action of two different shape strains as in (a) (for single laths).

The first suggestion seems to be an unlikely possibility in view of the observed unique relationship between the habit plane and the orientation relationship.

The second argument depends on there being a small angle ( $< 5^\circ$ ) between the traces of the laths in the relief surface, but because the sense of the tilt was not recorded when the habit plane determinations were made, evaluation of this proposal is not possible.

Since in the case of double laths the two parts junction along the habit plane, crystallographically they represent the same situation as two parallel single laths, of opposite tilt, butted together. The only obvious suggestion is that two shape strains are involved but, like the single laths, the Kossel method failed to detect X-ray reflections from two different lattice orientations in any of the cases examined. The suggestion (b) cannot be invoked in this case since the habit plane is common to both "halves" of the lath. In the absence of accurate shape strain data the possibility that there may be two values of  $d_1$  associated with the transformation must remain speculative.

Although it is possible that the formation of the laths studied

was strongly influenced by the specimen free surface, no attempts were made to compare their properties with those obtained from bulk precipitates, mainly because there is no known method for determining shape strains of bulk precipitates. Also, in iron/carbon alloys which undergo eutectoidal decomposition, the orientation relationship and habit plane determinations are rendered extremely difficult once the relief surface (and hence the austenite annealing twin traces) have been removed. Several attempts were made to produce iron/nickel alloys, with microstructures containing Widmanstätten precipitates and austenite, in which bulk habit planes and orientation relationships could be compared more readily with those of surface transformations. These attempts to produce structures containing both ferrite and austenite were unsuccessful due to the extreme sluggishness of the austenite to ferrite transformation in this system. An alloy containing 12% nickel, for example, austenized at  $1150^{\circ}\text{C}$  and treated isothermally for two weeks at  $500^{\circ}\text{C}$ , showed no evidence of decomposition to ferrite (even at the austenite grain boundaries). The extremely long times required to produce precipitates of reasonable size in iron/nickel and similar iron/cobalt alloys (15, 16) seems to preclude them from studies of the present type. Furthermore, any shape change occurring during transformation would be expected to be destroyed by surface tension forces during sustained holding at the transformation temperature.

## 9.2 Comparison of Experiment with the Predictions of Martensite

### Crystallographic Theory

By reference to the work of Bowles and Kennon (56) a value of the parameter  $\theta$ , which accounted for the observed habit plane, was chosen and the predictions of the theory for  $(110) [uvw]_F$  and  $(hk1) [\bar{1}10]_F$  (including  $(111) [\bar{1}10]_F$ ) as the elements of the complementary strain, were examined. It was concluded that shears on these systems could not account for the observed orientation relationship and the direction and magnitude of the shape strain, when the habit plane was specified. For the case of  $(111) [\bar{1}10]_F$  the orientation relationship predicted was about  $1\frac{1}{2}^\circ$  from that observed while the direction of the shape strain was  $5 - 10^\circ$  from the measured value. The shear component of the calculated shape strain magnitude was double that observed.

An alternative approach, when no experimental evidence of the possible nature of the complementary strain exists, is to predict the elements of this strain from a knowledge of other properties of the transformation. This method relies on the strain remaining when a small dilatation is removed from the total lattice strain, being an invariant line strain. This can then be factorized into two invariant plane strains. If the complementary strain is not a simple shear, or a combination of shears either on the same plane or in the same direction, the strain  $S$  will not be an invariant line strain and the factorization cannot be achieved in the usual way (36).

When the invariant line strain  $S_0$  was formed using the measured habit plane and a value for  $\theta$  consistent with the product phase being either equilibrium or supersaturated ferrite, the observed orientation

relationship could not be achieved exactly by the introduction of a small rotation through an angle  $\psi$  about the invariant line  $x_i$  of  $S_0$ . Choosing a value for  $\psi$  which gave most reasonable agreement with the observed orientation relationship and carrying out the factorization of  $S$  (for  $\delta = 1$ ), resulted in solutions for  $d_1$  which were some  $20^\circ$  from the experimental value. These results strongly suggest that either

- (a) The experimental observations are in error.
- (b) The calculated values for  $S$  are incorrect because of the models chosen.
- (c) The calculated values of  $S$  are correct, but the  $S$  is not an invariant line strain.

The construction of the strain  $S$  requires the habit plane and the lattice parameters of the parent and product phases to be known. Although exhibiting some scatter, the majority of the habit plane determinations fell within  $\pm 4^\circ$  of the mean value, an experimental scatter little greater than that often reported for martensite plates (7). The values of the lattice parameters were assigned with less certainty for reasons already discussed. In particular the method of determining the supersaturated ferrite parameter is most open to criticism and indeed the application of a supersaturation model to the Widmanstätten transformation may not even be valid since diffusion must necessarily take place ahead of the interface. Small changes in the lattice parameters, however, produced only small changes in the theoretical predictions. This circumstance has been previously reported by Srinivasan and Wayman (72) in their analysis of the bainite transformation, and changes in the degree of supersaturation would be expected not to

contribute to any marked changes in the results.

The suggestion that the complementary strain may not be a simple shear has been advanced in both the plastic accommodation model (60) and the general theories of martensitic transformations developed by Acton and Bevis (58) and Ross and Crocker (59). In these theories there need be no invariant line strain and factorization of the total strain into its component strains becomes more difficult. This being the case, a possible way in which the present transformation could be analysed would be to determine the total lattice strain defined by the pure strain and the observed orientation relationship, and to remove from this the experimental shape strain. The problem is then the decomposition of the remaining strain into a combination of shears. If the complementary strain is a combination of two shears it must be an invariant line strain and the factorization could, in principle, be carried out if one of the shears is specified. It is pointed out however, that extremely accurate experimental measurements of the shape strain and orientation relationship would be necessary to ensure that the complementary strain derived in this way is an invariant line strain. Because of experimental error this could probably never be achieved, and the present results are neither precise nor complete enough to allow such an approach to be implemented. It would further appear that the iron/carbon system is not the one most suited to an investigation of this kind because of the inherent difficulties of obtaining accurate shape strain data.

The final justification for using a given shear or combination of shears as the complementary strain in the crystallographic theory, is

firstly the agreement between the proposed shear and the experimental observations of slip and/or twinning of the product phase. As yet very little direct experimental evidence has been obtained for any fine scale internal structure of Widmanstätten precipitates which are known to be accompanied by shape changes, and there is no experimental evidence to support any of the cases considered in the calculations. The methods of the general theory, namely systematic variation of the component shears of the complementary strain, applied to the present transformation, may allow the shear elements to be predicted and could therefore provide some clue as to the nature of at least a component of the complementary strain.

Within the range of solutions obtained using the observed properties of the transformation it is felt that the geometric and crystallographic properties, and especially the change of shape cannot be dismissed lightly as coincidental "geometric" features which bear no significance to the transformation mechanism. The mathematical analysis has failed to allow any of the proposed models to be preferred, nevertheless it is believed that the transformation is martensitic in nature since there is a correspondence implied by the shape change, which is manifested in a unique set of geometric and crystallographic properties associated with the transformation.

---

APPENDIX 1

Twin Trace Analysis

Referring to Figure 6.11 and defining:

$t_{jk}$  = trace of the  $j^{\text{th}}$  twin in face  $k$ ,

$T_j$  = determined twin pole.

$\alpha_{jk}$  = angle between the trace of the  $j^{\text{th}}$  twin in face  $k$  and the direction  $I_1$ .

$\gamma$  = angle between the normals to face 1 and face 2.

then each trace may be expressed in the I basis as follows:

$$t_{11} = (\cos \alpha_{11}, \sin \alpha_{11}, 0)_I$$

$$t_{12} = (\cos \alpha_{12}, -\sin \alpha_{12} \cdot \cos \gamma, -\sin \alpha_{12} \cdot \sin \gamma)_I$$

$$t_{21} = (\cos \alpha_{21}, \sin \alpha_{21}, 0)_I$$

$$t_{22} = (\cos \alpha_{22}, -\sin \alpha_{22} \cdot \cos \gamma, -\sin \alpha_{22} \cdot \sin \gamma)_I$$

$$T_1 = t_{11} \times t_{12}$$

$$T_2 = t_{21} \times t_{22}$$

The angle between the poles  $T_1$  and  $T_2$  should be  $70^{\circ}32'$  but because of experimental error this is generally not found and some correction must be applied.

APPENDIX 2

A Quick Method of Locating the Vector  $[h\ k\ l]$   
in Cubic Crystals.

When two crystal directions  $[p\ q\ r]_I$  and  $[u\ v\ w]_I$  are experimentally determined and are of known Miller indices, a third, required direction  $[h\ k\ l]_I$  of known form, can be located approximately without the need to define the crystal basis relative to the specimen geometry. The method requires that the two angles,  $\theta_1$  and  $\theta_2$ , between  $[h\ k\ l]$  and the two experimental vectors be expressed as the correct angle for the crystallographic identities involved. By solving the three simultaneous equations:

$$h^2 + k^2 + l^2 = 1 \quad \dots 1$$

$$p.h + q.k + r.l = \cos \theta_1 \quad \dots 2$$

$$u.h + v.k + w.l = \cos \theta_2 \quad \dots 3$$

any crystal direction can be found expressed in the I basis. Since the method uses experimental vectors the determined vector will be in error by an amount of the order of magnitude of the experimental error. This is generally true, but differences will accrue depending upon the geometrical relationship of the determined vector to the two experimental vectors. The most accurate results require the two experimental vectors to be well separated,  $\approx 90^\circ$ , and accuracy is also high for vectors contained in the locus of points equidistant from both experimental poles. Less accurate results are obtained when the two experimental vectors are close together. Where small errors are involved this simple solution obviates the need for complicated refinements of the experimental

data and lengthy matrix calculations.

The solution was programmed on computer and for the initial orientation work (Tables 9.3 and 9.4) the method was used to locate all the directions not determined experimentally.

APPENDIX 3The Least Squares Analysis (127)

One way of describing the orientation of a crystal in space is to define the rotation required to carry a standard orientation into the observed orientation. An observed orientation however, will necessarily be determined experimentally and the experimental crystal poles subject to error, so that some method of adjustment of their positions is necessary. Mackenzie proposed a least squares method of adjustment which allows the estimation of a highly precise value of the orientation-defining rotation when the experimental errors are small.

Defining:

$y_a$  as a unit vector parallel to a measured plane normal,

$x_a$  as a unit vector parallel to the normal of the corresponding plane in the standard orientation,

$R$  as the rotation (matrix) which is to be determined.

The "true" position of the measured vector  $y_a$  is therefore  $Rx_a$  and the angular deviation of  $y_a$  from  $Rx_a$  is given by  $\theta_a$ .

$$\dots \cos \theta_a = y_a' Rx_a \quad (a = 1, 2, 3, \dots, n)$$

where the dashed notation refers to the transposed matrix or vector.

Using least squares, the sum of the type:

$$\sum w_a \theta_a^2$$

should be a minimum, or equivalently:

$$S = \sum_{a=1}^n w_a \cos \theta_a = \sum_{a=1}^n w_a y_a' Rx_a$$

should be a maximum, where  $w_a$  is a weight related to the variance of  $\theta_a$ .

Now, defining X and Y as (3 x n) matrixes with  $x_a$  and  $y_a$  (a = 1,2,3...n) in the respective columns

$$S = \text{Trace} (W Y' R X) \quad \dots(1)$$

In the present analysis only one estimate of each experimental pole was made and  $W = I$ .

Mackenzie then factorises  $A = X W Y'$  into two rotation matrixes  $R_1$  and  $R_2$  and a diagonal matrix  $\Lambda$ , such that:

$$A = R_2 \Lambda R_1'$$

Equation (1) becomes:

$$\begin{aligned} S &= \text{Trace} (R_1' R R_2 \Lambda) \\ &= \text{Trace} (R_0 \Lambda) \end{aligned}$$

when  $R_0 = I$

then  $R = R_1 R_2' \quad \dots(2)$

and  $S_{\max} = \text{Trace} (\Lambda)$

The evaluation of  $R_1$  and  $R_2$  determines  $\Lambda$  and allows R to be calculated. By finding the three roots  $\lambda_1^2$ ,  $\lambda_2^2$  and  $\lambda_3^2$ , of the determinantal equation:

$$\det | A'A - \lambda^2 I | = 0$$

and substituting these in turn into the equation

$$A' A u_a = \lambda_a^2 u_a$$

three mutually orthogonal unit vectors  $u_1$ ,  $u_2$  and  $u_3$  are found if  $\lambda_a$  is positive.

The (3 x 3) matrix  $R_1$  has as successive columns  $u_1$ ,  $u_2$  and  $u_3$ . Similarly three vectors  $v_1$ ,  $v_2$  and  $v_3$ , corresponding to the three  $Au_a$ , can be determined and the matrix  $R_2$  has as successive columns

$v_1/\lambda_1$ ,  $v_2/\lambda_2$  and  $v_3/\lambda_3$ .

$$R_1 = (u_1 \ u_2 \ u_3) \quad \dots(3)$$

$$R_2 = (v_1/\lambda_1 \ v_2/\lambda_2 \ v_3/\lambda_3) \quad \dots(4)$$

By substituting the values of  $R_1$  and  $R_2$  from (3) and (4) into (2) the rotation matrix defining the crystal orientation is determined.

This analysis was programmed on an IBM 360/50 computer with five input vectors  $y_a$  and  $x_a$ . The choice of five was made on the basis of the number of high quality conics generally observed on a Kossel film for the particular prevailing geometry and specimen material.

The value of:

$$\cos \theta = \frac{1 - (\text{Trace } (W) - S_{\max})}{n \text{ Trace } (W)}$$

given by Mackenzie as a measure of the standard deviation was also calculated.

A print-out of the programme, which incorporates the least squares analysis of the ferrite data (Part A) and the austenite orientation determination from a knowledge of the orientation of two or more ferrite variants (Part B), is included overleaf.

```

C-----C
C PART A
C A LEAST SQUARES REFINEMENT OF KUSSEL DATA USING HACKENZIES METHOD
C REF. ACTA. CRYST. (1957.)
C ONLY THE FIVE BEST VECTORS (POLES) ARE USED.
C Y IS THE VECTOR WHICH IN STANDARD PROJECTION IS X
C CARD PUNCH Z0
C LAST DATA CARD IS @END DATA@
C-----C

```

```

IMPLICIT REAL*8(A-H,U-Z,S)
DATA END/@END @/,DATA/@DATA@/
DIMENSION X(5,5),Y(5,5),A(3,3),ADASHA(3,3),AMDASH(3),AMDA(3),U(3),
IV(3,5),R1(3,3),R2(3,3),R0(3,3,2),RM(3,3),HEAD(20)
DIMENSION SYN(5,5,48),RUT(3,3,24),KAK(3,3),TRACE(24),T(6),
IAXIS(5,3),IAR(5,3),ANTI(5,3),DETER(48)
1 READ(1,2)HEAD
2 FORMAT(20A4)
IF (HEAD(1).EQ.END.AND.HEAD(2).EQ.DATA) GO TO 300
WRITE(3,4) HEAD
4 FORMAT(@1@,20X,20A4)
5 READ,NUMVAR
WRITE(5,6) NUMVAR
6 FORMAT(//5X,@VARIANT NUMBER @,11)
DO 10 I=1,5
READ,(X(I,J),J=1,5)
10 CONTINUE
DO 11 L=1,5
READ,(Y(L,M),M=1,5)
11 CONTINUE
WRITE(3,7)
7 FORMAT(//15X,@X IS THE MATRIX@)
DO 12 I=1,5
WRITE(3,14)(X(I,J),J=1,5)
12 CONTINUE
WRITE(3,8)
8 FORMAT(//15X,@Y IS THE MATRIX@)
DO 13 L=1,5
WRITE(3,15)(Y(L,M),M=1,5)
13 CONTINUE
14 FORMAT( 18X,@(F10.7,2F15.7,@)@)
15 FORMAT( 18X,@(F10.7,2F15.7,@)@)
C DASH NOTATION ALWAYS REFERS TO A TRANSPOSE OPERATION
C A=X*YDASH
DO 21 J=1,3
DO 20 M=1,3
A(J,M)=X(1,J)*Y(1,M)+X(2,J)*Y(2,M)+X(3,J)*Y(3,M)+X(4,J)*Y(4,M)+
IX(5,J)*Y(5,M)
20 CONTINUE
21 CONTINUE
DO 22 J=1,3
22 CONTINUE
C ADASHA=ADASH*A
DO 31 J=1,3
DO 30 M=1,3
ADASHA(J,M)=A(1,J)*A(1,M)+A(2,J)*A(2,M)+A(3,J)*A(3,M)

```

30 CONTINUE  
31 CONTINUE

-----C  
C THE EIGENVALUES OF THE 3\*3 MATRIX ADASHA ARE FOUND BY FINDING THE C  
C DETERMINANT OF ADASHA (DET) WITH THE TERMS ADASHA(J,J) WRITTEN AS C  
C (A(J,J)-AMDASQ), THE ROOTS OF THE RESULTING CUBIC EQUATION IN C  
C AMDASQ ARE THE CHARACTERISTIC ROOTS OF THE MATRIX. C  
C AS A FIRST APPROXIMATION THE TWO ROOTS OF THE FIRST DERIVATIVE C  
C (GRAD) OF THE CUBIC EQUATION (DET) ARE USED TO OBTAIN APPROXIMATE C  
C VALUES OF AMDASQ. C  
-----C

```
P=-1.0000000
Q=ADASHA(1,1)+ADASHA(2,2)+ADASHA(3,3)
R=-ADASHA(1,1)*(ADASHA(2,2)+ADASHA(3,3))-(ADASHA(2,2)*ADASHA(3,3))
1+(ADASHA(2,3)*ADASHA(3,2))+(ADASHA(1,2)*ADASHA(2,1))+(ADASHA(1,3)*
2ADASHA(3,1))
S=(ADASHA(1,1)*ADASHA(2,2)*ADASHA(3,3))-(ADASHA(1,1)*ADASHA(2,3)*
1ADASHA(3,2))+(ADASHA(1,2)*ADASHA(2,3)*ADASHA(3,1))-(ADASHA(1,2)*
2ADASHA(2,1)*ADASHA(3,3))+(ADASHA(1,3)*ADASHA(2,1)*ADASHA(3,2))-
3(ADASHA(1,3)*ADASHA(2,2)*ADASHA(3,1))
ROOT1=(-Q+DSQRT(Q**2-3.0*P*R))/(3.0*P)
ROOT2=(-Q-DSQRT(Q**2-3.0*P*R))/(3.0*P)
AMDASQ(1)=ROOT1+((ROOT1+ROOT2)/2.0-ROOT2)
AMDASQ(2)=(ROOT1+ROOT2)/2.0
AMDASQ(3)=ROOT2-((ROOT1+ROOT2)/2.0-ROOT2)
```

-----C  
C NEWTON APPROXIMATION BEGINS HERE. C  
-----C

```
DO 42 N=1,3
40 DET=P*AMDASQ(N)**3+Q*AMDASQ(N)**2+R*AMDASQ(N)+S
GRAD=3.0*P*AMDASQ(N)**2+2.0*Q*AMDASQ(N)+R
BETTER=AMDASQ(N)-DET/GRAD
ACC=.0000000000001
TEST=DABS(AMDASQ(N)-BETTER)-ACC
IF (TEST)42,42,41
41 AMDASQ(N)=BETTER
GO TO 40
42 CONTINUE
```

-----C  
C ADASHA\*U(J)=AMDASQ(N)\*U(J) C  
C THREE SIMULTANEOUS EQUATIONS IN U ARE SOLVED BY TAKING RATIOS OF C  
C UNKNOWN AND THEN MAKING SUM OF SQUARES EQUAL ZERO. C  
C RATIO U(1)/U(2)=RAT12 C  
C RATIO U(3)/U(2)=RAT32 C  
-----C

```
DO 51 N=1,3
RAT12=-((ADASHA(2,3)/ADASHA(1,3))*ADASHA(1,2)-ADASHA(2,2)+
1AMDASQ(N))/((ADASHA(2,3)/ADASHA(1,3))*(ADASHA(1,1)-AMDASQ(N))-
2ADASHA(2,1))
RAT32=-((ADASHA(3,1)/ADASHA(2,1))*(ADASHA(2,2)-AMDASQ(N))
1-ADASHA(3,2))/((ADASHA(3,1)/ADASHA(2,1))*ADASHA(2,3)-ADASHA(3,3)+
2AMDASQ(N))
SUM=RAT12**2+1.0+RAT32**2
SQTSUM=DSQRT(SUM)
U(1)=RAT12/SQTSUM
U(2)=1.0/SQTSUM
```

```

U(3)=KAT32/SWTSUM
C THE FIRST COLUMN OF K1 IS THE VECTOR U AND SO FORTH.
DU 50 J=1,3
K1(J,N)=U(J)
50 CONTINUE
51 CONTINUE
WRITE(3,54)
DU 52 J=1,3
WRITE(3,55)(K1(J,N),N=1,3)
52 CONTINUE
53 FORMAT(18X, '(a,F10.7,2F15.7,a)')
54 FORMAT(/14X, 'K1 IS THE MATRIX')
C V(N)=A*U(N)
C V(N)=A*U(N) AND V(N)/AMDA(N) IS THE FIRST COLUMN OF K2
DU 61 N=1,3
DU 60 J=1,3
V(J,N)=A(J,1)*K1(1,N)+A(J,2)*K1(2,N)+A(J,3)*K1(3,N)
60 CONTINUE
61 CONTINUE
DU 70 I=1,3
AMDA(I)=DSQRT(AMDA2(I))
70 CONTINUE
DU 81 I=1,3
DU 80 J=1,3
R2(I,J)=V(I,J)/AMDA(J)
80 CONTINUE
81 CONTINUE
WRITE(3,84)
DU 82 I=1,3
WRITE(3,83)(R2(I,J),J=1,3)
82 CONTINUE
83 FORMAT(18X, '(a,F10.7,2F15.7,a)')
84 FORMAT(/14X, 'K2 IS THE MATRIX')
C R0=K1*K2DASH
DU 91 I=1,3
DU 90 J=1,3
R0(I,J,NUMVAR)=K1(1,I)*R2(J,1)+K1(1,2)*R2(J,2)+K1(1,3)*R2(J,3)
90 CONTINUE
91 CONTINUE
WRITE(3,95)
DU 92 I=1,3
WRITE(3,93)(R0(I,J,NUMVAR),J=1,3)
92 CONTINUE
93 FORMAT(18X, '(a,F10.7,2F15.7,a)')
95 FORMAT(/14X, 'R0 IS THE MATRIX')
TR=R0(1,1,NUMVAR)+R0(2,2,NUMVAR)+R0(3,3,NUMVAR)
THETA=(DARCOS((TR-1.)/2.))*(180./3.1415926535)
WRITE(3,160) THETA
DU 87 I=1,3
DU 86 J=1,3
ANTI(I,J)=(R0(I,J,NUMVAR)-R0(J,I,NUMVAR))/(2.*DSIN(THETA))
86 CONTINUE

```

```

87 CONTINUE
D1=AN11(3,2)
D2=AN11(1,3)
D3=AN11(2,1)
DEESQ=D1**2+D2**2+D3**2
D1=D1/DSQRT(DEESQ)
D2=D2/DSQRT(DEESQ)
D3=D3/DSQRT(DEESQ)
WRITE(3,162) D1,D2,D3
-----C
C ESTIMATION OF THE ERROR
C AK=ADASH*K2
C RAK=RIDASH*AK
-----C
DO 101 I=1,3
DO 100 J=1,3
AR(I,J)=A(1,I)*K2(1,J)+A(2,I)*K2(2,J)+A(3,I)*K2(3,J)
100 CONTINUE
101 CONTINUE
DO 103 I=1,3
DO 102 J=1,3
RAK(I,J)=R1(1,I)*AK(1,J)+R1(2,I)*AK(2,J)+R1(3,I)*AK(3,J)
102 CONTINUE
103 CONTINUE
TK=KAK(1,1)+KAK(2,2)+KAK(3,3)
IF(TK.GE.5) GO TO 98
DEV=(DARCOS(1-(5-TK)/25)**2*(180/3.1415926535))
WRITE(3,97) DEV
97 FORMAT(/732X,DEV= ,F10.4)
98 WRITE(3,164) TK
WRITE(3,165)
-----C
IF(NUMVAR.EQ.1) GO TO 5
-----C
C END PART A
-----C
C PART B
C DETERMINATION OF AN ORIENTATION RELATIONSHIP FROM A KNOWLEDGE OF
C THE ORIENTATION OF TWO OR MORE VARIANTS OF THIS RELATIONSHIP
C THE ROTATION WHICH CARRIES VARIANT 2 INTO COINCIDENCE WITH VARIANT 1
C IS OBTAINED BY COMBINING THE TWO RU MATRICES
C RM=RU(1)DASH * RU(2)
-----C
DO 105 I=1,3
DO 104 J=1,3
RM(I,J)=RU(1,1,1)*RU(1,J,2)+RU(2,1,1)*RU(2,J,2)+RU(3,1,1)*
1RU(3,J,2)
104 CONTINUE
105 CONTINUE
WRITE(3,106)
DO 99 I=1,3
WRITE(3,107)(RM(I,J),J=1,3)
99 CONTINUE
106 FORMAT(/714X, RM IS THE MATRIX)
107 FORMAT( 18X, ( ,F10.7,2F10.7, /))

```

```

TR=RM(1,1)+RM(2,2)+RM(3,3)
THETA=(ARCCOS((TR-1.)/2.))*(180./3.1415926535)
WRITE(3,161) THETA
DO 112 I=1,3
DO 111 J=1,3
ANTI(I,J)=(RM(I,J)-RM(J,I))/(2.*DSIN(THETA))
111 CONTINUE
112 CONTINUE
D1=ANTI(3,2)
D2=ANTI(1,3)
D3=ANTI(2,1)
DEESQ=D1**2+D2**2+D3**2
D1=D1/DSQRT(DEESQ)
D2=D2/DSQRT(DEESQ)
D3=D3/DSQRT(DEESQ)
WRITE(3,163) D1,D2,D3

```

-----C  
TO GENERATE 24 UNITARY MATRICES CAPABLE OF DESCRIBING THE  
OPERATIONS OF A CUBE  
-----C

```

T(1)=1.
T(2)=0
T(3)=0
T(4)=-1.
T(5)=0
T(6)=0
N=1
109 DO 114 I=1,6
DO 115 J=1,6
NTEST=I-J-(I/3)*3+(J/3)*3
IF (NTEST)110,113,110
110 CONTINUE
I1=I
I2=I+1-(I/6)*6
I3=I+2-((I+1)/6)*6
J1=J
J2=J+1-(J/6)*6
J3=J+2-((J+1)/6)*6
FK1=1.-DABS(T(I1)-T(J1))
FK2=1.-DABS(T(I2)-T(J2))
FK3=1.-DABS(T(I3)-T(J3))

```

-----C  
SYM IS A 3\*3 MATRIX WITH ROW1 T(I),ROW2 T(J),ROW3 K  
THE 48 POSSIBLE MATRICES ARE GIVEN BY ROT(N)=RM\*SYM(N)  
-----C

```

SYM(2,2,N)=T(J2)
SYM(3,3,N)=FK3
SYM(3,2,N)=FK2
SYM(3,1,N)=FK1
SYM(2,3,N)=T(J3)
SYM(2,1,N)=T(J1)
SYM(1,3,N)=T(I3)
SYM(1,2,N)=T(I2)
SYM(1,1,N)=T(I1)
N=N+1

```

```

113 CONTINUE
114 CONTINUE
DU 151 N=1,24
N=N+24
SYM(1,1,M)=SYM(1,1,N)
SYM(1,2,M)=SYM(1,2,N)
SYM(1,3,M)=SYM(1,3,N)
SYM(2,1,M)=SYM(2,1,N)
SYM(2,2,M)=SYM(2,2,N)
SYM(2,3,M)=SYM(2,3,N)
SYM(3,1,M)=-SYM(3,1,N)
SYM(3,2,M)=-SYM(3,2,N)
SYM(3,3,M)=-SYM(3,3,N)
151 CONTINUE
K=1
DU 156 N=1,48
152 DETER(N)=SYM(1,1,N)*(SYM(2,2,N)*SYM(3,3,N)-SYM(2,3,N)*SYM(3,2,N))
1+SYM(1,2,N)*(SYM(2,3,N)*SYM(3,1,N)-SYM(2,1,N)*SYM(3,3,N))+
2SYM(1,3,N)*(SYM(2,1,N)*SYM(3,2,N)-SYM(2,2,N)*SYM(3,1,N))
TEST=DETER(N)
IF (TEST)156,156,153
153 DU 153 I=1,3
DU 154 J=1,3
SYM(I,J,K)=SYM(I,J,N)
154 CONTINUE
155 CONTINUE
K=K+1
156 CONTINUE
WRITE(3,157)
157 FORMAT(/'30X,@THE 24 SYMMETRY MATRICES@)
DU 170 I=1,3
WRITE(3,158)((SYM(I,J,K),J=1,3),K=1,8)
158 FORMAT(@ @,8(3F5,1,1X))
170 CONTINUE
WRITE(3,173)
173 FORMAT(@0@)
DU 171 I=1,3
WRITE(3,158)((SYM(I,J,K),J=1,3),K=9,16)
171 CONTINUE
WRITE(3,173)
DU 172 I=1,3
WRITE(3,158)((SYM(I,J,K),J=1,3),K=17,24)
172 CONTINUE

```

---

```

C
N=1
115 DU 117 I=1,3
DU 116 J=1,3
ROT(I,J,N)=RM(I,1)*SYM(1,J,N)+RM(I,2)*SYM(2,J,N)+RM(I,3)*
1SYM(3,J,N)
116 CONTINUE
117 CONTINUE
N=N+1
118 IF(N.LE.24) GO TO 115
119 CONTINUE
DU 122 N=1,24
TRACE(N)=ROT(1,1,N)+ROT(2,2,N)+ROT(3,3,N)

```

```

122 CONTINUE
WRITE(3,124)
124 FORMAT(/755X,@THE 24 TRACES OF ROT@)
WRITE(3,125)(TRACE(N),N=1,24)
125 FORMAT(@ @12F10.7,/ @12F10.7)

```

```

-----
C IT IS REQUIRED TO FIND WHICH ROT HAS A TRACE EQUAL TO -1,+1,OR 0
C REQUIRED MATRIX NUMBER=NUK
C REQUIRED TRACE=RIT
C NOMINAL TRACE VALUE=NTV
C REQUIRED NOMINAL TRACE VALUE=NRIV
-----

```

```

DIG=100
NTV=-1
TEST=DIG
129 DO 132 N=1,24
IF (TRACE(N)) 126,127,127
126 GOOD=DABS(NTV+(TRACE(N))**2)
GO TO 128
127 GOOD=DABS(NTV-(TRACE(N))**2)
128 CONTINUE
IF (TEST-GOOD)132,132,130
130 TEST=GOOD
RIT=TRACE(N)
NUK=N
NRIV=NTV
132 CONTINUE
IF (NTV.GE.1) GO TO 133
NTV=NTV+1
GO TO 129
133 CONTINUE
WRITE(3,131) NUK
131 FORMAT(/710X,@REQUIRED SYMMETRY MATRIX NUMBER= @,I2)
WRITE(3,134)
134 FORMAT(/713X,@ROT IS THE MATRIX@)
DO 135 I=1,3
WRITE(3,136)(ROT(I,J,NUK),J=1,3)
135 CONTINUE
136 FORMAT( 18X,@( @,F10.7,2F15.7,@)@)
TEST=DABS(RIT)-0.9999999
IF (TEST) 138,146,146
146 TEST=RIT
IF (TEST) 148,147,147
147 THETA=90.0
GO TO 139
148 THETA=180.0
WRITE(3,137) THETA
D1=DSQRT((ROT(1,1,NUK)+1.0)/2.0)
D2=DSQRT((ROT(2,2,NUK)+1.0)/2.0)
D3=DSQRT((ROT(3,3,NUK)+1.0)/2.0)
GO TO 142
138 THETA=(DARCOS((RIT-1)/2))*(180./3.1415926535)

```

```

139 WRITE(5,137) THETA
137 FORMAT(//30X,@THETA= @,F10.5)
DO 141 I=1,3
DO 140 J=1,3
AXIS(I,J)=(ROT(I,J,NOK)-ROT(J,I,NOK))/(2.*DSIN(THETA))
140 CONTINUE
141 CONTINUE
C THE ANTISYMMETRICAL PART OF ROT GIVES THE ROTATION AXIS
D1=AXIS(3,2)
D2=AXIS(1,3)
D3=AXIS(2,1)
142 DEESQ=D1**2+D2**2+D3**2
D1=D1/DSQRT(DEESQ)
D2=D2/DSQRT(DEESQ)
D3=D3/DSQRT(DEESQ)
WRITE(5,145) D1,D2,D3
145 FORMAT(//30X,@D1= @,F10.7,/30X,@D2= @,F10.7,/30X,@D3= @,F10.7)
150 GO TO 1
160 FORMAT(//30X,@THETA= @,F10.5)
161 FORMAT(//30X,@THETA= @,F10.5)
162 FORMAT(//30X,@D1= @,F10.7,/30X,@D2= @,F10.7,/30X,@D3= @,F10.7)
163 FORMAT(//30X,@D1= @,F10.7,/30X,@D2= @,F10.7,/30X,@D3= @,F10.7)
164 FORMAT(//30X,@TRACE= @,F20.16)
165 FORMAT(@1@)
300 CONTINUE
STOP
END

```

APPENDIX 4Determination of the Shear.

All measurements are made in the I basis:

$I_1$  = A unit vector in the positive direction of the edge  
between the two surfaces.

$I_2$  =  $(I_1 \times I_3)$

$I_3$  = A unit vector normal to surface 1.

$\beta$  = angle between surface normals.

If  $p_1'$  is the habit plane defined by traces in the two surfaces, the plane with normal  $I_3$  is tilted through an angle  $\theta_1$  about the habit plane trace to a new position  $I_3^*$ . Similarly, the normal to surface 2, denoted  $n_2$  and defined by the angle  $\beta$  ( $n_2 = I_2$  for  $\beta = 90^\circ$ , where  $\beta$  is the angle between  $I_3$  and  $n_2$ ) is tilted about the second trace through an angle  $\theta_2$ , to a new position  $n_2^*$ . The new position of the intersection of the two surfaces, originally  $I_1$ , is defined by:

$$I_1^* = (I_3^* \times n_2^*)$$

$I_1$  rotates to  $I_1^*$  in a plane defined by:

$$n_3 = (I_1^* \times I_1)$$

This plane must therefore contain the direction of displacement. In a shear the shear plane, in this case the habit plane  $p_1'$ , also contains the direction of displacement,  $d_1$ .

$$\therefore d_1 = (n_3 \times p_1')$$

If the strain carrying  $I_1$  to  $I_1^*$  is a simple shear then:

$$I_1^* = S I_1$$

where

$$S = (I + m_1^* d_1^* p_1')$$

$$m_1^* = \text{magnitude of shear.}$$

$$d_1^* = \text{direction of shear.}$$

The calculation is most easily achieved if a new basis D is defined such that:

$$d_1^* = [100]_D$$

$$p_1^* = [010]_D$$

$$(d_1^* \times p_1^*) = [001]_D$$

The shear then takes the simple form:

$$S = \begin{pmatrix} 1 & m_1^* & 0 \\ 0 & 1 & 0 \\ 0 & 0 & 1 \end{pmatrix}$$

and the shear magnitude results from the solution of

$$I_1^* = S I_1$$

where both  $I_1^*$  and  $I_1$  are referred to the D basis. (The transformation matrix  $\mathbb{T}$  is found by writing as successive columns the direction cosines of  $d_1^*$ ,  $p_1^*$  and  $(d_1^* \times p_1^*)$  referred to the I basis).

REFERENCES.

1. J.W. Christian, "The Theory of Transformations in Metals and Alloys". Pergamon (1965).
2. B.A. Bilby and J.W. Christian in Symposium: "The Mechanisms of Phase Transformations in Metals". Inst. Metals Monograph Series No.18 (1956).
3. J. Mackenzie, J. Aust. Inst. Metals 5, 90 (1960).
4. A.R. Troiano and A.B. Greninger, Metal Progress 50, 303 (1946).
5. J.W. Christian in Symposium: "The Physical Metallurgy of Martensite and Bainite". B.I.S.R.A./I.S.I. Special Report No.93.
6. J.W. Christian in Symposium: "The Decomposition of Austenite by Diffusional Processes". Interscience (1962).
7. C.M. Wayman, "Introduction to the Crystallography of Martensitic Transformations". Macmillan (1964).
8. H.M. Clark and C.M. Wayman, to be published.
9. P.G. McDougall, unpublished research.
10. R.D. Garwood in Symposium: "The Physical Metallurgy of Martensite and Bainite". B.I.S.R.A./I.S.I. Special Report No.93.
11. H.I. Aaronson in Symposium: "The Mechanisms of Phase Transformations in Crystalline Solids". Inst. Metals Monograph and Report Series No.33 (1969).
12. A.H. Geisler, Acta Met. 1, 260 (1953).
13. J.S. Bowles and W.J. McG. Tegart, Acta Met. 3, 590 (1955).
14. J.S. Bowles and C.S. Barrett, Prog. Met. Phys. 3, 1 (1952).
15. P.L. Ryder, W. Pitsch and R.F. Mehl, Acta Met. 15, 1431 (1967).

16. P.L. Ryder and W. Pitsch, *Acta Met.* 14, 1437 (1966).
17. J.N. Hobstetter in Symposium: "The Decomposition of Austenite by Diffusional Processes". Interscience (1962).
18. F.R.N. Nabarro, *Proc. Roy. Soc.* 175, 519 (1940).
19. H.I. Aaronson in Symposium: "The Mechanisms of Phase Transformations in Metals". *Inst. Metals Monograph Series No.18* (1956).
20. H.I. Aaronson in Symposium: "The Decomposition of Austenite by Diffusional Processes". Interscience (1962).
21. C.S. Smith, *T.A.S.M.* 45, 533 (1953).
22. M. Hillert in Symposium: "The Decomposition of Austenite by Diffusional Processes". Interscience (1962).
23. J.W. Christian in Symposium: "The Mechanisms of Phase Transformations in Crystalline Solids". *Inst. Metals Monograph and Report Series No.33* (1969).
24. C. Laird and H.I. Aaronson, *Acta Met.* 14, 171 (1966).
25. C. Laird and H.I. Aaronson, *Acta Met.* 15, 73 (1967).
26. C. Laird and H.I. Aaronson, *Acta Met.* 17, 505 (1969).
27. N.F. Kennon and G.R. Purdy, unpublished research.
28. J.S. Bowles and J. Mackenzie, *Acta Met.* 2, 129 (1954).
29. P.M. Kelly and J. Nutting, *Proc. Roy. Soc.* 259, 45 (1960).
30. M.A. Jaswon and J.A. Wheeler, *Acta Cryst.* 1, 216 (1948).
31. W.M. Lomer in Symposium: "The Mechanism of Phase Transformations in Metals". *Inst. of Metals Monograph and Report Series No.18*.
32. A.B. Greninger and A.R. Troiano, *T.A.I.M.E.* 185, 590 (1949).
33. M.S. Wechsler, D.S. Lieberman and T. Read, *T.A.I.M.E.* 197, 1503 (1953).

34. J.S. Bowles and J. Mackenzie, *Acta Met.* 2, 138 (1954).
35. J.S. Bowles and J. Mackenzie, *Acta Met.* 2, 224 (1954).
36. J.S. Bowles and J. Mackenzie, *Acta Met.* 10, 625 (1962).
37. E.S. Machlin and M. Cohen, *J. Metals*, 3, 1019 (1951).
38. J.S. Bowles and A. Morton, *Acta Met.* 12, 629 (1964).
39. A. Morton and C.M. Wayman, *Acta Met.* 14, 1567 (1966).
40. D.P. Dunne and J.S. Bowles, *Acta Met.* 17, 201 (1969).
41. P. Krauklis and J.S. Bowles, *Acta Met.* 17, 997 (1969).
42. H.M. Otte and T.A. Read, *T.A.I.M.E.* 209, 412 (1957).
43. K.A. Johnson and C.M. Wayman, *Acta Cryst.* 16, 480 (1963).
44. D.S. Lieberman, M.S. Wechsler and T. Read, *J. App. Phys.* 26, 473 (1955).
45. M.W. Burkart and T.A. Read, *T.A.I.M.E.* 197, 1516 (1953).
46. J. Mackenzie and J.S. Bowles, *Acta Met.* 5, 137 (1957).
47. N.F. Kennon and J.S. Bowles, *Acta Met.* 17, 373 (1969).
48. A.H. Cottrell and B.A. Bilby, *Phil. Mag.* 42, 573 (1951).
49. B.A. Bilby, *Phil. Mag.* 44, 782 (1953).
50. B.A. Bilby in Symposium: "Defects in Crystalline Solids". *Phys. Soc.* (1955).
51. R. Bullough and B.A. Bilby, *Proc. Phys. Soc.* 69, 1276 (1956).
52. F.C. Frank, *Acta Met.* 1, 15 (1953).
53. B.A. Bilby and F.C. Frank, *Acta Met.* 8, 239 (1960).
54. M.S. Wechsler, T.A. Read and D.S. Lieberman, *T.A.I.M.E.* 218, 202 (1960).
55. H.M. Otte, *T.A.I.M.E.* 218, 342 (1960).
56. J.S. Bowles and N.F. Kennon, *J. Aust. Inst. Metals*, 5, 90 (1960).

57. A.G. Crocker and B.A. Bilby, *Acta Met.* 9, 678 (1961).
58. A.F. Acton and M. Bevis, *Mat. Sci. Eng.* 5, 19 (1969-70).
59. N.D.H. Ross and A.G. Crocker, *Acta Met.* 18, 405 (1970).
60. J.S. Bowles and D.P. Dunne, *Acta Met.* 17, 678 (1969).
61. N.F. Kennon, M.Sc. Thesis, U.N.S.W. (1959).
62. D.S. Lieberman in Symposium: "The Mechanisms of Phase Transformations in Crystalline Solids". Inst. Metals Monograph and Report Series No.33 (1969).
63. A.P. Miodownik in Symposium: "The Mechanism of Phase Transformations in Metals". Inst. Metals Monograph and Report Series No.18 (1956) (Discussion).
64. K. Tsuya, T. Mitsuhashi and Y. Sakami, *J. Mech. Lab. (Japan)* 9, 243 (1955).
65. M.A. Guzovskaya and A.P. Gulyayev, *Izvest. Akad. Nauk. S.S.S.R. Metally.* 1, 112 (1967).
66. B.A. Leont'ev, V.F. Zubarev, M.P. Matveyeva and T.I. Shelyagina *Izvest. Akad. Nauk. S.S.S.R. Metally.* 1, 116 (1967).
67. B.A. Leont'ev and E.G. Katshanov, *Fizika Metallov i Metallovedenie* 24, 177 (1967).
68. R.S. Davenport and E.C. Bain, *T.A.I.M.E.* 90, 117 (1930).
69. R.F. Mehl in Symposium: "Transformations and Hardenability in Steels". Climax Molybdenum Co. (1967) (closing remarks).
70. G.V. Smith and R.F. Mehl, *T.A.I.M.E.* 150, 211 (1942).
71. T. Ko and S.A. Cottrell, *J.I.S.I.* 172, 307 (1953).
72. G.R. Srinivasan and C.M. Wayman, *Acta Met.* 16, 609, 621 (1968).

73. A. Hultgren, T.A.S.M. 39, 915 (1947).
74. W.S. Owen and J. White, J.I.S.I. 197, 241 (1961).
75. G.R. Speich and M. Cohen, T.A.I.M.E. 218, 1050 (1960).
76. G.R. Speich in Symposium: "The Decomposition of Austenite by Diffusional Processes". Interscience (1962).
77. L. Kaufman, S.V. Radcliffe and M. Cohen, *ibid.*
78. R.H. Goodenow, S.J. Matas and R.F. Heheman, T.A.I.M.E. 227, 651 (1963).
79. K. Kinsman, E. Eichen and H.I. Aaronson, to be published (as reported in Reference 11).
80. K.J. Irvine and F.B. Pickering in Symposium: "The Physical Metallurgy of Martensite and Bainite". B.I.S.R.A./I.S.I. Special Report No.93.
81. R.H. Goodenow, R.H. Barkalow and R.F. Heheman, *ibid.*
82. J.M. Oblak and R.F. Heheman in Symposium: "Transformations and Hardenability in Steels". Climax Molybdenum Co. (1967).
83. F.B. Pickering, *ibid.*
84. R.F. Mehl and A. Dube in Symposium: "Phase Transformations in Solids". John Wiley (1951).
85. K. Shimizu, T. Ko and Z. Nishiyama, Trans. J.I.M. 5, 225 (1964).
86. D.N. Shackelton and P. Kelly in Symposium: "The Physical Metallurgy of Martensite and Bainite". B.I.S.R.A./I.S.I. Special Report No.93.
87. A.B. Greninger and A.R. Troiano, Metals Tech. 7, 1212 (1940).
88. S.V. Radcliff and E.C. Rollandson, J.I.S.I. 191, 56 (1959).
89. R.I. Entin in Symposium: "The Decomposition of Austenite by Diffusional Processes". Interscience (1962).

90. C. Zener, T.A.I.M.E. 167, 513 (1946).
91. J.C. Fisher in: "Thermodynamics in Physical Metallurgy". A.S.M. (1950).
92. K.R. Kinsman and H.I. Aaronson discussion on Reference 82.
93. R. Smith and J.S. Bowles, Acta Met. 8, 405 (1960).
94. R.T. Gunther, Nature 143, 667 (1939).
95. R.F. Mehl in "The Sorby Centennial Symposium on the History of Metallurgy". A.I.M.E. Conference (1963).
96. J. Young, Proc. Roy. Soc. A 112, 630 (1926).
97. J. Young, Phil. Trans. Roy. Soc. A 238, 393 (1939).
98. R.F. Mehl and C.S. Barrett, T.A.I.M.E. 93, 78 (1931).
99. R.F. Mehl and O.T. Marzke, T.A.I.M.E. 93, 123 (1931).
100. R.F. Mehl, C.S. Barrett and F.N. Rhines, T.A.I.M.E. (1932).
101. R.F. Mehl, C.S. Barrett and D.W. Smith, T.A.I.M.E. 105, 215 (1933).
102. R.F. Mehl and D.W. Smith, T.A.I.M.E. 113, 203 (1934).
103. R.F. Mehl, C.S. Barrett and H.S. Jerabek, Metals Tech. 1, (1934).
104. R.F. Mehl, C.S. Barrett and F. Kaiser, Metals Tech. 2, (1935).
105. R.F. Mehl and G. Derge, Metals Tech. 4, (1937).
106. N.T. Bellaiew, J. Inst. Met. 29, 379 (1923).
107. C.S. Barrett, "Structure of Metals". McGraw-Hill (1952).
108. C. Zener and C. Wert, J. App. Phys. 21, 5 (1950).
109. F. Laszlo, J.I.S.I. 164, 5 (1950).
110. J.A. Malcolm and G.R. Purdy, T.A.I.M.E. 239, 1391 (1967).
111. J.W. Spretnak and R. Speiser, T.A.S.M. 46, 1089 (1954).
112. E. Eichen and J.W. Spretnak, T.A.S.M. 51, 454 (1959).
113. H.M. Otte and T.B. Massalski, Acta Met. 6, 494 (1958).

114. P.E.J. Flewitt and J.M. Towner, *J. Inst. Metals* 95, 273 (1967).
115. E. Hornbogen and H. Warlimont, *Acta Met.* 15, 943 (1967).
116. P.E.J. Flewitt in Symposium: "The Mechanisms of Phase Transformations in Crystalline Solids". *Inst. Metals Monograph and Report Series No.33* (1969).
117. C.M. Wayman and G.R. Srinivasan, discussion of Reference 11.
118. H.I. Aaronson, discussion of Reference 23.
119. D.P. Dautovich, Ph.D. Thesis, U.N.S.W. (1968).
120. M. Oka and C.M. Wayman, *T.A.I.M.E.* 242, 337 (1968).
121. H. Suzuki, *Sci. Rep. Res. Inst. Tohoku Uni.* A6, 309 (1954).
122. D.P. Dunne, Ph.D. Thesis, U.N.S.W. (1968).
123. H.M. Otte and M.P. Drazin, "Tables for Determining Cubic Crystal Orientations from Surface Traces of Octahedral Planes". Harrod Co. (1964).
124. M. McGirr and A.S. Malin, private communication.
125. M. McGirr and A.S. Malin, unpublished research presented at the Annual Meeting of Australian Crystallographers (1966).
126. J.S. Bowles, private communication.
127. J. Mackenzie, *Acta Cryst.* 10, 61 (1957).
128. W.B. Pearson, "Handbook of Lattice Spacings". Pergamon Press (1967).
129. N. Ridley, H. Stuart and L. Zwell, *T.A.I.M.E.* 245, 1834 (1969).
130. A.R. Marder and G. Krauss, *T.A.S.M. Quart.* 62, 957 (1969).
131. A. Morton, Ph.D. Thesis, U.N.S.W. (1964).